Light-Powered Plasmonic Heaters: Extracting the Heat Out of Plasmons for Photothermal Applications

विद्या वाचस्पति की
उपाधि की अपेक्षाओं की आंशिक पूर्ति में प्रस्तुत शोध प्रबंध

A thesis submitted in partial fulfillment of the requirements of the
degree of Doctor of Philosophy

द्वारा / By

राधा कृष्ण कश्यप / Radha Krishna Kashyap

पंजीकरण सं.: २०१९३६७८ / Registration No.: 20193678

शोध प्रबंध पर्यवेक्षक / Thesis Supervisor:

डॉ. प्रमोद पि. पिल्लई / Pramod P. Pillai

IISER PUNE

भारतीय विज्ञान शिक्षा एवं अनुसंधान संस्थान पुणे
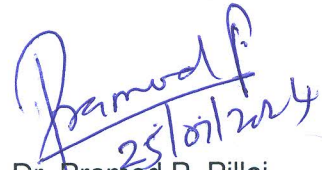INDIAN INSTITUTE OF SCIENCE EDUCATION AND RESEARCH PUNE
2024

Dedicated to,

Maiya, Papa, Puja, Didi, Siyaram and Sonika

Certificate

Certified that the work incorporated in the thesis entitled "Light-Powered Plasmonic Heaters: Extracting the Heat Out of Plasmons for Photothermal Applications" Submitted by Radha Krishna Kashyap was carried out by the candidate, under my supervision. The work presented here or any part of it has not been included in any other thesis submitted previously for the award of any degree or diploma from any other University or institution.

Dr. Pramod P. Pillai

(Thesis Supervisor)

Date: 25/07/2024

Declaration by Student

Name of Student: **Radha Krishna Kashyap**

Reg. No.: **20193678**

Thesis Supervisor(s): Dr. Pramod P. Pillai

Department: Department of Chemistry

Date of joining program: 01st August 2019

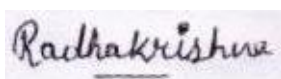Date of Pre-Synopsis Seminar: 29th January 2024

Title of Thesis: '**Light-Powered Plasmonic Heaters: Extracting the Heat Out of Plasmons for Photothermal Applications**'

   I declare that this written submission represents my idea in my own words and where others' ideas have been included; I have adequately cited and referenced the original sources. I declare that I have acknowledged collaborative work and discussions wherever such work has been included. I also declare that I have adhered to all principles of academic honesty and integrity and have not misrepresented or fabricated or falsified any idea/data/fact/source in my submission. I understand that violation of the above will be cause for disciplinary action by the Institute and can also evoke penal action from the sources which have thus not been properly cited or from whom proper permission has not been taken when needed.

   The work reported in this thesis is the original work done by me under the guidance of Dr. Pramod P. Pillai

Date: 25/07/2024

Signature of the student

Acknowledgement

To start with first I would like to thank the almighty god for guiding the path and giving me so much to cherish in my life one of the most beautiful and memorable is the present outcome the *Ph.D. thesis*. As I believe any journey is as good as the companion and without support and presence of well-wishers there is no meaning of success. My journey to date is crafted and supported by many and I find it difficult to sum up all their contribution in words. In the process, if it feels that I degraded any contribution it is not intentional. I wholeheartedly thank all who associated, supported, and inspired me throughout my Ph.D. journey.

To begin with, I would like to thank my Ph.D. supervisor, **Dr. Pramod P. Pillai** for splendidly navigating the way of this journey and sculpting the person I am today. I feel so overwhelmed to be able to join his esteemed group which has a life-changing impact on my career. He has not only taught me science and how to communicate it clearly but he has also molded me into a person who can imagine or think like a scientist. I enjoyed all our discussions which are always thought-provoking and encouraging, and they have greatly inspired me at difficult times. Most importantly I admire the way he always pushed me to achieve higher by pointing out all the mistakes critically. The attribute that he is never busy and always curious to have a scientific discussion has motivated me and supported me immensely. I have seen rise and fall in the desired circumstances whether it is COVID time or fire in the chemistry department which has heavily affected us. However, I have never seen him frustrated and he always keeps smiling and spreading positivity in his group which shows that he is a true leader in all senses and I aspire to attain these 'If I can'. Personally, I see an elder brother, a true teacher, an exceptional leader and guardian figure in him and I words will never be able to explain his contribution in either this thesis or overall in life.

I would like to thank both my RAC members **Prof. Santhosh Babu Sukumaran** and **Prof. G. V. Pavan Kumar** for their suggestions and discussions during RAC meetings. I would like to thank **Prof. C. Subramaniam** and **Ms. Itisha Dwivedi** for their incredible collaboration experience as well as the enriching scientific discussions.

I was blessed with some highly compassionate and brilliant minds as lab members during my Ph.D. adventure. It all began with my three wonderful seniors, **Dr. Soumendu**, **Dr. Gayathri**, and **Dr. Anish**. They have truly taught me experimental skills and set an extraordinary lab culture.

They have been amazingly wonderful mentors during the early years of my Ph.D. In addition to helping me with the technical components of my job, they also taught me numerous soft skills that I found useful in many other situations. They have been and continue to be very good friends with whom I can share all of my good and negative things in addition to being mentors.

Next comes the contemporary lab members without whom I cannot imagine to be able to finish my Ph.D. journey. Starting with **Dr. Sumit**, who has a brilliant mind and a clear thought process. We share a good bond and I would like to continue throughout my life. I would like to thank him to the deepest of my heart for all the initial days discussing on planning of various projects along with his endless support during experiments and discussions. **Dr. Indra Narayan** next in the list is again an excellent human being and amazing lab partner in terms of scientific or non-scientific support. I would like to thank **Pradyut** for being amazing support in scientific support and discussion as well as nonscientific endeavors and would hopefully make more memories to cherish and continue a lifelong collaboration. I adore the time management and communication skills of **Vanshika** and thank her for inspiring me. **Ankit** is a hard worker and a person of great help in and out of the lab I thank him for helping me with various experimental works as well as supporting me through ups and downs. The lab juniors (**Adhra** and **Shreya**) are extraordinarily talented and I am sure they will make the group proud and can't wait to see them grow further. The story will be incomplete without mentioning and thanking all the master thesis and short-term students who worked in the group (**Sara, Shana, Jasmine, Sriram, Rohith, Jibin, Namitha, Angela, Ajinkya, Jewel, Aishwarys, Aparna, Madhushmita, Anuradha, Sujitha, Namitha K. S., Thrisha,** and **Mridul**).

All the faculty members of the chemistry department are a support and encouragement system for all of us and I thank all of them with special mention to **Prof. Angshuman Nag**, **Prof. Pinaki Talukdar**, **Dr. Muhammed Musthafa**, **Prof. Partha Hazra** for teaching me during the coursework. I would like to express my gratitude to **Prof. Sunil S. Bhagwat,** Director, IISER Pune, the past directors, and all the department chairs I have worked under throughout my PhD journey **Prof. Nirmalya Ballav**, **Prof. Hosahudya N. Gopi**, and **Prof. Manickam Jayakannan** for providing an excellent scientific environment to the department.

After the mentors I would like to thank all the mentees (**Jasmine, Jibin, Angela, Jewel, Aparna, Madhushmita, Anuradha, Sujitha, Shreya** and **Mridul**) with whom I got the opportunity to

work apart from the brilliant mind they have a really good interpersonal skills and all of them supported and taught me a lot.

I would take this opportunity to thank all my teachers who taught me and instilled the required ability and knowledge to pursue a Ph.D. along with their constant motivation to do well in life. I thank all the instances and people involved in motivating and constantly guiding me through my dark phases.

I am grateful to the almighty god to have a family like Gem. **Maiya** has the maximum credit to start my educational journey she was the one who constantly used to push me towards excellence and not satisfied with what I had. Apart from taking care entire family and me she has played a great role in instilling the discipline and the necessary human properties in me along with teaching me life lessons to date. Next comes **Papa** who has been the piller of my life whether it is teaching me invaluable lessons through his life experiences or filling me with endless positivity and self-confidence. I am nothing without them. **Siyaram** and **Didi** are my biggest cheerleaders and well-wishers I thank them. I miss my youngest sister, **Puja**; a great motivator in my all endeavors which give my heart a sense of great void. I hope know she is watching me and will continue motivating me from heaven. Finally a very special one Sonika my wife for first joining in my life journey and enormously supporting afterwords

It is needless to say the contribution of true friends in life. It is true for this journey as well I thank all of my friends for their endless support (**Vineet, Gangeshwar, Bharat, Diggi, Bharat, Viksit, Sandeep, Kamboj, Harmesh,** and **all the 7th floor gang**). Finally, other than human beings, I would thank mother nature, the soul of my India, the '*Janmabhumi*' Jharkhand, and '*Karmabhumi*' Maharashtra for nourishing me.

Table of Contents

Thesis Abstract

The thermal energy (heat) dissipated during light-matter interactions is considered as a 'loss' in energy science. However, this process of heat dissipation is inevitable in all light-matter interactions. Recently, attention has gained towards designing systems that can generate and dissipate large amount of heat, so that they can be used for various applications. Plasmonic nanomaterials are one of the promising materials that can generate and dissipate huge amount of heat upon illumination. This dissipated heat is termed as 'plasmonic heat' and the area that studies this plasmonic heat is defined as 'thermoplasmonics'. There are multiple theoretical studies in this domain on the generation, dissipation, timescale, factors and so on, with very limited experimental validations. The proposed thesis is an effort to provide adequate experimental results on the factors influencing the generation, dissipation, quantification, and utilization of plasmonic heat.

In one of the studies, insights into the effect of shape and geometry on the generation of plasmonic heat were provided. Here, an assembled-geometry (bundled nanowires) was found to be a better nanostructure to generate the plasmonic heat, compared to the spherical counterpart. Photothermal experiments such as polymerization, solar-vapor generation, and Diels–Alder reaction, were used as a proxy to quantify the plasmonic heat dissipated by various nanostructures. Next, a novel quantification technique based on the property of 'thermochromism' was developed to qualitatively quantify plasmonic heat close to the surface of nanomaterials. This approach is a cost effective and reliable technique, which was validated with standard quantification techniques based on melting point, Raman, and IR imaging. In another study, the role of hot-charge carriers was separated from plasmonic heat in a photothermal chemical reaction. An ingenious design of a closed reactor setup was used to perform solar driven Claisen rearrangement reaction, which prevented the flow of hot-charge carriers into the reaction. This led to a sole plasmonic heat-driven high-temperature chemical transformation. In another set of studies, the plasmonic heat generated under sunlight illumination was converted into electricity through solar thermoelectric generators (STEG). The incorporation of AuNPs as the solar absorber led to ~9 times enhancement in the overall solar-to-electricity conversion efficiency of concentrated-STEG (under 75 sun), with an efficiency of 9.6% at ambient conditions. This, to the best of our knowledge, is the highest efficiency reported for STEGs at ambient conditions. The electricity generated from the plasmon-powered STEG was used to run low-to-medium power electrical devices (35 mW to 500 mW), as well as for the green-H_2 production via the electrolysis of water.

Thus, various aspects of thermoplasmoincs including generation, quantification, utilization and conversion of plasmonic heat were studied in detail. Alongside, the plasmonic heat was used for performing energy-intensive chemical transformations, which showcases the suitability of plasmonic heat in high-temperature applications. In short, our studies demonstrate that plasmonic heat could emerge as a greener alternative to conventional thermal energy sources in science and engineering.

Thesis Synopsis

Plasmonic nanomaterials are known to release large heat via nonradiative relaxation pathways, which is often termed as plasmonic heat. This heat generation was considered a *loss* in energy research and plasmonic community for a long time. However, it has been recently shown that plasmonic heat can indeed be used for a broad class of thermally-driven applications. The study domain dealing with the generation, manipulation, and utilization of plasmonic heat is termed as *thermoplasmonics,* which constitute the central theme of the thesis. The thesis focuses on both fundamental and applied aspects of plasmonic heat generation and utilisation, that require immediate attention to propel the area of thermoplasmonics. From a fundamental level, the factors affecting thermalization and dissipation processes were experimentally studied, wherein the effect of nanoparticle size, shape, and assembly was studied. Alongside, a simple, yet effective, quantification technique was developed for measuring the temperature-rise caused by the plasmonic heat. Form applied perspective, plasmonic heat was used for a broad range of studies, such as thermal polymerization, solar vapor generation, high-temperature organic reactions, and crystal-to-crystal phase transformation. Further, the plasmonic heat produced from the sunlight irradiation was used as the thermal energy source to boost the electricity generation efficiency of solar thermoelectric generators.

First Chapter discusses the concept of thermoplasmonics along with a summary of its evolution and progress. The discussion includes a brief introduction about the relaxation dynamics in photoexcited plasmonic nanoparticles leading to the generation and dissipation of heat. Next, the advantages of plasmonic heating over other forms of heat are discussed. Subsequently, theoretical predictions on the fundamental parameters of plasmonic nanoparticles affecting the thermalization and dissipation processes have been summarized. Following that, conventional applications of plasmonic heat in biology (photothermal imaging, drug and gene delivery, and photothermal therapy) and chemistry (solar-vapor generation and chemical reactions) are discussed. In the subsequent section, we discussed some of the challenges and opportunities in the field, leading towards the objective of the thesis.

The second Chapter summarizes our efforts in studying the effect of nanostructural shape and assembly on plasmonic heat generation and dissipation. In view to achieve the goal of studying assembly effect, an array of bundled gold nanorod was fabricated using the combination of thermal vapor deposition and electrochemical growth. The yield of the photothermal Diels-Alder reaction between trans-β-nitrostyrene and 2,3-dimethyl-1,3-butadiene was used as a marker for

the generation and dissipation of plasmonic heat. The detailed study suggested that the AuNR is a better photothermal converter than its spherical counterpart. The photothermal efficiency of the bundled AuNR array-based thermoplasmonic substrate was estimated to be ~93% , which is one the best reported so far. Further, the plasmonic heat generated from the bundled AuNR array was used for a broad range of studies such as PDMS polymerization, solar-vapor generation, and Diels-Alder reaction (**Scheme 1**). Thus, bundled AuNR array was projected as an efficient plasmonic heater for diverse studies both under aqueous and organic solvents.
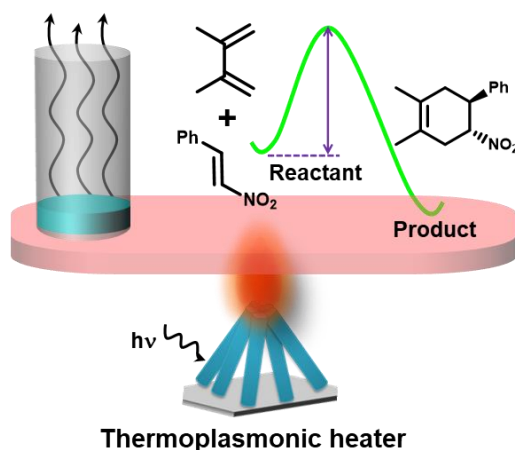
Scheme 1. Schematic representation of thermoplasmonic bundled AuNR array driving solar vapor generation and Diels-Alder reaction. **Kashyap, R. K.**; Dwivedi, I.; Roy, S.; Roy, S.; Rao, A.; Subramaniam, C.; Pillai, P. P. *Chem. Mater.* **2022**, *34*, 7369–7378.

In the third chapter, we could develop a simple technique based on thermochromism to quantify the temperature rise caused by the plasmonic heat (**Scheme 2**). Lead carbonate ($PbCO_3$) was used as a thermochromic molecule which is known to change its color from white to yellow as a result of thermal decomposition forming lead oxide (PbO). The activation temperature for thermochromic crystal-to-crystal transformation in $PbCO_3$ is reported to be ~250 °C. The successful color change from white to yellow in $PbCO_3$ adsorbed on the bundled AuNR array, upon illuminating with a 532 nm CW diode laser, suggested the attainment of temperature ~250 °C. The measured temperature was verified using three independent techniques: infrared-based thermometric imaging, melting point, and Raman spectroscopy. Infrared-based thermometric imaging study confirmed a sharp increase in the temperature caused by plasmonic heat, followed by its saturation at ~250 °C.
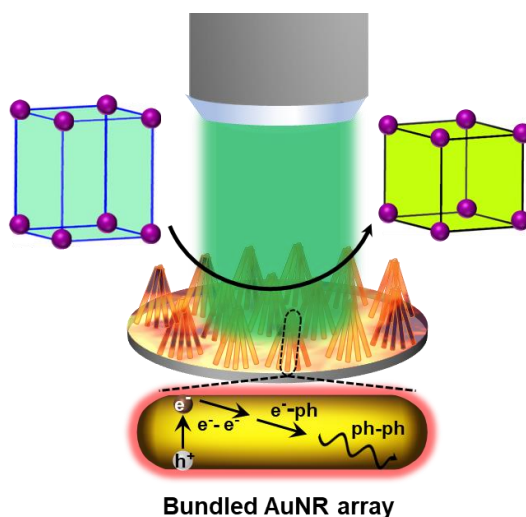
Bundled AuNR array

Scheme 2. Schematic representation of thermochromic phase change-based quantification of plasmonic heat in bundled AuNR array. **Kashyap, R. K.**; Dwivedi, I.; Roy, S.; Roy, S.; Rao, A.; Subramaniam, C.; Pillai, P. P. *Chem. Mater.* **2022***, 34,* 7369–7378.

The fourth Chapter discusses the prospect of plasmonic heat for high-temperature reactions in synthetic organic chemistry. Plasmonic-heat generated from the solar irradiation of gold nanoparticles was used as the thermal energy source for the Claisen rearrangement of allyl phenyl ether to 2-allylphenol, which is conventionally performed with electrical heating at 250 °C. The use of a closed reactor enables the physical separation of the reactants from the source of plasmonic-heat, thereby preventing the interference of the hot-charge carriers in the plasmon-driven Claisen rearrangement (**Scheme 3**). In this way, the sole effect of plasmonic-heat in driving a high temperature organic transformation is demonstrated. Our study reveals the prospects of plasmonic nanostructures in conducting energy intensive chemical synthesis in a sustainable fashion.
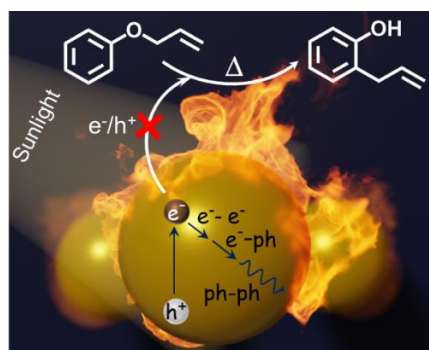
Scheme 3. Schematic representation of plasmonic heat driven 1,3-sigmatropic Claisen rearrangement, which is conventionally performed with electrical heating at 250 °C. **Kashyap, R. K.**; Tyagi, S. *Chem. Commun.* **2023**, *59*, 13293-13296.

The fifth Chapter explores the possibility of the conversion of plasmonic heat into electricity. A plasmon-powered solar thermoelectric generator (STEG) was fabricated by depositing a thin film of plasmonic AuNPs on commercially available thermoelectric generator. The use of plasmonic solar absorber film has improved the overall efficiency of solar-to-electricity conversion by ~9 times, yielding an overall efficiency of ~9.6% at ambient condition (**Scheme 4**). The device was found durable for more than a year, without any noticeable change in its efficiency. the electricity generated from plasmon-powered STEGs was used to run electrical devices, as well as store energy in the form of hydrogen via the electrolysis of water.
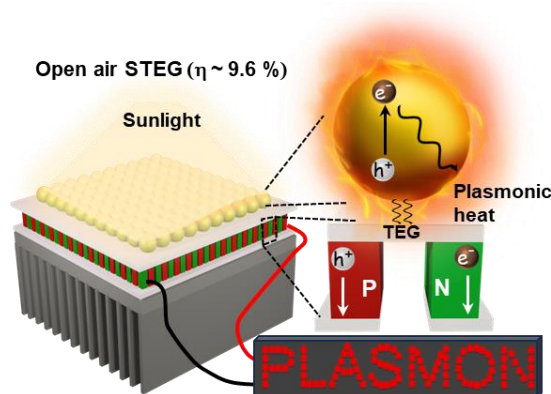
Scheme 4. Schematic representation of plasmonic gold nanoparticles boosting the solar-to-electricity conversion efficiency of solar thermoelectric generator. **Kashyap, R. K.**; Pillai, P. P. Plasmonic Nanoparticles Boost Solar-to-Electricity Generation at Ambient Conditions. *Nano Lett.* **2024**, *24*, 5585–559210.

In summary, the current thesis is an attempt to fill some of the gaps in the field of thermoplasmonics with respect to fundamental as well as applied perspectives. Various aspects of thermoplasmoincs including generation, quantification, utilization and conversion of plasmonic heat were studied in detail. Alongside, the plasmonic heat was used for performing energy intensive chemical transformations, which showcases the suitability of plasmonic heat in high-temperature applications. In short, our studies demonstrate that plasmonic heat could emerge as a greener and sustainable alternative to conventional thermal energy sources in science and engineering.

Chapter – 1

Introduction to Thermoplasmonics: Concepts and Applications
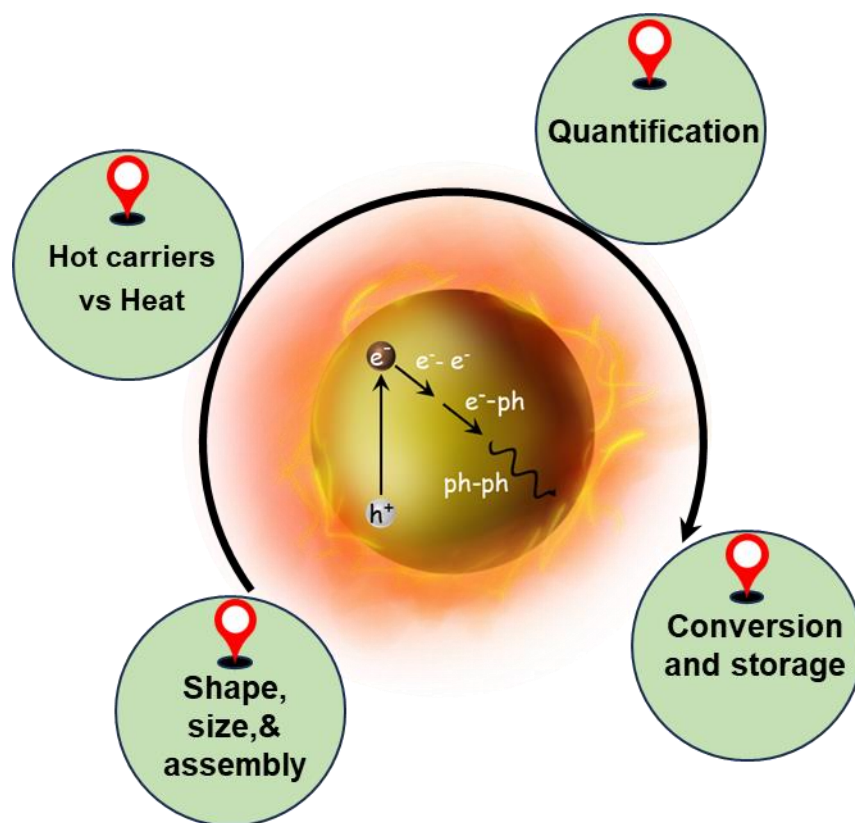
A part of this Chapter has been adapted from the following paper with permission. Copyright 2022, Wiley-VCH: Jain, V.; Kashyap, R. K.; Pillai, P. P. Plasmonic Photocatalysis: Activating Chemical Bonds through Light and Plasmon. *Adv. Opt. Mater.* **2022**, *10*, 2200463.

1.1. Introduction

The continuous rise in global energy consumption and overreliance on fossil fuels to meet this increasing demand has resulted in an energy crisis and climate change. Therefore, it is needless to say that we require sustainability in the energy sector. Among all the renewable energy sources, solar energy has shown promise in meeting global energy demand with net zero carbon emission. Therefore, solar research has attracted significant scientific attention in the area of energy research. In that direction, attention has been given to the direct utilization, conversion as well as storage of solar energy. The important requirement to harvest solar energy for various applications is a material that can absorb sunlight efficiently, often termed as a solar absorber. Characteristics of an ideal solar absorber include a high absorption coefficient along with high photostability. Among all the solar absorbers, plasmonic materials have gained immense attention in the past two decades. One of the standout reasons is the plasmonic effects, which arise due to the collective oscillation of conduction electrons of metal nanoparticles (NPs) under the influence of electromagnetic radiation (**Figure 1.1a**).[1-3] As a result, the amount of light absorbed by a plasmonic material is exceptionally high. For example, the molar extinction coefficient of plasmonic metal NPs are in the range of 10^8 - 10^{10} M^{-1} cm^{-1}, which is approximately 10^4 - 10^6 times higher than most of the light-absorbing species known.[1-3] Because of the collective oscillation of surface electrons, the absorption cross-section of LSPR can extend up to ten times the geometrical cross-section of metal NPs (**Figure 1.1a**).[1] The light energy is confined on the surface of plasmonic NPs in the form of an elevated electric field, which then decays through two main relaxation pathways: (i) radiative pathways via the re-emission of photons (luminescence or scattering) or (ii) non-radiative pathways via the generation of hot charge carriers.[1] The radiative photon emission or scattering is a dominant pathway for larger particles (say > 50 nm for Ag), and has been extensively used for numerous applications such as Surface Enhanced Raman Scattering (SERS), imaging, and sensing. The non-radiative pathway is dominant for smaller-sized particles and leads to the generation of hot electron-hole pairs, which are used in fueling various chemical transformations. Following the plasmonic excitation, either through intra- or inter-band transitions, there is a creation of non-Fermi electronic distribution within the time frame of 1-100 fs via Landau damping, which thermalizes internally through electron-electron

scattering in the time scale of 100 fs to 1 ps leading to the distribution of hot electrons and holes close to the Fermi energy level (**Figure 1.1b**). Subsequently, these hot charge carriers thermally equilibrate by dissipating their energy via electron-phonon scattering, and releases heat to the NP lattice in the time frame of 1-100 ps (local or plasmonic heating; **Figure 1.1c**). Finally, the NP lattice reaches a thermal equilibration with the surrounding by dissipating heat, in the time frame of 0.1 – 10 ns via phonon-phonon interactions (**Figure 1.1d**). The heat dissipated is termed as plasmonic heat. It is worth mentioning that all these relaxation processes can occur simultaneously in a photoexcited plasmonic NP. Thus, it is essential to understand and control various factors influencing these relaxation processes, for realizing the desired outcome from the plasmon decay. For instance, one needs to focus on hot-charge carrier generation, separation, and extraction steps for performing useful chemical reactions using plasmonic NPs. Having said that the thermal dissipation is the end product of the pathway and hence the thermal effect cannot be avoided in a plasmonic nanomaterial.
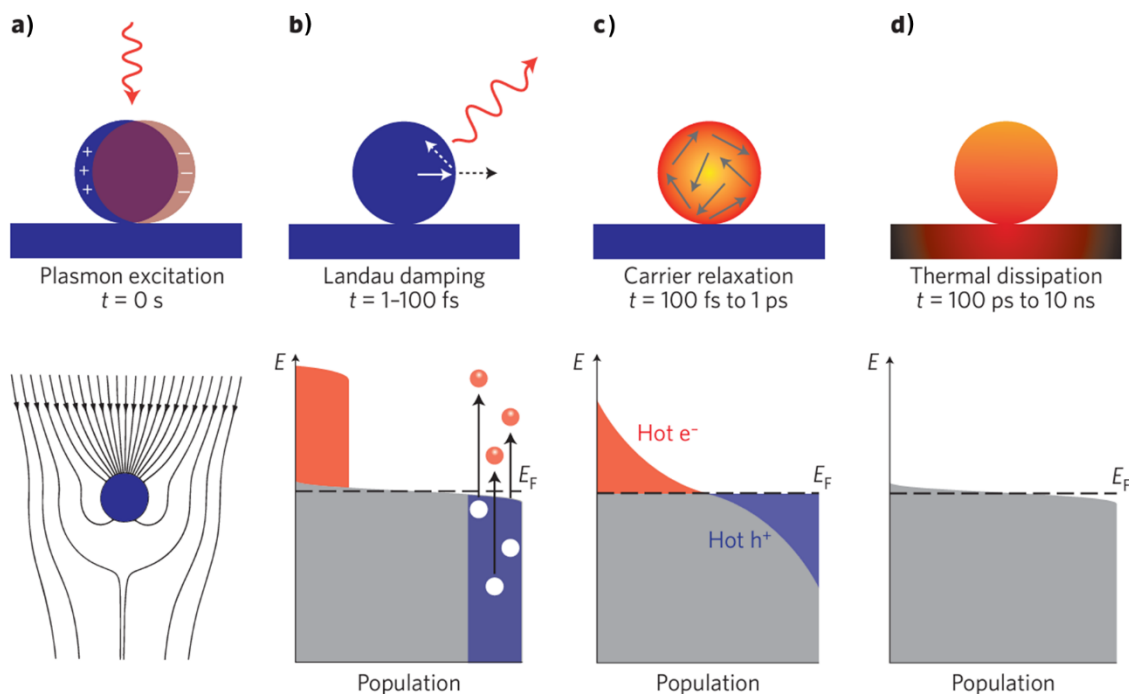
Figure 1.1. The light-matter interaction in plasmonic nanoparticles. (a) Light illumination triggers the collective and coherent oscillation in conduction band electrons which is called as localized surface plasmon polaritons. Due to oscillation, the effective size for optical interaction is higher than the physical cross-section of the particle and hence plasmonic nanoparticles are known to absorb light beyond its physical cross-section. (b) The excited plasmons relax via Landau damping resulting in the generation of excited electron-hole pairs which are in a thermal distribution. (c) Next, in the time scale of 100 fs to 1 ps the electron-electron interatom equilibrates the energy to result in the Fermi-Dirac distribution of hot

charge carriers (electron: red, hole: blue). (d) Finally, hot charge carriers transfer the absorbed energy to the nanoparticle lattice via electron-phonon interaction which dissipates to the local environment via phonon-phonon interaction resulting in a local elevation in temperature known as plasmonic heat. Reproduced with permission from ref 1. Copyright: 2015, Nature Publishing Group.

1.2. Thermoplasmonics: The area and its evolution

In plasmonics initially, light concentration was considered the most useful property, as at that time the most attractive applications were surface-enhanced Raman spectroscopy (SERS) and plasmonic devices.[2] Hence, the absorbed energy was considered as a loss.[2] On the other hand, plasmonic nanomaterials absorb most of the illuminated optical energy and undergo non-radiative relaxation.[1-3] Acknowledging this fact, some research groups reached the conclusion that if absorption in metal is inevitable, it might as well be utilized.[1-3] In that direction two independent research domains have come into existence (i) utilizing hot charge carriers for chemical transformation, popularly known as plasmonic photocatalysis and (ii) utilizing the thermal energy dissipated into the crystal, named as thermoplasmonics. Initially, research was focused predominantly on fundamentals of plasmonic heating along with its applications in the medical field. The first application reported was the protein denaturation all the way back in 1999.[4] However, the property of plasmonic heating and its potential application has got prominent attention after a series of seminal works by Orrit, Halas, West, and El-Sayed in medical applications such as cell imaging and photothermal therapy.[3-6] Following that, thermoplasmonics has evolved as an independent area of research having a broad range of applications (**Figure 1.2**).[4-30]

Applications of plasmonic heat

Biology	Physical and material sciences	Chemistry
➤Protein denaturation: 1999	➤ Phase change: Melting/Boiling	➤ Chemical reactions
➤Photothermal imaging: 2002	➤ Nanofabrication	➤ Solvothermal reactions
➤Photothermal therapy:2003	➤ Microbubble formation	
➤Drug/gene delivery	➤ Temperature-induced liquid flows	
➤Plasmonic sensing	➤ Water evaporation/desalination	
	➤ Solar light harvesting: Thermophotovoltaics	

Figure 1.2. List of broad range applications of plasmonic heat in demonstrating the importance of thermoplasmonics in energy and fundamental applications.

1.3. What is so special about plasmonic heating?

1.3.1. Localized nature: Nanoscopic control of the processes

The thermal conductivity of widely used noble metals such as Au and Ag, as plasmonic materials, is high as compared to the surrounding medium and therefore the temperature throughout the nanostructure is same. However, there is an inverse relation of temperature increase with distance as described in the following equation: [2]

$$\Delta T = \frac{V_{NP}\ Q}{4\pi k_0 r}$$

Where, r is the distance from the center of NP, k_0 is thermal conductivity of the surrounding medium, V_{NP} is the NP volume, and Q is the energy coming from the light. The outcome of the equation can be further subdivided into two cases with respect to distance r

$$\delta T\ (r) =\ \delta T_{NP}\frac{R}{r}, \qquad r > R,$$

$$\delta T\ (r) \approx\ \delta T_{NP}, \qquad r < R$$

As a result, the maximum temperature achieved due to plasmonic heating is at the nanoparticle lattice which is equally distributed throughout. However, the temperature decreases sharply going away from the nanoparticle as depicted in **Figure 1.3**. This depicts the localized nature of plasmonic heating.
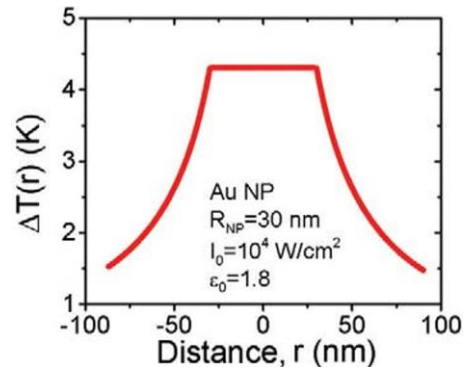
Figure 1.3. Localized nature of plasmonic heat. The calculated temperature increase arising from plasmonic heating in illuminated gold nanoparticles of radius 30 nm, where water is the surrounding medium. The temperature increase was maximum throughout the nanoparticle and decreased sharply going away from it indicating its localized nature. Reproduced with permission from ref 2. Copyright: 2007, Elsevier.

Now an obvious advantage of the plasmonic nanoparticle heater is that it provides the nanoscopic control of the processes. For example, Brongersma and co-workers[13] demonstrated the photothermal growth of silicon nanorods (SiNR) mediated by gold nanoparticles (AuNPs) (**Figure 1.4**). The authors were able to achieve the spatial as well as orientational control upon optimizing the illumination parameters. For instance, the SiNR growth was observed only at the illumination point, whereas smaller beam diameter had resulted into horizontal growth. The excellent spatial control has installed the control towards the fabrication of designed patterns of SiNR (**Figure 1.4g,h**). Therefore, plasmonic heat can be utilized to manipulate the processes at nanoscale with great ease.
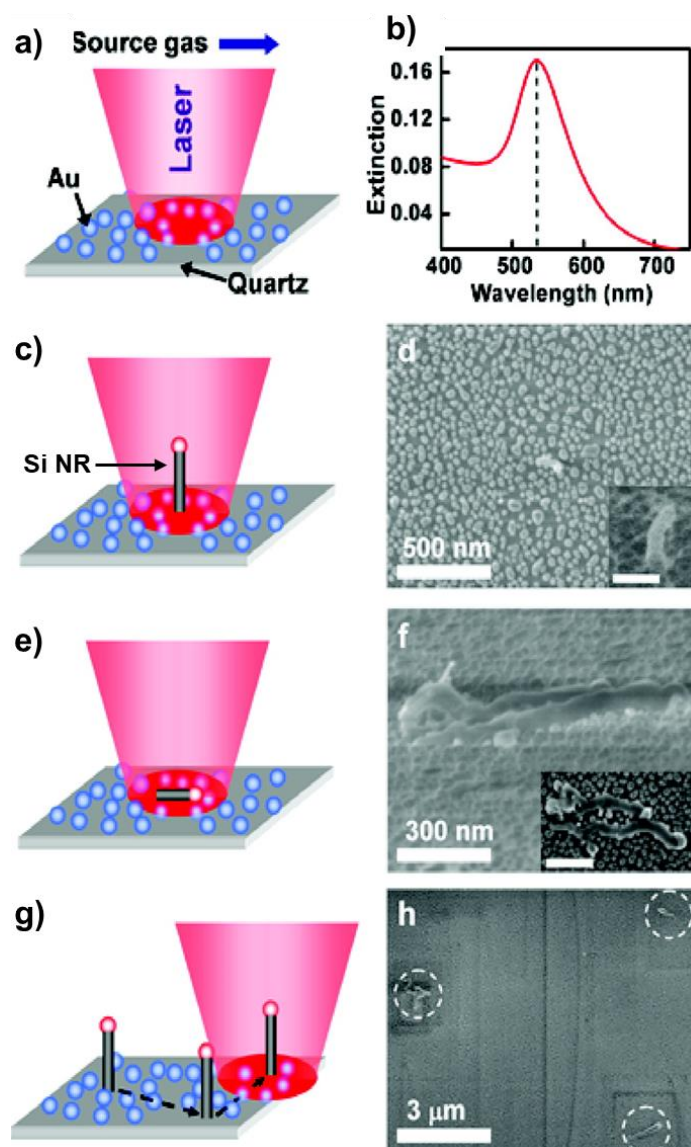
Figure 1.4. Nanoscopic control on photothermal growth of Si nanorod. (a) and (b) Schematic representation of the experimental setup consisting of a film of AuNPs on a glass slide submerged in a silicon precursor solution and UV-vis absorption spectrum of AuNPs used as a photothermal agent. (c) and (d) Scheme and FESEM study show Si NR growth was observed at the position of laser spot. (e) and (f) An experiment showing orientation control in the growth of Si NR where horizontal growth was observed upon decreasing the laser spot dimension. (g,h) Patterning individual Si NRs at the surface just by moving the laser spot from one place to the other. The SEM image shows the Si NR position in a white circle coinciding with the laser spot. The positional as well as orientational control was achieved due to the localized nature of plasmonic heat. Reproduced with permission from ref. 13. Copyright: 2007, American Chemical Society.

1.3.2. Generation of high local temperature: High-temperature processes with light at room temperature

As discussed in **Section 1.1**, plasmonic excitation involves a sea of electrons of metal nanostructure. As a result, the molar extinction coefficient of plasmonic materials are at least 4-6 orders higher than that of a standard light-absorbing molecule. Now, it has been found that nonradiative relaxation is the major relaxation pathway for excited surface plasmon polaritons. Since thermal dissipation is the outcome of nonradiative pathway, it is expected that plasmonic nanomaterials dissipate majority of the absorbed optical energy into heat. Indeed, the photothermal conversion efficiencies of plasmonic nanoparticle of size below 25 nm was found to be >90%. Therefore, a high temperature can be generated locally upon optical illumination of plasmonic nanoparticles, which provides room to perform high-temperature transformations at ambient reaction conditions.[24,27] For example, Scaiano and co-workers reported the photothermal decomposition of dicumyl peroxide in a drop containing reactant and AuNP (**Figure 1.5a**).
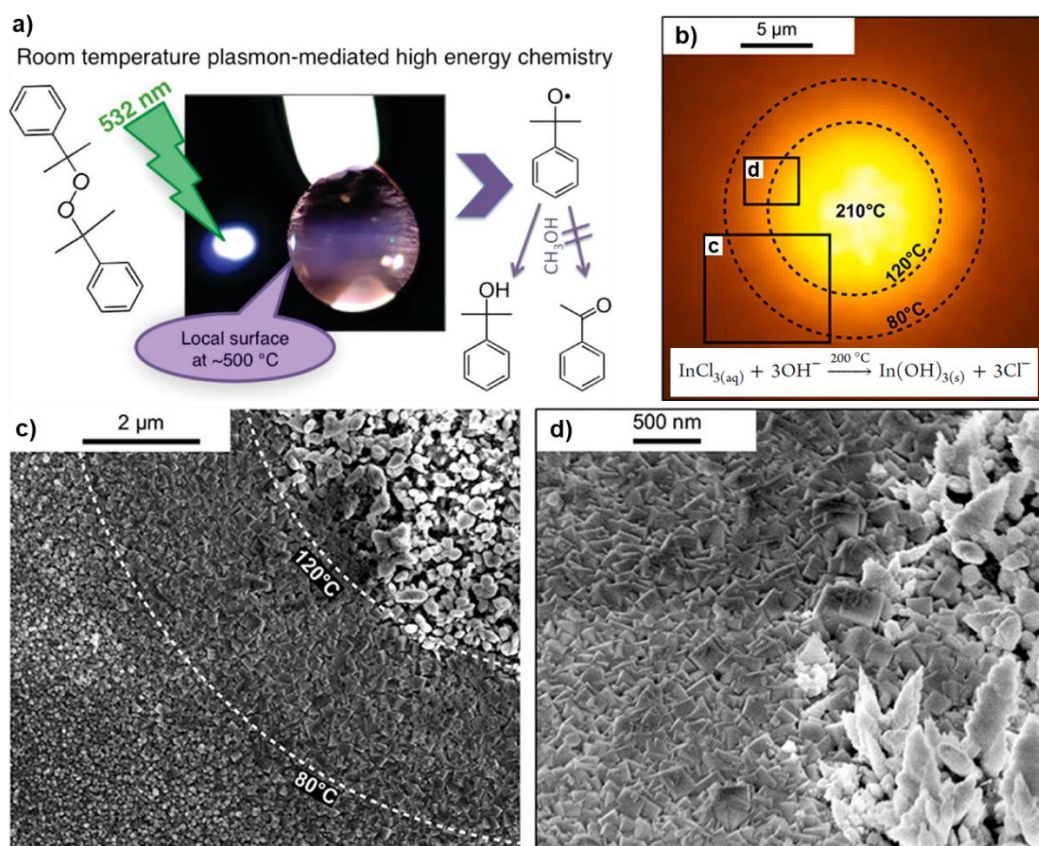
Figure 1.5. High-temperature transformation at ambient conditions. (a) The photothermal decomposition of dicumyl peroxide was reported with Au nanoparticle-based plasmonic heater in a drop

resulting in a surface temperature of 500 °C locally. Reproduced with permission from ref. 24. Copyright: 2011, American Chemical Society. (b), (c) and (d) Photothermal transformation of $InCl_3$ to $In(OH)_3$ under ambient reaction environment. The reaction under thermal conditions is only possible with hydrothermal conditions using an autoclave. Moreover, authors were able to observe two distinct crystal shapes of $In(OH)_3$ (pine tree type and rectangular) which was not be possible in a single hydrothermal setup. Reproduced with permission from ref. 27. Copyright: 2016, American Chemical Society.

The temperature attained was estimated to be ~500 °C using Arrhenius equation from the known value of activation energy and rate constant of the reaction. In another report, Baffou and co-workers[27] were able to perform a high-temperature chemical transformation of indium chloride to indium hydroxide at room temperature. The AuNPs were used as a photothermal heaters and the temperature map suggested a temperature gradient around the illuminated area (**Figure 1.5 b**). The FESEM analysis has suggested the formation of two distinct type of crystals i.e. rectangular and palm tree shaped following the thermal profile of the sample. The palm like structure being formed at the area of highest temperature. Therefore, an exciting outcome of two distinct product type was achieved, which is impossible in a single solvothermal reaction setup.

1.3.3. Catalytic behavior of plasmonic material: Collective thermal and catalytic effect

As it is discussed in the **Section 1.1**, plasmonic nanomaterials concentrate electromagnetic radiation around them and because of plasmonic relaxation process they are an efficient catalyst. They can be individually used as a catalyst or can strongly influence the catalytic efficiency of a material around it. On the other hand, plasmonic materials are efficient photothermal converters and generate high temperature locally. Both these properties: catalytic as well as thermal platform can have a co-operative effect in driving a chemical transformation. For example, Cronin and co-workers[14] used a hybrid material comprising of a plasmonic material of Au and a catalytic material Fe_2O_3. The cooperativity of catalytic enhancement and photothermal effect were able to perform CO oxidation upon light illumination (**Figure 1.6**).
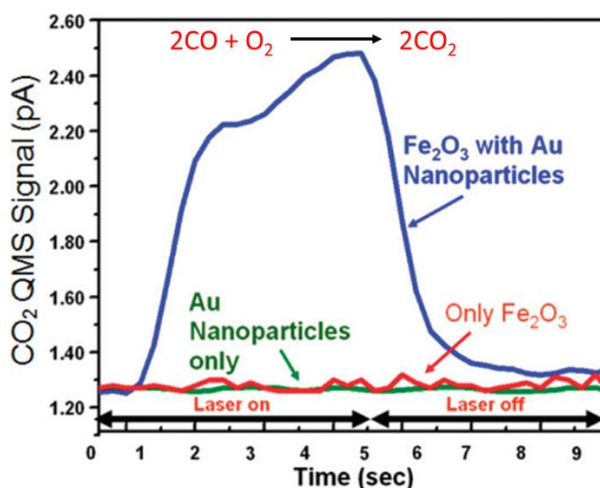
Figure 1.6. Cooperative effect of catalytic and photothermal behaviors of Au-Fe₂O₃ particle in driving CO oxidation. The reaction was only possible in the presence of hybrid Au-Fe₂O₃ structure under light illumination. Reproduced with permission from ref. 14. Copyright: 2010, American Chemical Society.

In summary, the plasmonic heat has various advantages over normal heating which can be explored to achieve exciting outcomes. Additionally, as plasmonic materials are visible and NIR active, direct sunlight can be used as an excitation source to perform thermal processes. This brings the sustainability aspect as well. Therefore, plasmonic materials hold the promise to tackle energy crisis and climate change, and hence it is an attractive area of research.

However, the utilization of plasmonic heating is limited by the following shortcomings:

    a) Difficulties in the quantification: Plasmonic heating is a local phenomenon of a nanostructure and hence accurate quantification of plasmonic heat is difficult as the regular thermometers cannot be used due to limitations in spatial resolution.

    b) Control over the amount of heat: It is challenging to precisely control the photothermal heat generated by plasmonic materials compared to normal electrical heating. In principle, one can achieve this by tuning the intensity of illumination. However, the lack of a standard quantification technique makes it difficult to know the exact temperature at a particular intensity.

1.4. Fundamentals of plasmonic heating

Localized surface plasmon resonance (LSPR) is the resonance condition of electronic oscillation frequency with illuminated light frequency which is the reason of light absorption by plasmonic nanostructure. The LSPR depend on (i) nature and geometric parameters of nanostructure such as size, shape, and assembly, (ii) wavelength of illumination, and (iii) nature of surrounding medium. Since plasmonic heating is also an outcome of LSPR, it also depends upon the above factors. In this section we will discuss the factors influencing the thermalization. According to the report by Kotov and co-workers,[3] the temperature increase follows the LSPR band of the nanoparticle (**Figure 1.7a**). The higher time of light exposure resulted in a higher temperature increase.
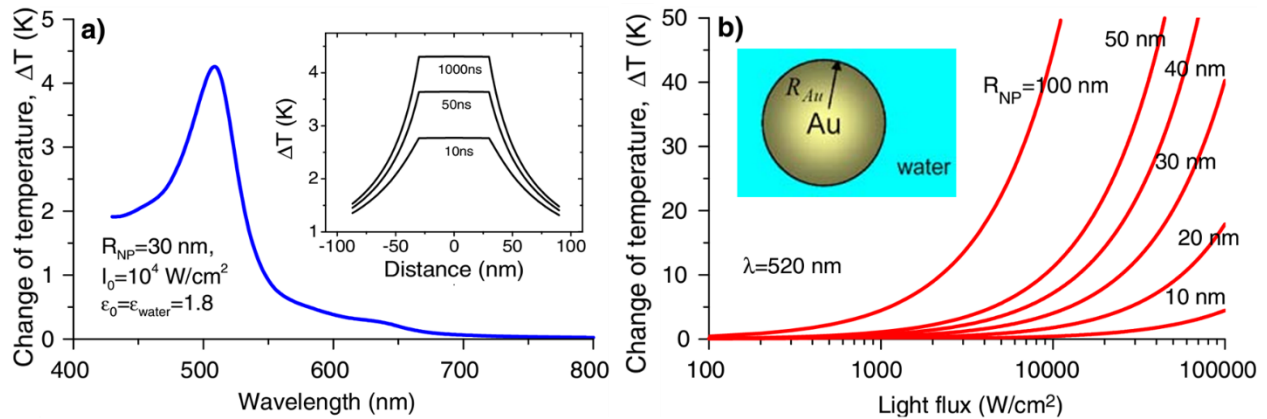
Figure 1.7. Effect of (a) wavelength of illumination and (b) nanoparticle size as well as illumination intensity. The heat generation follows the absorption profile and maximum heat generated is at plasmon maxima. On the other hand, thermalization has a direct dependence on size as well as illumination intensity. Reproduced with permission from ref. 3. Copyright: 2006, Springer.

Govorov and co-workers have developed the following expression to show the effect of size and illumination intensity on the plasmonic heat generation:[2]

$$\Delta T_{max}(I_0) = \frac{R_{NP}^2}{3k_0}\frac{\omega}{8\pi}\left|\frac{3\varepsilon_0}{2\varepsilon_0 + \varepsilon_{NP}}\right|^2 Im\,\varepsilon_{NP}\frac{8\pi.I_0}{c\sqrt{\varepsilon_0}}$$

where, ΔT_{max} is the maximum temperature increase at the nanoparticle lattice, R_{NP} is the radius of NP, k_0 is thermal conductivity of the surrounding medium, ε_{NP} and ε_0 are the dielectric constants of the NP and surrounding medium is the NP volume, I_0 is the intensity of light, and ω

is the LSPR frequency. The equation clearly suggests that the temperature increase is proportional to the second power of the radius of NP. On the other hand, the thermalization is directly proportional to the illumination intensity as shown in the **Figure 1.7b**.

Kotov and co-workers in the same report,[3] discussed the effect of light polarization and assembly of NPs (**Figure 1.8**). Two closely spaced nanoparticles showed collective effect on thermalization, when the electric field polarization is parallel to the interparticle axis; whereas the optical polarizations in the other direction showed reduced heat dissipation.
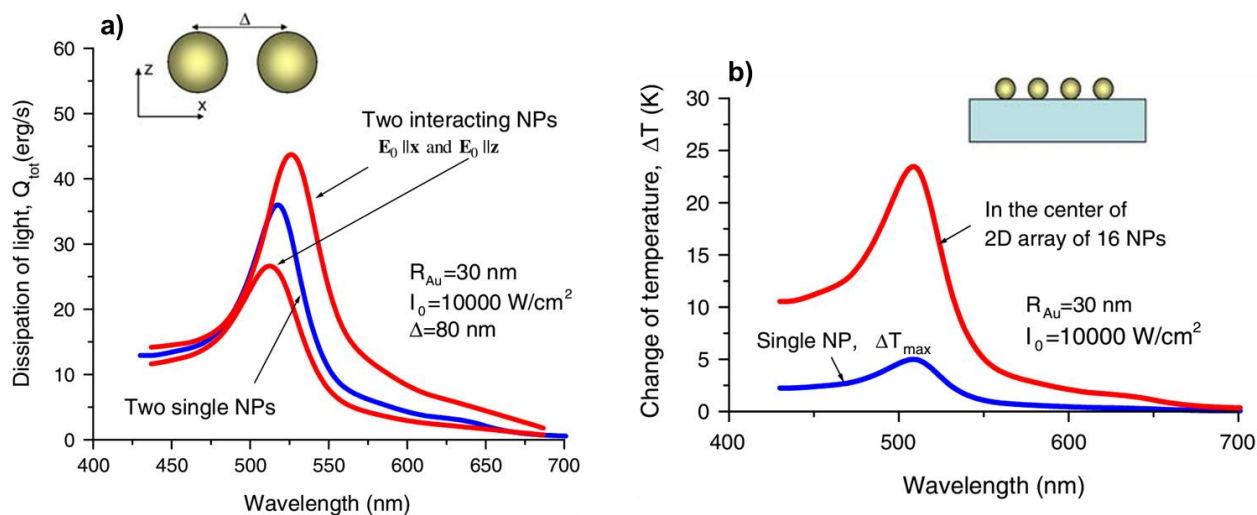
Figure 1.8. Effect of light polarization and assembly on plasmonic heat generation. (a) The light polarization direction affects the extent of collective heating by closely spaced two nanoparticles where the electric field parallel to the interparticle axis resulted in higher heat generation compared to any other polarization. (b) An array of 16 nanoparticle has shown higher change in temperature as compared to the individual particle, indicating that thermalization has collective effect. Reproduced with permission from ref. 3. Copyright: 2006, Springer.

The temperature change for an array of 16 AuNPs (4 × 4) under irradiation was calculated to study the assembly effect (**Figure 1.8b**). An increase in the temperature was found for the array as compared to the single nanoparticle, which conclusively proves the collective effect of thermalization. The effect of shape and material composition was studied by Baffou and co-workers.[30] A dimensionless quantity Joule's number (J_o) was introduces through this study, as a marker of photothermal conversion efficiency as described below:

$$J_o = \frac{\sigma_{abs}\lambda_{ref}}{2\pi V_{NP}}$$

where, **Jo** is Joule's number, σ_{abs} is the absorption cross-section of the NP, V_{NP} is the volume of the NP, and λ_{ref} = 1240 nm is an arbitrary reference wavelength to make **Jo** dimensionless. Higher the **Jo**, higher is the photothermal conversion efficiency. Further, **Figure 1.9** shows that **Jo** increases with increase in nanoparticle aspect ratio. Therefore, it can be concluded that the anisotropic nanostructures are better photothermal converters compared to isotropic ones. It is important to mention that the influence of most of the fundamental nanostructural parameters (geometry and assembly) have been studied theoretically. However, their experimental verification is scarcely discussed which present an opportunity in the field.
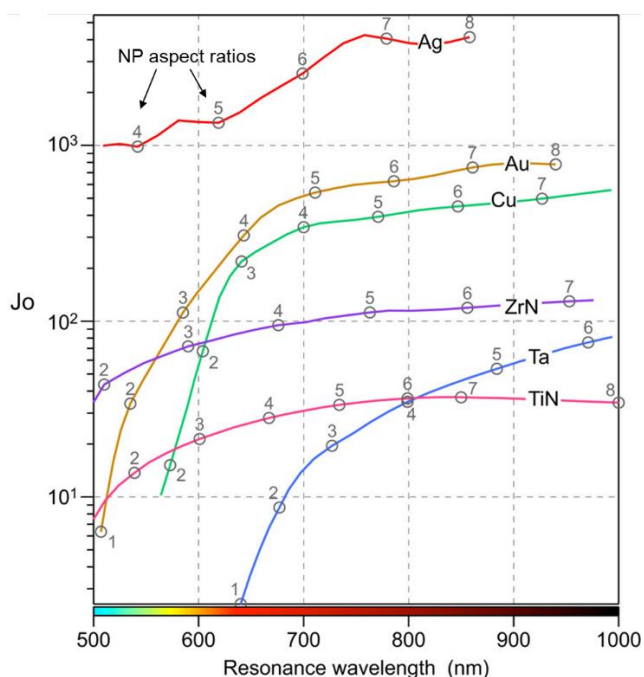
Figure 1.9. Effect of nanoparticle shape and material composition on thermalization. Joule's number was defined as an indicator of photothermal conversion efficiency. The plot clearly shows that anisotropic particles are better photothermal convertors as compared to their spherical counterparts. Reproduced with permission from ref. 30. Copyright: 2015, American Chemical Society.

1.5. Conventional applications

The first application of plasmonic heat was reported in 1999 for protein denaturation.[4] Since then, the plasmonic photothermal property was predominantly explored for biomedical applications (**Figure 1.10**) including photothermal imaging, drug and gene delivery, and plasmonic photothermal therapy (PPTT).[5-8,10,12,16,19,20] The basic principle behind plasmonic photothermal

therapy is the targeted delivery of NIR absorbing nanoparticles to the tumor cells followed by illumination which initiate apoptosis leading to the destruction of cancerous cells.
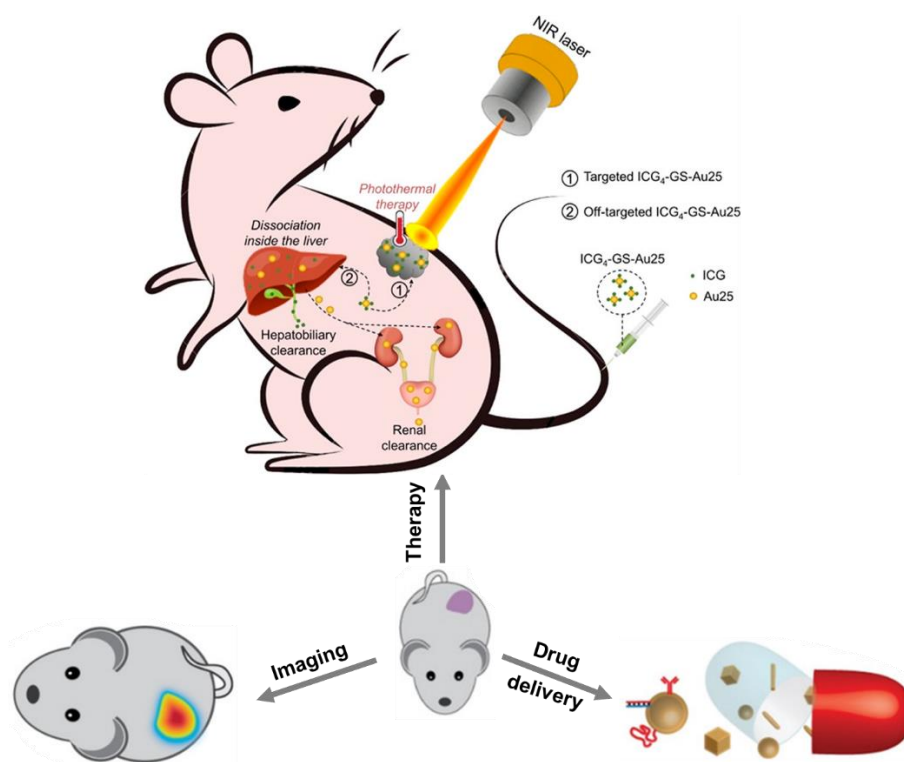
Figure 1.10. Representative biomedical applications of plasmonic heating. The top panel is reproduced with permission from ref. 8. Copyright: 2020, American Chemical Society. The bottom panel is reproduced with permission from ref. 20. Copyright: 2019, Wiley-VCH.

This is an effective way to treat cancer and the field has progressed to the extent where human trials on prostate cancer have also been performed with promising output.ref The other widely studied application of plasmonic heat is solar vapor generation and desalination of water.[21,22] As it is already discussed, the plasmonic nanostructure presents opportunity for direct solar energy utilization to drive thermal processes. Keeping this in mind, researchers have used the plasmonic photothermal property for vaporization and desalination to tackle the shortage of drinking water in a sustainable fashion. The principle here is that plasmonic based solar evaporator film absorbs sunlight and convert it efficiently to heat. The water at plasmonic material interfacial feels the heat and starts boiling, which can be condensed, collected, and stored (**Figure 1.11**).
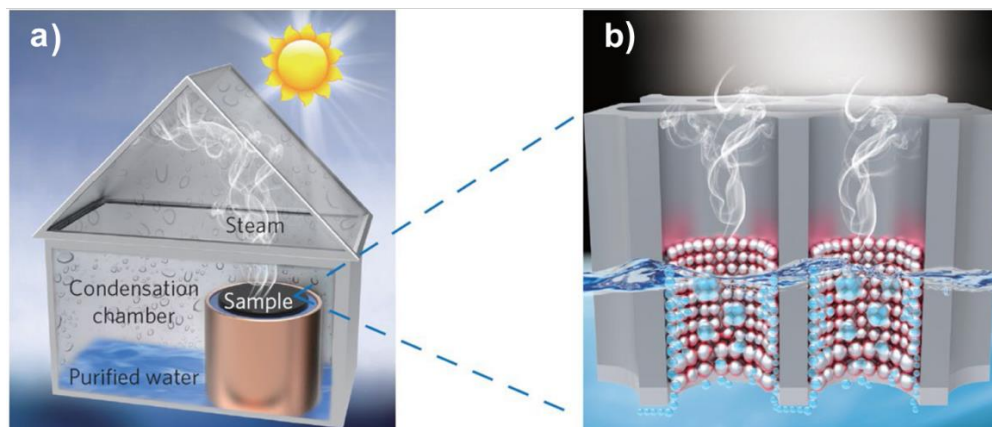
Figure 1.11. Plasmonic heat-driven solar vapor generation. (a) A prototype design of the desalination setup and (b) plasmonic photothermal platform consisting of Al nanoparticles in a porous template. The solar illumination generate heat at the surface of Al NP, in turn heating and evaporation of water in contact with it. Reproduced with permission from ref. 22. Copyright: 2016, Nature Publishing Centre.

1.6. Applications in chemistry

The chemical synthesis comprises up of ~40 % of global energy consumption and therefore attention has been given to install sustainability in this sector. Solar energy being the green and perennial source is considered to be a sustainable alternate, where there is a must requisite for efficient solar absorbing materials. The plasmonic nanostructures has found applications to drive chemistry using light, where the chemical transformation has been reported via three distinct driving forces: local field, hot charge carriers, and plasmonic heat. Thermally-driven chemical transformations can be successfully performed using light and plasmons. In the very first attempt in this direction, Branda and co-workers[23] reported a bond dissociation reaction at the surface of Au coated silica nanoparticles using plasmonic heat (**Figure 1.12a**). The potential of plasmonic nanoparticles were further investigated for high temperature transformation. In a seminal work by Scaiano and co-workers,[23] the thermal decomposition of dicumyl peroxide was achieved in a drop of reactant and AuNPs illuminated with high energy pulsed laser. From the known value of activation energy and rate constant, the temperature of the reaction was estimated to be ~500 ℃. Accordingly, the temperature reached from plasmonic heating was reported to be ~500 ℃. In a subsequent report by Correa-Duarte and co-workers, a reactor comprising AuNPs in a silica shell was reported for [2+4] cycloaddition reaction. Therefore, different classes of thermal transformation can be performed using plasmonic noble metal nanostructures without affecting

their (i) structural integrity and (ii) chemical purity, as they are chemical inert. However, it is worth mentioning here that the direct solar energy utilization for driving thermoplasmonic chemistry is yet to be established, which is under exploration in this area. This present an opportunity where the goal is to achieve lab-to-industrial scale transition towards sustainability in chemical synthesis.
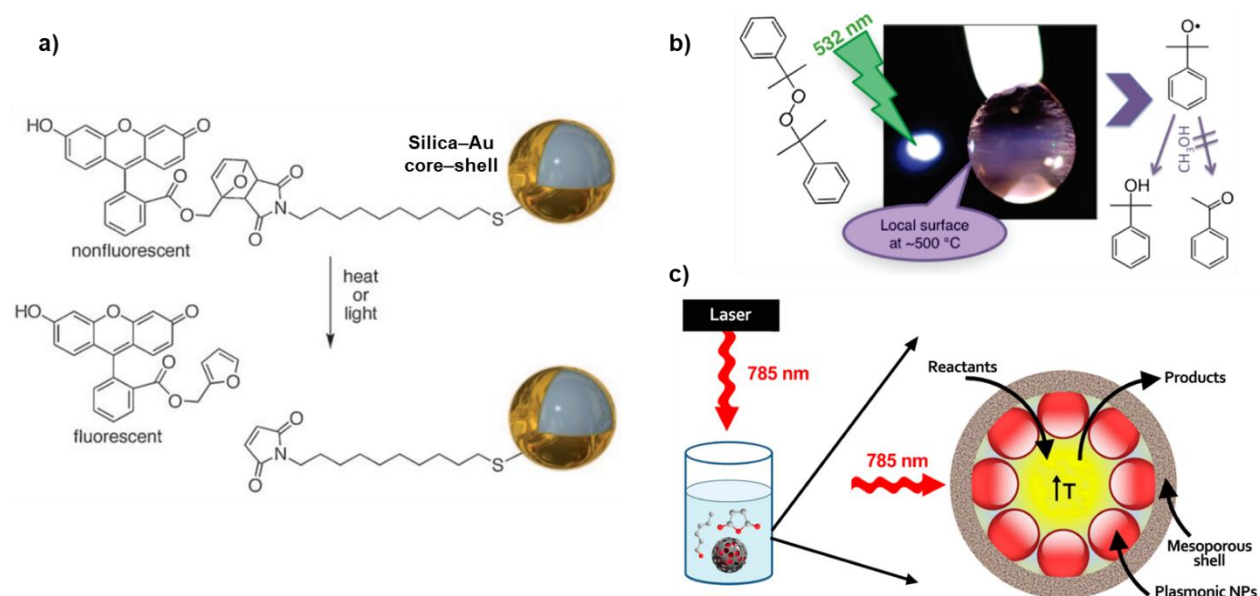
Figure 1.12. Applications of plasmonic heat in performing thermally -driven chemical transformation. (a) Bond dissociation reaction using silica-Au core-shell NP as the plasmonic material. Reproduced with permission from ref 23. Copyright: 2009, Wiley-VCH. (b) Photothermal dissociation of dicumyl peroxide in a drop illuminated with a high energy pulsed laser. AuNPs were used as plasmonic heater and a temperature of 500 ℃ was estimated using the Arrhenius equation. Reproduced with permission from ref 24. Copyright: 2011, American Chemical Society. (c) Plasmonic heat-driven Diels-Alder reaction in a mesoporous shell reactor. Reproduced with permission from ref. 29. Copyright: 2013, American Chemical Society.

1.7. Challenges and opportunities

Thermoplasmonics is a well-matured research field where studies have been done both in fundamental as well as applied perspectives. For example, concerning the fundamental part, the ultrafast carrier dynamics have already been studied which allowed the scientific community to come up with the mechanistic insight of the plasmonic heat generation and dissipation. Despite this, there are several key aspects that still need to be studied to realize the full potential of thermoplasmonics in science, especially in chemistry.

1.7.1. Experimental verification of fundamental studies

As discussed in **Section 1.4**, adequate theoretical studies are available to predict the effect of geometrical and orientational parameters of nanostructures as well as light intensity dependence of plasmonic heating. However, the experimental verification is scarcely reported. This is mainly due to the challenges in measuring the temperature at nanoscale. Having said that, this presents an opportunity in the field where the effect of various parameters on effective plasmonic heat generation can be studied experimentally.

1.7.2. Disentangling thermal effect from hot charge carriers

One of the most debated aspects in plasmon-driven chemistry is deconvoluting the role of hot charge carriers and heat (**Figure 1.13**). It is very important to find out the driving factor of a plasmon-driven chemical transformation to deduce their mechanism, which will be crucial in meeting the desired outcome towards the establishment of plasmonic materials for sustainable chemical synthesis. However, the task is extremely challenging as hot charge carriers and heat are the outcomes of the same ultrafast nonradiative relaxation pathway. It is due to this reason a great attention has been given to the problem.[31-54]
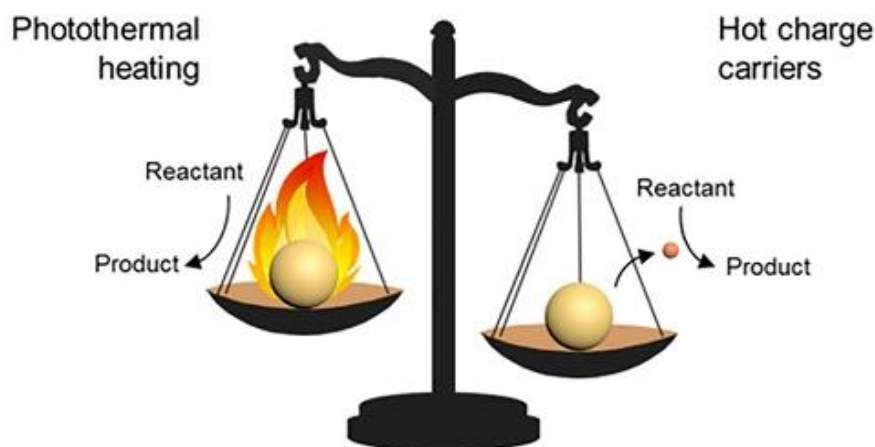
Figure 1.13. An illustration showing the competing role of hot charge carriers and plasmonic heat in a plasmon-driven chemical transformation. Reproduced with permission from ref. 37. Copyright 2018, American Chemical Society.

1.7.3. Quantification of plasmonic heat

Plasmonic heat being a nanoscopic phenomenon poses an inevitable challenge of measurement of temperature, as common thermometers cannot be used due to their spatial resolution. But, the measurement of temperature at nanoscale is extremely important to regulate thermoplasmonic applications. This is very crucial in the case of biomedical applications to avoid damaging healthy cells. This challenge has led to the emergence of a separate research domain named as nanothermometry. Some of the commonly used nanothermometers are listed in **Figure 1.14**.[55-109] Most of these techniques require sophisticated instrumentation facilities and expertise. Therefore, this is an active area of research where the goal is to estimate either accurate or utilizable heat around a plasmonic nanostructure.
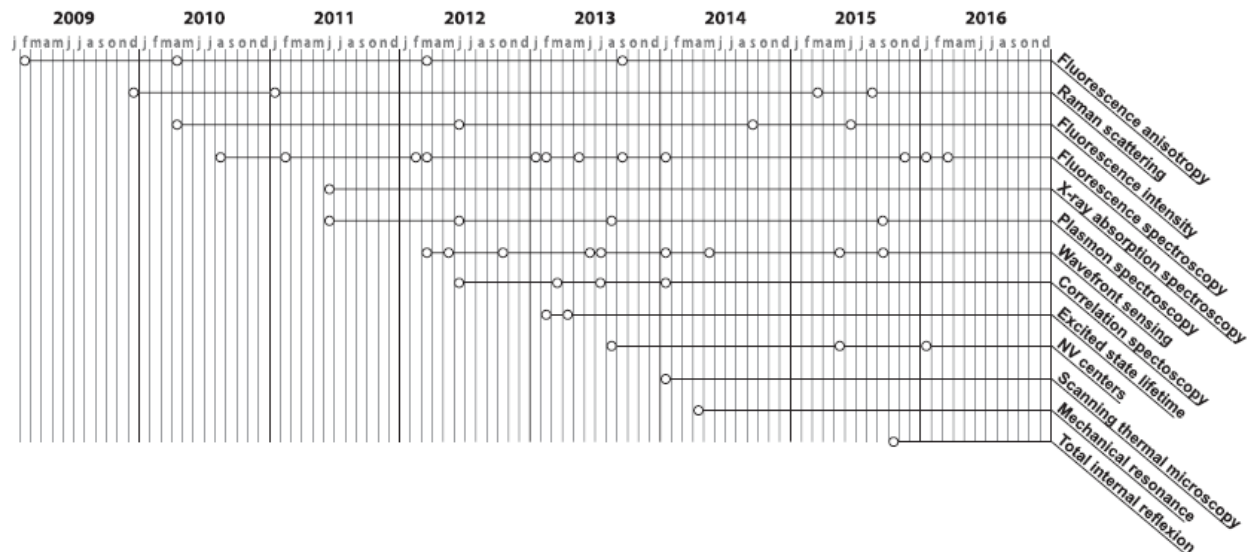
Figure 1.14. Evolution and progress of various nanothermometric techniques. The circles represent the publication, whereas the alphabet at the bottom of each year represent month name. Reproduced with permission from ref. 55. Copyright: 2017, Cambridge University Press.

1.7.4. Applications of plasmonic heat for solar harvesting

Plasmonic nanostructures are promising light-harvesting material due to their high extinction coefficient as well as excellent photostability. Additionally, the existence of plasmonic behavior ranging in visible and near infrared region make them ideal candidate for solar harvesting. Briefly, plasmonic nanomaterials can absorb solar light and convert efficiently into heat. Harnessing the

feature of excellent sunlight-to-heat conversion efficiency by a plasmonic nanomaterial can be a crucial step towards sustainability in energy research. The thermoplasmonic heat can be utilized to (i) drive thermal processes such as chemical transformation, solar vapor generation and desalination, other thermally driven phase changes etc or (ii) can be converted into some universal form of energy such as electricity.

1.8. Motivation and objectives of the thesis

As discussed above, there lies many opportunities and challenges in thermoplasmonics both with respect to fundamental, as well as applied perspectives, which motivated us to enter into the field. For example, the experimental verification of the factors affecting the plasmonic heat generation and dissipation is scarcely discussed. Moreover, the quantification of plasmonic heat with simple and reliable techniques is also a challenging task to achieve. All these information are crucial for establishing the plasmonic material as a sustainable alternative to thermally drive chemical transformations, and this forms the basis of the thesis.

Keeping the above points in mind, the present thesis revolves around thermoplasmonics with the goal of filling the gaps and gaining significant advancement in the area. The thesis is designed to study both the fundamental as well as applied perspectives of plasmonic heating. In the direction of fundamental aspect, we envisage to experimentally study the factors influencing the thermalization such as nanoparticle size shape and assembly. The crucial step towards the goal was an appropriate design of the plasmonic heater, which was successfully achieved by fabricating bundled gold nanorod structure. This was followed by experimentally studying the influence of shape and assembly effects, which was achieved by selecting a thermally driven organic transformation as a proxy for the temperature measurement. The normalization of different materials is crucial in comparing the properties, which was also kept in mind and appropriate normalizations have been adopted throughout different studies.

In the applied direction, our objective was to use the solar-driven plasmonic heater for high temperature reaction in synthetic organic chemistry. Moreover, we were interested in deconvoluting the role of hot carriers from plasmonic heat to perform a sole plasmonic heat driven chemistry. Secondly, our idea was also to develop a simple and cost effective, yet effective, strategy to quantify of temperature-rise caused by the plasmonic heat. Finally, our goal was to use

the plasmonic heaters to convert and store the sunlight in other forms of energy, such as electricity and H₂ fuel.
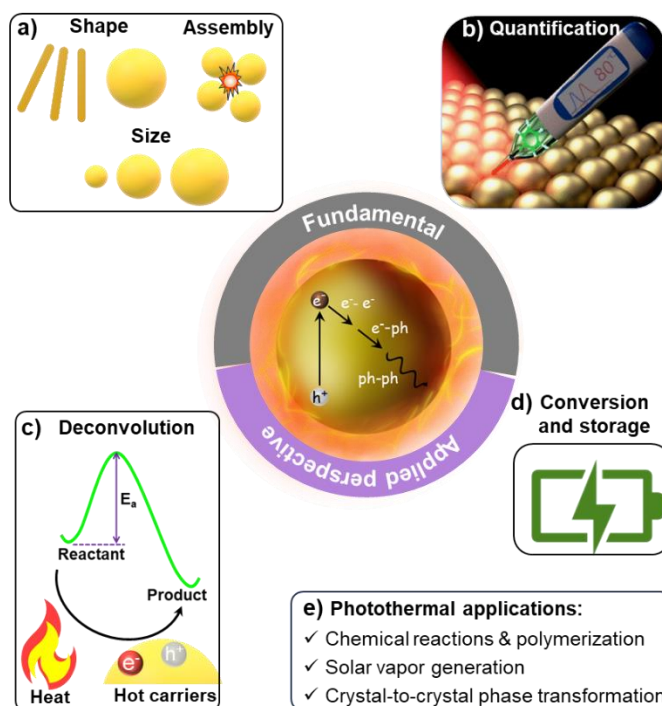
Figure 1.15. A scheme of the overall objective of the thesis, which can be subdivided into two portions: fundamental and applied studies. (a) The effect of nanostructural geometry and arrangement on plasmonic heat generation was studied experimentally. (b) Likewise, efforts were dedicated for developing a simple, yet effective, strategy to quantify the temperature-rise caused by the plasmonic heat. (c) Plasmonic heat was aimed to be used as an alternate thermal energy source for doing high-temperature reactions in synthetic organic chemistry, along with developing strategies to deconvolute the thermal effects from hot charge carriers. (d) The final objective was to use plasmonic heaters to convert and store the sunlight in other forms of energy, such as electricity and H₂ fuel. (e) Throughout the thesis the objective was to effectively utilize plasmonic heat for various photothermal applications. The scheme used in (b) is reproduced with permission from ref. 109. Copyright: 2018, American Chemical Society.

1.8.1. Brief overview of the Chapters

The current thesis is subdivided into five chapters followed, by conclusions and future directions. After the present discussion of the field thermoplasmonics as a part of the first Chapter. the second Chapter discusses the role of nanoparticle shape as well as assembly on the generation and dissipation of plasmonic heat. Additionally, the plasmonic heat was utilized for various thermally driven transformations such as PDMS polymerization, solar vapor generation, and crystal-to-

crystal phase transformation. The yield of photothermally driven Diels-Alder reaction was used as a proxy to monitor the effect of NP shape and assembly effect on the generation and dissipation of plasmonic heat. Insights into thermal dissipation was also discussed, which was largely dependent on the surrounding medium.

In Chapter four, the plasmonic heat was quantified using a novel irreversible thermochromism technique. The measured temperature was verified with three independent techniques, such as (i) melting point measurement, (ii) Raman spectroscopy, and (iii) infra-red-based thermometric imaging studies. The next Chapter discusses the utilization of plasmonic heat for high-temperature reactions in synthetic organic chemistry, namely Claisen rearrangement. A thermodynamically closed reactor setup was designed to physically separate the plasmonic heater from the reaction mixture, which enabled the sole plasmonic heat-driven chemical transformation.

In Chapter five, the prospect of conversion and storage of plasmonic heat is discussed. The solar energy has been converted into electricity using plasmon-powered solar thermoelectric generator. The solar-to-electricity conversion efficiency was found to be 9.6% under ambient conditions using plasmonic gold nanoparticles as the solar absorber. Further, the electrical outputs from plasmon-powered solar thermoelectric generator was used as a proxy to study the effect of size on plasmonic heat generation and dissipation. Finally, the electricity generated was stored as chemical energy in the form of hydrogen via electrolysis of water.

1.8. References

(1)   Brongersma, M. L.; Halas, N. J.; Nordlander, P. Plasmon-Induced Hot Carrier Science and Technology. *Nat. Nanotechnol.* **2015**, *10*, 25– 34.

(2)   Govorov, A. O.; Richardson, H. H. Generating Heat with Metal Nanoparticles. *Nano Today* **2007**, *2*, 30– 38.

(3)   Govorov, A. O.; Zhang, W.; Skeini, T.; Richardson, H.; Lee, J.; Kotov, N. A. Gold Nanoparticle Ensembles as Heaters and Actuators: Melting and Collective Plasmon Resonances. *Nanoscale Res. Lett.* **2006**, *1*, 84– 90.

(4)   Hüttmann, G.; Birngruber, R. On the Possibility of High-Precision Photothermal Microeffects and the Measurement of Fast Thermal Denaturation of Proteins. *IEEE J. Sel. Top. Quant.* **1999**, *5*, 954–962.

(5)   Boyer, D.; Tamarat, P.; Maali, A.; Lounis, B.; Orrit, M. Photothermal Imaging of Nanometer-Sized Metal Particles Among Scatterers. *Science* **2002**, *297*, 1160.

(6)   Hirsch, L. R.; Stafford, R. J.; Bankson, J. A.; Sershen, S. R.; Rivera, B.; Price, R. E.; Hazle, J. D.; Halas, N. J.; West, J. L. Nanoshell-Mediated Near-Infrared Thermal Therapy of Tumors under Magnetic Resonance Guidance. *Proc. Natl. Acad. Sci. U.S.A.* **2003**, *100*, 13549–13554.

(7)   Huang, X.; El-Sayed, I. H.; Qian, W.; El-Sayed, M. A. Cancer Cell Imaging and Photothermal Therapy in the Near-Infrared Region by Using Gold Nanorods. *J. Am. Chem. Soc.* **2006**, *128*, 2115-2120.

(8)   Jiang, X.; Du, B.; Huang, Y.; Yu, M.; Zheng, J. Cancer Photothermal Therapy with ICG-Conjugated Gold Nanoclusters. *Bioconjugate Chem.* **2020**, *31*, 1522– 1528.

(9)   Adleman, J. R.; Boyd, D. A.; Goodwin, D. G.; Psaltis, D. Heterogenous Catalysis Mediated by Plasmon Heating. *Nano Lett.* **2009**, *9*, 4417–4423.

(10)   Agarwal, A.; Huang, S. W.; O'Donnell, M.; Day, K. C.; Day, M.; Kotov, N.; Ashkenazi, S. Targeted Gold Nanorod Contrast Agent for Prostate Cancer Detection by Photoacoustic Imaging. *J. Appl. Phys.* **2007**, *102*, 064701.

(11)   Baffou, G.; Quidant, R. Nanoplasmonics for Chemistry. *Chem. Soc. Rev.* **2014**, *43*, 3898–3907.

(12)   Boisselier, E.; Astruc, D. Gold Nanoparticles in Nanomedicine: Preparations, Imaging, Diagnostics, Therapies and Toxicity. *Chem. Soc. Rev.* **2009**, *38*, 1759–1782.

(13)   Cao, L.; Barsic, D. N.; Guichard, A. R.; Brongersma, M. L. Plasmon-Assisted Local Temperature Control to Pattern Individual Semiconductor Nanowires and Carbon Nanotubes. *Nano Lett.* **2007**, *7*, 3523– 3527.

(14)   Hung, W. H.; Aykol, M.; Valley, D.; Hou, W. B.; Cronin, S. B. Plasmon Resonant Enhancement of Carbon Monoxide Catalysis. *Nano Lett.* **2010**, *10*, 1314– 1318.

(15)   Boyd, D. A.; Greengard, L.; Brongersma, M.; El-Naggar,M. Y.; Goodwin, D. G. Plasmon-Assisted Chemical Vapor Deposition. *Nano Lett.* **2006**, *6*, 2592–2597.

(16)   Carregal-Romero, S.; Ochs, M.; Rivera-Gil, P.; Ganas, C.; Pavlov, A. M.; Sukhorukov, G. B.; Parak, W. J. NIR-Light Triggered Delivery of Macromolecules into the Cytosol. *J. Control. Release* **2012**, *159*, 120–127.

(17)   Chen, X.; Zhu, H. Y.; Zhao, J. C.; Zheng, Z. F.; Gao, X. P. Visible-Light-Driven Oxidation of Organic Contaminants in Air with Gold Nanoparticle Catalysts on Oxide Supports. *Angew. Chem. Int. Ed.* **2008**, *47*, 5353–5356.

(18)   Ding, T. X.; Hou, L.; van der Meer, H.; Alivisatos, A. P.; Orrit, M. Hundreds-fold Sensitivity Enhancement of Photothermal Microscopy in Near-Critical Xenon. *J. Phys. Chem. Lett.* **2016**, *7*, 2524–2529.

(19)   Doane, T. L.; Burda, C. The Unique Role of Nanoparticles in Nanomedicine: Imaging, Drug Delivery and Therapy. *Chem. Soc. Rev.* **2012**, *41*, 2885–2911.

(20)   Kim, M.; Lee, J. H.; Nam, J. M. Plasmonic Photothermal Nanoparticles for Biomedical Applications. *Adv. Sci.* **2019**, *6*, 1900471.

(21)   Dou, Y.; Zhigilei, L. V.; Winograd, N.; Garrison, B. J. Explosive Boiling of Water Films Adjacent to Heated Surfaces: A Microscopic Description. *J. Phys. Chem. A* **2001**, *105*, 2748–2755.

(22)   Zhou, L.; Tan, Y.; Wang, J.; Xu, W.; Yuan, Y.; Cai, W.; Zhu, S.; Zhu, J. 3D Self-Assembly of Aluminium Nanoparticles for Plasmon-Enhanced Solar Desalination. *Nat. Photonics* **2016**, *10*, 393– 398.

(23)   Bakhtiari, A. B. S.; Hsiao, D.; Jin, G.; Gates, B. D.; Branda, N. R. An Efficient Method Based on The Photothermal Effect for The Release Of Molecules From Metal Nanoparticle Surfaces. *Angew. Chem. Int. Ed.* **2009**, *48*, 4166– 4169.

(24)   Fasciani, C.; Bueno Alejo, C. J.; Grenier, M.; Netto-Ferreira, J. C.; Scaiano, J. C. High-Temperature Organic Reactions at Room Temperature Using Plasmon Excitation: Decomposition of Dicumyl Peroxide. *Org. Lett.* **2011**, *2*, 204–207.

(25)   Hrelescu, C.; Stehr, L.; Ringler, M.; Sperling, R. A.; Parak, W. J.; Klar, T. A.; Feldmann, J. DNA Melting in Gold Nanostove Clusters. *J. Phys. Chem. C* **2010**, *114*, 7401–7411.

(26)   Ni, W.; Ba, H.; Lutich, A. A.; Jäckel, F.; Feldmann, J. Enhancing Single-Nanoparticle Surface-Chemistry by Plasmonic Overheating in an Optical Trap. *Nano Lett.* **2012**, *12*, 4647–4650.

(27)   Robert, H.; Kundrat, F.; Bermúdez Ureña, E.; Rigneault, H.; Monneret, S.; Quidant, R.; Polleux, J.; Baffou, G. Light-Assisted Solvothermal Chemistry Using Plasmonic Nanoparticles. *ACS Omega* **2016**, *1*, 2–8.

(28)   Urban, A. S.; Fedoruk, M.; Horton, M. R.; Rädler, J. O.; Stefani, F. D.; Feldmann, J. Controlled Nanometric Phase Transitions of Phospholipid Membranes by Plasmonic Heating of Single Gold Nanoparticles. *Nano Lett.* **2009**, *9*, 2903–2908.

(29)   Vásquez Vásquez, C.; Vaz, B.; Giannini, V.; Pérez-Lorenzo, M.; Alvarez-Puebla, R. A.; Correa-Duarte, M. A. Nanoreactors for Simultaneous Remote Thermal Activation and Optical Monitoring of Chemical Reactions. *J. Am. Chem. Soc.* **2013**, *135*, 13616–13619.

(30)   Lalisse, A.; Tessier, G.; Plain, J.; Baffou, G. Quantifying the Efficiency of Plasmonic Materials for Near-Field Enhancement and Photothermal Conversion. *J. Phys. Chem. C* **2015**, *119*, 25518– 25528.

(31) Yen, C.-W.; El-Sayed, M. A. Plasmonic Field Effect on the Hexacyanoferrate (III)-Thiosulfate Electron Transfer Catalytic Reaction on Gold Nanoparticles: Electromagnetic or Thermal? J. Phys. Chem. C **2009**, 113, 19585– 19590.

(32) Bora, T.; Zoepfl, D.; Dutta, J. Importance of plasmonic heating on visible light driven photocatalysis of gold nanoparticle decorated zinc oxide nanorods. *Sci. Rep.* **2016**, *6*, 26913.

(33) Li, K.; Hogan, N. J.; Kale, M. J.; Halas, N. J.; Nordlander, P.; Christopher, P. Balancing Near-Field Enhancement, Absorption, and Scattering for Effective Antenna-Reactor Plasmonic Photocatalysis. *Nano Lett.* **2017**, *17*, 3710– 3717.

(34) Dubi, Y.; Sivan, Y. "Hot" Electrons in Metallic Nanostructures—Non-Thermal Carriers or Heating?. *Light: Sci. Appl.* **2019**, *8*, 89.

(35) Sivan, Y.; Un, I. W.; Dubi, Y. Assistance of Metal Nanoparticles in Photocatalysis - Nothing More than a Classical Heat Source. *Faraday Discuss.* **2019**, *214*, 215– 233.

(36) Zhou, L.; Swearer, D. F.; Zhang, C.; Robatjazi, H.; Zhao, H.; Henderson, L.; Dong, L.; Christopher, P.; Carter, E. A.; Nordlander, P. Quantifying Hot Carrier and Thermal Contributions in Plasmonic Photocatalysis. *Science* **2018**, *362*, 69– 72.

(37) Kamarudheen, R.; Castellanos, G. W.; Kamp, L. P. J.; Clercx, H. J. H.; Baldi, A. Quantifying Photothermal and Hot Charge Carrier Effects in Plasmon-Driven Nanoparticle Syntheses. *ACS Nano* **2018**, *12*, 8447– 8455.

(38) Zhang, X.; Li, X.; Reish, M. E.; Zhang, D.; Su, N. Q.; Gutiérrez, Y.; Moreno, F.; Yang, W.; Everitt, H. O.; Liu, J. Plasmon-Enhanced Catalysis: Distinguishing Thermal and Nonthermal Effects. *Nano Lett.* **2018**, *18*, 1714– 1723.

(39) Keller, E. L.; Frontiera, R. R. Ultrafast Nanoscale Raman Thermometry Proves Heating is Not a Primary Mechanism for Plasmon-Driven Photocatalysis. *ACS Nano* **2018**, *12*, 5848– 5855.

(40) Yu, Y.; Sundaresan, V.; Willets, K. A. Hot carriers versus thermal effects: Resolving the enhancement mechanisms for plasmon-mediated photoelectrochemical reactions. *J. Phys. Chem. C* **2018**, *122*, 5040– 5048.

(41) Dubi, Y.; Un, I. W.; Sivan, Y. Thermal Effects - An Alternative Mechanism for Plasmon-Assisted Photocatalysis. *Chem. Sci.* **2020**, *11*, 5017– 5027.

(42) Maley, M.; Hill, J. W.; Saha, P.; Walmsley, J. D.; Hill, C. M. The Role of Heating in the Electrochemical Response of Plasmonic Nanostructures under Illumination. *J. Phys. Chem. C* **2019**, *123*, 12390– 12399.

(43) Zhan, C.; Liu, B. W.; Huang, Y. F.; Hu, S.; Ren, B.; Moskovits, M.; Tian, Z. Q. Disentangling Charge Carrier from Photothermal Effects in Plasmonic Metal Nanostructures. *Nat. Commun.* **2019**, *10*, 2671.

(44) Sivan, Y.; Baraban, J.; Un, I.; Dubi, Y. Comment on "Quantifying Hot Carrier And Thermal Contributions in Plasmonic Photocatalysis". *Science* **2019**, *364,* eaaw9367.

(45) Zhou, L.; Swearer, D. F.; Robatjazi, H.; Alabastri, A.; Christopher, P.; Carter, E. A.; Nordlander, P.; Halas, N. J. Response on Comment to "Quantifying Hot Carrier and Thermal Contributions in Plasmonic Photocatalysis. *Science* **2019**, *364*, 69– 72.

(46) Sivan, Y.; Baraban, J.; Dubi, Y. Eppur Si Riscalda – And yet, it (Just) Heats Up: Further Comments On "Quantifying Hot Carrier and Thermal Contributions in Plasmonic Photocatalysis. Preprint at https://arxiv.org/abs/1907.04773 (2019).

(47) Sarhan, R. M.; Koopman, W.; Schuetz, R.; Schmid, T.; Liebig, F.; Koetz, J.; Bargheer, M. The Importance of Plasmonic Heating for the Plasmon-Driven Photodimerization of 4-Nitrothiophenol. *Sci. Rep.* **2019**, *9*, 3060.

(48) Li, X.; Everitt, O. H.; Liu, J. Confirming Nonthermal Plasmonic Effects Enhance CO_2 Methanation on Rh/TiO_2 Catalysts. *Nano Res.* **2019**, *12*, 1906– 1911.

(49) Jain, P. K. Taking the Heat off of Plasmonic Chemistry. *J. Phys. Chem. C* **2019**, *123*, 24347– 24351.

(50) Zhang, Q.; Zhou, Y.; Fu, X.; Villarreal, E.; Sun, L.; Zou, S.; Wang, H. Photothermal Effect, Local Field Dependence, and Charge Carrier Relaying Species in Plasmon-Driven Photocatalysis: A Case Study of Aerobic Nitrothiophenol Coupling Reaction. *J. Phys. Chem. C* **2019**, *123*, 26695– 26704.

(51) Rodio, M.; Graf, M.; Schulz, F.; Mueller, N. S.; Eich, M.; Lange, H. Experimental Evidence for Nonthermal Contributions to Plasmon-Enhanced Electrochemical Oxidation Reactions. *ACS Catal.* **2020**, *10*, 2345– 2353.

(52) Ou, W.; Zhou, B.; Shen, J.; Lo, T. W.; Lei, D.; Li, S.; Zhong, J.; Li, Y. Y.; Lu, J. Thermal and nonthermal effects in plasmon-mediated electrochemistry at nanostructured Ag electrodes. *Angew. Chem. Int. Ed.* **2020**, *59*, 6790– 6793.

(53) Schorr, N. B.; Counihan, M. J.; Bhargava, R.; Rodríguez-López, J. Impact of Plasmonic Photothermal Effects on the Reactivity of Au Nanoparticle Modified Graphene Electrodes Visualized Using Scanning Electrochemical Microscopy. *Anal. Chem.* **2020**, *92* (5), 3666– 3673.

(54) Sivan, Y.; Baraban, J. H.; Dubi, Y. Experimental practices required to isolate thermal effects in plasmonic photo-catalysis: lessons from recent experiments. *OSA Continuum* **2020**, *3*, 483.

(55) Baffou, G. *Thermoplasmonics: Heating Metal Nanoparticles Using Light*, 1st ed.; Cambridge University Press, 2017.

(56)   Acosta, V. M.; Bauch, E.; Ledbetter, M. P.; Waxman, A.; Bouchard, L. S.; Budker, D. Temperature Dependence of The Nitrogen-Vacancy Magnetic Resonance In Diamond. *Phys. Rev. Lett.* **2010**, *104*, 1– 4.

(57)   Baffou, G.; Kreuzer, M. P.; Kulzer, F.; Quidant, R. Temperature Mapping Near Plasmonic Nanostructures Using Fluorescence Polarization Anisotropy. *Opt. Express* **2009**, *17*, 3291– 3298.

(58)   Baffou, G.; Girard, C.; Quidant, R. Mapping Heat Origin in Plasmonic Structures. *Phys. Rev. Lett.* **2010**, *104*, 136805.

(59)   Baffou, G.; Bon, P.; Savatier, J.; Polleux, J.; Zhu, M.; Merlin, M.; Rigneault, H.; Monneret, S. Thermal Imaging Of Nanostructures By Quantitative Optical Phase Analysis. *ACS Nano* **2012**, *6*, 2452– 2458.

(60)   Baral, S.; Johnson, S. C.; Alaulamie, A. A.; Richardson, H. H. Nanothermometry Using Optically Trapped Erbium Oxide Nanoparticle. *Appl. Phys. A: Mater. Sci. Process.* **2016**, *122*, 340.

(61)   Bendix, P. M.; Reihani, S. N.; Oddershede, L. B. Direct Measurements of Heating By Electromagnetically Trapped Gold Nanoparticles On Supported Lipid Bilayers. *ACS Nano* **2010**, *4*, 2256– 2262.

(62)   Carlson, M. T.; Khan, A.; Richardson, H. H. Local Temperature Determination of Optically Excited Nanoparticles and Nanodots. *Nano Lett.* **2011**, *11*, 1061– 1069.

(63)   Chen, Z.; Shan, X.; Guan, Y.; Wang, S.; Zhu, J.-J.; Tao, N. Imaging Local Heating and Thermal Diffusion of Nanomaterials with Plasmonic Thermal Microscopy. ACS Nano **2015**, 9, 11574– 11581.

(64)   Chiu, M. J.; Chu, L. K. Quantifying the Photothermal Efficiency of Gold Nanoparticles Using Tryptophan as an *in Situ* Fluorescent Thermometer. *Phys. Chem. Chem. Phys.* **2015**, *17*, 17090– 17100.

(65)   Clarke, M. L.; Chou, S. G.; Hwang, J. Monitoring Photothermally Excited Nanoparticles via Multimodal Microscopy. *J. Phys. Chem. Lett.* **2010**, *1*, 1743– 1748.

(66)   Coppens, Z. J.; Li, W.; Walker, D. G.; Valentine, J. G. Probing and Controlling Photothermal Heat Generation in Plasmonic Nanostructures. *Nano Lett.* **2013**, *13*, 1023– 1028.

(67)   Debasu, M. L.; Ananias, D.; Pastoriza-Santos, I.; Liz-Marzán, L. M.; Rocha, J.; Carlos, L. D. All-In-One Optical Heater-Thermometer Nanoplatform Operative From 300 to 2000 K Based on Er^{3+} Emission and Blackbody Radiation. *Adv. Mater.* **2013**, *25*, 4868– 4874.

(68)   Desiatov, B.; Goykhman, I.; Levy, U. Direct Temperature Mapping of Nanoscale Plasmonic Devices. *Nano Lett.* **2014**, *14*, 648– 652.

(69) Donner, J. S.; Thompson, S. A.; Alonso-Ortega, C.; Morales, J.; Rico, L. G.; Santos, S. I. C. O.; Quidant, R. Imaging of Plasmonic Heating in a Living Organism. *ACS Nano* **2013**, *7*, 8666– 8672.

(70) Donner, J. S.; Thompson, S. A.; Kreuzer, M. P.; Baffou, G.; Quidant, R. Mapping Intracellular Temperature Using Green Fluorescent Protein. *Nano Lett.* **2012**, *12* (4), 2107– 2111.

(71) Ebrahimi, S.; Akhlaghi, Y.; Kompany-Zareh, M.; Rinnan, Å. Nucleic Acid Based Fluorescent Nanothermometers. *ACS Nano* **2014**, *8*, 10372– 10382.

(72) Freddi, S.; Sironi, L.; D'Antuono, R.; Morone, D.; Dona, A.; Cabrini, E.; D'Alfonso, L.; Collini, M.; Pallavicini, P.; Baldi, G.; Maggioni, D.; Chirico, G. A Molecular Thermometer for Nanoparticles for Optical Hyperthermia. *Nano Lett.* **2013**, *13*, 2004– 2010.

(73) Gomès, S.; Assy, A.; Chapuis, P. O. Scanning Thermal Microscopy: A review. *Phys. Status Solidi A* **2015**, *212*, 477–494.

(74) Hao Vu, X.; Levy, M.; Barroca, T.; Nhung Tran, H.; Fort, E. Gold Nanocrescents for Remotely Measuring and Controlling Local Temperature. *Nanotechnology* **2013**, *24*, 325501.

(75) Herzog, J. B.; Knight, M. W.; Natelson, D. Thermoplasmonics: Quantifying Plasmonic Heating in Single Nanowires. *Nano Lett.* **2014**, *14*, 499–503.

(76) Honda, M.; Saito, Y.; Smith, N. I.; Fujita, K.; Kawata, S. Nanoscale Heating of Laser Irradiated Single Gold Nanoparticles in Liquid. *Opt. Express* **2011**, *19*, 12375–12383.

(77) Hormeño, S.; Gregorio-Godoy, P.; Pérez-Juste, J.; Liz-Marzán, L. M.; Juárez, B. H.; Arias-Gonzalez, J. R. Laser Heating Tunability by Off-Resonant Irradiation of Gold Nanoparticles. *Small* **2014**, *10*, 376–384.

(78) Ito, S.; Sugiyama, T.; Toitani, N.; Katayama, G.; Miyasaka, H. Application of Fluorescence Correlation Spectroscopy to the Measurement of Local Temperature in Solutions under Optical Trapping Condition. *J. Phys. Chem. B* **2007**, *111*, 2365.

(79) Jaque, D.; Vetrone, F. Luminescence Thermometry. *Nanoscale* **2012**, *4*, 4301–4326.

(80) Jaque, D.; Maestro, L. M.; Escudero, E.; Martín Rodriguez, E.; Capobianco, J. A.; Vetrone, F.; Juarranz de la Fuente, A.; Sanz-Rodríguez, F.; Iglesias-de la Cruz, M. C.; Jacinto, C.; Rocha, U.; García Solé, J. Fluorescent Nano-Particles for Multi-Photon Thermal Sensing. *J. Luminescence* **2013**, *133*, 249–253.

(81) Jonsson, G. E.; Milijkovic, V.; Dmitriev, A. Nanoplasmon-Enabled Macroscopic Thermal Management. *Sci. Rep.* **2014**, *4*, 5111.

(82)   Kim, K.; Chung, J.; Hwang, G.; Kwon, O.; Sik Lee, J. Quantitative Measurement with Scanning Thermal Microscope by Preventing Preventing the Distortion Due to the Heat Transfer through the Air. *ACS Nano* **2011**, *5*, 8700–8709.

(83)   Kinkhabwala, A. A.; Staffaroni, M.; Suze, O.; Burgos, S. Nanoscale Thermal Mapping of HAMR Heads Using Polymer Imprint Thermal Mapping. *IEEE Trans. Magn.* **2016**, *52*, 1.

(84)   Ma, H.; Bendix, P. M.; Oddershede, L. B. Large-Scale Orientation Dependent Heating from a Single Irradiated Gold Nanorod. *Nano Lett.* **2012**, *12*, 3954–3960.

(85)   Maestro, L. M.; Haro-González, P.; Coello, J. G.; Jaque, D. Absorption Efficiency of Gold Nanorods Determined by Quantum Dot Fluorescence Thermometry. *Appl. Phys. Lett.* **2012**, *100*, 201110.

(86)   Pacardo, D. B.; Neupane, B.;Wang, G.; Gu, Z.;Walker, G. M.; Ligler, F. S. A Temperature Microsensor for Measuring Laser-Induced Heating in Gold Nanorods. *Anal. Bioanal. Chem.* **2015**, *407*, 719–725.

(87)   Petriashvili, G.; De Santo, M. P.; Chubinidze, K.; Hamdi, R.; Barberi, R. Visual Micro-Thermometers for Nanoparticles Photo-Thermal Conversion. *Opt. Express* **2014**, *22*, 14705–14711.

(88)   Plakhotnik, T.; Gruber, D. Luminescence of Nitrogen-Vacancy Centers in Nanodiamonds at Temperatures between 300 and 700 K: Perspectives on Nanothermometry. *Phys. Chem. Chem. Phys.* **2010**, *12*, 9751–9756.

(89)   Pozzi, E. A.; Zrimsek, A. B.; Lethiec, C. M.; Schatz, G. C.; Hersam, M. C.; Van Duyne, P. 2015. Evaluating Single-Molecule Stokes and Anti-Stokes SERS for Nanoscale Thermometry. *J. Phys. Chem. C*, **119**, 21116–21124.

(90)   Rocha, U.; Jacinto da Silva, C.; Ferreira Silva, W.; Guedes, I.; Benayas, A.; Martínez Maestro, L.; Acosta, Elias, M.; Bovero, E.; van Veggel, F. C. J. M.; Garcí Solé, J. A.; Jaque, D. Thermal Sensing Based on Neodymium-Doped LaF$_3$ Nanoparticles. *ACS Nano* **2013**, *7*, 1188–1199.

(91)   Rodríguez-Sevilla, P.; Zhang, Y.; Haro-González, P.; Sanz-Rodríguez, F.; Jaque, F.;García Solé, J.; Liu, X.; Jaque, D. Thermal Scanning at the Cellular Level by an Optically Trapped Upconverting Fluorescent Particle. *Adv. Mater.* **2016**, *28*, 2421–2426.

(92)   Rohani, S.; Quintanilla, M.; Tuccio, S.; De Angelis, F.; Cantelar, E.; Govorov, A. O.; Razzari, L.; Vetrone, F. Enhanced Luminescence, Collective Heating, and Nanothermometry in an Ensemble System Composed of Lanthanide-Doped Upconverting Nanoparticles and Gold Nanorods. *Adv. Opt. Mater.* **2015**, *3*, 1606–1613.

(93)   Rycenga, M.; Wang, Z.; Gordon, E.; Cobley, C. M.; Schwartz, A. G.; Lo, C. S.; Xia, Y. Probing the Photothermal Effect of Gold-Based Nanocages with Surface-Enhanced Raman Scattering (SERS). *Angew. Chem. Int. Ed.* **2009**, *48*, 9924–9927.

(94)   Savchuk, O. A.; Carvajal, J. J.; Pujol, M. C.; Barrera,W.; Massons, J.; Aguilo, M.; Diaz, F. Ho,Yb:KLu(WO$_4$)$_2$ Nanoparticles: A Versatile Material for Multiple Thermal Sensing Purposes by Luminescent Thermometry. *J. Phys. Chem. C* **2015**, *119*, 18546–18558.

(95)   Schiebener, P.; Straub, J.; Levelt Sengers, J. M. H.; Gallagher, J. S. Refractive Index of Water and Steam as Function of Wavelength, Temperture and Density. *J. Phys. Chem. Ref. Data* **1990**, *19*, 677.

(96)   Schmid, S.;Wu, K.; Larsen, P. E.; Rindzevicius, T.; Boisen, A. Low-Power Photothermal Probing of Single Plasmonic Nanostructures with Nanomechanical String Resonators. *Nano Lett.* **2014**, *14*, 2318–2321.

(97)   Setoura, K.; Werner, D.; Hashimoto, S. Optical Scattering Spectral Thermometry and Refractometry of a Single Gold Nanoparticle under CW Laser Excitation. *J. Phys. Chem. C* **2012**, *116*, 15458–15466.

(98)   Setoura, K.; Okada, Y.; Werner, D.; Hashimoto, S. Observation of Nanoscale Cooling Effects by Substrates and the Surrounding Media for Single Gold Nanoparticles under CW-Laser Illumination. *ACS Nano* **2013**, *7*, 7874–7885.

(99)   Tetienne, J. P.; A.; Lombard, Simpson, D. A.; Ritchie, C.; Lu, J.; Mulvaney, P.; Hollenberg, C. L. Scanning Nanospin Ensemble Microscope for Nanoscale Magnetic and Thermal Imaging. *Nano Lett.* **2016**, *16*, 326–333.

(100)   Toshimitsu, M.; Matsumura, Y.; Shoji, T.; Kitamura, N.; Takase, M.; Murakoshi, K.; Yamauchi, H.; Ito, S.; Miyasaka, H.; Nobuhiro, A.; Mizumoto, Y.; Ishihara, H.; Tsuboi, Y. Metallic-Nanostructure-Enhanced Optical Trapping of Flexible Polymer Chains in Aqueous Solution as Revealed by Confocal Fluorescence Microspectroscopy. *J. Phys. Chem. C* **2012**, *116*, 14610–14618.

(101)   Yamauchi, H.; Ito, S.; Yoshida, K.; Itoh, T.; Tsuboi, Y.; Kitamura, N.; Miyasaka, H. Temperature near Gold Nanoprticles under Phtotexcitation: Evaluation Using a Fluorescence Correlation Technique. *J. Phys. Chem. C* **2013**, *117*, 8388–8396.

(102)   Van de Broek, B.; Grandjean, D.; Trekker, J.; Ye, J.; Verstreken, K.; Maes, G.; Borghs, G.; Nikitenko, S.; Lagae, L.; Bartic, C.; Temst, K.; Van Bael, M. J. Temperature Determination of Resonantly Excited Plasmonic Branched Gold Nanoparticles by X-Ray Absorption Spectroscopy. *Small* **2011**, *7*, 2498–2506.

(103)   Velghe, S.; Primot, J.; Guérineau, N.; Cohen, M.; Wattellier, B. Wavefront Reconstruction from Multidirectional Phase Derivatives Generated by Multilateral Shearing Interferometers. *Opt. Lett.* **2005**, *30*, 245–247.

(104)   Vetrone, F.; Naccache, R.; Zamarrón, A.; Juarranz de la Fuente, A.; Sanz-Rodríguez, F.; Martinez Maestro, L.; Martín Rodriguez, E.; Jaque, D.; García Solé, J.;, Capobianco, J. A. Temperature Sensing Using Fluorescent Nanothermometers. *ACS Nano* **2010**, *4*, 3254.

(105) Šiler, M.; Ježek, J.; Jákl, P.; Zdeněk, P.; Zemánek, P. Direct Measurement of the Temperature Profile Close to an Optically Trapped Absorbing Particle. *Opt. Lett.* **2016**, *41*, 870–873.

(106) Xie, X.; Cahill, D. G. Thermometry of Plasmonic Nanostructures by Anti-Stokes Electronic Raman Scattering. *Appl. Phys. Lett.* **2016**, *109*, 183104.

(107) Yashchenok, A.; Masic, A.; Gorin, D.; Inozemtseva, O.; Sup Shim, B.; Kotov, N.; Skirtach, A.; Möhwald, H. Optical Heating and Temperature Determination of Core–Shell Gold Nanoparticles and Single-Walled Carbon Nanotube Microparticles. *Small* **2015**, *11*, 1320–1327.

(108) Yokota, Y.; Ueno, K.; Misawa, H. Highly Controlled Surface-Ehnaced Raman Scattering Chips using Nanoengineered Gold Blocks. *Small* **2011**, *2*, 252–258.

(109) Hu, S.; Liu, B.-J.; Feng, J.-M.; Zong, C.; Lin, K.-Q.; Wang, X.; Wu, D.-Y.; Ren, B. Quantifying Surface Temperature of Thermoplasmonic Nanostructures. *J. Am. Chem. Soc.* **2018**, *140*, 13680– 13686.

Chapter – 2

Effect of Shape and Configuration on Generation of Plasmonic Heat in Gold Nanostructures
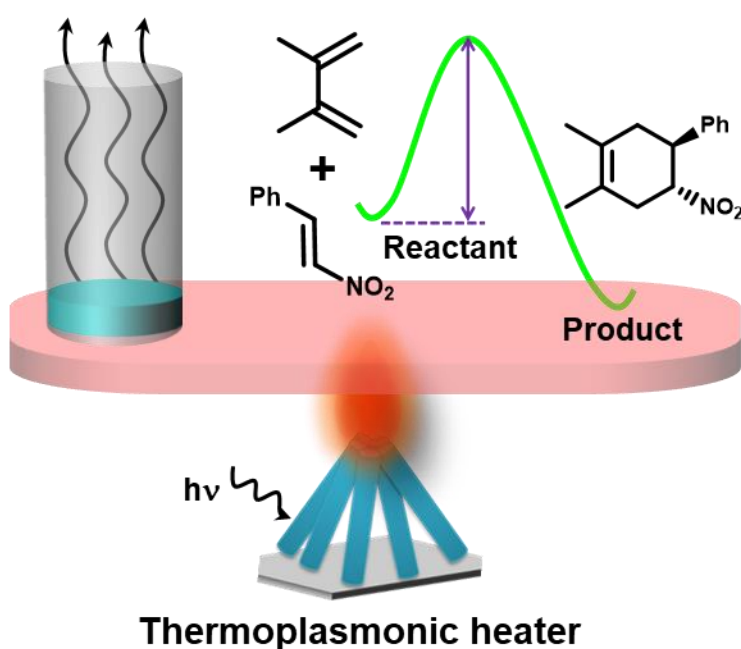
This chapter has been adapted from the following paper. Copyright 2022, American Chemical Society:

2.1. Abstract

A plasmonic material is a hub of many intriguing processes that often compete with each other while performing a function. Doing chemistry with plasmons is rewarding but is often challenged by the competition between the intriguing relaxation processes in plasmonic materials. One of the currently debated and prominent examples of this is the interference of the thermalization process in bringing out different physicochemical transformations. A thoughtful use of nanostructured materials as well as reaction conditions is crucial in minimizing the interference between the different plasmonic processes. This chapter deals here the fabrication design of an ideal thermoplasmonic heater based on gold nanorods and its broad range of application. We present here insights into the utilization of thermoplasmonic properties in configurable arrays of gold nanorods (AuNRs), which will help in accomplishing the desired outcome from the thermalization process. The plasmonic heat generated in AuNR arrays is used to perform versatile and useful photothermal processes, such as polymerization, solar-vapor generation, and Diels–Alder reaction. Also, we have tried to explore the effect of shape and configuration of gold nanostructures on the generation and dissipation of plasmonic heat. The solar vapor generation studies revealed that the efficiency of bundled AuNR-based thermoplasmonic heater is ~93% which is one of the best reported so far in the literature using plasmonic materials. Thus the bundled AuNR arrays developed by us possess strong thermoplasmonic properties to act as an efficient heating platform for future photothermal applications. The insights provided here will have far-reaching implications in the emerging area of plasmonically powered processes, especially in plasmonic photocatalysis.

2.2. Introduction

Forming and breaking of high-energy chemical bonds with plasmons is an emerging paradigm in materials science.[1–7] A photoexcited plasmonic nanostructure can initiate a series of de-excitation pathways via radiative (scattering or emission of photons) and nonradiative processes (electron-electron, electron-phonon, or phonon–phonon interactions), resulting in unique plasmonic outcomes.[8,9] Each of these intriguing relaxation processes has earned them a special place in the areas of surface-enhanced Raman scattering (SERS),[10,11] plasmonic photocatalysis,[1–7,12,13] and thermoplasmonics.[14–20] Thoughtful use of nanostructured materials as well as reaction conditions is crucial to minimize the interference between the different relaxation processes, and thereby achieve the desired outcome. For example, the success of plasmonic photocatalysis relies on the timely and efficient extraction of hot charge carriers from the nanostructures (in the order of a few femtoseconds).[4,8] Failing this, the entire excitation energy will be dissipated as heat to the nanoparticle lattice, and finally, to the surroundings (often termed as thermalization or the local heating process. The heat dissipated is called as plasmonic heat),[4,8] which triggers different photothermal processes. The contributions from hot charge carriers and thermalization in a plasmon-driven physicochemical transformation are often debated[21] as they are outcomes of the same nonradiative relaxation pathway. Thus, a better understanding as well as appropriate design of experiments is essential to minimize the interference between these two intriguing processes.[21,22] We present here insights into the utilization, and dissipation of local heating in plasmonic nanostructures, which will be vital in accomplishing the desired outcome from the thermalization process.

The idea of converting light-to-heat energy using plasmonic architectures has gained immense scientific importance due to its direct technological relevance in energy and medical research.[14–29] Thermoplasmonics is a well-matured research field that studies the generation, manipulation, and dissipation of plasmonic heat. There are studies on factors affecting thermalization and dissipation processes. For example, Richardson and coworkers[15] reported the localized nature of plasmonic heat. They established a relationship between temperature increase (ΔT) and distance from the nanostructure as follows:

$$\Delta T(r) = \frac{V_{NP}Q}{4\pi k_o r} \tag{1}$$

Where, $\Delta T(r)$ is the temperature increase at a distance r from the center of nanoparticle, V_{NP} is the volume of the nanoparticle, k_o is the thermal conductivity of the surrounding medium and Q is the heat generated. The equation is applicable for the condition r > R_{NP}, where R_{NP} is the radius of the nanoparticle.

Authors have theoretically calculated the temperature increase around optically illuminated AuNP (R_{NP} = 30 nm) in a water medium and found that the temperature decreases drastically when moving away from the nanoparticle (**Figure 2.1a**). The thermal conductivity of Au is high as compared to the surrounding media (water) and hence the temperature increase is almost equal throughout the nanoparticle. Similarly, the effect of nanoparticle assembly, size, and light intensity on plasmonic heat generation was theoretically demonstrated by Kotov and coworkers.[30] Firstly, the wavelength-dependent study suggested that the temperature increase is maximum at LSPR (**Figure 2.1b**). Further, the temperature increase with a single nanoparticle under illumination was compared with an array of closely spaced 16 nanoparticles. The higher temperature increase in the case of nanoparticles array has suggested the collective effect on thermalization which might be due to plasmon coupling or hot-spots generation (**Figure 2.1b**). Secondly, the authors deduced a mathematical expression to elucidate the size dependence of plasmonic heating which suggested the temperature increase is proportional to the second power of the nanoparticle radius, i.e. $\Delta T_{max} \propto R_{NP}^2$ (**Figure 2.1c**). Finally, authors have found a direct relation between the intensity of light on the temperature increase.
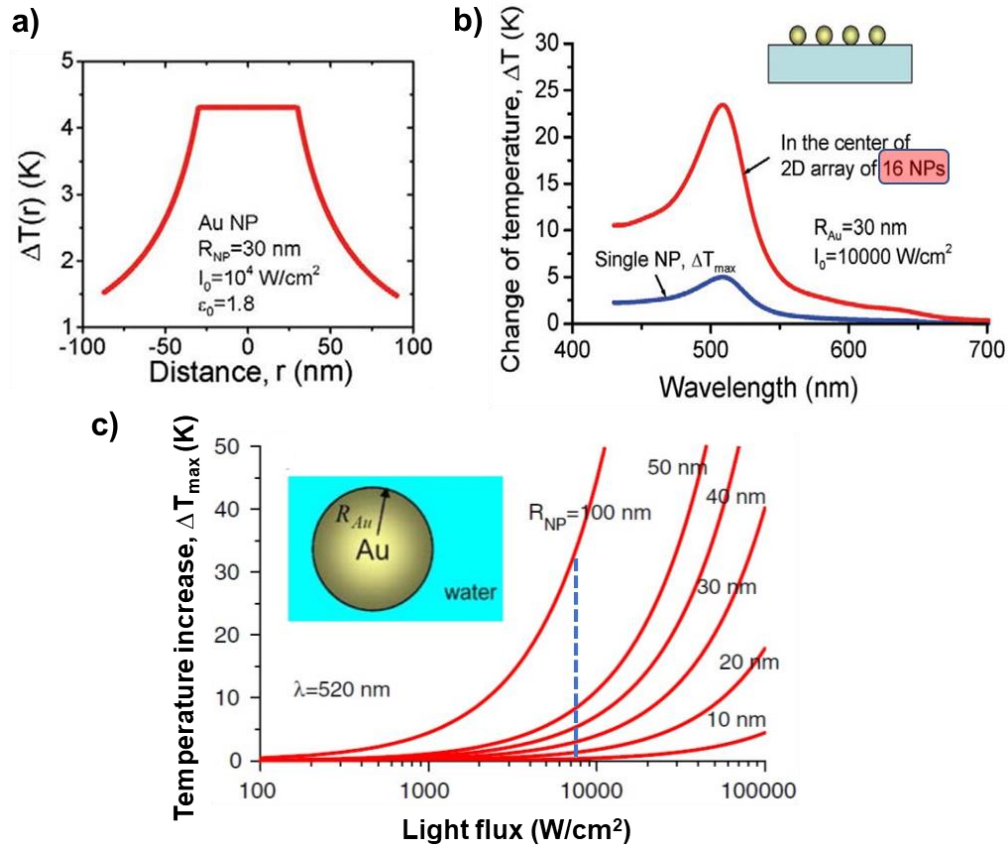
Figure 2.1. Fundamental aspects of plasmonic heating. (a) The calculated temperature profile of a plasmonic AuNP as a function of distance from its center in an aqueous environment. Reproduced with permission from ref. 15. Copyright: 2007, Elsevier. (b) comparison of the temperature increase caused by a single AuNP and an array of closely spaced 16 AuNPs. A clear collective effect can be seen in the amount of photothermal heat generated. (c) Effect of nanoparticle size and light intensity on the thermalization process. The temperature increase has a direct relation with intensity as well as the radius of a nanoparticle. (b) and (c) are reproduced with permission from ref. 30. Copyright: 2006, Springer.
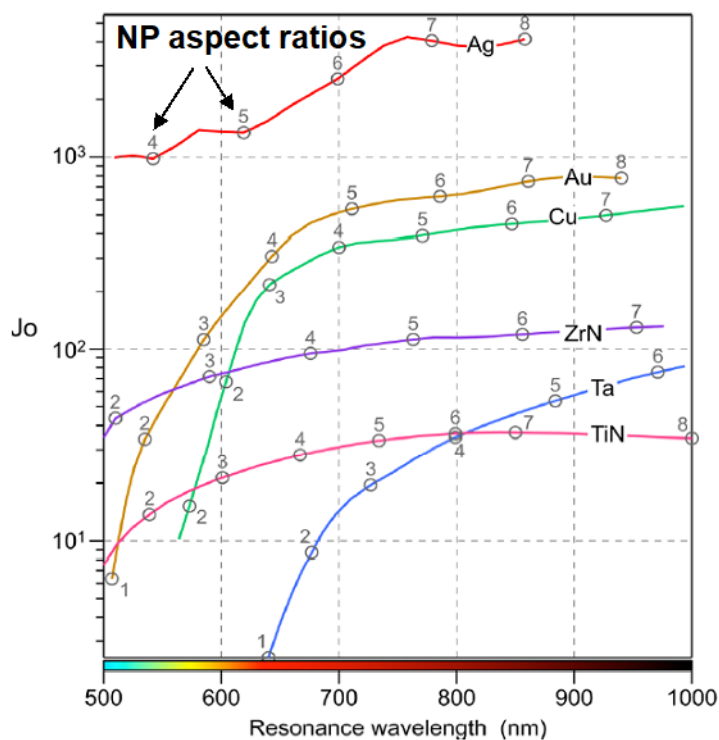
Figure 2.2. Effect of composition and shape anisotropy on plasmonic heat generation. Joules number is proposed as an indication of photothermal conversion efficiency, which was estimated to increase with an increase in aspect ratio. This suggests the anisotropic nanoparticle to be a superior photothermal converter compared to its isotropic counterparts. Reproduced with permission from ref. 31. Copyright: 2015, American Chemical Society

Although the area is rich with various studies, predominantly theoretical ones, however there are certain limitations both with respect to fundamental and applied perspectives. For example, the results explained above are theoretical studies and their experimental verification is missing in the literature. In this Chapter, we were interested in experimentally studying the effect of assembly as well as shape-anisotropy on plasmonic heat generation and dissipation. For this, we have fabricated thermoplasmonic heaters based on configurable one-dimensional gold nanorod (AuNR) arrays and performed various photothermal transformations in solution (both aqueous and organic) as well as in solid states. The thermoplasmonic properties of AuNR arrays were effectively demonstrated in thermally driven polymerization, solar-vapor generation, and Diels–Alder reaction (**Figure 2.3**).
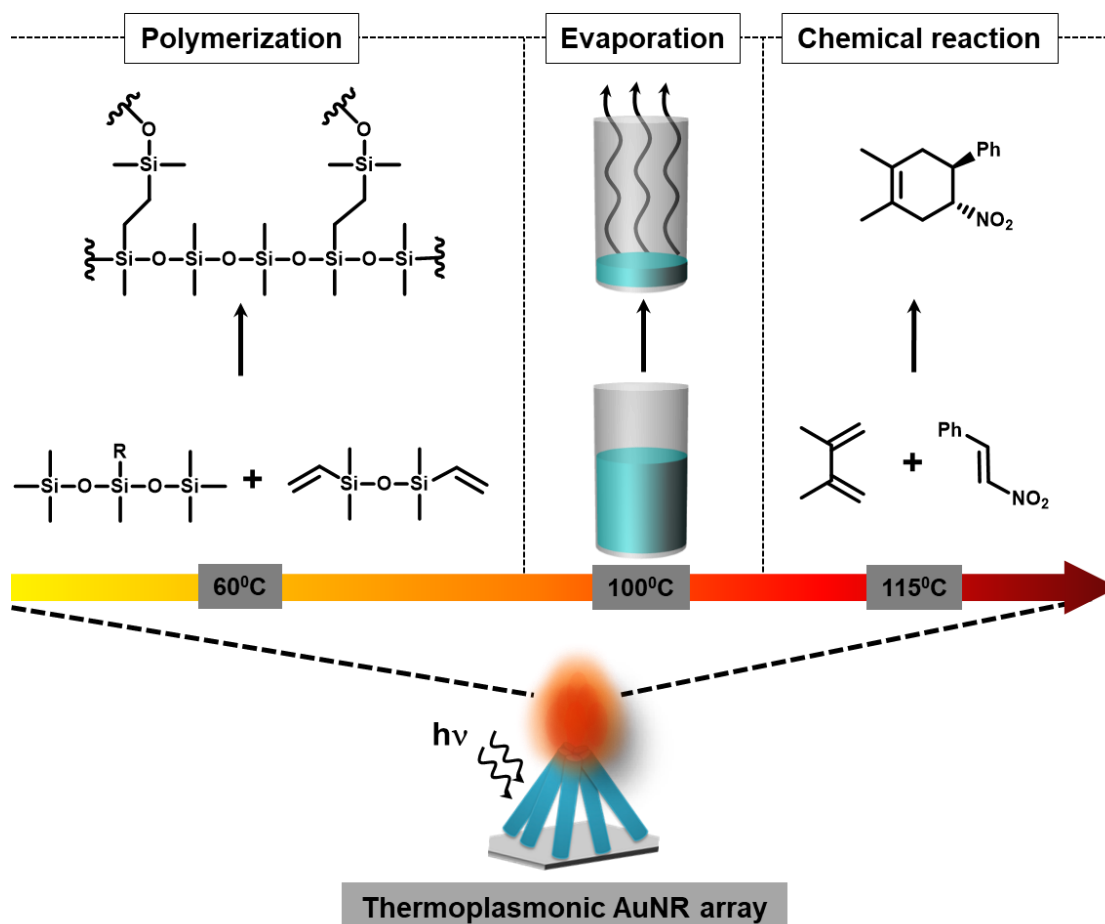
Figure 2.3. Generic Use of Thermoplasmonic AuNR Arrays for Performing Photothermally Driven PDMS Polymerization, Solar-Vapor Generation, and Diels–Alder [4 + 2] Cycloaddition.

2.3. Methods and Experimental Section

2.3.1. Materials and reagents

Anodic alumina oxide (AAO) (pore diameter = 75 nm, pore length = 50 μm, and interpore distance 150 nm) templates were purchased from Smart Membranes. Au plating solution (Orotemp 24 RTU) was purchased from Lectrachem Ltd. (TECHNIC UK). For PDMS experiments, Sylgard 184 was purchased from Ellsworth Adhesives India Pvt. Ltd (Dow Corning, Midland, MI). FTO glass, hydrochloric acid, tetrachloroauratetrihydrate ($HAuCl_4.3H_2O$), tetramethylammonium hydroxide (TMAOH) 25% wt. in water, 11-mercaptoundecanoic acid (MUA), hydrazine

monohydrate ($N_2H_4.H_2O$ 50-60%), tetrabutylammonium borohydride (TBAB), sodium hydroxide pellets, *trans*β-Nitrostyrene (99%), 2,3-dimethyl-1,3-butadiene (98%), lead carbonate, and cadmium acetate dihydrate were purchased from Sigma-Aldrich. (Di-n-dodecyl) dimethylammonium bromide (DDAB) and dodecylamine (DDA) were purchased from Alfa Aesar. All the reagents were used as received without any further purification.

2.3.2. Fabrication of gold nanorod (AuNR) arrays

Gold nanorod (AuNR) arrays of varying morphologies were fabricated following the reported three-step fabrication protocol, using anodic aluminum oxide (AAO) membranes as a template (**Figure 2.5a**).[32,33] In a typical experiment, metallic silver (Ag) was thermally evaporated (growth rate 0.2 Å/s) to generate a high-quality ∼200 nm Ag film on one side of the AAO template. Next, the AAO film was placed in the electrochemical cell for the deposition of Au, as shown in **Figure 2.5b,c**. Au was electrodeposited in the pores of the AAO template by applying a constant potential of −975 mV (vs Ag/AgCl electrode) using a Au plating solution (Orotemp 24 RTU). Note that the charge limit was kept at 40 mC. The electrodeposition time was varied from 280 to 350 s for fabricating AuNR arrays with different morphologies. The AAO template was then etched by placing it in ∼5 mL of 3 M NaOH for ∼12 h and washed 4 times with Milli-Q water. The AuNR arrays were then carefully transferred onto a glass support and kept in an oven at 90 °C for ∼10 min. The prepared AuNR arrays were stored in a vacuum desiccator to minimize aerial oxidation.

2.3.3. Scanning electron microscopy (SEM) imaging:

The AuNR arrays immobilized on glass slide was dried under vacuum for imaging. The Field Emission Scanning Electron Microscopic (FE-SEM) imaging was performed on ZEISS Ultra Plus FESEM instrument.

2.3.4. Inductively coupled plasma-mass spectrometry (ICP-MS):

ICP-MS study was performed with ICP-Q (Thermo Fischer) instrument to estimate the number of Au atoms present in the bundled AuNR array. The sample was prepared in 2 % (V/V) HCl in Milli Q water, after carefully dissolving the AuNR array by adding minimal amount of freshly prepared

aqua regia. The number of Au atoms in bundled AuNR arrays was estimated to be ~7.4 ×10^{17} from the ICP-MS experiment.

2.3.5. Synthesis of AuNPs:

Spherical gold nanoparticles (AuNPs) were synthesized following a modified literature procedure.[34,35] Hydrazine monohydrate ($N_2H_4.H_2O$) was used as the reducing agent. In a typical experiment, $HAuCl_4.3H_2O$ (12 mg), DDA (140 mg), and DDAB (140 mg) were mixed in toluene (4 mL) and sonicated for ~10 min for complete solubilization of Au (III) ions. This was followed by a rapid injection of another toluene solution containing 30 mg of TBAB and 46 mg of DDAB. The resulting solution was left stirring overnight to ensure the complete reduction of Au (III) ions. The seed particles were then grown to ~5.5 nm DDA-Au NPs. For this, a growth solution was prepared by adding 460 mg of DDAB, 1.4 g of DDA, 120 mg of $HAuCl_4.3H_2O$ and seed solution in 30 mL toluene. The growth solution was further reduced with a dropwise addition of another toluene solution containing 160 μL of $N_2H_4.H_2O$ and 560 mg of DDAB. The solution was stirred overnight for complete growth of the particles yielding monodisperse 5.5 ± 0.7 nm of DDAAu NPs. The particles were further grown to ~12 nm DDA-AuNPs. A growth solution was prepared by adding 8 g of DDAB, 13.0 g of DDA, 1.1 g of $HAuCl_4.3H_2O$ and seed solution in 200 mL toluene. The growth solution was further reduced with a dropwise addition of another toluene solution containing 650 μL of $N_2H_4.H_2O$ and 4.4 g of DDAB. The solution was stirred overnight for complete growth of the particles yielding monodisperse 11.9 ± 1.0 nm of DDA-Au NPs, as confirmed through TEM analysis.

2.3.6. Place exchange of AuNP with 11-mercaptoundecanoic acid (MUA) ligands:

In a typical synthesis, 11.9 ± 1.0 nm DDA-Au NPs (15 mL) were first precipitated by adding 50 mL of methanol which yielded a black precipitate. The supernatant was carefully removed, and the precipitate was then re-dispersed in 20 mL toluene. MUA ligand (equal to the moles of Au (III) in solution) dissolved in 10 mL dichloromethane (DCM)) was added. The solution was left overnight to ensure a complete ligand exchange. Next, the supernatant was decanted, and the precipitate was washed with DCM (3 × 50 mL) and acetone (50 mL), respectively. The precipitate

was then dried and redispersed in Milli Q water by adding ~20 µL of TMAOH base (25 % wt. in water), to deprotonate the carboxylic acid group for further studies.

2.3.7. Transmission electron microscopy (TEM) imaging:

The TEM sample for the AuNP was prepared by drop casting the nanoparticle solution on a 400-mesh carbon coated copper grid (Tedpella Inc.), followed by drying under vacuum. The High-Resolution Transmission Electron Microscopic (HRTEM) imaging was performed on JEOL JEM2200FS (200 kV) HRTEM instrument.

2.3.8. UV-vis absorption studies:

UV-vis absorbance data for AuNPs was recorded on a Shimadzu UV 3600 spectrophotometer, over the wavelength range of 300-800 nm.

2.3.9. Powder X-ray diffraction (PXRD) studies:

Powder X-ray diffraction (PXRD) patterns for thermochromic studies were recorded on Bruker D8 X-ray diffractometer with Cu Kα radiation of 1.54 Å.

2.3.10. NMR and HRMS studies:

^{1}H NMR studies were recorded on Bruker 400 MHz spectrometer and Jeol 400 MHz. High-resolution mass spectroscopy (HRMS) was performed using an ESI-TOF mass analyser.

2.3.11. Photothermal curing of polydimethylsiloxane (PDMS)

In a typical experiment, PDMS elastomer and the curing agent were mixed thoroughly in 10:1 weight ratio. The mixture was then degassed to remove the air bubbles, and AuNR arrays were immersed into the mixture. The AuNR array was then irradiated with a 532 nm continuous wave 1W diode laser for ~1 h. Control experiment was per-formed in the absence of AuNR arrays, while keeping other parameters constant.

2.3.12. Diels-Alder reaction

The [4+2] cycloaddition between 2,3-dimethyl-1,3-butadiene (diene) and trans-β-nitrostyrene (dienophile) was performed in a 15 mL glass test tube under continuous irradiation with a 1W 532 nm CW diode laser (**Scheme 2.1**). The beam diameter was set to be 1 cm and the light intensity on the test tube wall was measured to be $1W.cm^{-2}$. In a typical experiment, AuNR arrays were carefully placed at the bottom of a 15 mL test tube. Next, ~880 mg (5.9 mmol) of trans-β-nitrostyrene was mixed with 1 mL (8.8 mmol) of 2,3-dimethyl-1,3-butadiene and purged with nitrogen for ~30 min.[36] Note, an excess of 2,3-dimethyl-1,3-butadiene was taken to compensate for evaporation losses during the irradiation. The AuNR array was then irradiated with a 532 nm 1W diode laser for ~15 h. The reaction mixture after irradiation was dried using a rotary evaporator to remove the unreacted diene. The conversion yield for all the reactions was calculated from the ^{1}H NMR studies in CDCl$_3$ of the crude reaction mixture, which mainly contained the Diels-Alder product and the unreacted dienophile. For purification, the crude reaction mixture was first subjected to rotary evaporation to separate the low boiling diene. Next, the dienophile was separated through vacuum distillation at ~170 °C, to get the pure product. The control experiment with thermal heating was performed under the exact experimental set-up as for the photothermal conditions.

2,3-Dimethyl-1,3-butadiene
(diene)

trans-β-nitrostyrene
(dienophile)

(1S,2R)-4,5-dimethyl-2-nitro-1,2,3,6-
tetrahydro-1,1'-biphenyl
(Diels-Alder adduct)
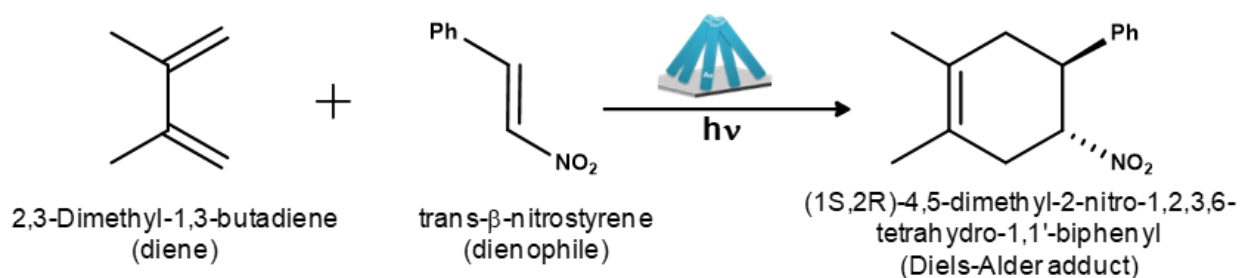
Scheme 2.1. Plasmonic heat driven Diels-Alder reaction between trans-β-nitrostyrene (dienophile) and 2,3-dimethyl-1,3-butadiene (diene) using bundled AuNR array as photothermal substrate.

2.3.13. Conversion yield calculation:

The conversion yield for [4+2] cycloaddition reactions was calculated from the ^{1}H NMR spectrum of the crude reaction mixture. The steps involved in calculating the yield are explained below with the help of a representative ^{1}H NMR spectrum.
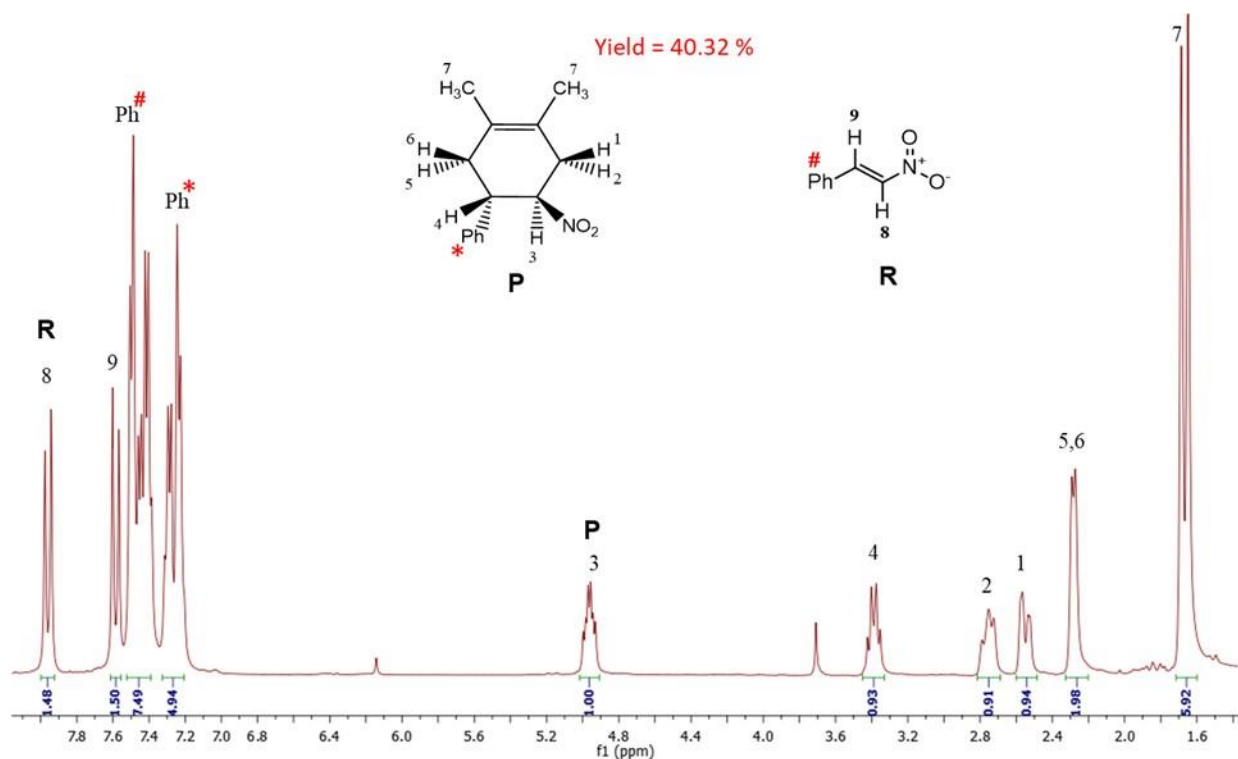
Figure 2.4. ^{1}H NMR spectrum of the crude reaction mixture (in CDCl$_3$) after irradiation with bundled AuNR array for 15h.

The peak marked as 3 corresponds to 1H of the product (P), and all the other peaks were integrated with respect to it. The peak marked 8 corresponds to 1H of dienophile reactant (R). Thus, the integration of peaks 3 and 8 can be taken as equivalents of product and reactant (dienophile), respectively.

In the above example, equivalents of product (P) = 1 and equivalents of reactant (R) = 1.48

Hence percentage yield was calculated as follows:

% yield of product = {Equivalents of product (P)/(sum of equivalents of P and R)} ×100

= {1/(1 + 1.48)} ×100

= {1/2.48} ×100

= 40.32 %

2.3.14. Calculation of nanoparticle concentration

The concentration of AuNPs in stock solution was calculated using Beer-Lambert's law:

$$A = \varepsilon \, . \, c \, . \, l$$

where,

A is the absorbance

ε is the molar extinction coefficient ($M^{-1}cm^{-1}$)

c is the concentration of the solution (M)

l is the optical path length (cm).

Molar extinction coefficient (ε) for AuNP was taken to be 2.7×10^8 M^{-1} cm^{-1} for ~12 nm diameter particles.[37]

The concentration of AuNP stock solution was estimated to be ~ 0.84 μM (in terms of AuNPs).

2.3.15. Determination of number of Au atoms present in each NP

The average no. of gold atoms in each nanoparticle sphere can be calculated as per the previous report[38]

$$N = 30.89602 \times D^3$$

where 'N' is the average number of gold atoms per nanoparticle and 'D' is the diameter of the particles.

The average diameter of the particles was 11.9 ± 1.0 nm as estimated from TEM analysis. So, the average no. of gold atoms per nanoparticle will be

$$N = 30.89602 \times (11.9)^3$$

$$= 52065$$

If the concentration of AuNP is 0.84 μM (**in terms of AuNPs**), then **number of gold atoms** in 28.2 μL of AuNPs will be

$28.2 \times 10^{-6} \times 0.84 \times 10^{-6} \times 6.022 \times 10^{23} \times 52065 = \sim7.4 \times 10^{17}$ Au atoms, which is equivalent to the number of Au atoms in the bundled AuNR array (1188 ± 162 nm) as calculated from ICP-MS

Number of mols (**in terms of Au atoms**) $= (7.4 \times 10^{17})/6.022 \times 10^{23}$

$$\sim 1.2 \text{ μmol}$$

2.3.16. [4+2] Cycloaddition reaction with spherical AuNPs

In a typical experiment, ~1.2 μmol of MUA capped AuNP (number of Au atoms was similar to that in the bundled AuNR arrays) was drop casted onto a clean glass slide. The glass slide was then heated slowly to get a homogeneous film of AuNPs.[39] Then the diene and dienophile were added in a 15 mL glass test tube as explained earlier, followed by carefully inserting the AuNP coated glass slide. The reaction medium was purged with nitrogen for ~30 min. The reaction medium containing AuNP coated glass slide was then irradiated with a 532 nm diode laser for 15 h.

2.3.17. Solar-vapor generation studies

In a typical experiment, 6 mL of DI water was taken in a 15 mL test tube containing the bundled AuNR arrays. Fresnel lens (19.5 cm ✕ 28.5 cm) was used to focus the sunlight onto the AuNR arrays immersed in water, as reported previously.[25] Control experiment was performed in the absence of bundled AuNR arrays and maintaining all other parameters. **Figure 2.12** clearly shows the solar vapor generation and condensation of water on the sides of the test tube, in the presence of bundled AuNR arrays.

2.3.18. Quantification of solar vapor generation

In a typical experiment, ~6 mL of DI water was taken in a 3.5 cm wide petri dish containing the bundled AuNR arrays. The petri dish was then placed onto a weighing balance (Mettler Toledo ME403/04) with 1 mg readability to monitor the weight loss. A thermocouple was set to note down

the variation in temperature. Fresnel lens (19.5 cm ✕ 28.5 cm) was used to focus the sunlight onto the bundled AuNR arrays immersed in water, the spot diameter was fixed to be 1 cm. A thermopile optical power sensor (Model LM-10 HTD; Coherent, Santa Clara, CA 95054 USA) was used for measuring the power of sunlight falling on the AuNR arrays, after focusing. The solar power measured was 13.6 W.cm^{-2}, under our experimental conditions. A complete evaporation of water was observed within 20 min of irradiation.

2.3.19. Calculation of evaporation rate

The evaporation rate was calculated using equation[40]

$$Evaporation\ rate = \frac{\Delta m}{A \Delta T} \tag{1}$$

Where **Δm** (in kg) is the mass loss of water during time interval **ΔT** (in h), and **A** (in m^2) is the area.

The evaporation rate was estimated for three different areas, for comparing with the values reported in the literature for other plasmonic materials.

The evaporation rate was 250.7 kg m^{-2}h^{-1}, when the area based on the spot size of radiation (d = 1 cm) falling onto the bundled AuNR arrays was considered in calculation.

The evaporation rate was 309.5 kg m^{-2}h^{-1}, when the area of bundled AuNR arrays (d = 9 mm) was considered in calculation.

The evaporation rate was ~20.5 kg m^{-2}h^{-1}, when the area of petri dish (d = 3.5 cm) was considered in calculation.

2.3.20. Calculation of solar vapor generation efficiency:

The thermodynamic equivalent reaction flow chart for the process of solar vapor generation, under our experimental condition is shown in **Scheme 2.2**.[40]

$$H_2O \ (l, \ 35 \ °C) \xrightarrow[C_{p,\,l}]{(i)} H_2O \ (l, \ 100 \ °C) \xrightarrow[h_{LV}]{(ii)} H_2O \ (v, \ 100 \ °C)$$

$$\xrightarrow[\quad H_{LV} \quad]{(iii)}$$
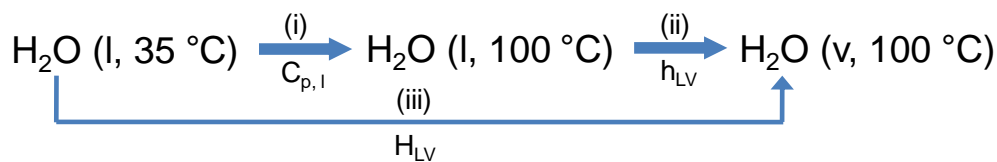
Scheme 2.2. Thermodynamic equivalent reaction flow chart for solar vapor generation under our experimental condition.

According to Hess's law,[40] the overall enthalpy of water evaporation, H_{LV}, is equal to the sum of the enthalpies for processes (i) and (ii)

$$\eta_{SVG}(\%) = \frac{Q_{LV}}{Q_{input}} \times 100 = \frac{mH_{LV}}{q_i \, C_{opt}} \times 100 \tag{2}$$

Where, η_{SVG} = efficiency of solar vapor generation,

Q_{LV} = energy consumed during water evaporation,

Q_{input} = energy of the incident solar radiation,

m = mass loss of water after evaporation (~6.04 g),

H_{LV} = enthalpy of liquid to vapor phase transformation, which includes specific heat capacity of water, C_p (4.18 J K^{-1}g^{-1}) as well as latent heat of vaporization, $h_{LV,373K}$ (2257.2 J g^{-1}), i.e., H_{LV} = $C_P\Delta T$ (373-306) + h_{LV}

q_i = power of illuminated solar light (6.5 W.cm^{-2}),

C_{opt} = optical concentration, which is obtained by multiplying the power with spot area (1 cm^2).

$$\eta_{SVG}(\%) = \frac{6.04 \text{ g} \times [4.18 \text{ J/K} \cdot \text{g} \times (373 \text{ K} - 306 \text{ K}) + 2257.2 \text{ j/g}]}{13.6 \text{ W/cm}^2 \times 1 \text{ cm}^2 \times 1200 \text{ s}} \times 100$$

$$= 93 \ \%$$

The efficiency of plasmonic AuNR arrays, reported here, is among the best of the materials developed for solar vapor generation (**Table 2.2**).

2.4. Results and Discussion

2.4.1. Fabrication of configurable thermoplasmonic AuNR arrays

Plasmon-driven processes are highly sensitive to the size, shape, and composition of nanostructured materials. In general, anisotropic nanostructures exhibit superior plasmonic properties over spherical nanomaterials because of their unique shape-dependent optoelectronic properties such as a high molar extinction coefficient, unidirectional charge transport, and edge effects.[41] In the present work, an array of highly configurable one-dimensional AuNRs was fabricated on a glass slide with the help of the template-mediated electrodeposition technique (**Figures 2.5** and **2.6**, **Section 2.3.2** in the Methods and Experimental Section).[32,33]
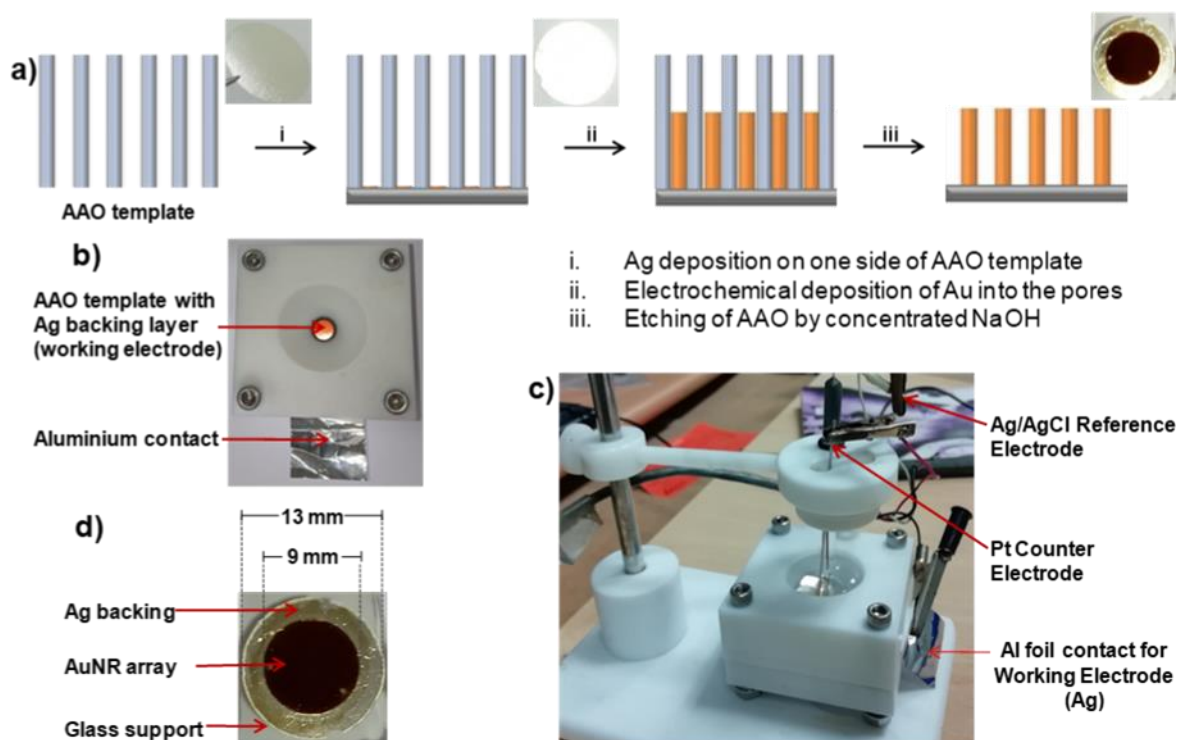
Figure 2.5. Fabrication of gold nanowire (AuNR) arrays. **(a)** Schematic representation for the fabrication of AuNR arrays with optical photographs of the AAO template at each stage. **(b)** Photograph of the electrochemical cell with the AAO template. **(c)** Photograph of the experimental setup for electrochemical deposition. **(d)** Optical photograph of AuNR arrays (with Ag backing) on a glass support.

Briefly, an array of AuNRs was electrochemically grown in an anodic aluminum oxide (AAO) template having a silver backing layer (~200 nm thick), followed by the etching of the template with a 3 M sodium hydroxide solution. The AuNRs in the array had a diameter of ~75 nm, and the length was varied by controlling the electrodeposition time (280–350 s; **Figures 2.6a–d, 2.15, and 2.16** in the Appendix). At 280 s deposition time, the length of AuNRs in the array was estimated to be 618 ± 47 nm, and the array was distributed in a hexagonal lattice (inset of **Figure 2.6a**). The AuNRs started to lose their free-standing ability as well as the hexagonal lattice arrangement, as the NRs were grown beyond 752 ± 52 nm in length. The insets of **Figure 2.6b–d** clearly show the bundling of AuNRs, corresponding to different electrodeposition times. Thus, different morphologies of AuNR arrays, ranging from straight to bundled arrangements, were uniformly fabricated over a large area (~0.6 cm^2). This flexibility in the fabrication protocol to form straight and bundled geometries can be beneficial in studying the influence of nanostructural morphology on various plasmonic properties.
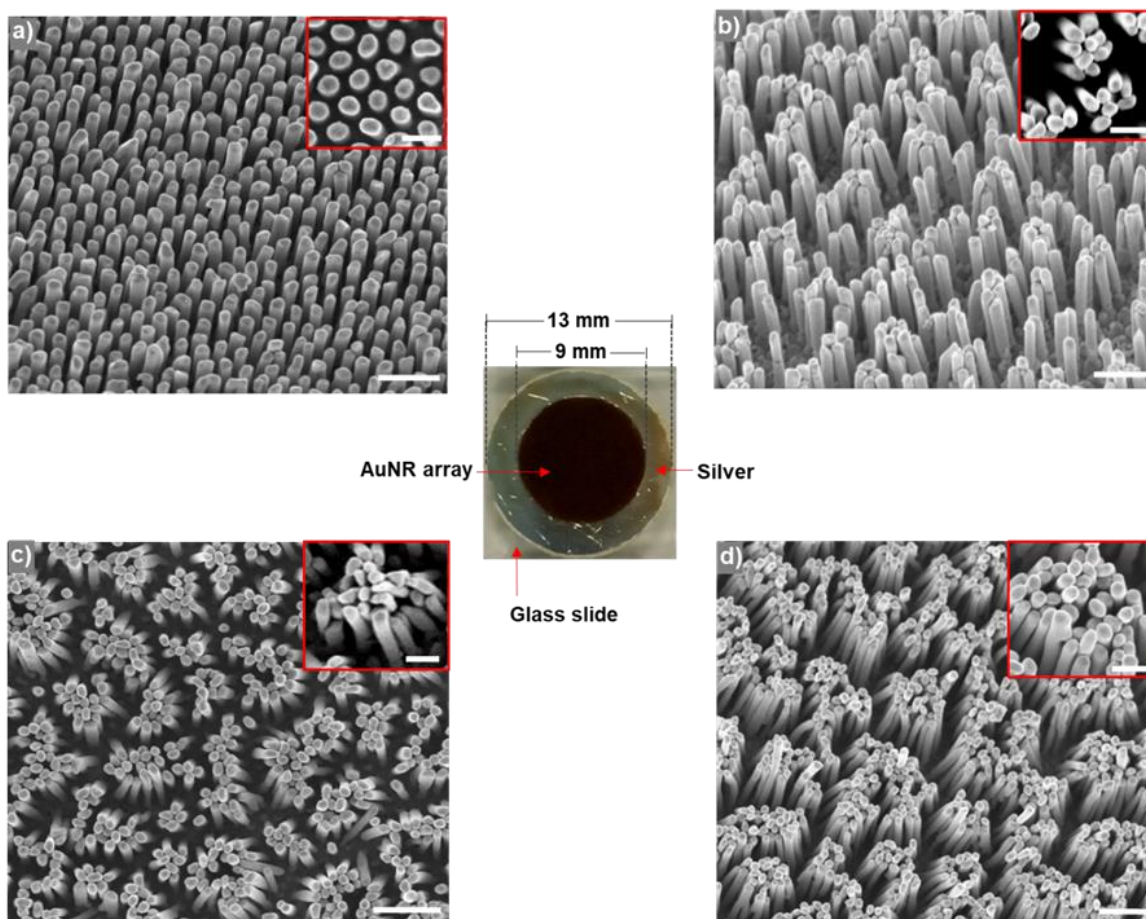
Figure 2.6. Microscopic characterization of configurable thermoplasmonic AuNR arrays. SEM images of (a) 618 ± 47 nm: long straight, (b) 752 ± 52 nm: long bundled, (c) 880 ± 64 nm: long bundled, and (d) 1188 ± 162 nm: long bundled AuNR arrays, corresponding to electrodeposition times of 280, 330, 340, and 350 s, respectively. The scale bar corresponds to 500 nm. The corresponding top-view images given in the insets clearly show the bundling of AuNRs. The scale bar of inset images corresponds to 200 nm. A representative optical photograph of the bundled array of the AuNR deposited on a glass slide is shown in the middle, with all the dimensions marked.

2.4.2. Thermoplasmonic polymerization and the Diels–Alder reaction

Our first target was to perform systematic thermoplasmonic studies to test the ability of AuNR arrays in converting light-to-heat energy. Solid-state ultraviolet (UV)–visible absorption studies proved that the bundled AuNR arrays exhibited strong absorption in the visible–near-infrared (NIR) region (**Figure 2.7**), thereby justifying the use of a green laser and sunlight as irradiation sources. Accordingly, a 1 W 532 nm continuous wave (CW) diode laser was used as an irradiation source (having a Gaussian beam distribution, with a maximum intensity of 1 W cm^{-2} measured at the center; **Figure 2.17** in the Appendix).
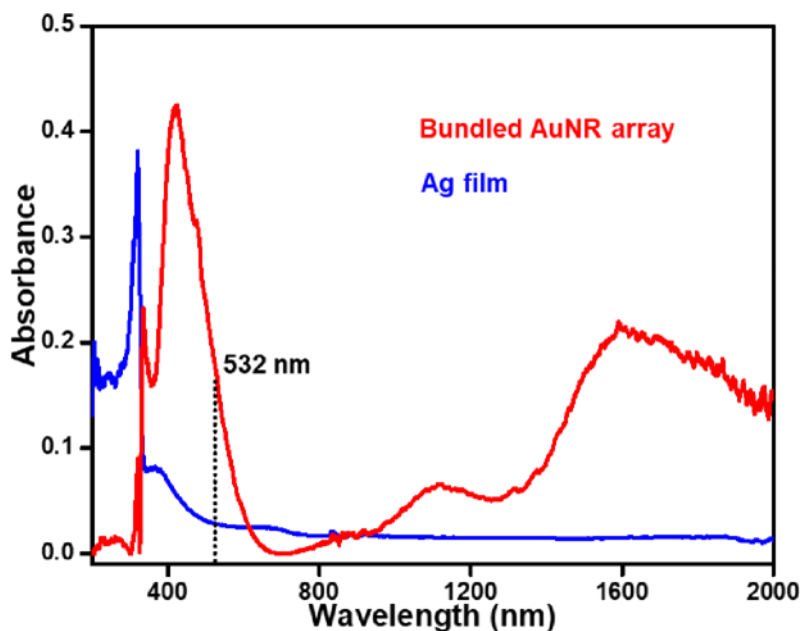
Figure 2.7. Solid-state UV-visible absorption spectrum of bundled AuNR arrays and Ag film, recorded under the reflectance mode. Diffuse reflectance data was converted to absorbance using the Kubelka–Munk transformation. The absorbance below 400 nm corresponds to glass slide and silver film, whereas the absorbance above ~450 nm corresponds to bundled AuNR array. The spectrum clearly shows strong absorbance in the visible-NIR region, thereby justifying the use of green laser and sunlight as irradiation sources.

To begin with, photothermally driven polymerization of polydimethylsiloxane (PDMS) was performed. The irradiation of AuNR arrays suspended in a solution of a PDMS monomer and a curing agent led to the complete polymerization within ~1 h of irradiation with a 1 W 532 nm CW laser (**Figure 2.8**). The bulk temperature increased to ~60 °C during the PDMS polymerization experiment (bulk temperature refers to the steady-state temperature achieved in the surrounding medium). It is well known that the plasmonic heat generated can dampen quickly to the surroundings based on the thermal conductivity of the medium,[15] resulting in a marginal increase in the bulk temperature.[12,13,42] We, therefore, envisaged that the AuNR arrays can generate temperatures much higher than ~60 °C close to their surface, and therefore performed a series of high-temperature photothermal transformations.
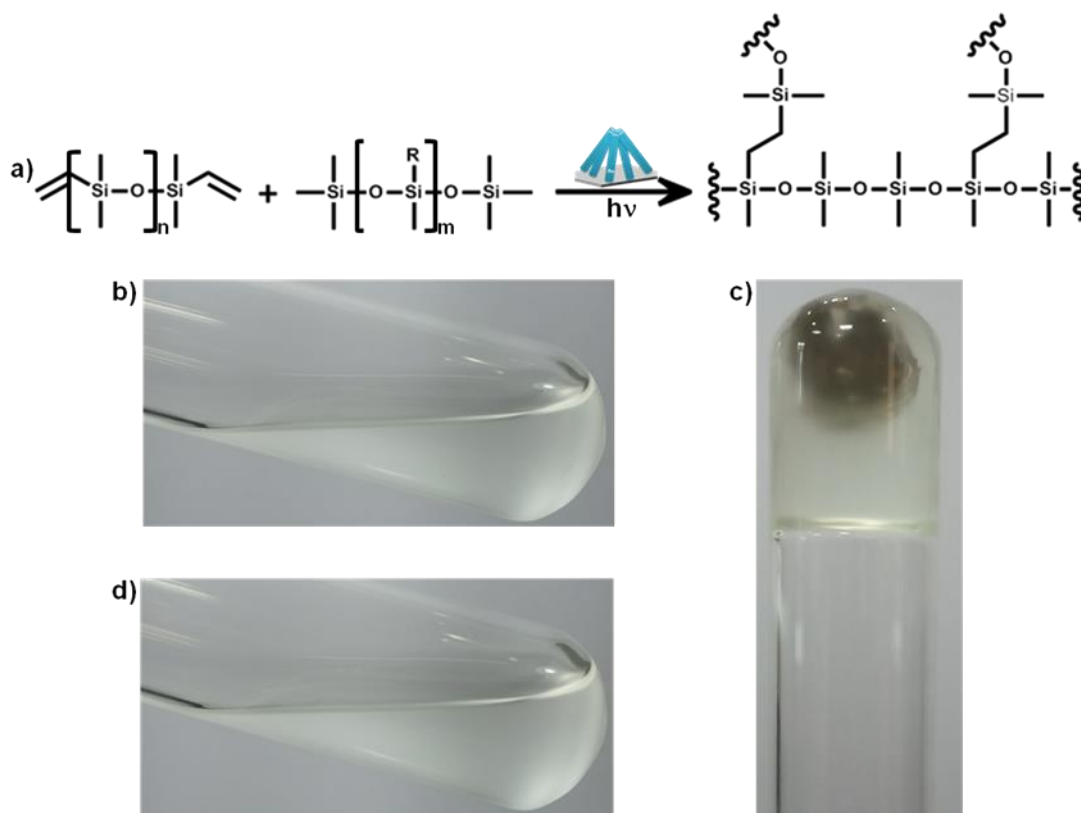
Figure 2.8. Photothermal PDMS curing. **(a)** Reaction scheme for the curing of PDMS. Photographs of the curing mixture **(b)** before, and after irradiation for ~1 h in the **(c)** presence and **(d)** absence of straight AuNR-3 arrays.

First, we performed an atom-economic and widely used reaction in synthetic organic chemistry, namely, the Diels–Alder cycloaddition. The [4 + 2] cycloaddition between 2,3-dimethyl-1,3-butadiene (diene) and *trans*-β-nitrostyrene (dienophile) was chosen as a representative example (**Figure 2.9a**), as this reaction is solely heat driven.[43] Our intention was also to use the Diels–Alder cycloaddition as a model reaction to test the role of the morphology of AuNR arrays (straight vs bundled) on plasmonic heat generation. The photoirradiation of diene and dienophile, for ∼15 h, in the presence of bundled AuNR arrays (with NR length 1188 ± 162 nm) with a 1 W green laser, yielded ∼40% of the Diels–Alder adduct (1*S*,2*R*)-4,5-dimethyl-2-nitro-1,2,3,6-tetrahydro-1,1'-biphenyl (**Figures 2.9b, Table 2.1**, and **2.18–2.20** in the Appendix). It is worth mentioning that no products corresponding to the photochemical [2 + 2] cycloaddition were observed in our studies. The reagents formed a uniform solution, and the bulk temperature under irradiation in the presence of bundled AuNR arrays reached ∼60 °C (bulk temperature refers to the steady-state temperature achieved in the reaction mixture). Control experiments in the absence of bundled one-dimensional (1D) AuNR arrays produced the Diels–Alder adduct in merely a ∼12% yield (**Figure 2.20c** in the Appendix), which is close to the thermal experiments performed at the bulk temperature in the absence of bundled AuNR arrays (∼60 °C; **Figure 2.21b** in the Appendix). Similarly, the Diels–Alder reaction performed in the presence of the bundled AuNR array at 60 °C without light irradiation gave a comparable yield to that obtained in the absence of nanorod arrays under similar conditions. (**Figure 2.21b, d** in the Appendix). Thus, all the control experiments conclusively prove the active role of thermoplasmonic heat from bundled AuNR arrays (photothermal effect) in driving the Diels–Alder reaction.
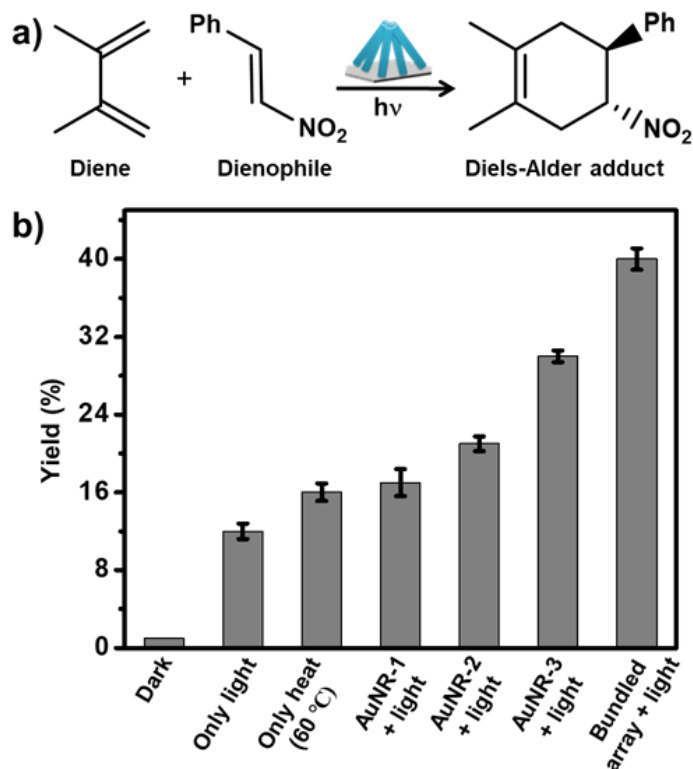
Figure 2.9. Thermoplasmonic Diels–Alder reaction. (a) Reaction scheme for the [4 + 2] cycloaddition between 2,3-dimethyl-1,3-butadiene (diene) and *trans*-β-nitrostyrene (dienophile), using the thermoplasmonic heat generated from bundled AuNR arrays. (b) Bar diagram summarizing the yield of the Diels–Alder adduct obtained under different reaction conditions.

The bundled AuNR arrays were found to be superior to straight AuNR arrays, as well as spherical Au nanoparticles with a similar number of Au atoms (**Section 2.3.16**, **2.9b**, **2.10, 2.11** and **Table 2.1, Figures 2.22, 2.23** in the Appendix,). This clearly proves the advantage of one-dimensional structures over their spherical counterparts in plasmonic heat generation as well.
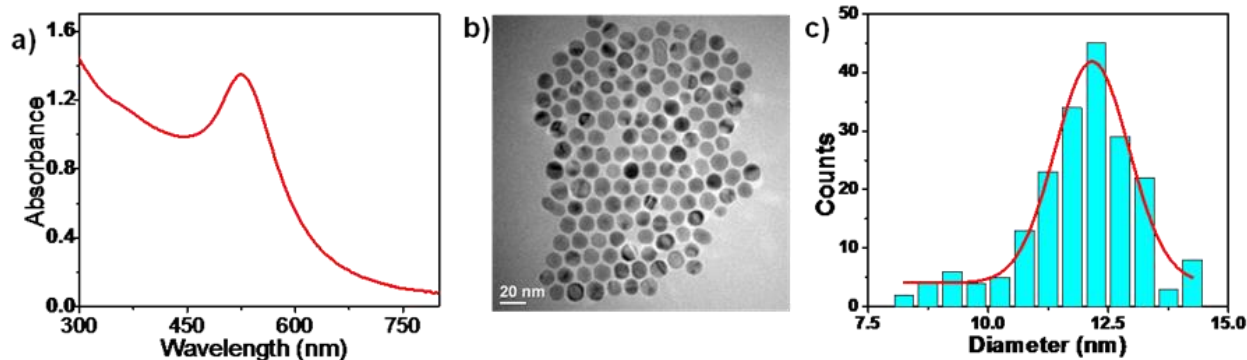
Figure 2.10. Spectroscopic and microscopic characterization of AuNPs. **(a)** UV-vis absorption spectrum, **(b)** a representative TEM image, and **(c)** a histogram showing the size distribution of AuNPs. The average size was estimated to be 11.9 ± 1.0 nm. The size distribution was estimated from ∼ 200 NPs.

Now, the higher thermalization in bundled morphology compared to straight AuNR arrays can be attributed to the (i) increase in the absorption cross-section of the bundled arrays, or (ii) enhanced concentration of the electromagnetic field at the tips of bundled nanorods (leading to the generation of plasmonic coupling and hot spots),[44−50] or (iii) the increase in the number of Au atoms in the bundled array. To get more insight, the Diels–Alder cycloaddition was performed in the presence of straight AuNR arrays with varying lengths (AuNR-1 with NR length 400 ± 51 nm, AuNR-2 with NR length 534 ± 47 nm, and AuNR-3 with NR length 618 ± 47 nm; **Figures 2.11** and **2.22** in the Appendix).
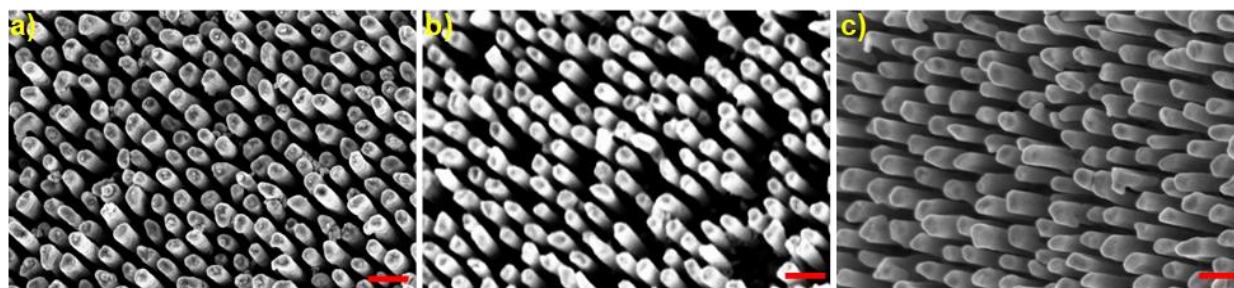
Figure 2.11. SEM images of straight AuNR arrays of different **(a)** AuNR-1 arrays with NR length 400 ± 51 nm, **(b)** AuNR-2 with NR length 534 ± 47 nm, and **(c)** AuNR-3 arrays with NR length 618 ± 47. Scale bar corresponds to 200 nm.

The yields of the Diels–Alder adduct increased as the length of the NRs in straight AuNR arrays was increased (essentially, the Au content increased as the AuNR arrays were grown longer; **Figure 2.9b**). It should be recalled that the bundled AuNR arrays were prepared by increasing the length of the NRs, which essentially will increase the Au content in the NR arrays. Even though the bundled AuNR arrays gave the maximum yield, it will be inappropriate at this stage to comment on the influence of plasmon coupling or hot spots on the thermalization process. Most probably, the primary reason for the observed variation in the product yield could be the difference in the absorption cross section of the samples at the excitation wavelength of ∼532 nm. Detailed and separate studies must be performed to analyze the influence of nanostructural assembly on thermoplasmonic properties. Having said that, it can be confirmed that the bundled

AuNR arrays showed the highest photothermal effect, and further thermoplasmonic studies were continued with bundled AuNR arrays.

Table 2.1. Summary of photothermally and thermally driven Diels-Alder reactions under different experimental conditions.

Photothermal reaction with 1 W 532 nm laser irradiation			Thermal reaction	
Materials	**Measured bulk temperature (^{0}C)**	**Yield^a (%)**	**Temperature (^{o}C)**	**Yield^a (%)**
StraightAuNR-1 arrays	~ 57	~ 17	~115	~ 82
StraightAuNR-2 arrays	~ 57	~ 21	~ 60	~ 15
StraightAuNR-3 arrays	~ 57	~ 30	~ 25	~ 1
Bundled AuNR arrays	~ 57	~ 40		
Spherical AuNPs	~ 57	~ 23		
Ag film	~ 55	~ 12		
Without AuNR arrays	~ 55	~ 12		

[a]Yields were calculated from NMR studies.

2.4.3. Thermoplasmonic solar-vapor generation.

It is essential to quantitatively analyze the thermoplasmonic properties of bundled AuNR arrays before projecting them as an efficient heating platform for generic photothermal applications. With this in mind, one of the well-studied thermoplasmonic experiments, namely, solar-vapor generation,[25,26] was performed using bundled AuNR arrays (see **Section 2.3.17-21** for detail). An instantaneous boiling of water, as well as a steady generation of steam, was observed upon irradiation of bundled AuNR arrays suspended in water (**Figures 2.12, 2.14a**, and **2.24** in the Appendix).
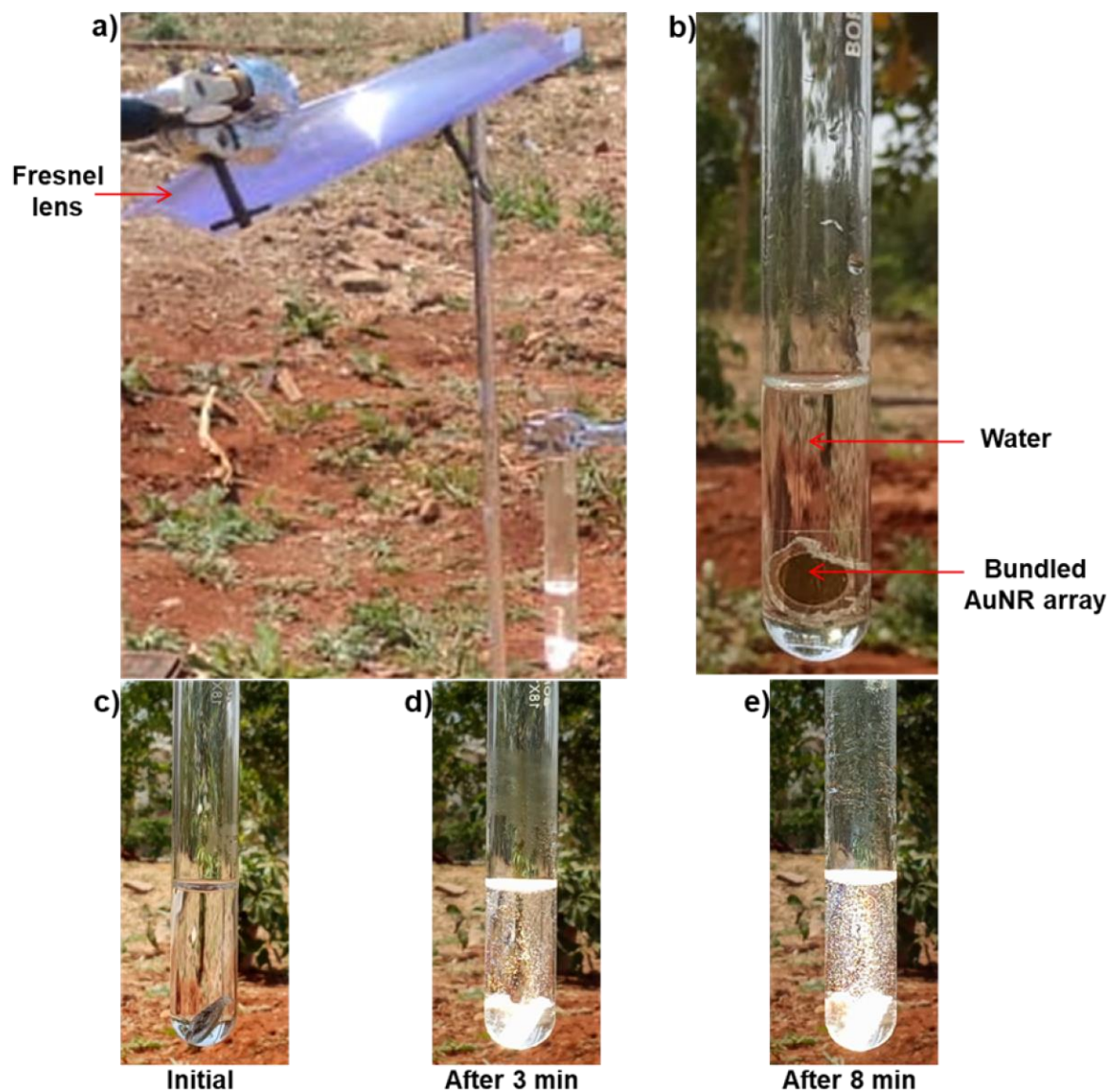
Figure 2.12. (a) Photograph of the experimental setup for studying solar vapor generation. **(b)** Photograph of test tube containing bundled AuNR array immersed in 5 mL of DI water. Photographs of test tubes **(c)** before, **(d)** after 3 min, and **(e)** 8 min of solar irradiation.

It is worth mentioning that sunlight was used as the light source for water evaporation experiments, which signifies the practical use of AuNR arrays as thermoplasmonic heaters (the sunlight was focused using a Fresnel lens,[25] as mentioned in the Methods and Experimental Section). Systematic solar-vapor generation experiments showed that ~6 g of water was evaporated within ~20 min of irradiation in the presence of bundled AuNR arrays (the water in the Petri dish was

completely evaporated, **Figure 2.14b**). Correspondingly, the bulk temperature of water increased to ∼80 °C within ∼5 min of irradiation of bundled AuNR arrays (**Figure 2.14c**). Control experiments, in the absence of bundled AuNR arrays as well as in the dark, confirmed the role of the thermalization process in solar-vapor generation. The evaporation rate and efficiency of a bundled AuNR array-based thermoplasmonic heater were estimated to be ∼20.5 kg m^{-2} h^{-1} and ∼93%, respectively (**Figures, 2.13, 2.14d**, **Scheme 2.1**, and **Section 2.3.18**).
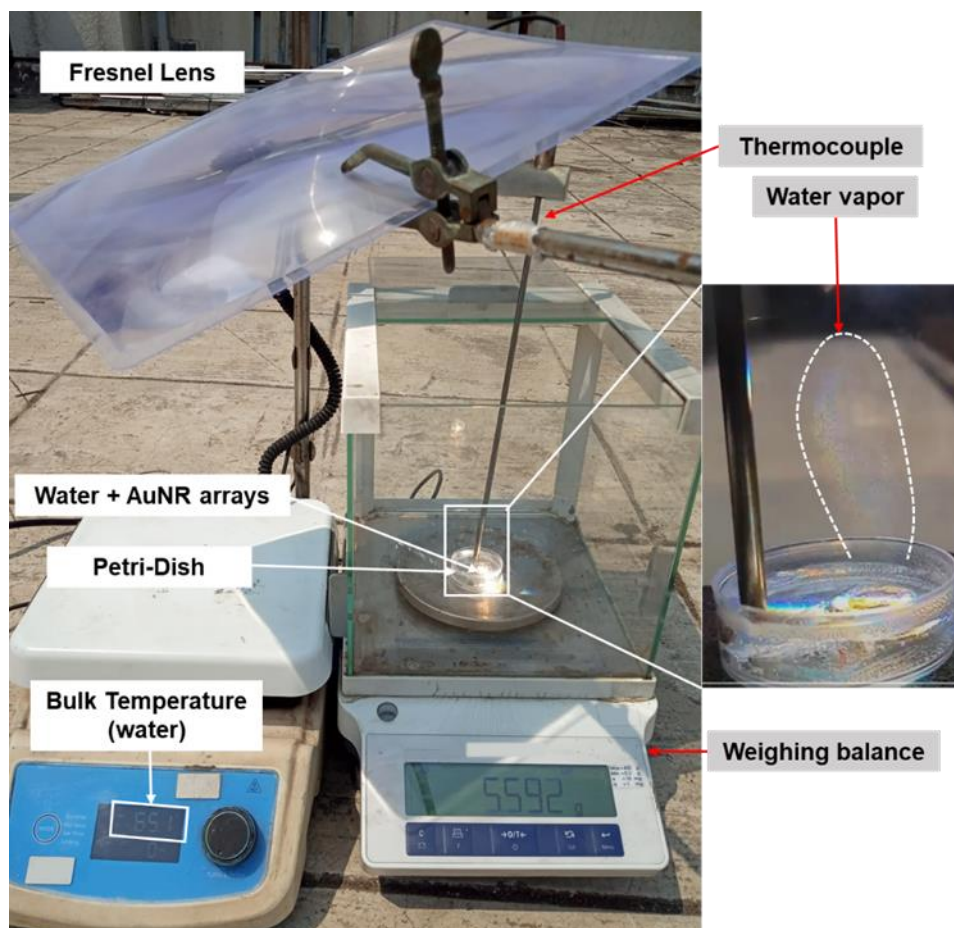
Figure 2.13. Thermoplasmonic solar-vapor generation. Optical photograph of the experimental setup for thermoplasmonic heat-driven solar-vapor generation (a thermocouple was used to measure the temperature).

Both these values are comparable to some of the best thermoplasmonic materials reported based on plasmonic nanostructures (**Table 2.2**). The rate of solar-vapor evaporation was ∼310 kg m^{-2} h^{-1} when the area of the bundled AuNR array was considered for the calculation (instead of the entire

area of the Petri dish). Thus, the bundled AuNR arrays possess strong thermoplasmonic properties to act as efficient light-to-heat energy converters for future photothermal applications.
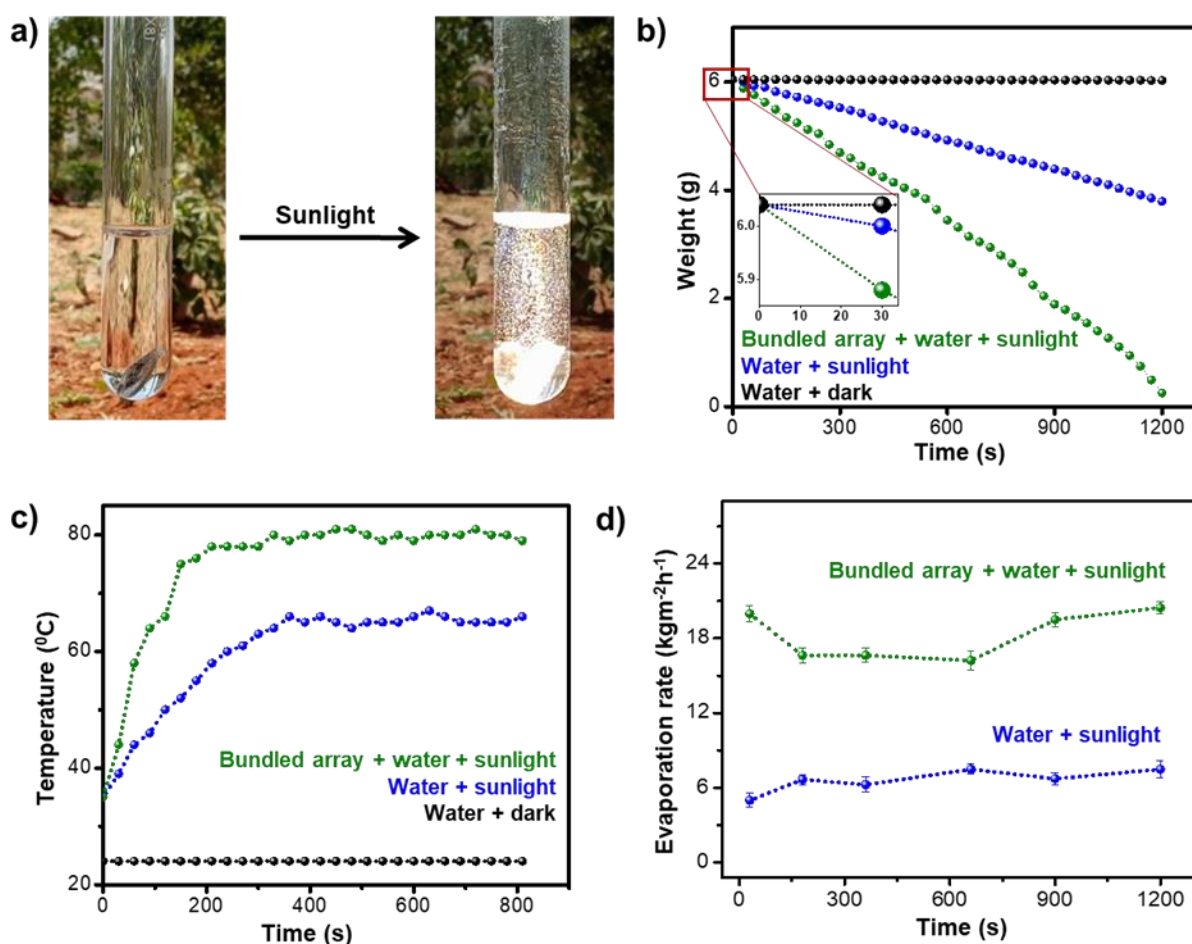
Figure 2.14. Thermoplasmonic solar-vapor generation. (a) Optical photographs showing the boiling of water by the thermoplasmonic heat produced from bundled AuNR arrays. Monitoring the (b) weight loss (inset shows that the first weight loss was noted after 30 s of irradiation) and (c) temperature increase of water under different experimental conditions. "Water + dark" corresponds to experiments performed inside the laboratory in the dark, under ambient temperature (~25 °C), and pressure (~1 atm). (d) Plot showing the difference in the evaporation rate in the presence and the absence of bundled AuNR arrays. The error was estimated from three independent measurements.

Table 2.2. Comparison of solar vapor generation studies.

Materials	Light source	Efficiency (%)	Evaporation Rate (kgm^{-2}h^{-1})	Final Temp. (°C)	Ref.
Ag NPs and poly (sodium-*p*styrenesulfonate, PSS) on agarose gel	Solar simulator (1 kWm^{-2})	92.8	2.1	-	51
Ag NPs in AAO template	Solar simulator (1 kWm^{-2})	80	1.2	-	52
Au Vapor deposited in AAO template	Solar simulator (1-4 kWm^{-2})	62-90	1-9	98 (Steam temp.)	53
Black Au	Solar simulator (1-20 kWm^{-2})	25-57	1-16	80	54
Au NPs	Sunlight with focusing	24	2.5 g in 4 min	80	25
Bundled AuNR arrays	**Sunlight with focusing**	**93**	**20.5**	**80**	**Our work 55**

2.5. Conclusions

We studied the effect of shape anisotropy along with assembly on plasmonic heat generation and dissipation. For that, we introduce configurable AuNR arrays as a versatile thermoplasmonic heater for the efficient conversion of light-to-heat energy. The spherical AuNPs were found to be a less efficient thermoplasmonic substrate as compared to AuNR arrays. On the other hand, the bundled morphology was found to be a superior photothermal platform compared to the straight morphology; however, the involvement of plasmon coupling or hot-spots generation cannot be confirmed. The plasmonic heat generated from AuNR arrays was used for polymerization, solar-vapor generation, and Diels–Alder cycloaddition, The bundled AuNR arrays developed by us possess strong thermoplasmonic properties to act as an efficient heating platform for future photothermal applications. Moreover, the reaction conditions played a crucial role in the dissipation of heat from the thermoplasmonic surface to the surroundings, with minimal influence on surface temperature observed in solution-state studies. Such information will definitely be

helpful in the emerging area of plasmonic photocatalysis, where the emphasis is to minimize or deconvolute the role of the thermalization process from hot electron chemistry. In a broader perspective, our thermoplasmonic studies demand the thoughtful design of nanostructures as well as reaction conditions for achieving the desired outcome from a plasmonic process.

2.6. References

(1)   Christopher, P.; Xin, H.; Linic, S. Visible-Light-Enhanced Catalytic Oxidation Reactions on Plasmonic Silver Nanostructures. *Nat. Chem.* **2011**, *3*, 467−472.

(2)   Mukherjee, S.; Libisch, F.; Large, N.; Neumann, O.; Brown, L. V.; Cheng, J.; Lassiter, J. B.; Carter, E. A.; Nordlander, P.; Halas, N. J. Hot Electrons Do the Impossible: Plasmon-Induced Dissociation of H2 on Au. *Nano Lett.* **2013**, *13*, 240−247.

(3)   Kale, M. J.; Avanesian, T.; Christopher, P. Direct Photocatalysis by Plasmonic Nanostructures. *ACS Catal.* **2014**, *4,* 116−128.

(4)   Kim, Y.; Torres, D. D.; Jain, P. K. Activation Energies of Plasmonic Catalysts. *Nano Lett.* **2016**, *16*, 3399−3407.

(5)   Yu, S.; Wilson, A. J.; Kumari, G.; Zhang, X.; Jain, P. K. Opportunities and Challenges of Solar- Energy-Driven Carbon Dioxide to Fuel Conversion with Plasmonic Catalysts. *ACS Energy Lett.* **2017**, *2*, 2058−2070.

(6)   Aslam, U.; Rao, V. G.; Chavez, S.; Linic, S. Catalytic Conversion of Solar to Chemical Energy on Plasmonic Metal Nanostructures. *Nat. Catal.* **2018**, *1*, 656−665.

(7)   Dasog, M. Transition Metal Nitrides Are Heating Up the Field of Plasmonics. *Chem. Mater.* **2022**, *34*, 4249−4258.

(8)   Link, S.; El-Sayed, M. A. Shape and Size Dependence of Radiative, Non-Radiative and Photothermal Properties of Gold Nanocrystals. *Int. Rev. Phys. Chem.* **2000**, *19*, 409−453.

(9)   Hartland, G. V. Optical Studies of Dynamics in Noble Metal Nanostructures. *Chem. Rev.* **2011**, *111*, 3858−3887.

(10)   Stiles, P. L.; Dieringer, J. A.; Shah, N. C.; Van Duyne, R. P. Surface-Enhanced Raman Spectroscopy. *Annu. Rev. Anal. Chem.* **2008**, *1*, 601−626.

(11)   Stranahan, S. M.; Willets, K. A. Super-resolution Optical Imaging of Single-Molecule SERS Hot Spots. *Nano Lett.* **2010**, *10,* 3777−3784.

(12) Roy, S.; Roy, S.; Rao, A.; Devatha, G.; Pillai, P. P. Precise Nanoparticle−Reactant Interaction Outplays Ligand Poisoning in Visible-Light Photocatalysis. *Chem. Mater.* **2018**, *30*, 8415−8419.

(13) Roy, S.; Jain, V.; Kashyap, R. K.; Rao, A.; Pillai, P. P. Electrostatically Driven Multielectron Transfer for the Photocatalytic Regeneration of Nicotinamide Cofactor. *ACS Catal.* **2020**, *10*, 5522− 5528.

(14) Boyer, D.; Tamarat, P.; Maali, A.; Lounis, B.; Orrit, M. Photothermal Imaging of Nanometer-Sized Metal Particles among Scatterers. *Science* **2002**, *297*, 1160−1163.

(15) Govorov, A. O.; Richardson, H. H. Generating Heat with Metal Nanoparticles. *Nano Today* **2007**, *2*, 30−38.

(16) Baffou, G. *Thermoplasmonics: Heating Metal Nanoparticles Using Light*, 1st ed.; Cambridge University Press, 2017.

(17) Jauffred, L.; Samadi, A.; Klingberg, H.; Bendix, P. M.; Oddershede, L. B. Plasmonic Heating of Nanostructures. *Chem. Rev.* **2019**, *119*, 8087−8130.

(18) Chang, L.; Besteiro, L. V.; Sun, J.; Santiago, E. Y.; Gray, S. K.; Wang, Z.; Govorov, A. O. Electronic Structure of the Plasmons in Metal Nanocrystals: Fundamental Limitations for the Energy Efficiency of Hot Electron Generation. *ACS Energy Lett.* **2019**, *4*, 2552−2568.

(19) Baffou, G.; Cichos, F.; Quidant, R. Applications and Challenges of Thermoplasmonics. *Nat. Mater.* **2020**, *19*, 946−958.

(20) Klemmed, B.; Besteiro, L. V.; Benad, A.; Georgi, M.; Wang, Z.; Govorov, A.; Eychmüller, A. Hybrid Plasmonic−Aerogel Materials as Optical Superheaters with Engineered Resonances. *Angew. Chem., Int. Ed.* **2020**, *59*, 1696−1702.

(21) Zhou, L.; Swearer, D. F.; Zhang, C.; Robatjazi, H.; Zhao, H.; Henderson, L.; Dong, L.; Christopher, P.; Carter, E. A.; Nordlander, P.; Halas, N. J. Quantifying Hot Carrier and Thermal Contributions in Plasmonic Photocatalysis. *Science* **2018**, *362*, 69−72.

(22) Kamarudheen, R.; Aalbers, G. J. W.; Hamans, R. F.; Kamp, L. P. J.; Baldi, A. Distinguishing Among All Possible Activation Mechanisms of a Plasmon-Driven Chemical Reaction. *ACS Energy Lett.* **2020**, *5*, 2605−2613.

(23) Hirsch, L. R.; Stafford, R. J.; Bankson, J. A.; Sershen, S. R.; Rivera, B.; Price, R. E.; Hazle, J. D.; Halas, N. J.; West, J. L. Nanoshell-mediated Near-infrared Thermal Therapy of Tumors Under Magnetic Resonance Guidance. *Proc. Natl. Acad. Sci. U.S.A.* **2003**, *100*, 13549− 13554.

(24) Huang, X.; El-Sayed, I. H.; Qian, W.; El-Sayed, M. A. Cancer Cell Imaging and Photothermal Therapy in the Near-Infrared Region by Using Gold Nanorods. *J. Am. Chem. Soc.* **2006**, *128*, 2115−2120.

(25) Neumann, O.; Urban, A. S.; Day, J.; Lal, S.; Nordlander, P.; Halas, N. J. Solar Vapor Generation Enabled by Nanoparticles. *ACS Nano* **2013**, *7*, 42−49.

(26) Zhao, F.; Guo, Y.; Zhou, X.; Shi, W.; Yu, G. Materials for Solar-Powered Water Evaporation. *Nat. Rev. Mater.* **2020**, *5*, 388−401.

(27) Karaballi, R. A.; Monfared, Y. E.; Dasog, M. Photothermal Transduction Efficiencies of Plasmonic Group 4 Metal Nitride Nanocrystals. *Langmuir* **2020**, *36*, 5058−5064.

(28) Vázquez-Vázquez, C.; Vaz, B.; Giannini, V.; Pérez-Lorenzo, M.; Alvarez-Puebla, R. A.; Correa-Duarte, M. A. Nanoreactors for Simultaneous Remote Thermal Activation and Optical Monitoring of Chemical Reactions. *J. Am. Chem. Soc.* **2013**, *135*, 13616−13619.

(29) Strozyk, M. S.; Carregal-Romero, S.; Henriksen-Lacey, M.; Brust, M.; Liz-Marzán, L. M. Biocompatible, Multiresponsive Nanogel Composites for Codelivery of Antiangiogenic and Chemotherapeutic Agents. *Chem. Mater.* **2017**, *29*, 2303−2313.

(30) Govorov, A. O.; Zhang, W.; Skeini, T.; Richardson, H.; Lee, J.; Kotov, N. A. Gold Nanoparticle Ensembles as Heaters and Actuators: Melting and Collective Plasmon Resonances. *Nanoscale Res. Lett.* **2006**, *1*, 84– 90.

(31) Lalisse, A.; Tessier, G.; Plain, J.; Baffou, G. Quantifying the Efficiency of Plasmonic Materials for Near-Field Enhancement and Photothermal Conversion. *J. Phys. Chem. C* **2015**, *119*, 25518– 25528.

(32) Banholzer, M. J.; Qin, L.; Millstone, J. E.; Osberg, K. D.; Mirkin, C. A. On-Wire Lithography: Synthesis, Encoding and Biological Applications. *Nat. Protoc.* **2009**, *4*, 838−848.

(33) Pillai, P. P.; Pacławski, K.; Kim, J.; Grzybowski, B. A. Nanostructural Anisotropy Underlies Anisotropic Electrical Bistability. *Adv. Mater.* **2013**, *25*, 1623−1628.

(34) Jana, N. R.; Peng, X. Single-Phase and Gram-Scale Routes toward Nearly Monodisperse Au and Other Noble Metal Nanocrystals. *J. Am. Chem. Soc.* **2003**, *125*, 14280–14281.

(35) Roy, S.; Roy, S.; Rao, A.; Devatha, G.; Pillai, P. P. Precise Nanoparticle–Reactant Interaction Outplays Ligand Poisoning in Visible-Light Photocatalysis. *Chem. Mater.* **2018**, *30*, 8415–8419.

(36) Zelisko, P. M.; Amarne, H. Y.; Bain, H. D.; Neumann, K. Extensions of a Basic Laboratory Experiment: [4 + 2] and [2 + 2] Cycloadditions. *J. Chem. Educ*. **2008**, *85*, 104–106.

(37) Kim, Y.; Smith, J. G.; Jain, P. K. Harvesting Multiple Electron–Hole Pairs Generated through Plasmonic Excitation of Au Nanoparticles. *Nat. Chem.***2018**, *10*, 763–769.

(38) Liu, X.; Atwater, M.; Wang, J.; Huo, Q. Extinction Coefficient of Gold Nanoparticles with Different Sizes and Different Capping Ligands *Colloids Surface B*. **2007**, *58*, 3-7.

(39) Burns, E. N. V.; Lear, B. J. Controlled Rapid Formation of Polyurethane at 700 K: Thermodynamic and Kinetic Consequences of Extreme Photothermal Heating. *J. Phys. Chem. C* **2019**, *123*, 14774−14780.

(40) Zhu, Q.; Ye, K.; Zhu, W.; Xu, W.; Zou, C.; Song, L.; Sharman, E.; Wang, L.; Jin, S.; Zhang, G.; Luo, Y.; Jiang, J. A. Hydrogenated Metal Oxide with Full Solar Spectrum Absorption for Highly Efficient Photothermal Water Evaporation. *J. Phys. Chem. Lett.* **2020**, *11*, 2502– 2509.

(41) Burda, C.; Chen, X.; Narayanan, R.; El-Sayed, M. A. Chemistry and Properties of Nanocrystals of Different Shapes. *Chem. Rev*. **2005**, *105*, 1025−1102.

(42) Jain, P. K. Taking the Heat Off of Plasmonic Chemistry. *J. Phys. Chem. C* **2019**, *123*, 24347−24351.

(43) Zelisko, P. M.; Amarne, H. Y.; Bain, A. D.; Neumann, K. Extensions of a Basic Laboratory Experiment: [4+2] and [2+2] Cycloadditions. *J. Chem. Educ.* **2008**, *85*, 104.

(44) Yan, X.; Liu, G.; Xu, J.; Wang, S. Plasmon Heating of OneDimensional Gold Nanoparticle Chains. *Sol. Energy* **2018**, *173*, 665− 674.

(45) Gluodenis, M.; Foss, C. A. The Effect of Mutual Orientation on the Spectra of Metal Nanoparticle Rod−Rod and Rod−Sphere Pairs. *J. Phys. Chem. B* **2002**, *106*, 9484−9489.

(46) Thomas, K. G.; Barazzouk, S.; Ipe, B. I.; Joseph, S. T. S.; Kamat, P. V. Uniaxial Plasmon Coupling through Longitudinal Self-Assembly of Gold Nanorods. *J. Phys. Chem. B* **2004**, *108*, 13066−13068.

(47) Lee, S. J.; Morrill, A. R.; Moskovits, M. Hot Spots in Silver Nanowire Bundles for Surface-Enhanced Raman Spectroscopy. *J. Am. Chem. Soc*. **2006**, *128*, 2200−2201.

(48) Pramod, P.; Thomas, K. G. Plasmon Coupling in Dimers of Au Nanorods. *Adv. Mater.* **2008**, *20*, 4300−4305.

(49) Rao, A.; Roy, S.; Unnikrishnan, M.; Bhosale, S. S.; Devatha, G.; Pillai, P. P. Regulation of Interparticle Forces Reveals Controlled Aggregation in Charged Nanoparticles. *Chem. Mater.* **2016**, *28*, 2348− 2355.

(50) Rao, A.; Roy, S.; Pillai, P. P. Temporal Changes in Interparticle Interactions Drive the Formation of Transiently Stable Nanoparticle Precipitates. *Langmuir* **2021**, *37*, 1843−1849.

(51) Sun, Z.; Wang, J.; Wu, Q.; Wang, Z.; Wang, Z.; Sun, J.; Liu, C. J. Plasmon based double-layer hydrogel device for a highly efficient solar vapor generation. *Adv. Funct. Mater.* **2019**, *29*, 1901312.

(52) Chen, C.; Zhou, L.; Yu, J.; Wang, Y.; Nie, S.; Zhu, S.; Zhu, J. Dual functional asymmetric plasmonic structures for solar water purification and pollution detection. *Nano Energy* **2018**, *51*, 451– 456.

(53) Zhou, L.; Tan, Y.; Ji, D.; Zhu, B.; Zhang, P.; Xu, J.; Gan, Q.; Yu, Z.; Zhu, J. Self-Assembly of Highly Efficient, Broadband Plasmonic Absorbers for Solar Steam Generation. *Sci. Adv.* **2016**, *2*, e1501227– e1501227.

(54) Bae, K.; Kang, G.; Cho, S. K.; Park, W.; Kim, K.; Padilla, W. J. Flexible Thin-Film Black Gold Membranes with Ultrabroadband Plasmonic Nanofocusing for Efficient Solar Vapour Generation. *Nat. Commun.* **2015**, *6*, 10103.

(55) Kashyap, R. K.; Dwivedi, I.; Roy, S.; Roy, S.; Rao, A.; Subramaniam, C.; Pillai, P. P. Insights into the Utilization and Quantification of Thermoplasmonic Properties in Gold Nanorod Arrays. *Chem. Mater.* **2022**, *34*, 7369– 7378.

2.7. Appendix

Characterization of AuNR arrays
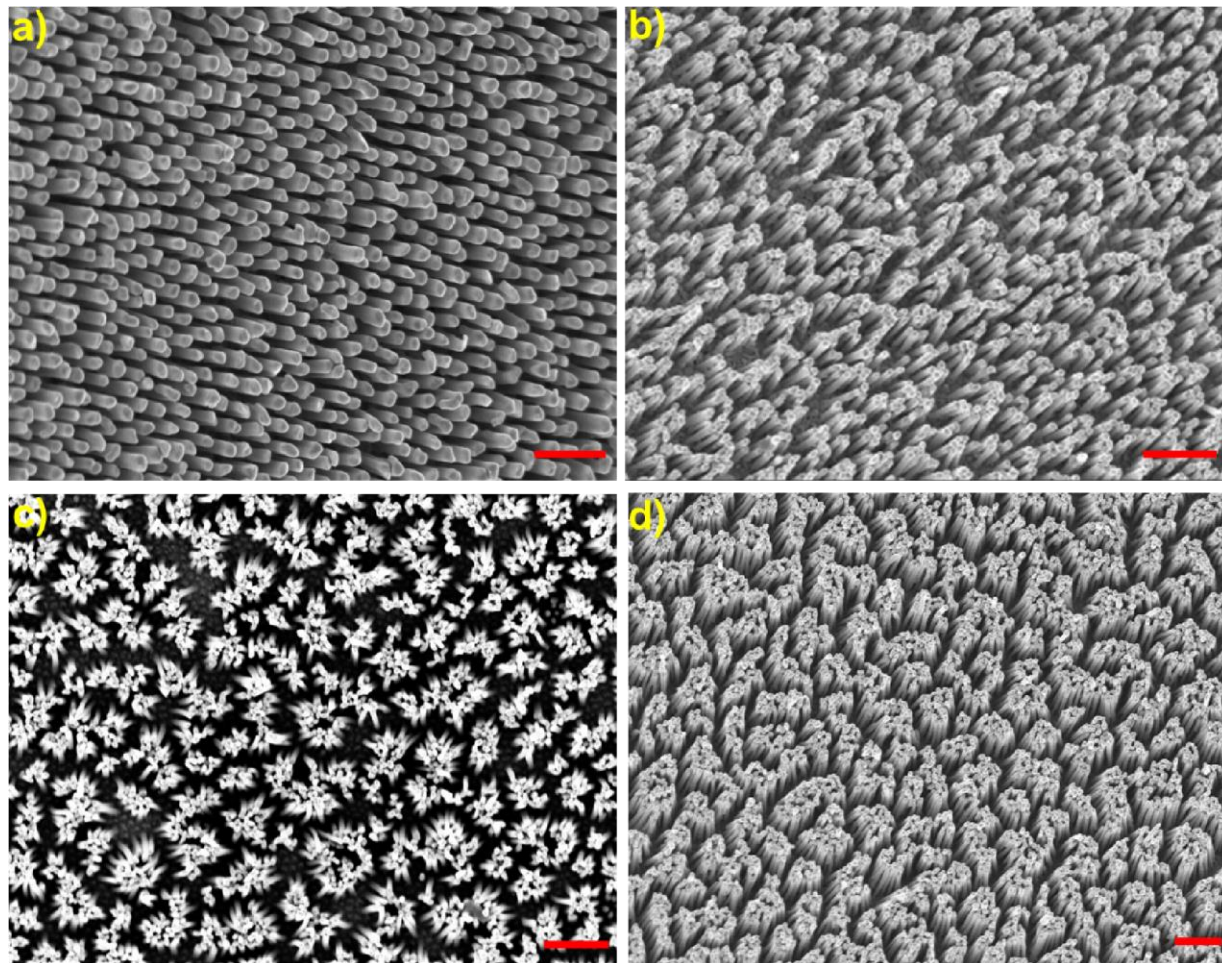
Figure 2.15. Large area SEM images of AuNR arrays: **(a)** 618 ± 47 nm long straight, **(b)** 752 ± 52 nm long bundled, **(c)** 880 ± 64 nm long bundled, and **(d)** 1188 ± 162 nm long bundled AuNR arrays, corresponding to electrodeposition times of 280, 330, 340, and 350 seconds, respectively. Scale bar corresponds to 1 μm.

Measurement of AuNR length:
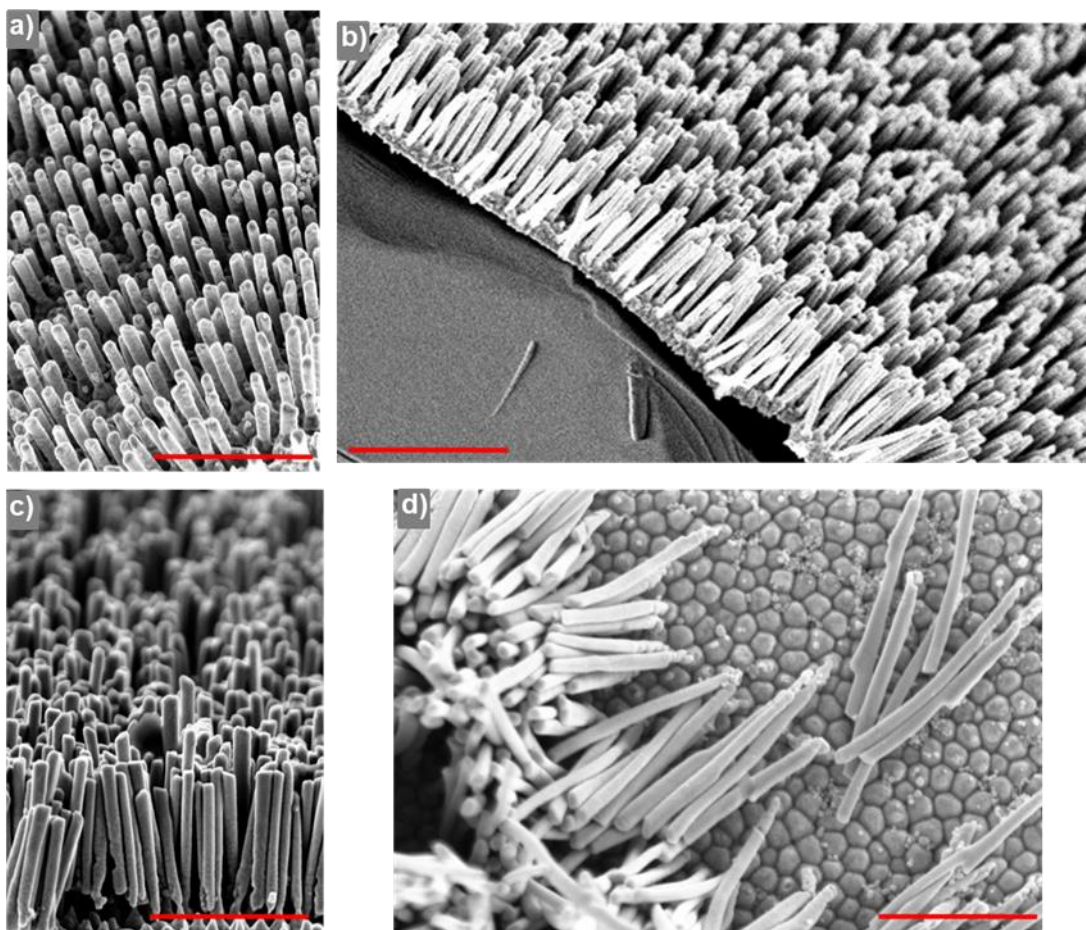
Figure 2.16. Representative SEM images of AuNR arrays used for the calculation of NR lengths: **(a)** 618 ± 47 nm long straight, **(b)** 752 ± 52 nm long bundled, **(c)** 880 ± 64 nm long bundled, and **(d)** 1188 ± 162 nm long bundled AuNR arrays. Scale bar corresponds to 1 µm.

Laser beam profile
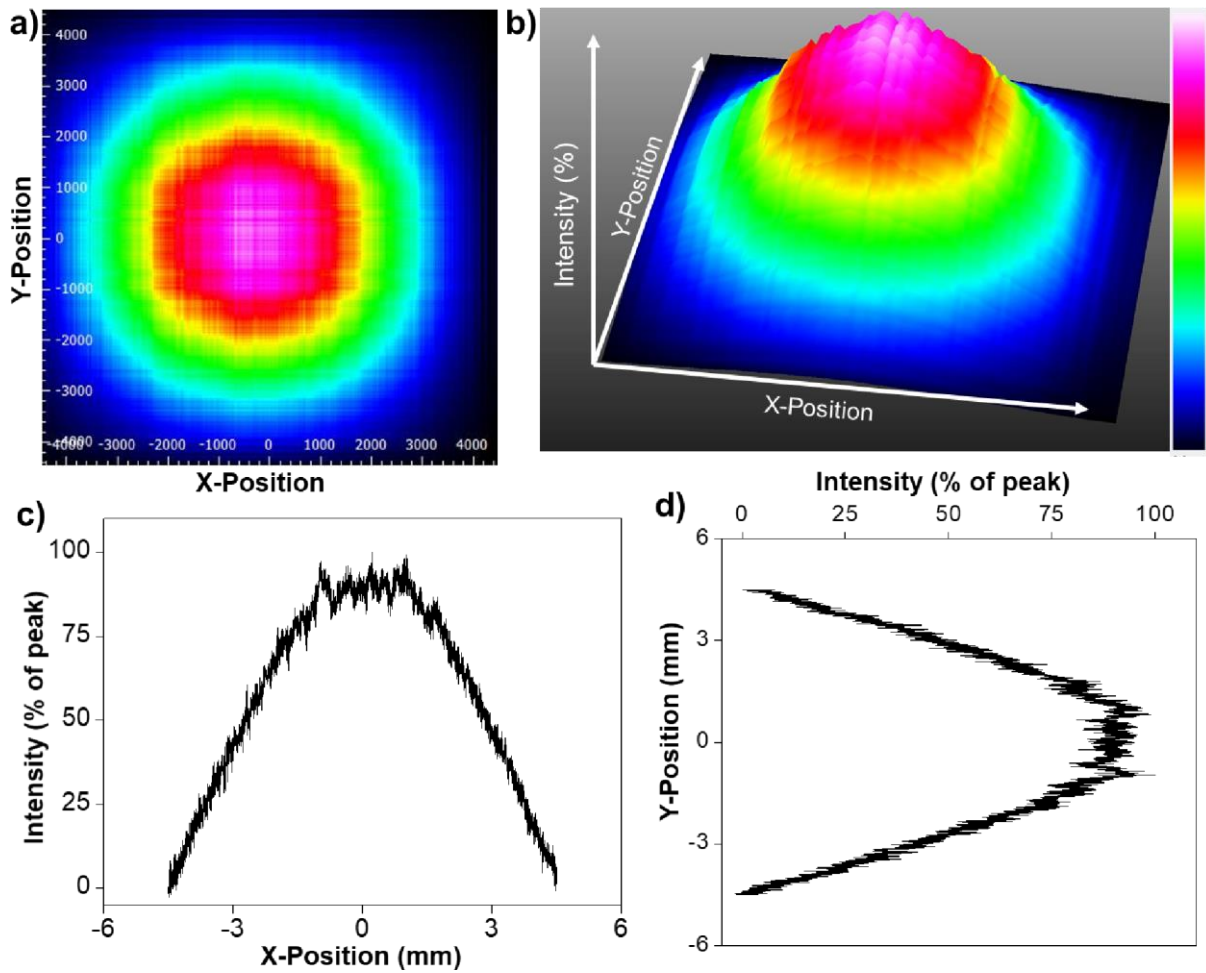
Figure 2.17. Laser beam profile measured at 1 cm beam diameter. **(a)** 2D and **(b)** 3D profiles of the beam clearly depict a gaussian distribution having maximum intensity at the central area of the beam, which decays away from the center point. The color code for the intensity is shown at right side of panel **(b)**. **(c)** and **(d)** The plots of beam profile along x-axis ($1/e^2$ diameter ~8 mm) and y-axis ($1/e^2$ diameter ~8 mm), showing the gaussian distribution.

Analysis of Diels-Alder reactions

Characterization of product:

^{1}H NMR Data: ^{1}H NMR (400 MHz, CDCl$_3$) δ 7.31 (dt, J = 13.4, 7.6 Hz, 5H), 5.00 (td, J = 10.8, 5.6 Hz, 1H), 3.53 – 3.37 (m, 1H), 2.92 – 2.74 (m, 1H), 2.63 (dd, J = 16.4, 4.5 Hz, 1H), 2.36 (t, J = 13.8 Hz, 2H), 1.72 (d, J = 16.9 Hz, 6H).
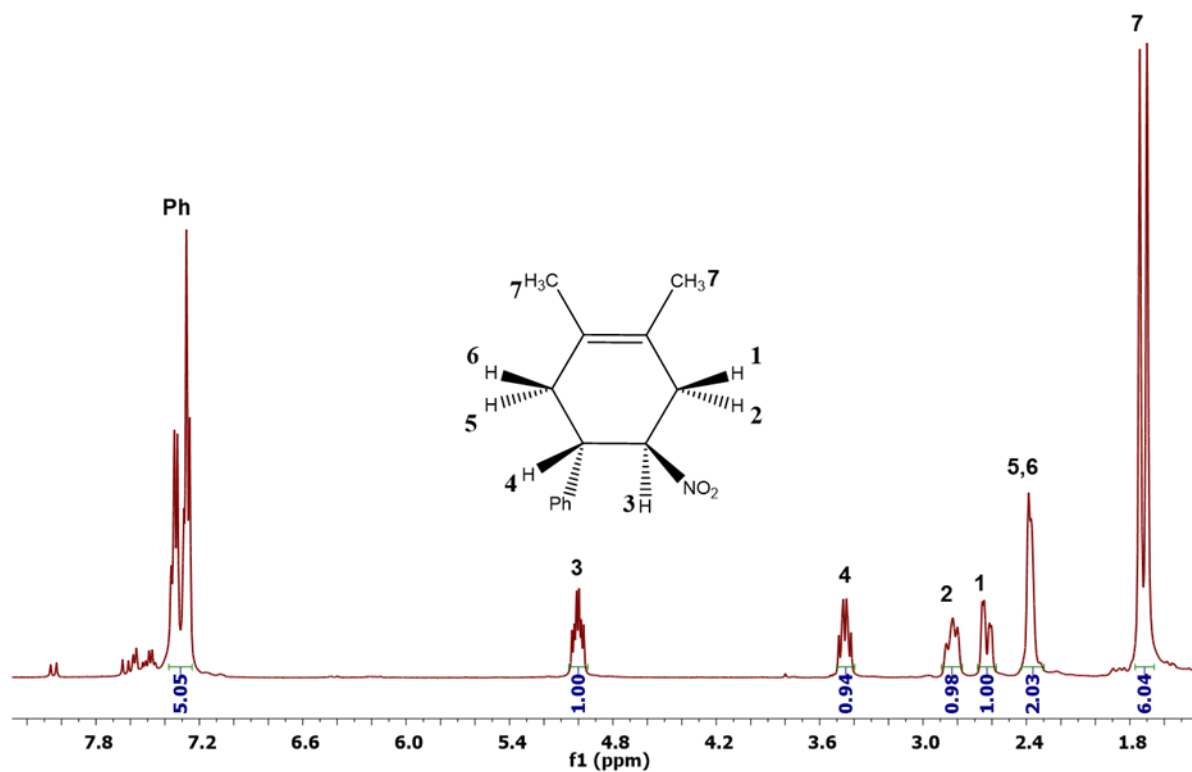
Figure 2.18. ^{1}H NMR spectrum of purified Diels-Alder product synthesized for the photothermal experiment, in the presence of bundled AuNR arrays. The NMR spectrum was collected in CDCl$_3$.

High-Resolution Mass Spectroscopy (HRMS):
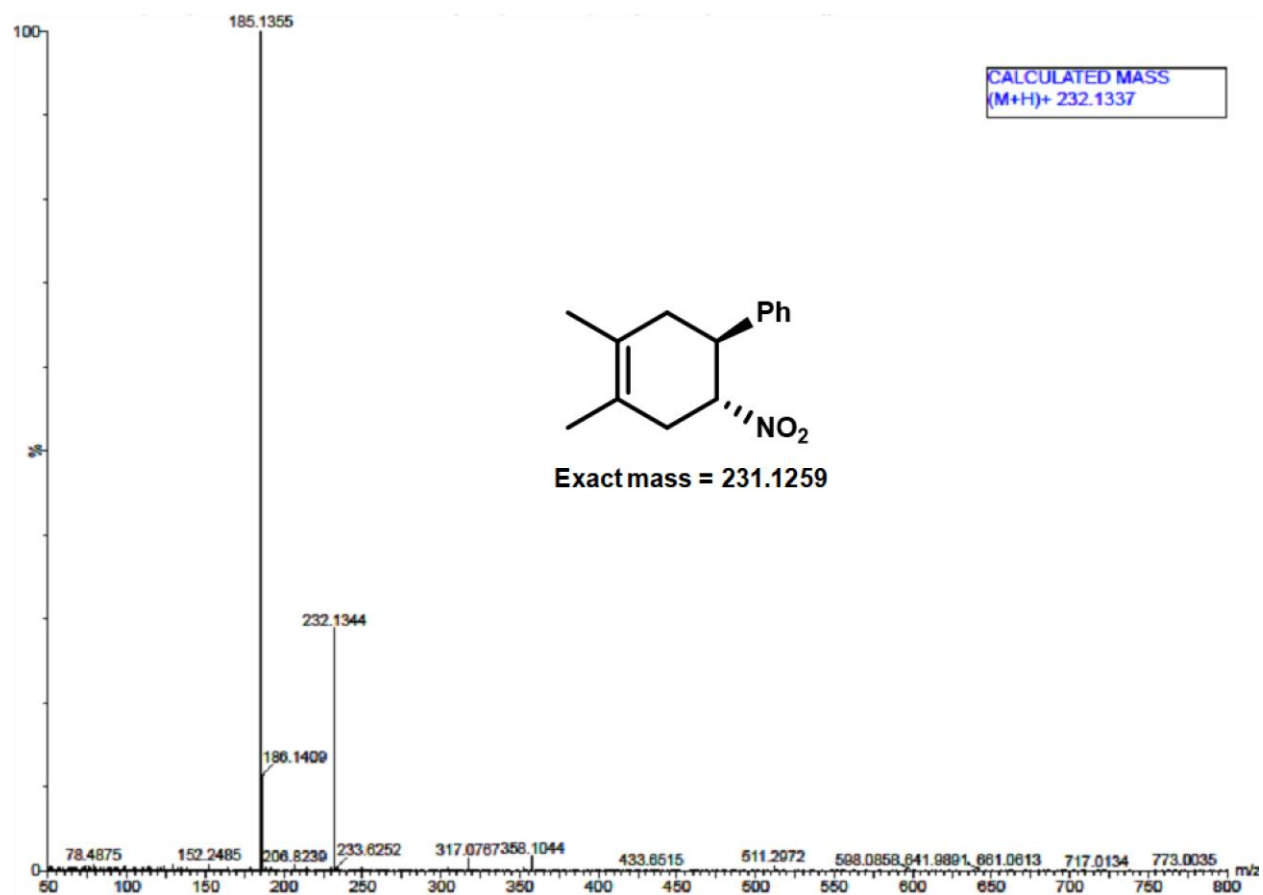
Figure 2.19. HRMS spectrum of purified Diels-Alder product synthesized from the photothermal experiment, in the presence of bundled AuNR arrays.
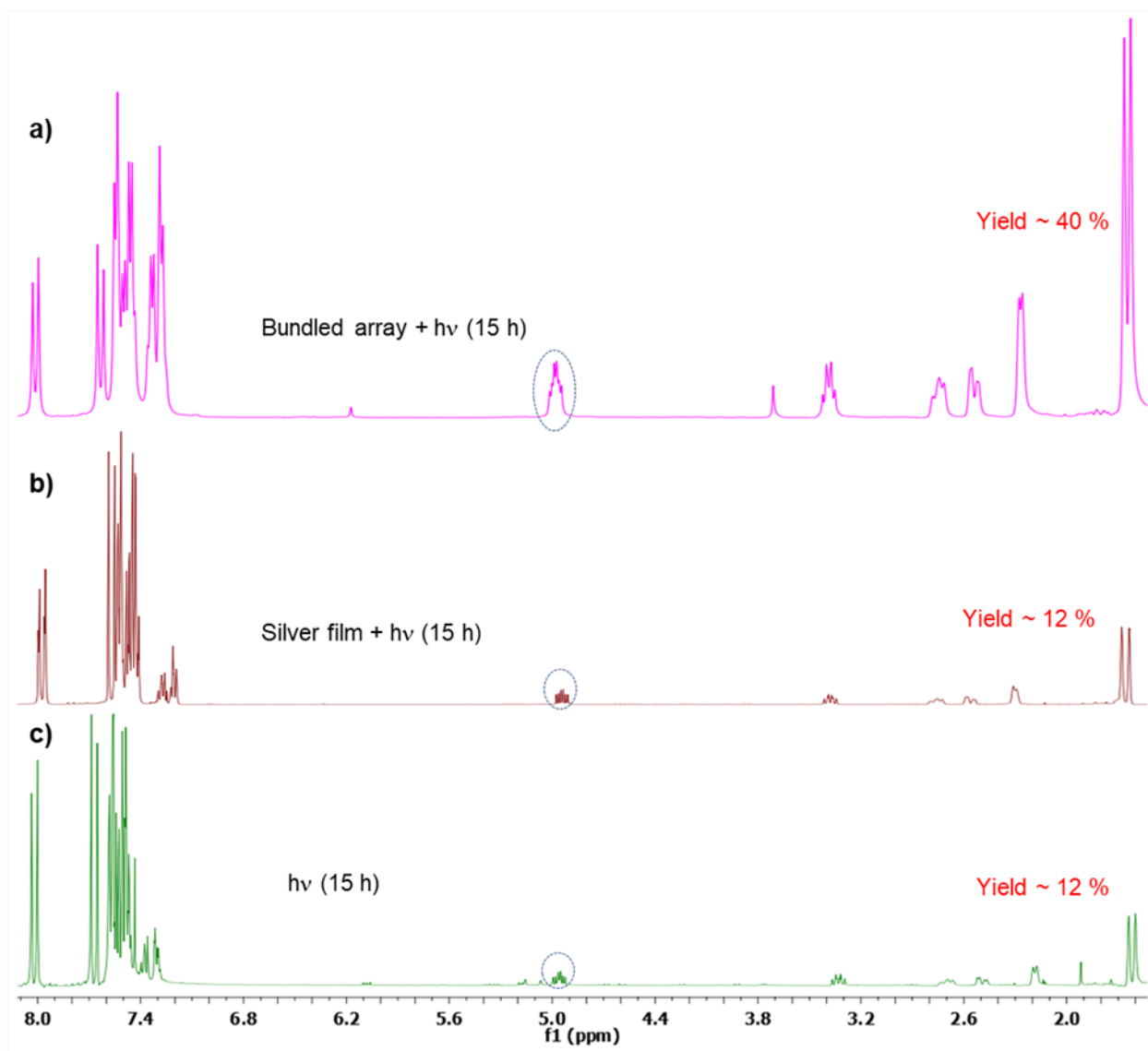
Figure 2.20. ¹H NMR spectra of crude reaction mixture for photothermal Diels-Alder reaction: **(a)** with bundled AuNR arrays under 532 nm laser irradiation, **(b)** with only silver film under 532 nm laser irradiation, and **(c)** with only the reactants under 532 nm laser irradiation.
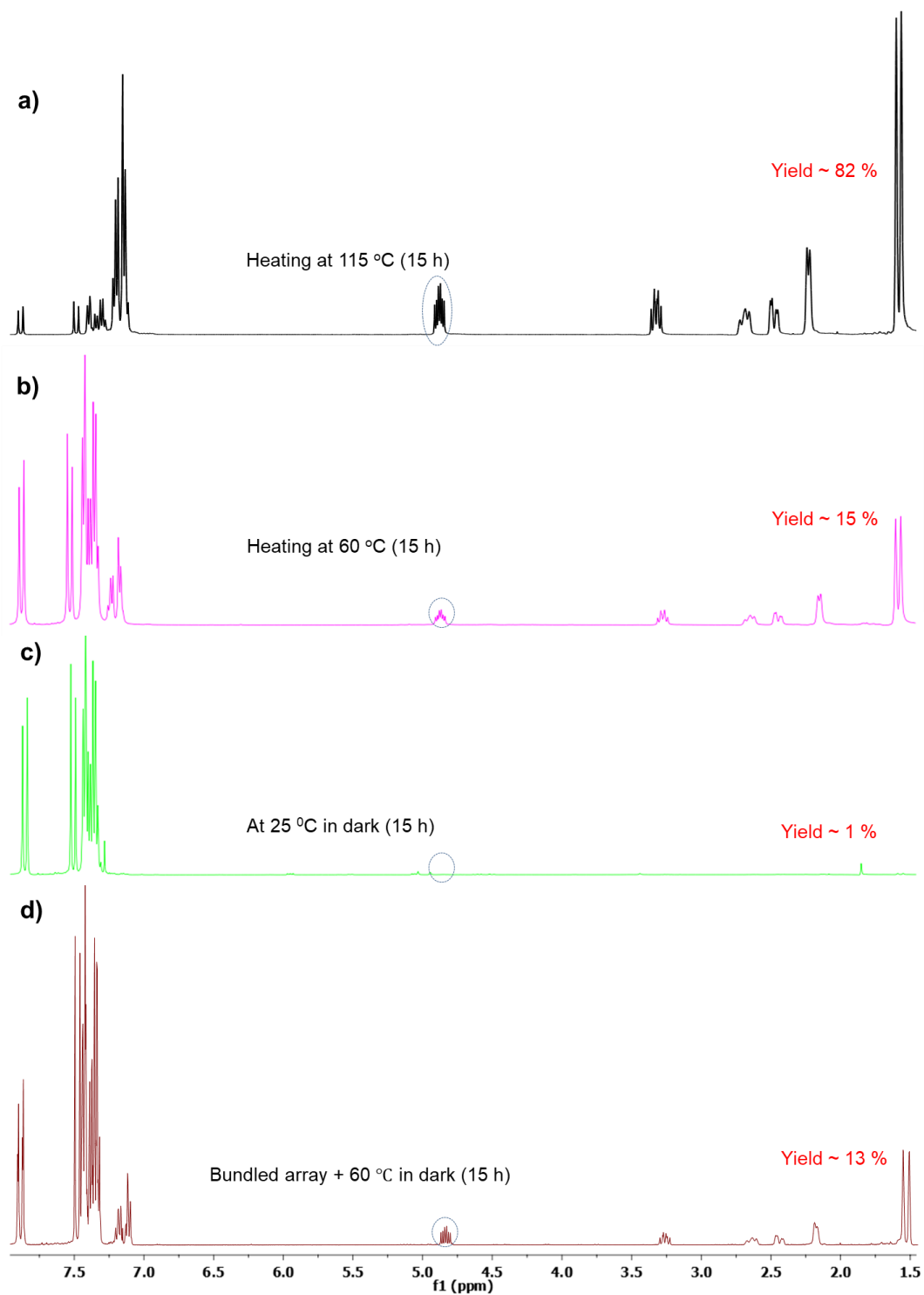
Figure 2.21. ^{1}H NMR spectra of the crude reaction mixture for Diels-Alder reaction in dark at **(a)**115 °C **(b)** 60 °C, **(c)** 25 °C in the absence of AuNR arrays, and **(d)** at 60 °C in the presence of bundled AuNR arrays.

Straight 1D-AuNR array with different lengths:
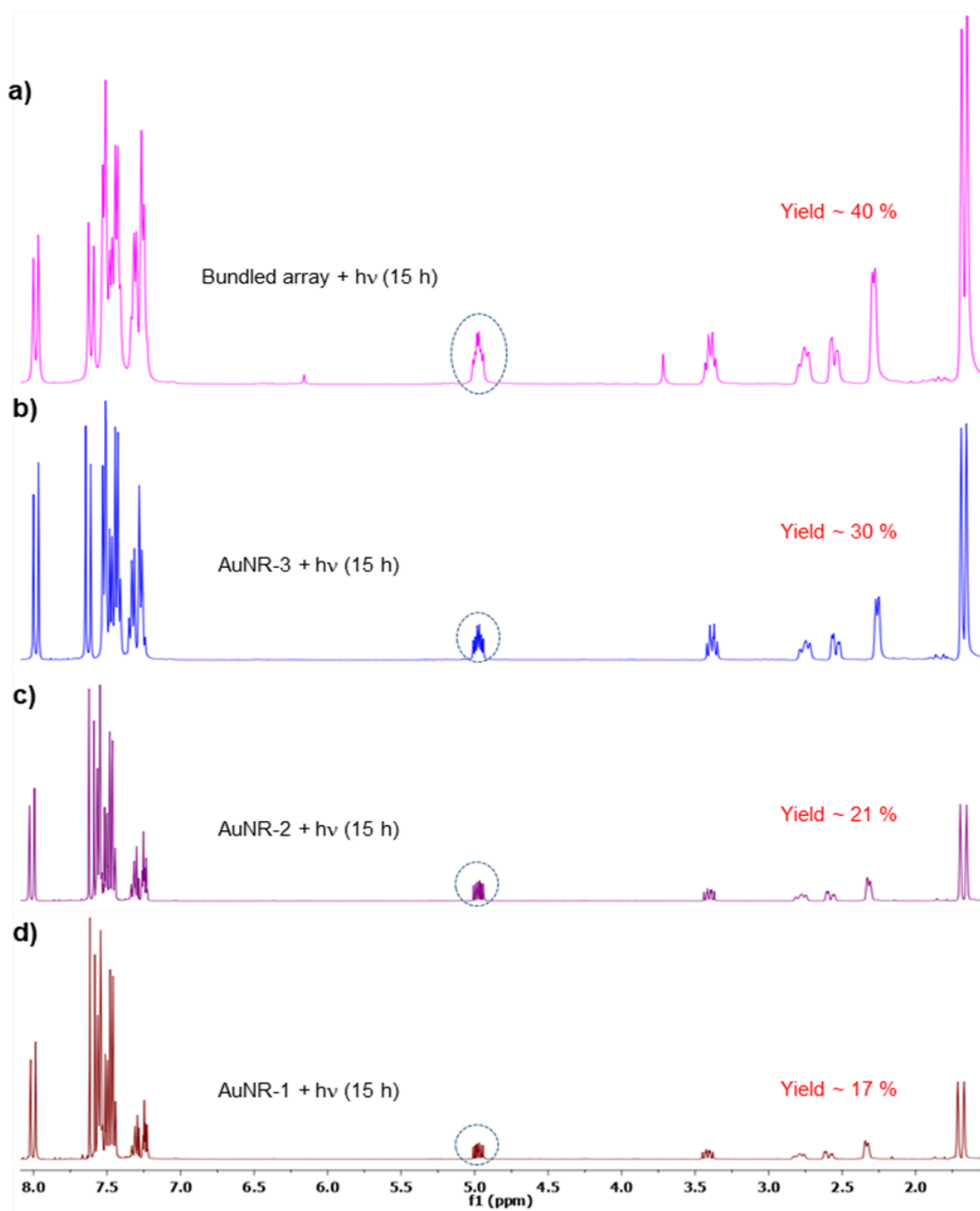
Figure 2.22. ^{1}H NMR spectra of crude reaction mixture for photothermal Diels-Alder reaction in the presence of **(a)** bundled AuNR arrays, **(b)** straight AuNR-3 arrays with NR length 618 ± 47, **(c)** straight AuNR-2 with NR length 534 ± 47 nm, and **(d)** straight AuNR-1 arrays with NR length 400 ± 51 nm.
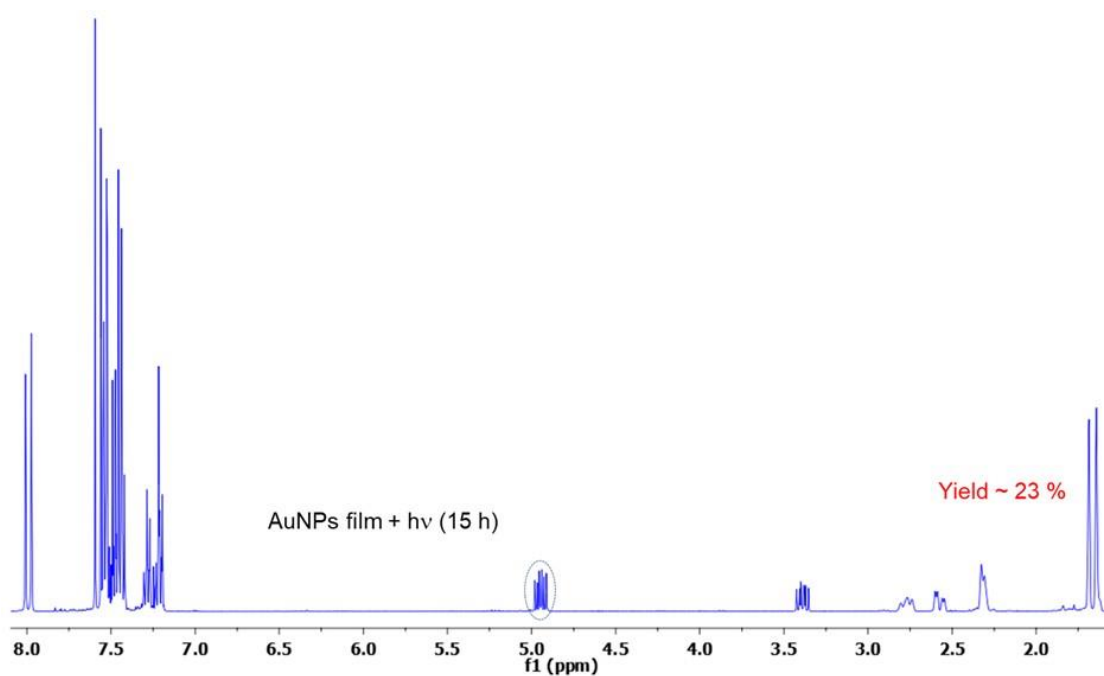
Figure 2.23. ¹H NMR spectra of crude reaction mixture for photothermal Diels-Alder reaction, in the presence of 11.9 ± 1.0 nm spherical AuNPs under 532 nm laser irradiation.

Solar-vapor generation without AuNR array
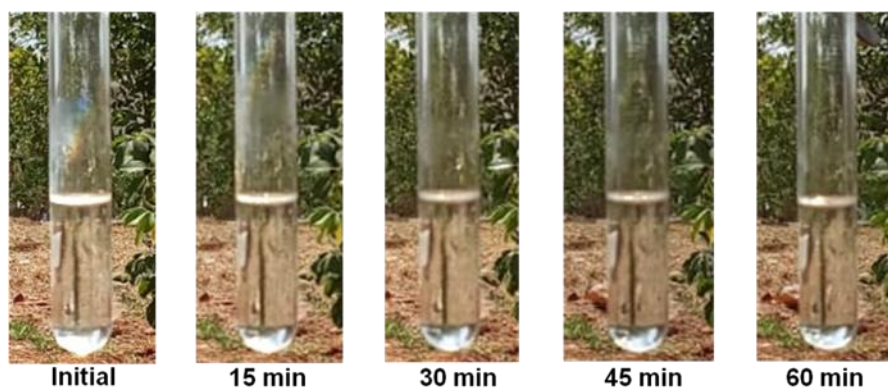
Figure 2.24. Photographs of test tubes containing 5 mL water in the absence of bundled AuNR arrays, at different time intervals of solar irradiation.

Chapter – 3

Quantification of Chemical Effectiveness of Plasmonic Heat

Bundled AuNR array

This chapter has been adapted from the following paper. Copyright 2022, American Chemical Society:

Kashyap, R. K.; Dwivedi, I.; Roy, S.; Roy, S.; Rao, A.; Subramaniam, C.; Pillai, P. P. Insights into the Utilization and Quantification of Thermoplasmonic Properties in Gold Nanorod Arrays. *Chem. Mater.* **2022**, *34*, 7369–7378.

3.1. Abstract

The quantification of plasmonic heat is necessary but challenging in the field of thermoplasmonics due to the localized nature of plasmonic heat. Conventional methods of measuring temperature cannot be used on the nanoscale because of restrictions in the size of the thermometers or lack of accessibility to the area of interest. There has been exploration of various quantification techniques and this area is popularly known as nanothermometry where the goal is to quantify the nanoscopic heat. In this Chapter, we will discuss our attempt to quantify the temperature-change in the surroundings caused due to the plasmonic heat. This is termed as chemical effectiveness of plasmonic heat which is the effective heat experienced by molecules around the nanostructure, which may trigger a chemical change. We have used the property of irreversible thermochromism as a marker to indirectly quantify the plasmonic heat where the heat from optically illuminated nanostructures could activate a color transition in the thermochromic molecule. The unprecedented use of thermochromism in quantifying the thermalization process shows that the surface of gold nanorod (AuNR) arrays can heat up to ~250 °C within ~15 min of irradiation. The measured temperature is independently validated with three different techniques photothermal melting studies, Raman spectroscopy, and standard infrared-based thermometric imaging studies. The plasmonic heat reported by the thermochromic studies is the lower limit corresponding to the phase change temperature of the thermochromic molecule, and the actual surface temperature of bundled AuNR arrays could be higher. Moreover, we have found that the amount of heat dissipated depends upon the nature of the surrounding medium as well as the reaction condition. The maximum impact of surface temperature was observed when substrates were adsorbed onto the AuNR arrays, whereas the influence of thermoplasmonic heat was minimum when the experiments were performed in a solution state.

3.2. Introduction

There are multiple techniques developed for nanoscopic temperature measurement which can be subdivided into two broad classes (**Figure 3.1**) based on their capability to measure the temperature.[1-8] The first class measures the surface-average temperature of an array of nanoparticles, while the second kind, known as single particle techniques, measures the temperature of individual nanoparticles. Both of these techniques are equally important for plasmon-driven processes depending upon the material type (single particle/multiparticle).[9-12]
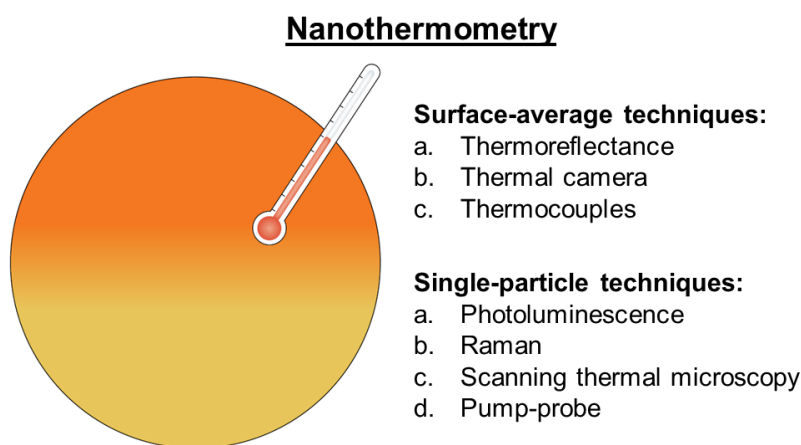
Figure 3.1. Schematic representation of various techniques used to measure the temperature at the nanoscale. This research field is known as *nanaothermometry*. Existing nanothermometers are divided based on their readout capabilities: surface average vs single-particle measurement. Reproduced with permission from ref. 8. Copyright: 2022, Nature Publishing Group.

Thermoreflectance-based techniques rely on the measurement of changes in temperature-dependent reflectance intensity by sample (**Figure 3.2a**). Although the normal reflectance intensity often changes very little with temperature, it can be linearized over a broad temperature range, which can render temperature measurement in plasmonic nanoscale assemblies.[13] A thermal camera detects the infrared radiation emitted by the heated material and converts it into a visual image of spatial thermal distribution (**Figure 3.2b**). It is a non-contact technique that is widely used to measure the temperature of plasmonic reactors in plasmon-driven chemistry.[14,15] On the other hand thermocouple-based measurement is a contact-based technique which works on the principle of the Seebeck effect arising due to thermal gradient across the thermocouple (**Figure 3.2c**).[16] All these techniques report the average temperature achieved under irradiation and have

poor spatial resolution. However, they could be extremely useful in analyzing the thermal effect resulting from the collective effect of nanoparticles in plasmon-driven processes.
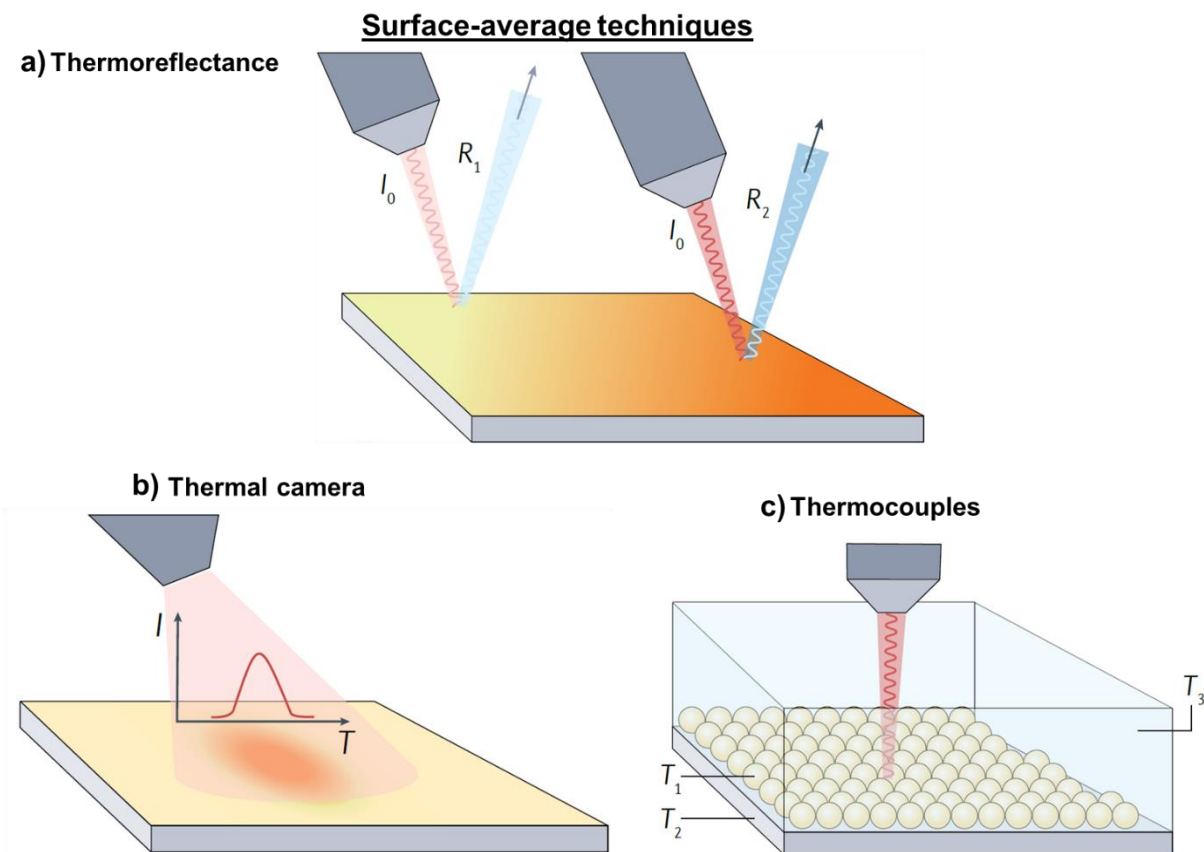
Figure 3.2. Schematic representation of working principle of nanothermometers capable of measuring surface-average temperature. (a) Thermoreflectance nanothermometer works on the principle of temperature-dependent reflectivity. (b) A thermal camera works on the principle of analyzing the black body radiation from a heated object to map the surface temperature. (c) Thermocouples work on the Seebeck effect arising as a result of the thermal gradient. Reproduced with permission from ref. 8. Copyright: 2022, Nature Publishing Group.

Sigle-particle techniques (**Figure 3.3**) are mostly tagging-based measurements where a nanostructure is tagged with a particular molecule whose temperature-sensitive properties analysis helps to measure the temperature at the nanoscale. For example, the photoluminescence-based technique relies on temperature-dependent photoluminescence changes of a fluorescent marker attached to a nanostructure (**Figure 3.3a**).[17] In the same line, one recently developed technique relies on an anti-Stokes photoluminescence signal from the nanostructure itself after fitting the data with Bose-Einstein distribution.[18,19] Similarly, temperature-dependent Raman signal

variations of a Raman marker tagged to the nanostructure can be monitored to estimate the nanoscopic temperature of individual particles (**Figure 3.3b**).[20] A separate method of directly measuring surface temperature with spatial resolution is using a nanoscopic thermally sensitive scanning probe termed as scanning thermal microscopy (SThM) (**Figure 3.3c**).[21] Lastly, a novel set of experiments that provide temperature data on the phonon and/or electrical system use pulsed illumination rather than continuous-wave illumination (**Figure 3.3d**). Ultrafast optical spectroscopy and ultrafast time-resolved electron diffraction are two techniques that may help us finish our comprehension of electron excitation and decay in plasmonic systems to move toward catalytic applications.[22]

Single-particle techniques

a) Photoluminescence
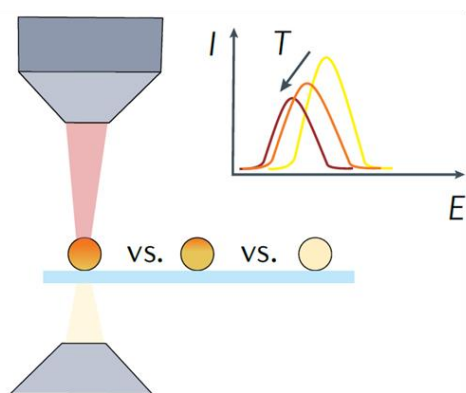
b) Raman
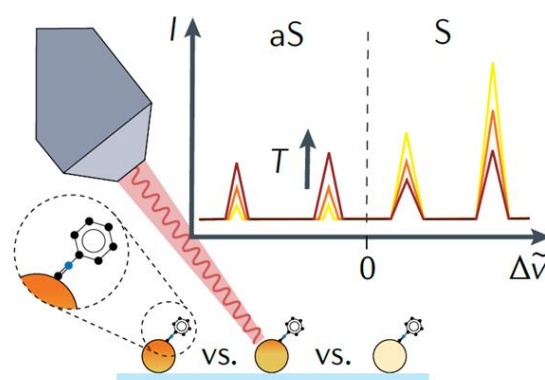
c) Scanning thermal microscopy
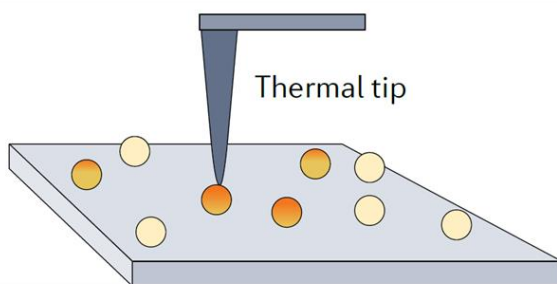
d) Pump–probe
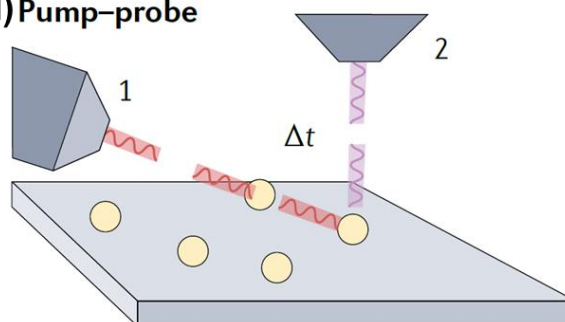
Figure 3.3. Working principle of single-particle nanothermometric techniques. (a) Photoluminescence-based techniques rely on the thermally sensitive photoluminescence changes in a fluorescence marker attached to a nanostructure. (b) Raman-based techniques measure temperature-dependent stokes and anti-stokes signal intensity variations of a Raman marker attached to the nanostructure to report temperature. (c) In a scanning thermal microscopy (SThM) the heat flow between the sample and a scanning thermally sensitive tip is exploited to map surface temperature with nanoscale spatial resolution. (d) Pump-probe

technique maps the dynamic temperature-dependent changes to report surface temperature. Reproduced with permission from ref. 8. Copyright: 2022, Nature Publishing Group.

As we can see, all the techniques discussed above require dedicated instrumentation and expertise to measure the temperature. Therefore, there is a need for a simple and cost-effective thermometric technique. In this direction, we have explored the phenomenon of thermochromism as a simple and reliable tool to quantify the practically usable thermoplasmonic heat close to the surface of nanostructures. The thermochromism studies reveal that the surface temperature on gold nanorod (AuNR) arrays can heat up to ~250 °C, within ~15 min of irradiation with a 1 W continuous wave green laser. The plasmonic heat reported by the thermochromic studies is the lower limit corresponding to the phase change temperature of the thermochromic molecule, and the actual surface temperature of bundled AuNR arrays could be higher. The thermoplasmonic heat was measured, independently, using melting, Raman spectroscopy, and direct infrared-based thermometric imaging techniques, which proves the suitability of thermochromism as a potential tool for the quantification of the thermalization process in plasmonic materials. Additionally, the analysis of the results from such direct thermometric imaging has provided insights into the heat-generation and heat-dissipative pathways. More importantly, the choice of reaction conditions turned out to be critical in utilizing as well as dissipating the thermoplasmonic heat to the surroundings.

3.3 Methods and Experimental Section

3.3.1. Materials and reagents:

Anodic alumina oxide (AAO) (pore diameter = 75 nm, pore length = 50 μm, and interpore distance 150 nm) templates were purchased from Smart Membranes. Au plating solution (Orotemp 24 RTU) was purchased from Lectrachem Ltd. (TECHNIC UK). Lead carbonate ($PbCO_3$), ammonium metavanadate (NH_4VO_3), cadmium acetate dihydrate ($Cd(CH_3COO)_2 \cdot 2H_2O$), and soybean oil were purchased from Sigma-Aldrich. All the reagents were used as received without any further purification.

3.3.2. Fabrication of gold nanorod (AuNR) arrays

Gold nanorod (AuNR) arrays of varying morphologies were fabricated following the reported three-step fabrication protocol, using anodic aluminum oxide (AAO) membranes as a template.[23,24] In a typical experiment, metallic silver (Ag) was thermally evaporated (growth rate 0.2 Å/s) to generate a high-quality ~200 nm Ag film on one side of the AAO template. Next, the AAO film was placed in the electrochemical cell for the deposition of Au. Au was electrodeposited in the pores of the AAO template by applying a constant potential of −975 mV (vs Ag/AgCl electrode) using a Au plating solution (Orotemp 24 RTU). Note that the charge limit was kept at 40 mC. The electrodeposition time was varied from 280 to 350 s for fabricating AuNR arrays with different morphologies. The AAO template was then etched by placing it in ~5 mL of 3 M NaOH for ~12 h and washed 4 times with Milli-Q water. The AuNR arrays were then carefully transferred onto a glass support and kept in an oven at 90 °C for ~10 min. The prepared AuNR arrays were stored in a vacuum desiccator to minimize aerial oxidation.

3.3.3. Thermochromic studies

Lead carbonate ($PbCO_3$) and ammonium meta vanadate (NH_4VO_3) were used as the thermochromic materials in our study.[25] The color changes were captured using a Macro Zoom Fluorescence Microscope System (Olympus MVX10). All of the snapshots were captured at 5X magnification. In a typical experiment, ~5 mg of lead carbonate was placed on bundled AuNR arrays and irradiated with a 1 W 532 nm CW diode laser for ~15 min under ambient conditions. **Figure 3.4** clearly shows that lead carbonate is localized solely at the surface of the Au nanorods. The snapshots were captured at different time intervals. Control experiments were carried out with a silver film as well as on glass substrates under the same conditions.

3.3.4. Intensity-dependent thermoplasmonically driven phase change in NH_4VO_3

In a typical experiment, ~1 g of NH_4VO_3 was uniformly distributed at the surface of the bundled AuNR arrays, which was then irradiated with a 532 nm CW diode laser at different intensities. The threshold light power required for the thermochromic phase change in NH_4VO_3 was 290 mW (it took ~3 h for the complete thermochromic phase change at 290 mW). Next, an intensity dependent

thermochromic phase change experiment was performed by gradually increasing the power of the laser source. As expected, the time required for the complete thermochromic phase change decreased as the power of the laser source was increased. Powder X-ray diffraction and Raman analyses confirmed that the final product contains a mixture of different phases of vanadium oxides (orthorhombic-V_2O_5, monoclinic-V_3O_7, monoclinic-V_6O_{13}, and tetragonal-VO_2), which is in good agreement with the literature reports.[26] **Figure 3.20** has been included in the Appendix for the intensity-dependent thermochromic study of ammonium metavanadate. It clearly shows that the time required for the complete thermochromic phase change decreased as the power of the laser source was increased.

3.3.5. Photothermal melting of cadmium acetate dihydrate

The melting of cadmium acetate dihydrate (melting point 255 °C) was performed using the thermoplasmonic heat generated from bundled AuNR arrays to validate the surface temperature measured from thermoplasmonic studies. In a typical experiment, ~5 mg of cadmium acetate dihydrate powder was uniformly placed at the surface of bundled AuNR arrays and irradiated with a 1 W 532 nm CW diode laser (1 W cm^{-2}) for ~1 min at 25 °C.

3.3.6. Photothermal polymerization of soybean oil

Soybean oil is a mixture of triglycerides, and its structure contains three fatty acids linked by a glycerol center. The unsaturated fatty acids have 1–3 double bonds. At 230 °C, polymerization occurs between these double bonds. The degree of unsaturation can be monitored by Raman spectroscopy and was defined by the ratio of stretching frequencies of vinyl C–H peak at 3014 cm^{-1} to the aliphatic C–H peak at 2855 cm^{-1}.[27] In a typical experiment, a drop of soybean oil was cast at the surface of bundled AuNR array, followed by irradiating the sample using a 1 W 532 nm CW diode laser for ~15 min. The Raman spectra of soybean oil were recorded on the bundled AuNR array before and after the irradiation (**Figure 3.13**). The ratio of unsaturated fatty acids to total fatty acids dropped from 0.41 to 0.31 after thermoplasmonic studies, which is characteristic of the initiation of the photothermal polymerization of soybean oil.[27] This again confirms that the surface temperature of the bundled AuNR array can reach at least 230 °C upon irradiation with a 1 W 532 nm CW diode laser. The Raman spectra were processed with baseline correction and smoothing.

3.3.7. Infrared thermometric studies

All of the thermometric studies were carried out using an A6703SC FLIR Thermal Camera having an InSb detector with an accuracy of ±2 °C. The thermal IR camera (A6703sc) by FLIR was calibrated upon heating the bundled AuNR arrays at an electrically heated thermal plate at known temperatures. The distance of the plate also affects the reading of the camera. Therefore, the same distance (20 cm) was maintained for flux measurement, as was used in calibration. The 1 W green laser source was kept vertically above the sample at a distance of ~10 cm. The thermal images were captured by keeping the thermal camera at an angle of 45°. Thermal images were recorded in the laser OFF state (0 s). This was followed by switching the laser ON to acquire temporal and spatial thermal images. Similarly, a control experiment was carried out by irradiating the silver substrate with a 1 W 532 nm CW diode laser till the saturation of its surface temperature.

3.3.8. Water evaporation experiments with laser irradiation

To study the role of reaction conditions, thermoplasmonic properties of bundled AuNR arrays were tested in liquid state transformation processes as well. For this, the water evaporation experiments were once again performed in the presence of bundled AuNR arrays, under irradiation conditions similar to the thermochromic study(with 1W green laser instead of focused sunlight). The weight of water merely decreased by ~180 mg in ~20 min, and the bulk temperature increased to ~ 45 °C, when 1W laser was used as the source of irradiation.

3.4. Results and Discussion

3.4.1. Fabrication of configurable thermoplasmonic AuNR arrays

Plasmon-driven processes are highly sensitive to the size, shape, and composition of nanostructured materials. In general, anisotropic nanostructures exhibit superior plasmonic properties over spherical nanomaterials because of their unique shape-dependent optoelectronic properties such as a high molar extinction coefficient, unidirectional charge transport, and edge effects.[28] In the present work, an array of highly configurable one-dimensional AuNRs was fabricated on a glass slide with the help of the template-mediated electrodeposition technique (**Section 3.3.2** in the Methods and Experimental Section).[23,24]

Briefly, an array of AuNRs was electrochemically grown in an anodic aluminum oxide (AAO) template having a silver backing layer (~200 nm thick), followed by the etching of the template with a 3 M sodium hydroxide solution. The AuNRs in the array had a diameter of ~75 nm, and the length was varied by controlling the electrodeposition time (280–350 s; already discussed in **Chapter 2**). At 280 s deposition time, the length of AuNRs in the array was estimated to be 618 ± 47 nm, and the array was distributed in a hexagonal lattice (already discussed in **Chapter 2**). The AuNRs started to lose their free-standing ability as well as the hexagonal lattice arrangement, as the NRs were grown beyond 752 ± 52 nm in length. The SEM studies clearly showed the bundling of AuNRs, corresponding to different electrodeposition times (already discussed in **Chapter 2**). Thus, different morphologies of AuNR arrays, ranging from straight to bundled arrangements, were uniformly fabricated over a large area (~0.6 cm^2). This flexibility in the fabrication protocol to form straight and bundled geometries can be beneficial in studying the influence of nanostructural morphology on various plasmonic properties.

The UV-visible spectrum showed appreciable absorption at a wavelength of 532 nm in the case of bundled AuNR arrays (already discussed in the **Chapter 2**) which motivated us to use a 532 nm excitation energy for studying the photothermal behavior of the geometry. Motivated by the scope of a broad range of photothermal applications shown by bundled AuNR arrays (already discussed in the **Chapter 2**) our next goal was to measure the plasmonic heat dissipated by these thermoplasmonic heaters.

3.4.2. Quantification of thermoplasmonic heat through thermochromism.

The direct monitoring and quantification of the thermalization process close to the surface of bundled AuNR arrays is discussed here. There are many elegant and reliable methodologies reported in the literature to measure the surface temperature of thermoplasmonic nanostructures.[1–8] We envisaged using the property of thermochromism to monitor the surface temperature of bundled AuNR arrays because an attractive visual color change will serve as the read out in this case (**Figure 3.4**). Moreover, the proposed thermal quantification technique based on thermochromism has multiple advantages over other quantification techniques. For example, it is cheaper, convenient, no dedicated instrumentation technique, calibration, or expertise is required (a visual color change acts as the readout) and could work in a liquid medium as well. Accordingly, a white-colored lead carbonate ($PbCO_3$) was chosen as the thermochromic molecule for the quantification of thermoplasmonic heat (~5 mg of $PbCO_3$ was homogeneously adsorbed on the surface of the bundled AuNR array, as shown in **Figure 3.4a,b**).
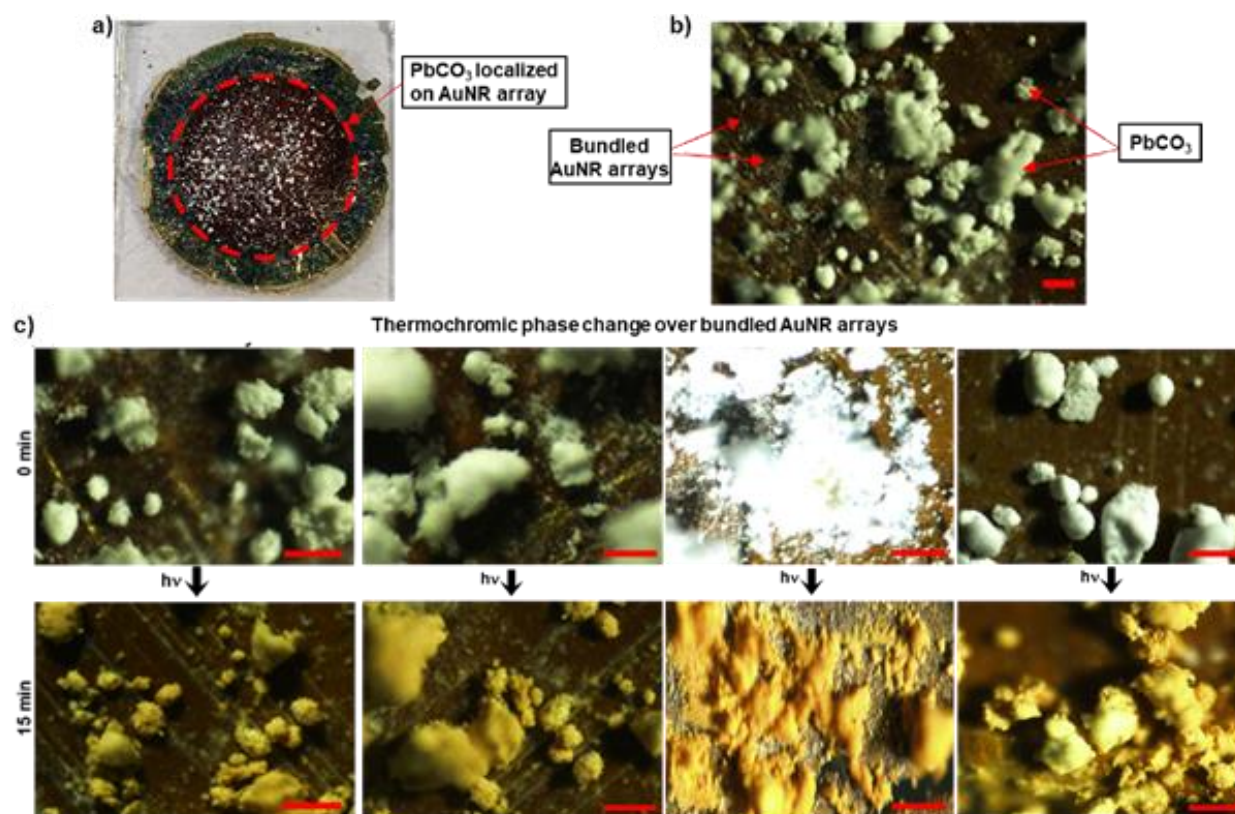

Figure 3.4. Photothermally driven thermochromic study of PbCO₃ at bundled AuNR array. (a) Full area and (b) magnified selected area optical images showing the uniform distribution of lead carbonate (white powder) on bundled AuNR array (reddish brown area). A large fraction of AuNR array is vacant to

have efficient optical absorption and thermoplasmonic heat generation. (c) A color change from white to yellow was observed after irradiating the $PbCO_3$ placed on the bundled AuNR arrays using a 1W 532 nm CW laser for ~ 15 min. Images from different areas are shown for proving the uniformity in color change over the entire sample. Note: The images marked as before (0 min) and after (15 min) does not correspond to the same area.

$PbCO_3$ is a well-known thermochromic molecule that will phase transform into a mixture of α- and β-lead oxide (PbO) at ~250 °C, accompanied by a visual color change from white to yellow.[29] The same color change was observed in our thermoplasmonic studies as well when $PbCO_3$ deposited on bundled AuNR arrays was irradiated with a 1 W CW green laser for ~15 min (**Figures 3.4a**). No noticeable color change was observed below 1 W. Detailed powder X-ray diffraction (PXRD) and Raman studies unambiguously confirm the quantitative photothermal transformation of $PbCO_3$ (orthorhombic *Pnma*) to PbO (a combination of tetragonal *P4/nmm* and orthorhombic Pbcm phases)[29,30] (**Figure 3.5a,b**).
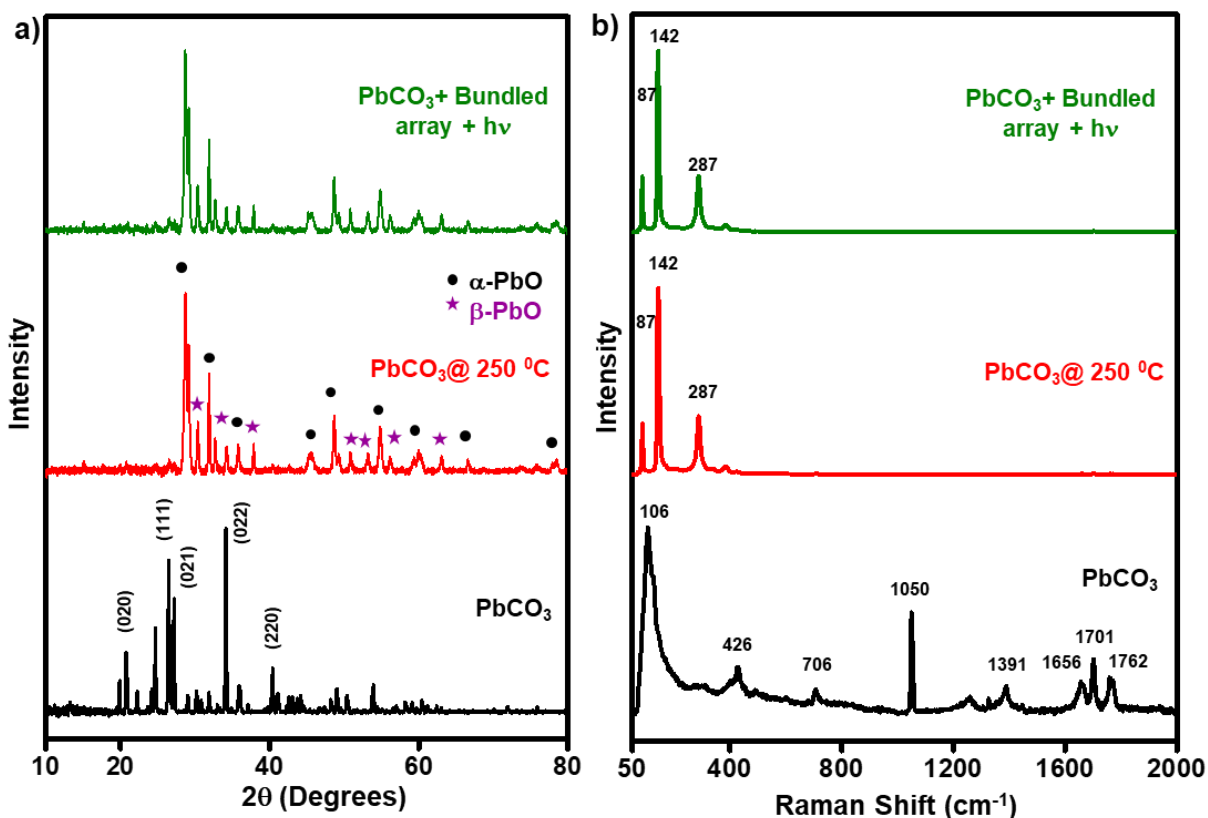
Figure 3.5. Characterization of the crystal-to-crystal transformation by thermochromism. The (a) PXRD and (b) Raman spectra confirm the transformation of orthorhombic $PbCO_3$ to a mixture of α- and β-lead oxide (tetragonal and orthorhombic phases). PXRD as well as Raman spectra of $PbCO_3$ before and

after the irradiation in the presence of bundled AuNR arrays, and thermally treated $PbCO_3$ at 250 °C confirm that the transformation in $PbCO_3$ was indeed triggered by the thermoplasmonic heat generated in bundled AuNR arrays.

Bare glass slide as well as silver film failed to show any thermochromic change, even when irradiated for 1 h under similar experimental conditions (**Figure 3.6a,b**). Thus, control experiments (with bare/silver-coated glass slides and thermal heating) confirm that the changes observed in thermochromic molecules were indeed triggered by the thermoplasmonic heat generated from bundled AuNR arrays (**Figure 3.6**).
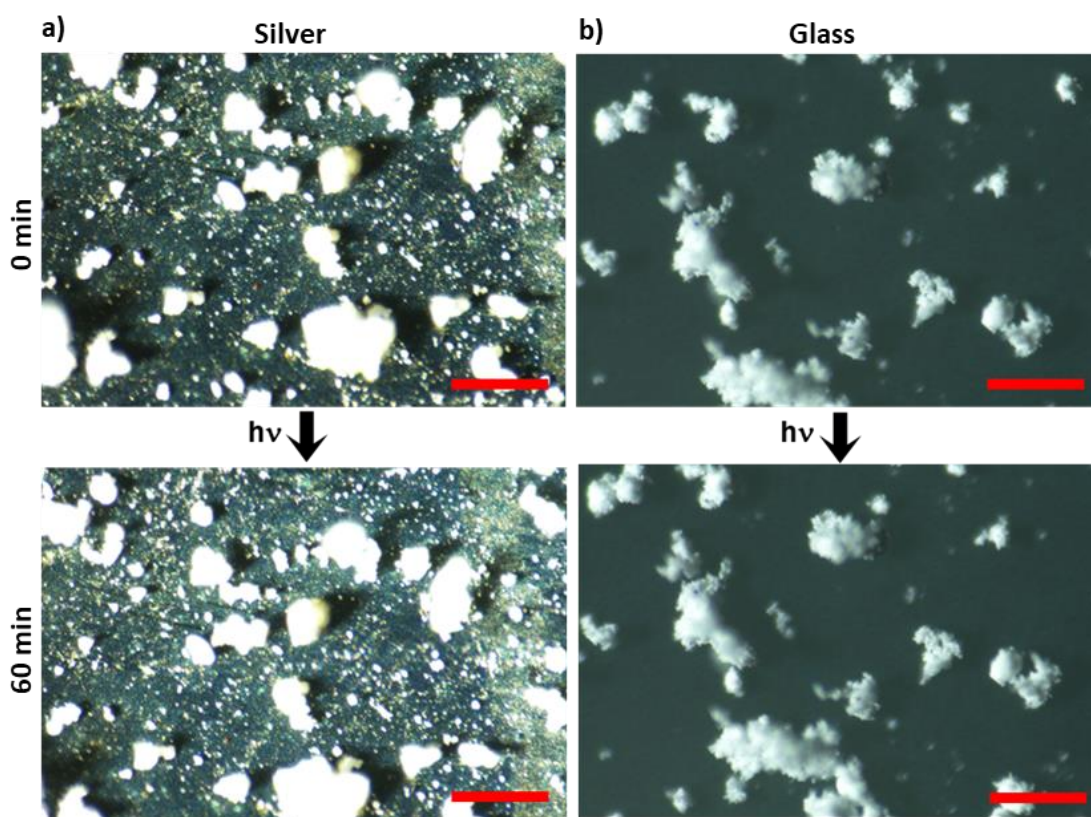
Figure 3.6. Optical images obtained before and after irradiating the $PbCO_3$ placed on (a) only silver film and (b) only glass surface using a 1W 532 nm CW laser for ~ 1 h. Scale bars correspond to 200 μm for all images. The absence of thermochromic phase change here confirms that the plasmonic heat generated by bundled AuNR array is the sole driving force for the crystal transformation in $PbCO_3$ with negligible contribution of silver backing film as well as glass slide.

The powder x-ray diffraction studies proved that the glass slide and Ag backing film have not produced any thermochromic crystal-to-crystal transition, conclusively excluding their potential role in the photothermal thermochromic change in $PbCO_3$ (**Figure 3.7**).
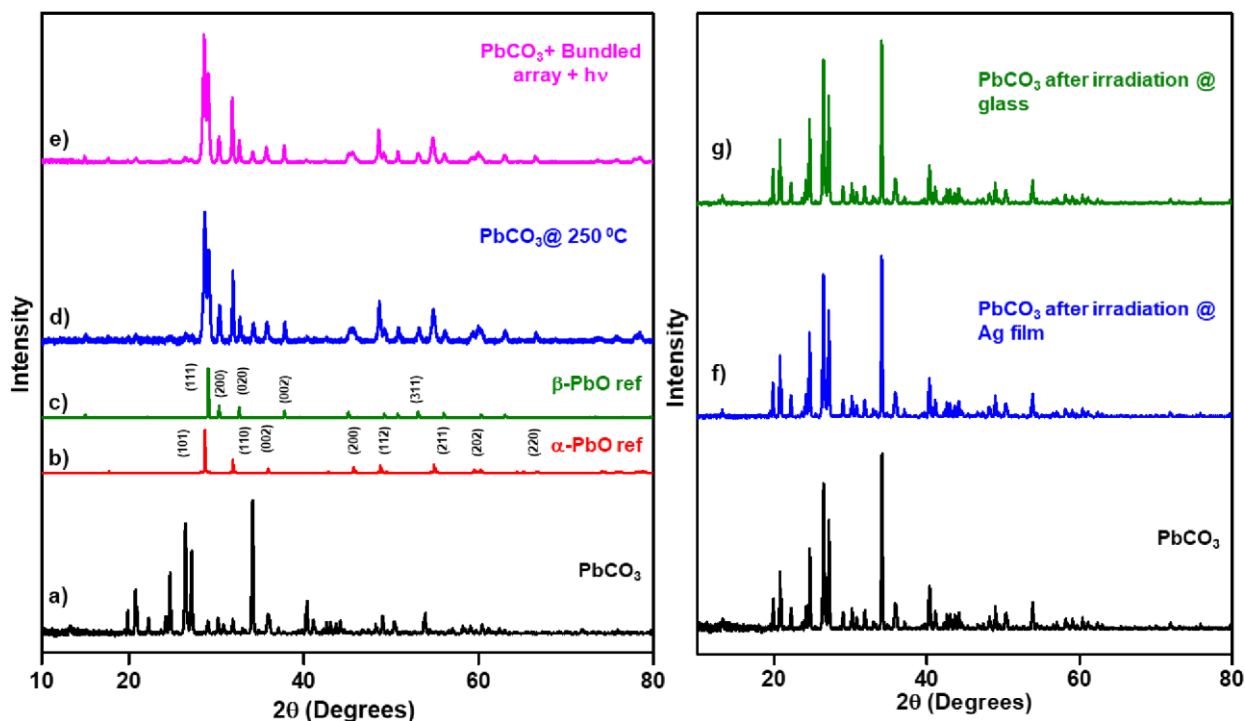
Figure 3.7. Left panel: Powder X-ray diffraction patterns of (a) PbCO₃, (b) a-PbO reference, (c) b-PbO reference, (d) PbCO₃ after thermal treatment at ~250 °C, and (e) PbCO₃ after photothermally heated (in the presence of bundled AuNR arrays after ~15 min of irradiation with a 1W 532 nm CW laser). The reference XRD patterns of expected products (tetragonal α-PbO, 00-005-0561 and orthorhombic β-PbO, 00-005-0570) are included for comparison. **Right panel:** Powder X-ray diffraction patterns of PbCO₃ before (black) and after irradiating the PbCO₃ placed on (f) only silver film and (g) only glass surface, using a 1W 532 nm CW laser for ~1 h.

The decomposition of PbCO₃ to PbO is well reported to strictly follow the thermal pathway, as shown in **Figure 3.8a**. The oxidation states of all of the elements in the reactant as well as in the products are the same, which confirms that plasmonic hot electrons are not involved in the decomposition process. Likewise, negligible absorption at ~532 nm by PbCO₃ and PbO molecules proves that the nonthermally activated chromism effects (such as photochemical) can be overruled in the present study (**Figure 3.8b**).
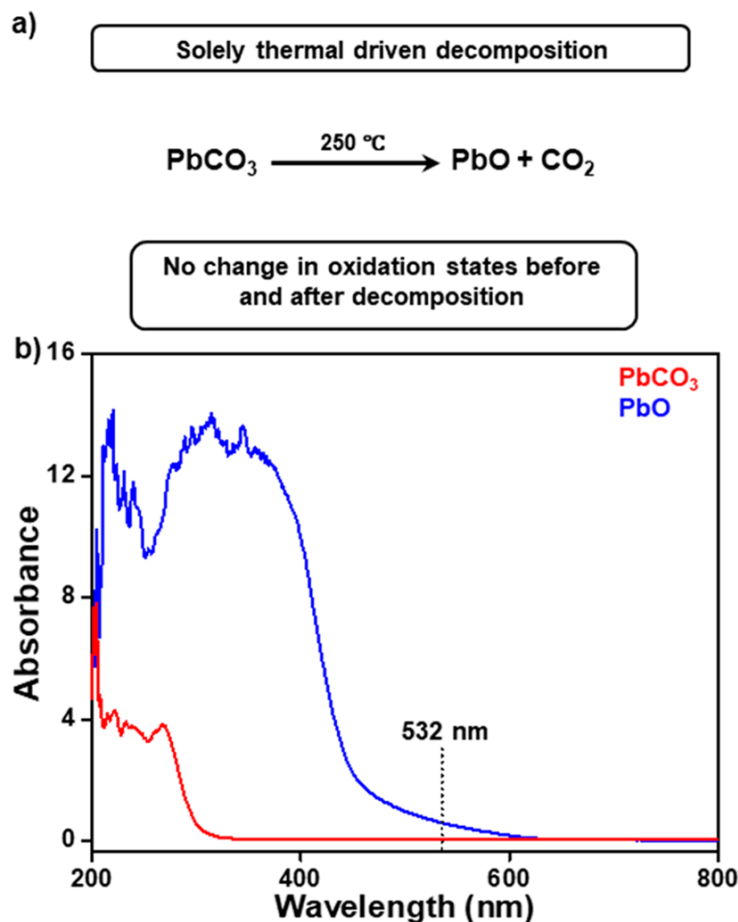
Figure 3.8. Overruling nonthermal effects. (a) Reaction scheme for the thermal decomposition of $PbCO_3$ to PbO. There is no change in the oxidation states of elements during the transformation, overruling the role of hot electron chemistry. (b) Solid-state UV–visible absorption spectra of $PbCO_3$ and PbO were recorded under the reflectance mode. A negligible absorbance of around 532 nm for both $PbCO_3$ and PbO confirms that the nonthermally activated chromism effects, such as the photochemical effect, can be overruled in the present study.

A considerable reshaping of AuNRs was observed after the thermoplasmonic studies (**Figure 3.9**) which is in accordance with the previous studies on the photothermal stability of AuNRs at high temperatures.[31,32] The reshaping of the AuNRs was observed only at the center of irradiation (a few micrometers, as the illumination was not uniform because of the Gaussian distribution of the laser beam (see **Figure 3.16** in the **Appendix**), whereas other regions were structurally intact. This allowed the multiple uses of bundled AuNR arrays, without any noticeable decrease in their thermoplasmonic properties.
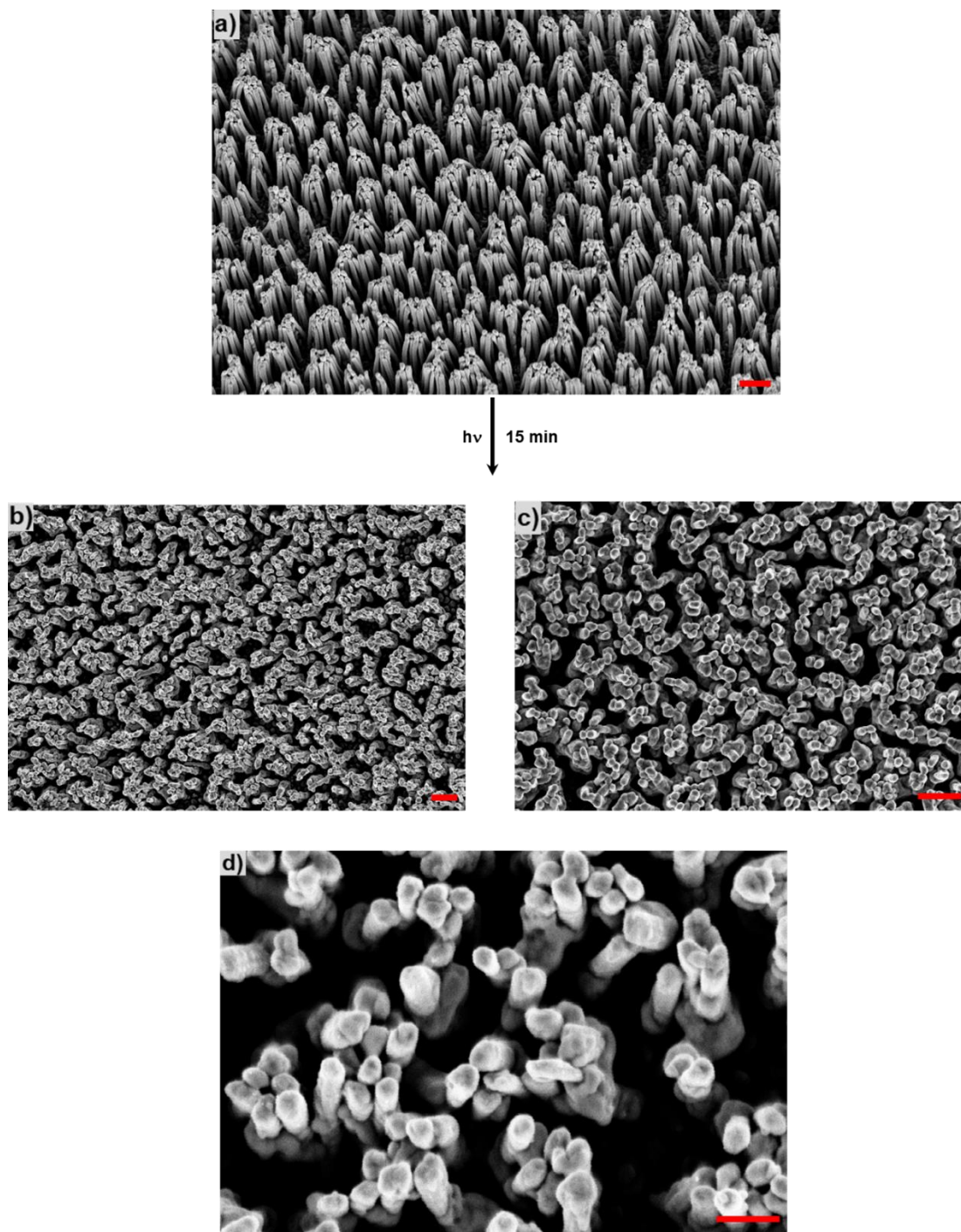
Figure 3.9. Characterization of photothermal re-shaping. SEM images of bundled AuNR arrays **(a)** before, and **(b), (c), (d)** after thermochromic studies with lead carbonate at different magnifications. The temperature reached to at least 250 ^{0}C during the thermochromic studies. Scale bar corresponds to 500 nm for **(a), (b)** and **(c)** and 200 nm for **(d)** A considerable re-shaping of the AuNRs was observed only at the center of irradiation (a few micrometer), whereas other regions were structurally intact.

The threshold intensity required for the thermochromic phase transition of $PbCO_3$ was 1 W, which was the maximum power limit of the laser source used. This prevented us to obtain a precise relationship between laser intensity and kinetics of phase transformation using $PbCO_3$. However, the intensity-dependent experiments could be performed using another thermochromic molecule that shows a phase change at a lower temperature. For this, ammonium metavanadate (NH_4VO_3) was selected as the thermochromic marker, which is well known to show a thermochromic phase change at 170 °C, accompanied by a color change from white to black.[47] The intensity-dependent studies show that the threshold light power required for the thermochromic phase change in NH_4VO_3 was 290 mW (it took ~3 h for the complete thermochromic phase change at 290 mW; **Figure 3.10**).
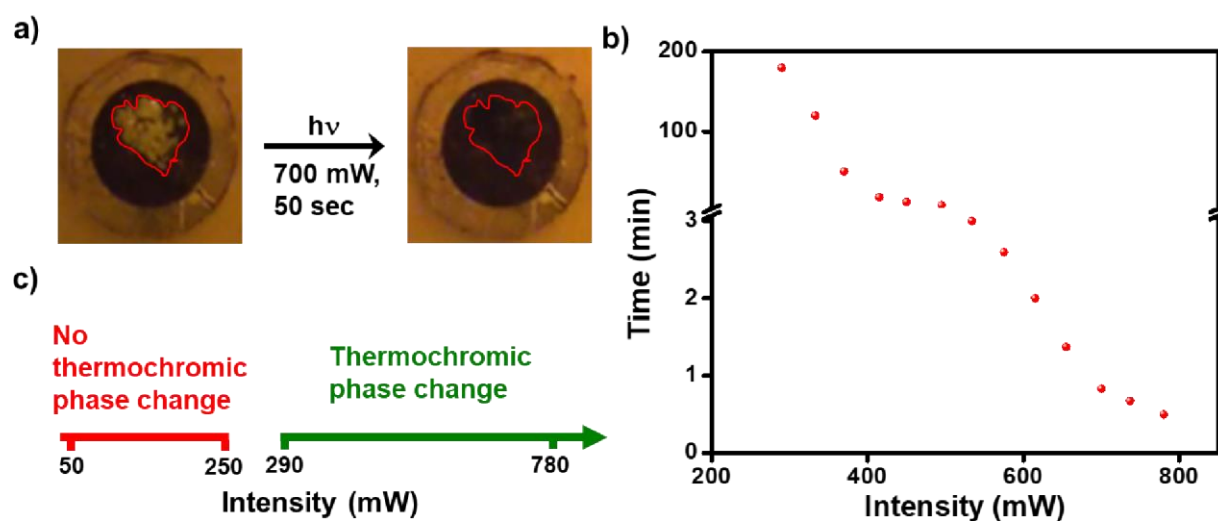
Figure 3.10. Intensity-dependent thermoplasmonically driven phase change in NH_4VO_3. (a) A typical thermochromic phase change (white to black) was observed in NH_4VO_3 placed on bundled AuNR array (marked in red boundaries), upon light irradiation using 532 nm CW (~700 mW) for ~50 sec. (b) The threshold light power required for the thermochromic phase change was 290 mW (it took ~3 h for the complete thermochromic phase change at 290 mW). The maximum time of light irradiation was fixed at ~3 h. (c) A plot showing the variation in the time taken for the complete thermochromic phase change, as a function of irradiation power.

Powder X-ray diffraction and Raman analyses (**Figure 3.11**) confirmed that the final product contains a mixture of different phases of vanadium oxides (orthorhombic–V_2O_5, monoclinic–V_3O_7, monoclinic–V_6O_{13}, and tetragonal–VO_2), which is in good agreement with the literature report.[45] Also, a precise relationship between the laser intensity and kinetics of phase

transformation was obtained using NH_4VO_3 as the thermochromic marker (**Figure 3.10b** and **Figure 3.17** in the Appendix). As expected, the time required for the complete thermochromic phase decreased as the power of the laser source was increased ($\sim$50 s @ 700 mW vs $\sim$3 h @ 290 mW; **Figure 3.10**). It is worth mentioning that the plasmonic heat reported by the thermochromic studies is the lower limit corresponding to the phase change temperature of the thermochromic molecule, and the actual surface temperature of bundled AuNR arrays could be higher.
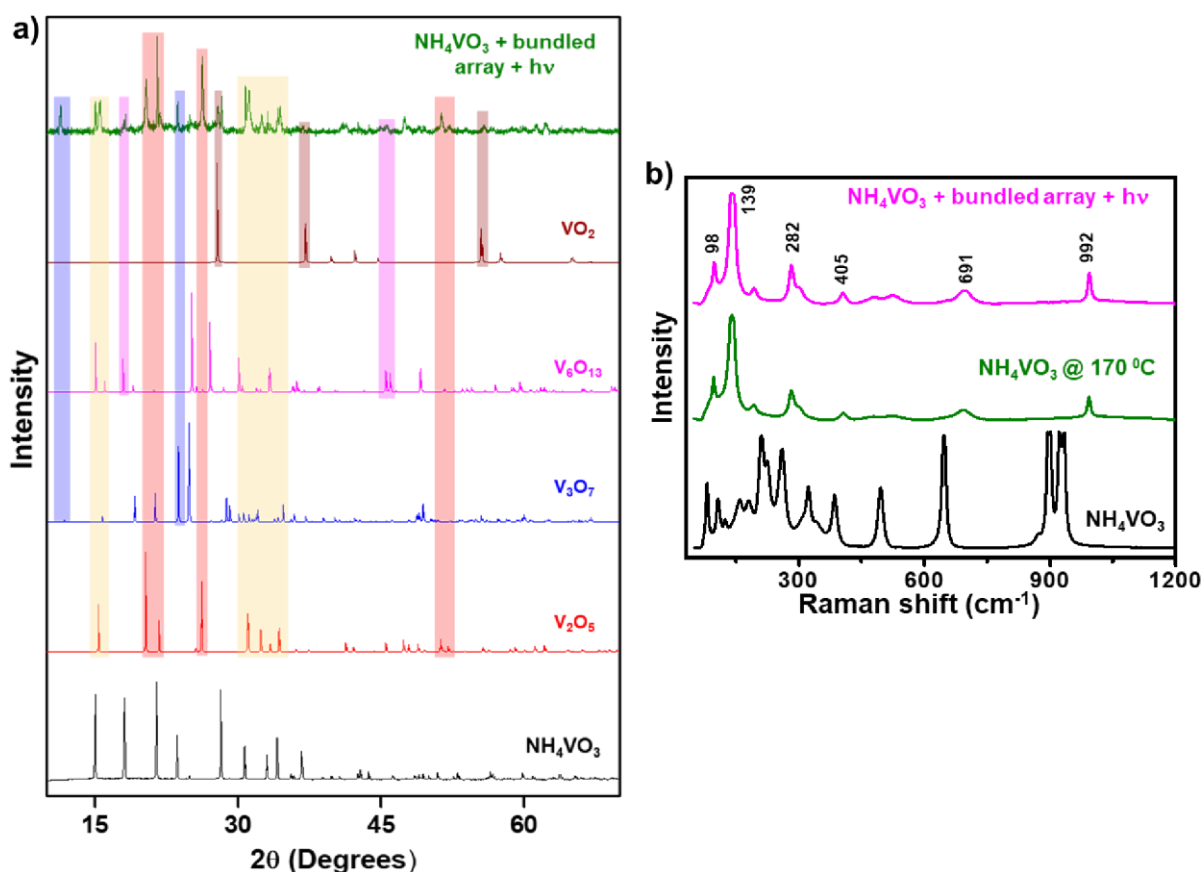
Figure 3.11. (a) Powder X-ray diffraction pattern of NH_4VO_3 before (black) and after irradiation (green) in the presence of bundled AuNR arrays, using a 532 nm CW diode laser ($\sim$700 mW) for $\sim$50s. The sample after irradiation contains all the peaks corresponding to orthorhombic-V_2O_5, monoclinic-V_3O_7, monoclinicV_6O_{13} and tetragonal-VO_2 phases. The reference XRD pattern for all the expected products (orthorhombicV_2O_5 (red), monoclinic-V_3O_7 (blue), monoclinic-V_6O_{13} (magenta) and tetragonal-VO_2 (wine red)) are included for the comparison. The colored bars show the overlap of major diffraction peaks in thermoplasmonically treated sample and references. (b) Raman analysis of NH_4VO_3 (black), the thermally heated NH_4VO_3 at 170 °C for $\sim$15 min (green), and thermoplasmonically heated NH_4VO_3 placed on bundled AuNR array (magenta) upon light irradiation using 532 nm CW diode laser ($\sim$700 mW) for $\sim$50s. Both the thermally as well as photothermally treated samples show similar Raman signals, confirming the efficacy of plasmonic heating in the thermochromic phase transition in NH_4VO_3.

3.4.3. Validation of thermochromism studies

A series of independent photothermal experiments were performed to validate the plasmonic heat measured through our thermochromism study. All of the following experiments were carried out under identical conditions as that of the thermochromic study (see the **Section 3.3.5** for details). The melting of cadmium acetate powder using the thermoplasmonic heat from bundled AuNR arrays confirms that the surface temperature reaches at least 255 °C (The melting point of cadmium acetate is 255 ^{0}C. **Figure 3.12**).
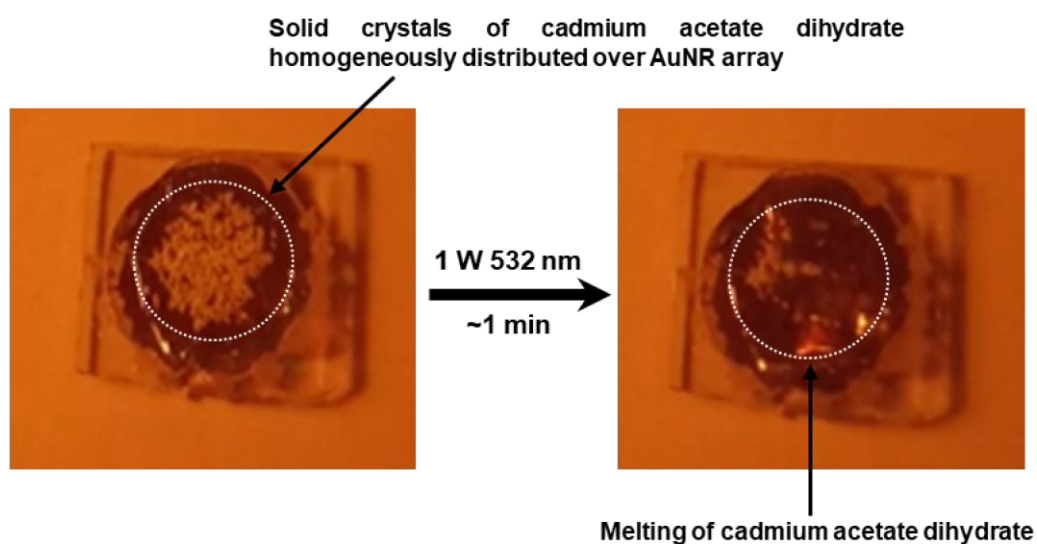
Figure 3.12. Thermoplasmonic melting of cadmium acetate dihydrate on bundled AuNR arrays. Transparency seen after the illumination of an opaque layer of cadmium acetate dihydrate adsorbed on bundled AuNR array is due to melting, which confirms the attainment of at least 255 ℃ (melting point of cadmium acetate dihydrate) under the experimental condition.

Next, a standard thermoplasmonic polymerization of soybean oil was performed on the surface of bundled AuNR arrays. The polymerization of soybean oil is known to initiate at ~230 °C, which is accompanied by a change in the ratio of stretching frequencies of vinylic to aliphatic C–H in Raman analysis.[27] The thermoplasmonic polymerization of soybean oil was observed on the bundled AuNR arrays, which ascertains the surface temperature to be at least ~230 °C (**Figure 3.13**).
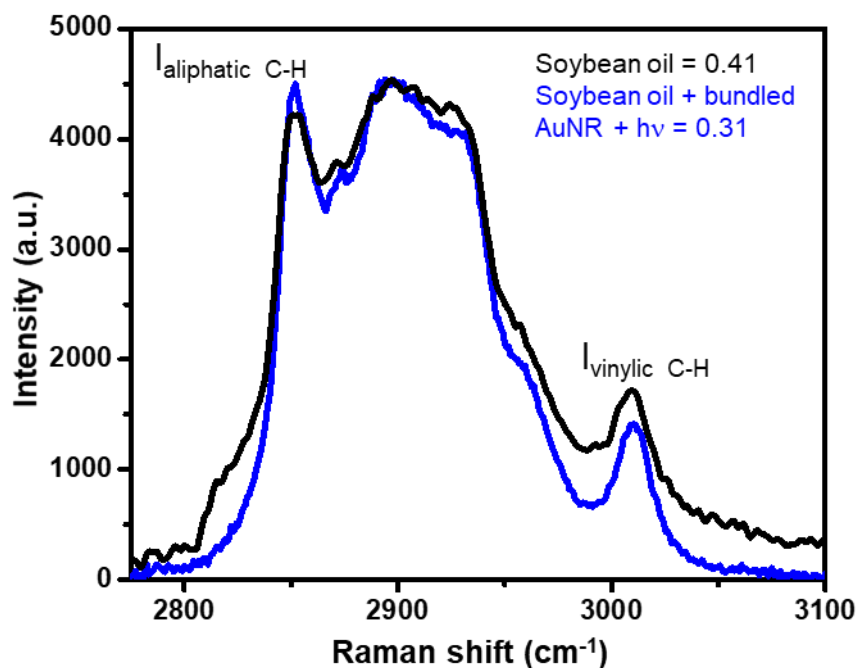
Figure 3.13. Raman spectra of the soybean oil before and after polymerization at the surface of bundled AuNR array. The ratio of vinylic to aliphatic C-H stretching peak intensity ($I_{vinylic\ C-H}/I_{aliphatic\ C-H}$) is shown in the inset. The commencement of polymerization on the AuNR array is confirmed by a drop in the ratio following illumination with a 1 W 532 nm CW laser. This indicates that the surface temperature reaches at least 230 °C, the temperature at which polymerization initiation occurs.

Finally, the thermoplasmonic heat was quantified using the infrared thermometric mapping,[7,35,36] which provides an in-situ, direct, and precise estimate of the surface temperature (**Figure 3.14**). The bundled AuNRs were irradiated with a 1 W 532 nm CW diode laser in an orthogonal geometry, with the infrared signatures captured at 45° with respect to the substrate. A rapid increase in the temperature at a rate of 7.5 °C/s was observed, which finally saturated at a surface temperature of ∼242 °C (**Figure 3.14a**). A thermometric image taken after 120 s clearly shows the heat map across the area of illumination, which qualitatively agrees with the beam profile maximum heating at the center of illumination (**Figure 3.14b,c** and **3.16** in the Appendix). Control experiments carried out on pristine silver substrates failed to provide any significant heat generation (**Figure 3.15b;** because silver substrates possess negligible absorption cross section at 532 nm), decisively pointing to the role of bundled AuNRs for the thermoplasmonic heat generation.
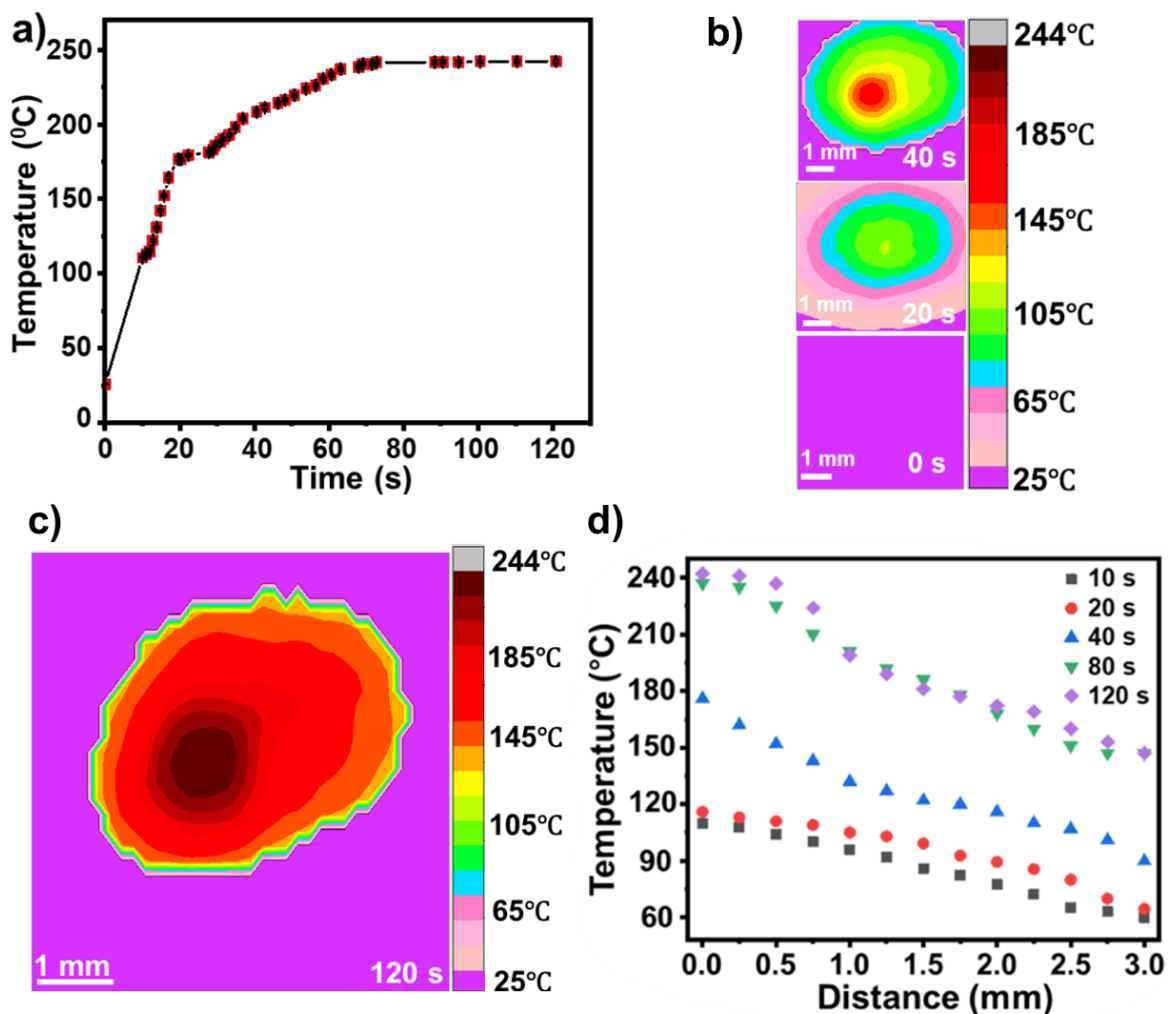
Figure 3.14. Quantification of thermoplasmonic temperature through direct infrared-based thermometric imaging studies. (a) Temporal evolution of thermoplasmonic temperature estimated from the surface of the bundled AuNR array with a 1 W 532 nm CW laser. (b) The thermometric images corresponding to different time periods with the color bar shown alongside. (c) A representative thermometric image taken after 120 s of laser irradiation is shown, with the maximum temperature saturation at ~242 °C at the center of the laser spot which is in accordance with the laser Gaussian beam profile (see **Figure 3.16** in the Appendix). (d) Spatiothermal gradient from the point of irradiation (distance = 0 mm) for varying time periods of laser irradiation.

Further, temporal thermal imaging provides important insights into the heat-dissipative pathways operating in the bundled AuNRs arrays. This assumes greater significance in the context of the applications including solar-vapor generation and thermochemical reactions, where efficient heat transfer to surroundings is critical. Accordingly, thermal profiles were extracted at
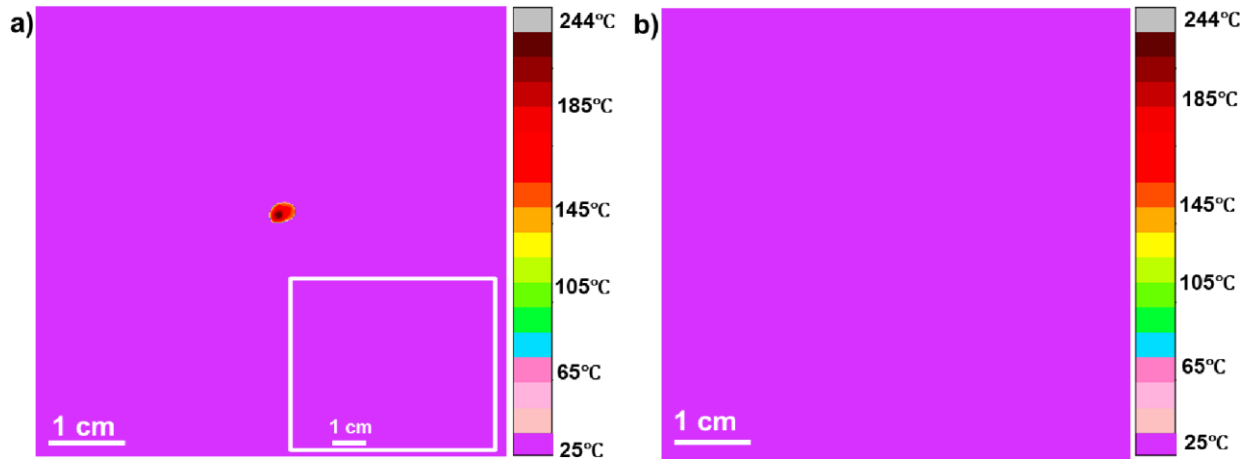
Figure 3.15. A representative thermal profile **(a)** at 120 s irradiation time showing the pinpoint as the laser irradiated spot on bundled AuNR arrays, reaching up to a maximum of ~242°C (Inset: The thermal profile when the laser was off). **(b)** Control experiment with silver substrate, reaching up to a maximum of ~27 °C.

different time periods of laser irradiation to estimate the spatial spread of heat from the point of laser irradiation across the bundled AuNR arrays (**Figure 3.14d**). It was observed that the surface temperature generated varies monotonically with the time of laser irradiation. Furthermore, the spatial thermal dissipation is also found to be directly proportional to the magnitude of heat difference between the source (bundled AuNRs arrays) and the sink (surroundings) (**Figure 3.14b and Table 3.1**). In short, a longer time of laser irradiation produces higher surface temperatures at the point of irradiation and consequently results in larger spatiothermal gradients (34 °C/mm for a temperature differential of 95 °C corresponding to 120 s of irradiation, Table 3.1). **Figure 2.7** proves that the Ag film has negligible absorption at the excitation wavelength of ~532 nm, which means that the bundled AuNR array is the primary absorber. Therefore, we propose that the bundled AuNRs were solely responsible for the thermoplasmonic heat generation, while both the bundled AuNRs and the underlying silver film contributed to the conductive heat transfer pathways. The details of heat dissipation pathways can be explained as follows:

3.4.4. Heat generation and dissipation pathways

The AuNRs are in physical contact with the underlying silver film. Therefore, the total heat conductance (G_{total}) will be the linear combination of the heat conductance as per the following equation:[37]

$$G_{total} = G_M + G_s + G_{rad}$$

Where,

G_{total} = total heat conductance,

G_M = heat conductance from metals: AuNR (G_{Au}), Au-Ag interface (G_{Au-Ag}) and Ag film (G_{Ag}), G_s = heat conductance from metal to surrounding, G_{rad} = radiative heat flow.

3.4.4.1. Effect of silver film

The thermal conductivity of the surrounding medium and support plays a crucial role in the heat dissipation from Au nanorods.[38] The thermal conductivity of silver is higher ($\geq$350 Wm^{-1}K^{-1}, with the lowest value of contact resistance) than all the surrounding medium used in our study. Thus, the underlying silver film will act as a heat sink for the dissipation of thermoplasmonic heat from the AuNR arrays.

3.4.4.2. Effect of Au nanorods length

The heat capacity will increase with an increase in the size of the nanoparticles.[39] As a result, the rate of heat dissipation will be slower for higher-sized nanoparticles.[40,41] Thus, it is clear that the rate of heat dissipation will decrease as the length of the AuNR is increased in our system.

Finally, we comment on the role of reaction conditions on the dissipation of heat from the surface of thermoplasmonic AuNR arrays. Controlling the amount of heat generated within a thermoplasmonic nanostructure is often a practically challenging task. Therefore, it is essential to regulate the process of dissipation to achieve the desired outcome from the remarkably high heat generated in thermoplasmonic nanostructures. Our studies show that the appropriate choice of reaction conditions is decisive in the utilization and dissipation of heat from the thermoplasmonic surface to the surroundings. The maximum surface temperature may be experienced when thermoplasmonic studies will be performed in the solid state under irradiation with a green laser. To study the role of reaction conditions, thermoplasmonic properties of bundled AuNR arrays were tested in the liquid-state transformation process as well. For this, the water evaporation experiments were once again performed in the presence of bundled AuNR arrays under irradiation conditions similar to thermochromism studies. The weight of water merely decreased by ∼180 mg in ∼20 min and the bulk temperature increased to ∼45 °C (measured using a thermometer, **Section**

3.3.7), when a 1 W 532 nm CW laser was used as the source of irradiation. Also, it is worth recollecting that the thermoplasmonically driven Diels–Alder reaction gave a moderate yield of ∼40% under the same irradiation condition, whereas the thermally performed Diels–Alder reaction at 115 °C yielded an ∼82% product (**Chapter 2**). This essentially confirms that the dissipation of heat from the surface of thermoplasmonic AuNR arrays is rapid in solution-state experiments. Thus, our studies provide direct and simultaneous insight into the utilization of the high surface temperature in thermoplasmonic nanostructures under different reaction conditions.

3.5. Conclusion

In conclusion, a visual color change-based quantification technique is proposed for the quantification of the chemical effectiveness of plasmonic heat. The phenomenon of thermochromism served as a reliable and simple tool to quantify the surface temperature of thermoplasmonic AuNR arrays. Thermochromism studies reveal that the temperature close to the surface of AuNR arrays can reach up to ∼250 °C, within ∼15 min of laser irradiation. It is important to mention here that the measurement of such a high temperature on the plasmonic substrate is scarcely reported in the literature. The measured temperature with the proposed thermochromism-based quantification is verified independently with three different techniques; melting point of crystalline solid, Raman spectroscopy, and IR-based thermometric imaging study, which proves the suitability of the methodology. The analysis of the results from direct IR thermometric imaging has provided important insights into the heat-generation and heat-dissipative pathways. A few advantages of the methodology are cost-effectiveness, and low response time for visualization of temperature through visual color change. Along with the advantages, the method possesses certain limitations, for example, it can measure only the minimum temperature corresponding to the thermochromic phase change temperature, whereas the actual temperature can be higher. Nonetheless, the method can be utilized to have a fair idea of effective surface-average temperature and hence can be utilized to find out the thermal effect in plasmon-driven chemistry.

3.6. References

(1) Quintanilla, M.; Liz-Marzán, L. M. Guiding Rules for Selecting a Nanothermometer. *Nano Today* **2018**, *19*, 126−145.

(2) Desiatov, B.; Goykhman, I.; Levy, U. Direct Temperature Mapping of Nanoscale Plasmonic Devices. *Nano Lett.* **2014**, *14*, 648− 652.

(3) Mauser, K. W.; Sola` Garcia, M.; Liebtrau, M.; Damilano, B.; Coulon, P.-M.; Vézian, S.; Shields, P. A.; Meuret, S.; Polman, A. Employing Cathodoluminescence for Nanothermometry and Thermal Transport Measurements in Semiconductor Nanowires. *ACS Nano* **2021**, *15*, 11385−11395.

(4) Baffou, G.; Kreuzer, M. P.; Kulzer, F.; Quidant, R. Temperature Mapping Near Plasmonic Nanostructures Using Fluorescence Polarization Anisotropy. *Opt. Express* **2009**, *17*, 3291−3298.

(5) Baffou, G.; Girard, C.; Quidant, R. Mapping Heat Origin in Plasmonic Structures. *Phys. Rev. Lett.* **2010**, *104*, 136805.

(6) Bendix, P. M.; Nader, S.; Reihani, S.; Oddershede, L. B. Direct Measurements of Heating by Electromagnetically Trapped Gold Nanoparticles on Supported Lipid Bilayers. *ACS Nano* **2010**, *4*, 2256−2262.

(7) Quintanilla, M.; Zhang, Y.; Liz-Marzán, L. M. Subtissue Plasmonic Heating Monitored with CaF_2:Nd^{3+}, Y^{3+} Nanothermometers in the Second Biological Window. *Chem. Mater.* **2018**, *30*, 2819−2828.

(8) Cortes, E.; Grzeschik, R.; Maier, S. A.; Schluecker, S. Experimental Characterization Techniques for Plasmon-Assisted Chemistry. *Nat. Rev. Chem.* **2022**, *6*, 259– 274.

(9) Baffou, G. Anti-Stokes thermometry in nanoplasmonics. *ACS Nano* **2021**, *15*, 5785–5792.

(10) Baffou, G.; Berto, P.; Bermúdez Ureña, E.; Quidant, R.; Monneret, S.; Polleux, J.; Rigneault, H. Photoinduced Heating of Nanoparticle Arrays. *ACS Nano* **2013**, *7*, 6478-6488.

(11) Govorov, A. O.; Zhang, W.; Skeini, T.; Richardson, H.; Lee, J.; Kotov, N. A. Gold Nanoparticle Ensembles as Heaters and Actuators: Melting and Collective Plasmon Resonances. *Nanoscale Res. Lett.* **2006**, *1*, 84– 90.

(12) Dubi, Y.; Un, I. W.; Sivan, Y. Thermal Effects - An Alternative Mechanism for Plasmon-Assisted Photocatalysis. *Chem. Sci.* **2020**, *11*, 5017– 5027.

(13) Wang, D.; Koh, Y. R.; Kudyshev, Z. A.; Maize, K.; Kildishev, A. V.; Boltasseva, A.; Shalaev, V. M.; Shakouri, A. Spatial and temporal nanoscale plasmonic heating quantified by thermoreflectance. *Nano Lett.* **2019**, *19*, 3796– 3803.

(14) Zhou, L.; Swearer, D. F.; Zhang, C.; Robatjazi, H.; Zhao, H.; Henderson, L.; Dong, L.; Christopher, P.; Carter, E. A.; Nordlander, P.; Halas, N. J. Quantifying Hot Carrier and Thermal Contributions in Plasmonic Photocatalysis. *Science* **2018**, *362*, 69– 72.

(15) Virk, M.; Xiong, K.; Svedendahl, M.; Käll, M.; Dahlin, A. B. A Thermal Plasmonic Sensor Platform: Resistive Heating of Nanohole Arrays. *Nano Lett.* **2014**, *14*, 3544– 3549.

(16) Zhang, X.; Li, X.; Reish, M. E.; Zhang, D.; Su, N. Q.; Gutiérrez, Y.; Moreno, F.; Yang, W.; Everitt, H. O.; Liu, J. Plasmon-Enhanced Catalysis: Distinguishing Thermal and Nonthermal Effects. *Nano Lett.* **2018**, *18*, 1714– 1723.

(17) Jaque, D.; Vetrone, F. Luminescence Nanothermometry. *Nanoscale* **2012**, *4*, 4301– 4326.

(18) Carattino, A.; Caldarola, M.; Orrit, M. Gold Nanoparticles as Absolute Nanothermometers. *Nano Lett.* **2018**, *18*, 874– 880.

(19) Barella, M.; Violi, I. L.; Gargiulo, J.; Martinez, L. P.; Goschin, F.; Guglielmotti, V.; Pallarola, D.; Schlucker, S.; Pilo-Pais, M.; Acuna, G. P.; Maier, S. A.; Cortes, E.; Stefani, F. D. *In Situ* Photothermal Response of Single Gold Nanoparticles through Hyperspectral Imaging Anti-Stokes Thermometry. *ACS Nano* **2021**, *15*, 2458– 2467.

(20) Hu, S.; Liu, B.-J.; Feng, J.-M.; Zong, C.; Lin, K.-Q.; Wang, X.; Wu, D.-Y.; Ren, B. Quantifying Surface Temperature of Thermoplasmonic Nanostructures. *J. Am. Chem. Soc.* **2018**, *140*, 13680–13686.

(21) Desiatov, B.; Goykhman, I.; Levy, U. Direct Temperature Mapping of Nanoscale Plasmonic Devices. *Nano Lett.* **2014**, *14*, 648–652.

(22) Jollans, T.; Caldarola, M.; Sivan, Y.; Orrit, M. Effective electron temperature measurement using time-resolved anti-Stokes photoluminescence. *J. Phys. Chem. A* **2020**, *124*, 6968–6976.

(23) Banholzer, M. J.; Qin, L.; Millstone, J. E.; Osberg, K. D.; Mirkin, C. A. On-Wire Lithography: Synthesis, Encoding and Biological Applications. *Nat. Protoc.* **2009**, *4*, 838−848.

(24) Pillai, P. P.; Pacławski, K.; Kim, J.; Grzybowski, B. A. Nanostructural Anisotropy Underlies Anisotropic Electrical Bistability. *Adv. Mater.* **2013**, *25*, 1623−1628.

(25) Galwey, A. K.; Brown, M. E. *Thermal decomposition of ionic solids*; Elsevier: Amsterdam, 1999.

(26) Akande, A. A.; Linganiso, E. C.; Dhonge, B. P.; Rammutla, K. E.; Machatine, A.; Prinsloo, L.; Kunert, H.; Mwakikunga, B. W. Phase Evolution of Vanadium Oxides Obtained through Temperature Programmed Calcinations of Ammonium Vanadate in Hydrogen Atmosphere and Their Humidity Sensing Properties. *Mater. Chem. Phys.* **2015**, *151*, 206–214.

(27) Qiu, J.; Wu, Y. C.; Wang, Y. C.; Engelhard, M. H.; McElwee-White, L.; Wei, W. D. Surface Plasmon Mediated Chemical Solution Deposition of Gold Nanoparticles on a Nanostructured Silver Surface at Room Temperature. *J. Am. Chem. Soc.* **2013**, *135*, 38–41.

(28) Burda, C.; Chen, X.; Narayanan, R.; El-Sayed, M. A. Chemistry and Properties of Nanocrystals of Different Shapes. *Chem. Rev.* **2005**, *105*, 1025−1102.

(29) Galwey, A. K.; Brown, M. E. *Thermal Decomposition of Ionic Solids*; Elsevier Science, 1999.

(30) Burgio, L.; Clark, R. J. H.; Firth, S. Raman spectroscopy as a means for the identification of plattnerite (PbO_2), of lead pigments and of their degradation products. *Analyst* **2001**, *126*, 222227.

(31) Petrova, H.; Juste, J. P.; Pastoriza-Santos, I.; Hartland, G. V.; Liz-Marzán, L. M.; Mulvaney, P. On the Temperature Stability of Gold Nanorods: Comparison between Thermal and Ultrafast Laser-Induced Heating. *Phys. Chem. Chem. Phys.* **2006**, *8*, 814−821.

(32) Harris-Birtill, D.; Singh, M.; Zhou, Y.; Elena-Gallina, M.; Cass, T.; Elson, D. In Gold Nanorod Reshaping Using a Continuous Wave Laser, Conference on Lasers and Electro-Optics (CLEO) - Laser Science to Photonic Applications; Optica Publishing Group, 2014.

(33) Day, J. H. Thermochromism of Inorganic Compounds. *Chem. Rev.* **1968**, *68*, 649−657.

(34) Akande, A. A.; Linganiso, E. C.; Dhonge, B. P.; Rammutla, K. E.; Machatine, A.; Prinsloo, L.; Kunert, H.; Mwakikunga, B. W. Phase Evolution of Vanadium Oxides Obtained through Temperature Programmed Calcinations of Ammonium Vanadate in Hydrogen Atmosphere and Their Humidity Sensing Properties. *Mater. Chem. Phys.* **2015**, *151*, 206−214.

(35) Sharma, S.; Sah, A.; Subramaniam, C.; Saha, S. K. Performance Enhancement of Tapered Helical Coil Receiver Using Novel Nanostructured Carbon Florets Coating. *Appl. Therm. Eng.* **2021**, *194*, 117065.

(36) Gupta, R.; Shinde, S.; Yella, A.; Subramaniam, C.; Saha, S. K. Thermomechanical Characterisations of PTFE, PEEK, PEKK as Encapsulation Materials for Medium Temperature Solar Applications. *Energy* **2020**, *194*, 116921.

(37) Yuksel, A.; Yu, E. T.; Cullinan, M.; Murthy, J. Investigation of Heat Transfer Modes in Plasmonic Nanoparticles. *Int. J. Heat Mass Transfer* **2020**, *156*, 119869.

(38) Park, J.; Huang, J. Y.; Wang, W.; Murphy, C. J.; Cahill, D. G. Heat Transport between Au Nanorods, Surrounding Liquids, and Solid Supports. *J. Phys. Chem. C* **2012**, *116*, 26335−26341.

(39) Johnson, R. J. G.; Schultz, J. D.; Lear, B. J. Photothermal Effectiveness of Magnetite Nanoparticles: Dependence upon Particle Size Probed by Experiment and Simulation. *Molecules* **2018**, *23*, 1234.

(40) Hu, M.; Hartland, G. V. Heat Dissipation for Au Particles in Aqueous Solution: Relaxation Time versus Size. *J. Phys. Chem. B* **2002**, *106*, 7029–7033.

(41) Yuksel, A.; Cullinan, M.; Murthy, J. Thermal Energy Transport Below the Diffraction Limit in Close-Packed Metal Nanoparticles. *In ASME 2017 Heat Transfer Summer Conference* **2017**, V002T13A005-V002T13A005.

3.7. Appendix

Laser beam profile
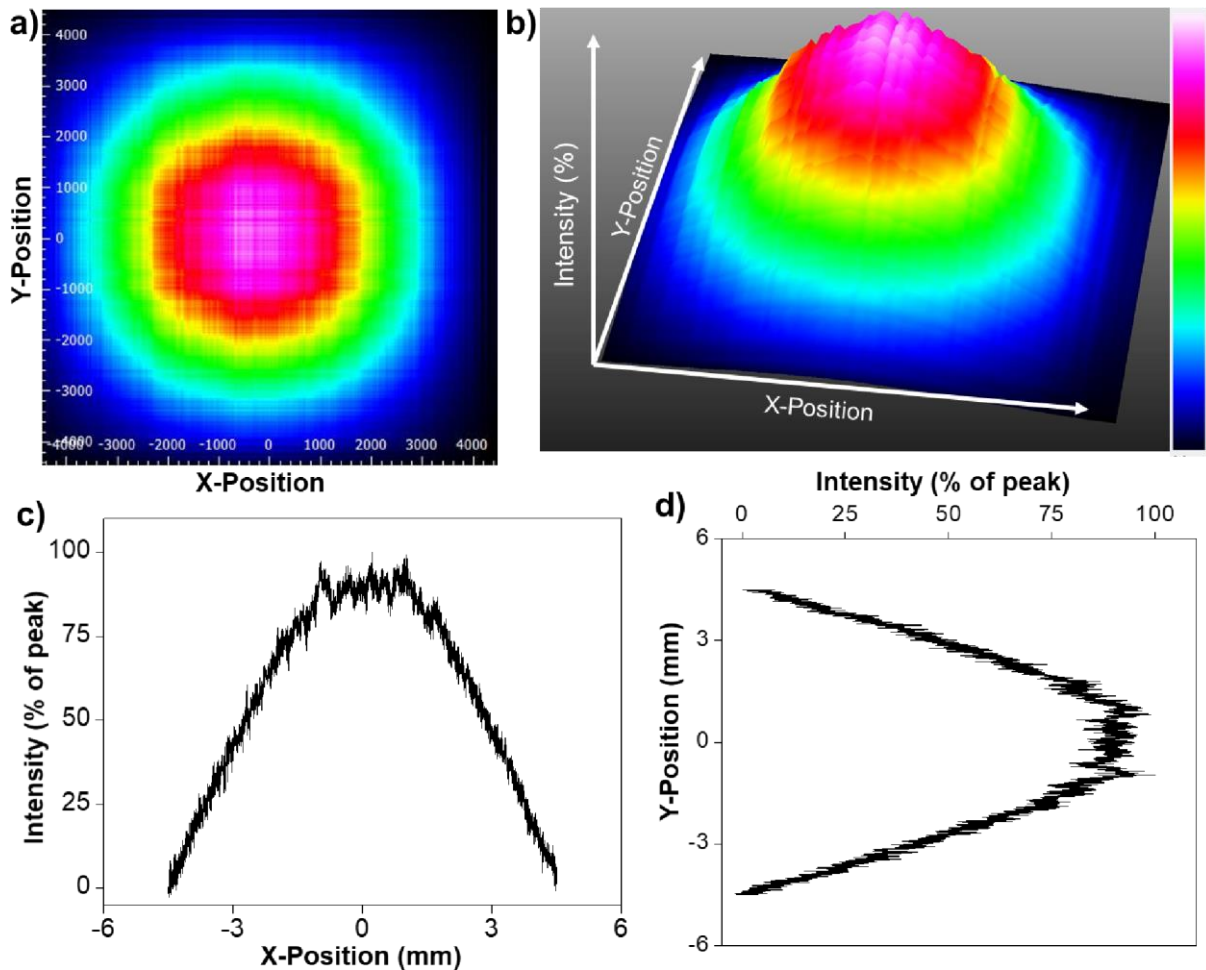
Figure 3.16. Laser beam profile measured at 1 cm beam diameter. **(a)** 2D and **(b)** 3D profiles of the beam clearly depict a Gaussian distribution having maximum intensity at the central area of the beam, which decays away from the center point. The color code for the intensity is shown at right side of panel **(b)**. **(c)** and **(d)** The plots of beam profile along x-axis ($1/e^2$ diameter ~8 mm) and y-axis ($1/e^2$ diameter ~8 mm), showing the Gaussian distribution.

Intensity-dependent photothermally driven thermochromic study
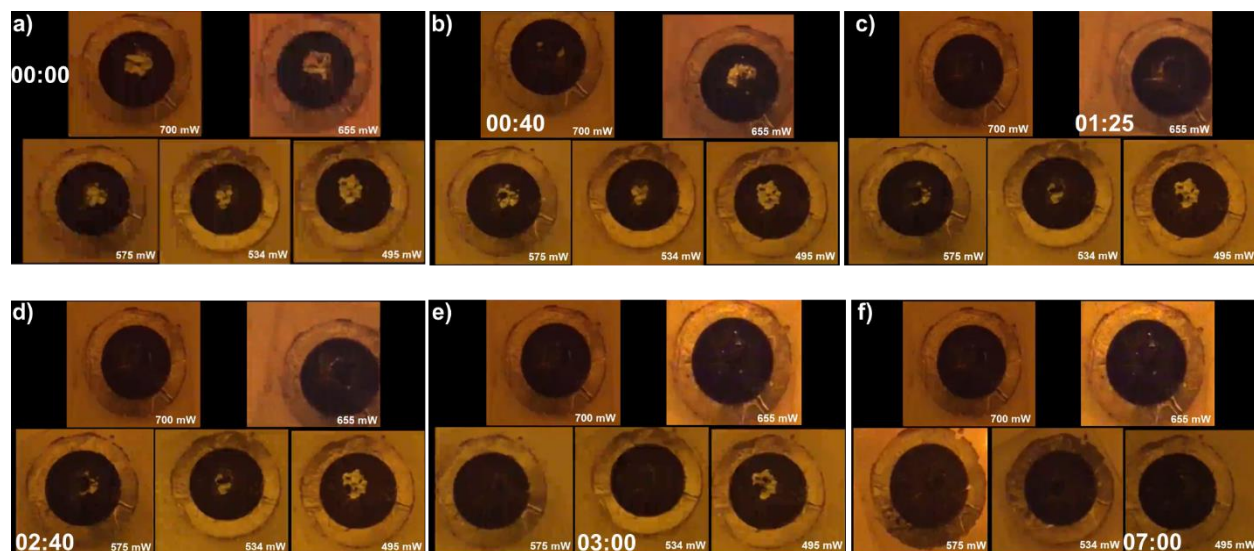
Figure 3.17. Intensity-dependent thermochromic study of NH_4VO_3 before irradiation (a) and after the complete thermochromic change of 1 g of NH_4VO_3 upon irradiation with (b) 700 mW, (c) 655 mW, (d) 575 mW, (e) 534 mW, and (f) 495 mW. The corresponding time of thermochromic change is written in the inset in the format mm:ss.

Table 3.1. Spatial thermal dissipation from the point of irradiation in bundled AuNR arrays with varying time periods of laser irradiation.

Time of irradiation (s)	Spatio-thermal gradient (°C/mm)	Temperature difference (°C)
10	16.6	50
20	17.7	51
40	25.0	86
80	33.0	90
120	34.2	95

Chapter − 4

Solely Plasmonic Heat Driven High-Temperature Organic Transformation: The Case of Claisen Rearrangement
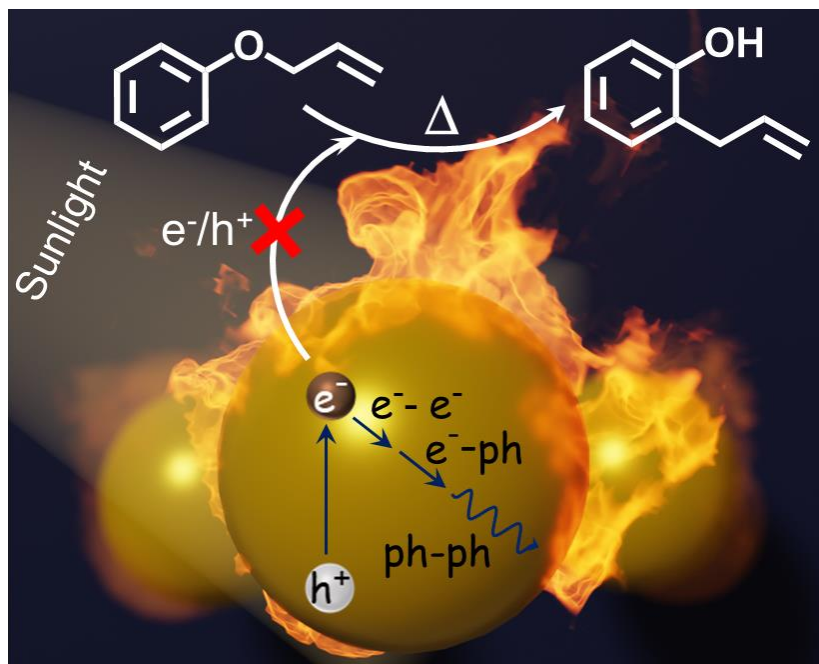
This chapter has been adapted from the following paper. Copyright 2023, Royal Society of Chemistry:

Kashyap, R. K.; Tyagi, S.; Plasmon enabled Claisen rearrangement with sunlight. *Chem. Commun.* **2023**, *59*, 13293-13296.

4.1. Abstract

The dampening of optically excited surface plasmon of nanostructures results in two major outcomes, hot charge carriers and heat which are part of the same non-radiative relaxation pathway. Therefore, the extent of involvement of hot charge carriers and heat in photothermal-driven chemistry is often debated. However, it is important to deconvolute the role of hot charge carriers and plasmonic heat to gain a complete mechanistic understanding. This Chapter deals with the extrication of the role of hot charge carriers from plasmonic heat-driven chemical transformation. Here, plasmonic-heat generated from the solar irradiation of gold nanoparticles is used as the thermal energy source for the Claisen rearrangement of allyl phenyl ether to 2-allylphenol, which is conventionally performed with electrical heating at 250 °C. The use of a closed reactor enables the physical separation of the reactants from the source of plasmonic-heat, thereby preventing the interference of the hot-charge carriers in the plasmon-driven Claisen rearrangement. In this way, the sole effect of plasmonic-heat in driving a high-temperature organic transformation is demonstrated. An attractive yield of 80% was achieved after 2 h of solar irradiation, which was at least double the yield obtained from the normal thermal reaction performed at 250 °C. This enhancement in the yield can be attributed to the higher steady-state temperature achieved with plasmonic-heat. The kinetic study revealed that the rate of the reaction under solar irradiation is at least twice that of the rection performed at 250 °C which could be attributed to the generation of higher temperature by plasmonic AuNP under solar irradiation. The reusability study revealed that the AuNP film can be used for at least till five cycles without any noticeable change in photothermal reaction yield. Our study reveals the prospects of plasmonic nanostructures in conducting energy intensive chemical synthesis in a sustainable fashion. Most importantly the study has shown a new avenue of disentangling the plasmonic heat from hot charge carriers in plasmon driven chemistry.

4.2. Introduction

The visible-light absorbing power of plasmonic nanoparticles (NPs) is exceptionally high (10^8 – 10^{10} M^{-1} cm^{-1}) because of their unique excitation pathway based on surface plasmon resonance.[1-3] A photoexcited NP can dissipate its excess energy through radiative and non-radiative pathways: ca. ~5% and ~95%, respectively, for NPs with size <25 nm.[4,5] The main outcomes of the radiative relaxation pathway are scattering and emission; whereas, hot-charge carrier generation and heat dissipation are the main outcomes of the non-radiative relaxation pathway.[6-10] Both hot-charge carrier generation and heat-dissipation can bring out important chemical and physical transformations, which constitute the areas of plasmonic photocatalysis[11-18] and thermoplasmonics,[19-26] respectively. The majority of the photoexcitation energy in plasmonic NPs is dissipated in the form of heat because of the fast charge recombination dynamics associated with non-radiative relaxation processes (100 fs–10 ps; Landau damping, electron–electron, electron–phonon, and phonon– phonon scattering).[6-10] In effect, the amount of heat dissipated by a photoexcited NP is huge because of the involvement of unique excitation and relaxation pathways (photothermal conversion efficiency is >90%).[27,28] This heat dissipated from a photoexcited NP is termed as plasmonic-heat, which has found use in various photothermal applications including therapy,[29,30] drug delivery,[31,32] solar-vapor generation,[33,34] azeotropic separation,[35] and material synthesis.[36]

Recent studies have proved the suitability of plasmonic-heat in synthetic organic chemistry as well, with the aim of achieving sustainability in chemical synthesis.[37-40] The idea here is to use plasmonic heat as the thermal energy source, instead of conventional electrical heating, for performing high-temperature organic reactions. For example, Scaiano and coworkers demonstrated that plasmon excitation of gold nanoparticles can perform high-temperature chemical reactions at room temperature, such as the decomposition of dicumyl peroxide (DCP).[37] The reaction was performed in a droplet containing gold nanoparticles and reactant, illuminated with 532 nm laser shots with energy 50 mJ/shot (**Figure 4.1**). Kinetic studies based on the known activation energy and rate constant values showed that gold nanoparticles can produce temperatures of 500 °C when excited by a 532 nm laser, causing the reaction to proceed in less than a minute.
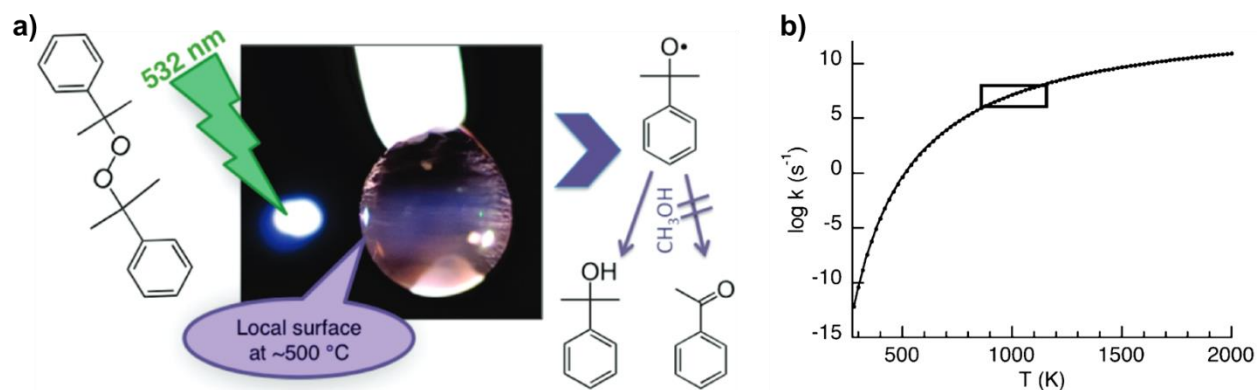
Figure 4.1. Photothermal decomposition of dicumyl peroxide. (a) The experimental setup where a drop of reaction mixture and gold nanoparticles was irradiated with 532 nm laser shots with energy 50 mJ/shot. (b) The calculated rate constant vs temperature plot. The temperature was estimation using already known value of activation energy and frequency factor (E_a = 34.25 kcal/mol and log A = 14.67). The range of temperatures where lifetime of DCP would fall between 10 ns and 1 μs is depicted by the rectangle. Reproduced with permission from ref. 37. Copyright: 2011, American Chemical Society.

Another study Correa-Duarte and coworkers presents the design of plasmonic hollow nanoreactors for concentrating light at the nanometer scale to perform and optically monitor the thermally activated Diels-Alder reaction in a confined volume without affecting the bulk solvent temperature.[38] The plasmonic nanoreactor (PNR) was made up of a mesoporous silica where the inner walls of the pore were decorated with gold nanoparticles (**Figure 4.2a**). The progress of the reaction was monitored by surface enhanced Raman spectroscopy (SERS), where a successive decrease in the C=C stretching frequency peak at 1660 cm^{-1} was observed as a function of irradiation time indicating the decrease in reactant amount (**Figure 4.2b, c**). The authors have observed a ~300% increase in the product yield with PNR under illumination as compared to the control experiments performed without light illumination, or without PNRs, or thermal reaction at bulk temperature (**Figure 4.2c**). The control experiments confirmed the active role of plasmonic heat in driving the Diels-Alder reaction. These studies motivated the researcher to use plasmonic based heater for synthetic organic chemistry as a greener alternative to electrical based heater.[39,40]
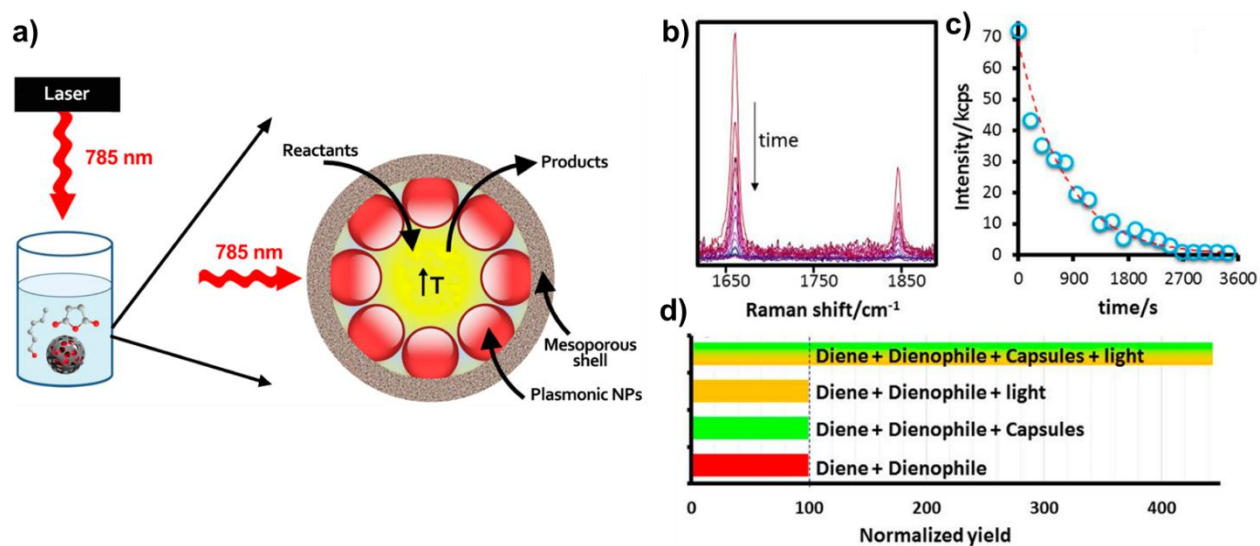
Figure 4.2. Photothermal Diels-Alder reaction and simultaneous monitoring with plasmonic nanoreactor (PNR). (a) The schematic cross-section of PNR with reaction setup. (b) and (c) Monitoring of progress of the reaction using surface enhance Raman spectroscopy (SERS). The time dependent SERS showed the decrease in the reactant peak at 1660 cm^{-1} which is plotted in (c). (d) The reaction yield showed ~300% enhancement as compared to the control experiments conclusively proved the involvement of plasmonic heat to drive the reaction. Reproduced with permission from ref. 38. Copyright: 2013, American Chemical Society.

However, it has been challenging to deconvolute the contribution of hot-charge carriers in a plasmonic-heat driven organic reaction, as both these outcomes are part of the same nonradiative decay process.[41] In this work, the use of a proper reactor system enabled us to prevent the interference of the hot charge carriers and study the sole effect of plasmonic-heat in high temperature organic reaction (**Scheme 4.1**). This was achieved by designing a thermodynamically closed reactor system, wherein the reaction mixture was physically separated from the plasmonic NPs (heating source). This will enable the exchange of energy (here, plasmonic-heat), whereas the exchange of matter (here, hot charge carriers) will be prevented. Our choice of the high temperature organic reaction was the thermally driven [3,3] sigmatropic Claisen rearrangement of allyl phenyl ether to 2-allylphenol, which is conventionally performed at 250 °C using electrical heating.[42-44] Also, Claisen rearrangement is one of the commonly practiced reactions in synthetic organic chemistry to form carbon–carbon bonds, further justifying the importance and choice of the reaction in the present study.[45] The plasmonic-heat dissipated from gold nanoparticles (AuNPs) was used as the thermal energy source for the Claisen rearrangement, which gave an excellent

yield of ~80% within 2 h of solar irradiation. Kinetic studies reveal that the rate of the reaction under plasmonic-heating was at least two times higher than the reaction performed with normal electrical heating, which can be attributed to the higher steady-state temperature achieved with plasmonic-heat.
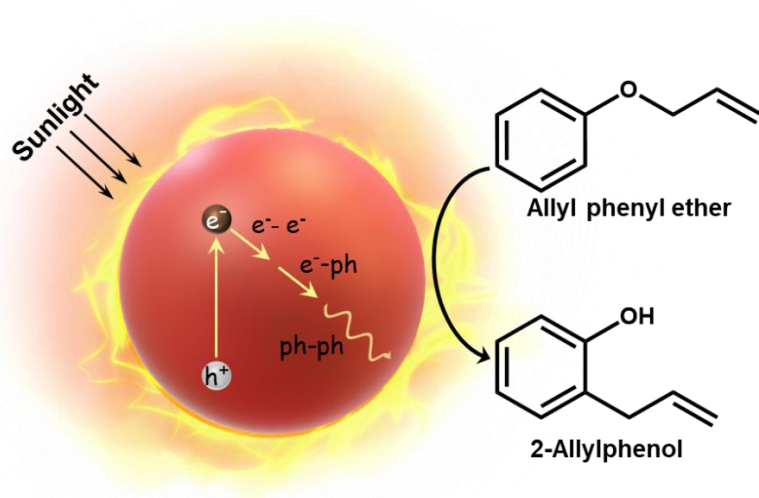
Scheme 4.1. Schematic representation of plasmonic-heat driven Claisen rearrangement of allyl phenyl ether to 2-allylphenol. The photoexcitation of plasmonic AuNPs leads to a series of nonradiative processes: Landau damping, electron-electron (e^-- e^-), electron-phonon (e^--ph), and finally heating-up the local environment via the phonon-phonon (ph-ph) interactions. This heat dissipated from the plasmonic AuNPs was used as the thermal energy source for the Claisen rearrangement.

4.3. Methods and Experimental Section

4.3.1. Materials and reagents

Tetrachloroaurate trihydrate ($HAuCl_4.3H_2O$), tetramethylammonium hydroxide (TMAOH) 25% wt. in water, 11-mercaptoundecanoic acid (MUA), hydrazine monohydrate ($N_2H_4.H_2O$ 50-60%), and tetrabutylammonium borohydride (TBAB) were purchased from Sigma-Aldrich. (Di-n-dodecyl) dimethylammonium bromide (DDAB) and dodecylamine (DDA) were purchased from Alfa Aesar. Allyl phenyl ether was purchased from Tokyo Chemical Industry (TCI). All the reagents were used as received without any further purification. All the stock solutions of metal ions were prepared in Milli-Q water.

4.3.2. UV-visible absorption spectroscopy

UV-vis absorbance data for AuNPs was recorded on a Shimadzu 3600 UV-VIS-NIR spectrophotometer, over the wavelength range of 200-1000 nm.

4.3.3. Transmission electron microscopy studies

The AuNPs were characterized using high resolution transmission electron microscopy (HR-TEM) studies on a JEOL JEM2200FS (200 kV) HRTEM instrument. AuNPs were drop-cast on a 400-mesh carbon-coated copper grid (Tedpella Inc.) and dried overnight under vacuum to prepare the TEM sample.

4.3.4. Synthesis of AuNPs

Spherical gold nanoparticles (AuNPs) were synthesized following a modified literature procedure (**Figure 4.4**).[46,47] Hydrazine monohydrate ($N_2H_4.H_2O$) was used as the reducing agent. In a typical experiment, $HAuCl_4.3H_2O$ (12 mg), DDA (140 mg), and DDAB (140 mg) were mixed in toluene (4 mL) and sonicated for ~10 min for complete solubilization of Au (III) ions. This was followed by a rapid injection of another toluene solution containing 30 mg of TBAB and 46 mg of DDAB. The resulting solution was left stirring overnight to ensure the complete reduction of Au (III) ions. The seed particles were then grown to ~5.5 nm DDA-AuNPs. For this, a growth solution was prepared by adding 460 mg of DDAB, 1.4 g of DDA, 120 mg of $HAuCl_4.3H_2O$ and seed solution in 30 mL toluene. The growth solution was further reduced with a dropwise addition of another toluene solution containing 160 µL of $N_2H_4.H_2O$ and 560 mg of DDAB. The solution was stirred overnight for complete growth of the particles yielding monodisperse 5.5 ± 0.7 nm of DDA-AuNPs. The particles were further grown to ~12 nm DDA-AuNPs. A growth solution was prepared by adding 8 g of DDAB, 13.0 g of DDA, 1.1 g of $HAuCl_4.3H_2O$ and seed solution in 200 mL toluene. The growth solution was further reduced with a dropwise addition of another toluene solution containing 650 µL of $N_2H_4.H_2O$ and 4.4 g of DDAB. The solution was stirred overnight for complete growth of the particles yielding monodisperse 12.09 ± 0.48 nm of DDA-AuNPs, as confirmed through TEM analysis (**Figure 4.5**).

4.3.5. Place-exchange of AuNPs with 11-mercaptoundecanoic acid (MUA) ligands

In a typical place exchange reaction, 12.09 ± 0.48 nm DDA-AuNPs (15 mL) were first precipitated by adding 50 mL of methanol which yielded a black precipitate. The supernatant was carefully removed, and the precipitate was then re-dispersed in 20 mL toluene. MUA ligand (equal to the moles of Au (III) in solution) dissolved in 10 mL dichloromethane (DCM) was added. The solution was left overnight to ensure a complete ligand exchange. Next, the supernatant was decanted, and the precipitate was washed with DCM (3 × 50 mL) and acetone (50 mL), respectively. The precipitate was then dried and redispersed in Milli Q water by adding ~20 µL of TMAOH base (25 % wt. in water), to deprotonate the carboxylic acid group for further studies.

4.3.6. Calculation of NP concentration

The concentration of AuNPs in stock solution was calculated using Beer-Lambert's law:

$$A = \varepsilon \cdot c \cdot l$$

where,

A is the absorbance

ε is the molar extinction coefficient ($M^{-1}cm^{-1}$)

c is the concentration of the solution (M)

l is the optical path length (cm).

Molar extinction coefficient (ε) for AuNP was taken to be 2.7×10^8 M^{-1} cm^{-1} for ~12 nm diameter particles.[48]

The concentration of AuNP stock solution was estimated to be ~ 0.38 µM (in terms of AuNPs).

4.3.7. Solar-driven Claisen rearrangement

Photothermal experiments were performed in a thermodynamically closed reactor system (**Figure 4.6**). Briefly, a 15 mL glass test tube was wrapped with an Al-foil. A film of AuNP (25 µL from 0.38 µM stock solution; 9.5 pmol) was coated onto the Al-foil and dried at room temp. Next, 1 mL of allyl phenyl ether was taken in this reactor followed by irradiating the AuNP film with focused sunlight (**Figure 4.6** and **4.7**). A Fresnel lens (28.5 cm × 19.5 cm) was used to focus the sunlight at the AuNP film. The solar beam diameter was measured to be ~1 cm after focusing and the optical

power illuminated at AuNP film was noted to be ~9 W.cm^{-2}. A thermopile optical power detector (Model LM-10 HTD; Coherent, Santa Clara, CA 95054 USA) was used for measuring the power of sunlight falling on the AuNP film, after focusing. The colorless reactant turned to reddish yellow within 2 h of solar irradiation, indicating the thermal conversion of allyl phenyl ether to 2-allylphenol. The reaction mixture was purified by column chromatography (silica column, 5 % ethyl acetate in hexane), and the product was characterized using proton-NMR and HRMS techniques (**Figure 4.8** and **4.18** in the **Appendix**). Control experiments were performed under focused sunlight without the AuNP film, under similar experimental conditions. Briefly, 1 mL of allyl phenyl ether in an Al-foil wrapped test tube ***without AuNP film*** (**Figure 4.6c**) was irradiated with focused sunlight for 2 h. The thermal experiment was performed in the laboratory at 250 °C with normal electrical heater.

4.3.8. Reaction yield calculation using NMR spectroscopy

The yield of the reaction was determined from ^{1}H-NMR of the crude reaction mixture. The ^{1}H-NMR spectrum of the reaction mixture contains the signals of the following organic molecules: allyl phenyl ether (the unreacted reactant), 2-allylphenol (the major product), and other possible side products.

In order to find the number of moles of product formed, a known amount of the internal standard (1,1,2,2-tetrachloroethane, 1 μL, 9.47 μmol) was added to the reaction mixture in CDCl$_3$. The signal for two equivalent protons of the internal standard appears as a singlet at δ5.95 ppm. This peak does not overlap with the NMR peaks of any other compounds in the reaction mixture. For more clarity, a representative ^{1}H-NMR spectrum and yield calculation are given below (**Figure 4.3**).

The reaction under consideration here is a 1:1 reaction, in which for every one mole of reactant reacted, an equivalent mole of product is expected to form. Thus, the yield (in percentage) was calculated as follows:

$$\text{Yield} = \frac{\text{number of moles of product formed}}{\text{number of moles of reactant used}} \times 100$$

Here, the number of moles of reactant used was 34.0 μmol, and the number of moles of product formed was determined from the NMR spectrum with a known amount of the internal standard (9.47 μmol).
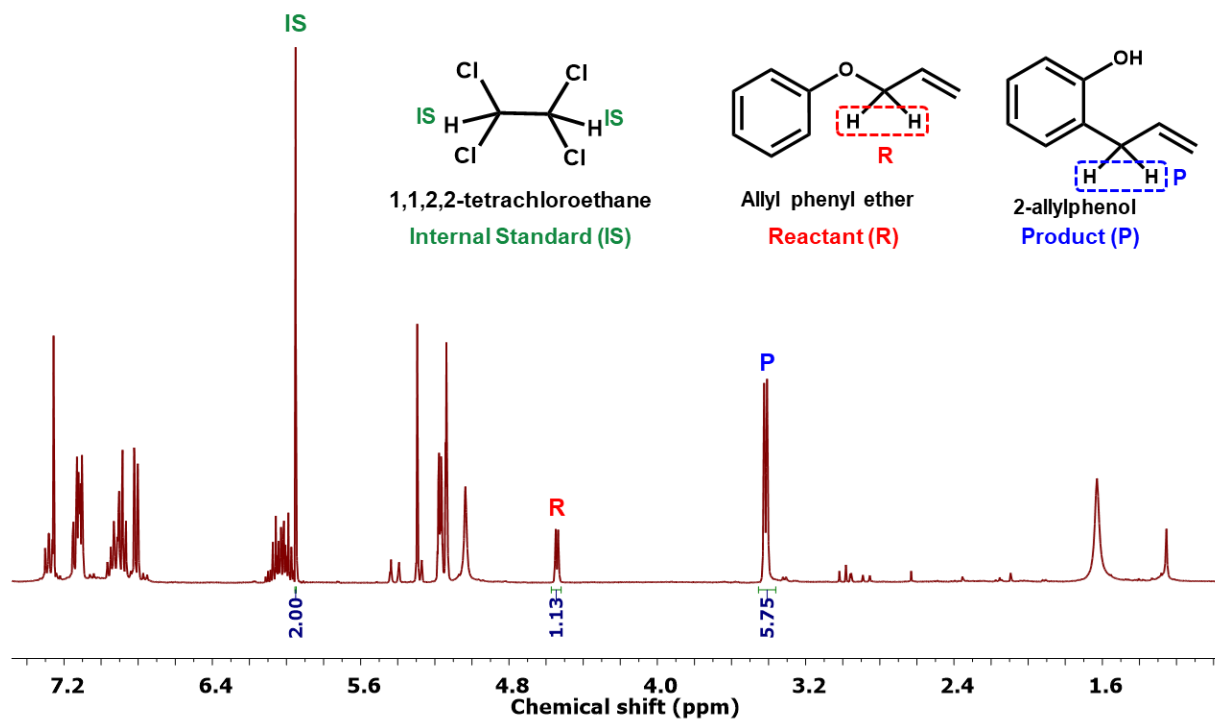
Figure 4.3. Representative ^{1}H-NMR spectrum of the crude reaction mixture with 1,1,2,2-tetrachloroethane as internal standard (IS). The characteristic peaks are marked with P, R and IS for product, reactant, and internal standard, respectively.

Since the peak of internal standard (IS) corresponds to 2 protons and peak of product (P) corresponds to 2 protons, the number of moles of product formed can be calculated using the following equation:

$$\text{number of moles of product} = \frac{\left(\frac{I_P}{2}\right)}{\left(\frac{I_{IS}}{2}\right)} \times \frac{w_{IS}}{M_{IS}} = \frac{I_P}{I_{IS}} \times n_{IS}$$

where,

I_P = integration value for NMR peak of product marked 'P' (5.75)

I_{IS} = integration value for NMR peak of internal standard marked 'IS' (2.00)

w_{IS}= weight of internal standard added after reaction (volume × density)

M_{IS}= molar mass of Internal standard

n_{IS}= number of moles of Internal standard used (9.47 μmol)

Substituting these values and relevant values from the NMR spectrum, we get:

$$\text{number of moles of product} = \frac{5.75}{2.00} \times 9.47 = 27.2262 \text{ μmol}$$

The number of moles of reactant used was 34.0 μmol. Therefore, percentage yield in this case is:

$$\text{Yield} = \frac{27.2262}{34.0} \times 100 = \mathbf{80.07} \text{ %}$$

4.3.9. In-situ visualization of photothermal Claisen rearrangement

In a typical experiment, film of AuNPs (25 μL from 0.38 μM stock solution) at the inner wall of a 15 ml glass test tube was made by drying its aqueous suspension at room temperature. Next, 1 mL of allyl phenyl ether (reactant) was added into the test tube. Finally, the AuNP film which was in physical contact with the reactant was irradiated with focused sunlight. Fresnel lens (19.5 cm × 28.5 cm) was used to focus the sunlight onto the AuNP film, the spot diameter was measured to be ~1 cm (**Figure 17a** in the **Appendix**). A thermopile optical power detector (Model LM-10 HTD; Coherent, Santa Clara, CA 95054 USA) was used for measuring the power of sunlight falling on the AuNP film, after focusing. The solar power measured under our experimental conditions was ~9 W.cm^{-2}. **Figure 4.17c** (in the **Appendix**) clearly shows the vigorous boiling of the reactant (b.p. = 191.7 °C), along with a distinct color change to reddish yellow (indicating the successful chemical transformation).

The control experiment in the absence of AuNP keeping other experimental parameter constant failed to show any boiling of the reactant as well as color change reaffirming the negligible chemical transformation (**Figure 17b** in the **Appendix**).

4.3.10. Reusability study

The reusability was performed using the same AuNP coated Al-foil wrapped test-tube set-up for five cycles. In each cycle, 1 mL of the allyl phenyl ether was taken in the test-tube and the same AuNP coated Al-foil was irradiated with focused sunlight for 90 min. The next cycle was performed after carefully washing and drying the inside of the test-tube. All the experimental parameters were kept identical in all cycles. The yield of the reaction was similar till five cycles, which can be attributed to the excellent photostability of AuNPs.

4.3.11. Reaction kinetics

Aliquots were taken from the reaction mixture at different time intervals, and the product yield was estimated. Briefly: for plasmonic-heat driven Claisen rearrangement, the aliquots were analyzed at 30, 45, 75, 90 and 120 mins. A continuous rise in the product peak (marked P) was observed along with simultaneous decrease in the reactant peak (marked R) upon increase in the reaction time. ~80% yield was obtained after 2 h of irradiation.

Likewise, kinetic studies for thermal reaction were performed. Here, the aliquots were taken out till 6 h as the reaction, so as to obtain a yield of ~80%. The amount of reaction mixture analyzed in each aliquot was the same.

4.4. Results and Discussion

AuNPs were chosen as the plasmonic NP in the present study because of their strong absorption power in visible-light and high photostability under continuous solar irradiation.[1-3] AuNPs of diameter 12.0 ± 0.4 nm were synthesized using a modified seed-mediated growth method[16] (see **Figures 4.4** and **4.5**).

Figure 4.4. General scheme for AuNPs synthesis and ligand exchange to obtain MUA-functionalized AuNPs in aqueous medium.

The surface of the AuNPs was functionalised with 11-mercaptoundecanoic acid (MUA) to enhance the colloidal stability of the NPs in the aqueous medium. This enabled the entire photothermal studies with AuNPs from the same batch. The rationale behind selecting ~12 nm AuNPs was based on the knowledge that AuNPs in the size range of 10–24 nm shows the highest photothermal conversion efficiency.[49] The surface plasmon band of AuNPs (centred at ~520 nm) has a strong overlap with the solar spectrum, enabling the use of sunlight as the irradiation source (**Figure 4.3a**).

Figure 4.5. Spectroscopic and microscopic characterization of AuNPs. (a) UV-visible absorption studies show a strong overlap between the surface plasmon band of AuNP (centred at ~520 nm) and the solar spectrum, confirming the suitability of sunlight as the irradiation source. Solar spectrum is the ASTM G173-03 AM1.5G reference spectrum adapted from DOE/NREL/ALLIANCE. (b) A representative transmission electron microscope (TEM) image of 12.0 ± 0.4 nm AuNPs. (c) A histogram showing the size distribution of MUA-functionalized AuNPs.

Along with testing the suitability of plasmonic heat in high temperature organic synthesis, our objective was to eliminate the contribution from hot-charge carriers in a plasmon-driven organic reaction. For this, a thin film of plasmonic AuNPs was coated on the surface of aluminium (Al) foil that was wrapped around the glass test tube (here, reactor) (see **Figure 4.6** and **4.7**). The Al-foil interface helped in achieving a stable coating of AuNPs on the test tube. Also, the high thermal conductivity of Al (205 W m^{-1} K^{-1}) ensured the effective transfer of the plasmonic-heat to the reactants inside the glass test tube. The physical separation of the reactants from the plasmonic-heat source (here, AuNPs) prevented the transfer of hot-charge carriers to the reactant. Furthermore, the wrapping of the reactor with Al-foil will block the direct exposure of the reactants to sunlight, thereby overruling the interference of photochemical effects as well. Yet another advantage of the closed reactor is that the reaction mixture will not be contaminated with the plasmonic heaters. In this way, a simple design of a closed reactor enabled us to study the sole effect of photothermal properties in a plasmon-driven organic reaction.
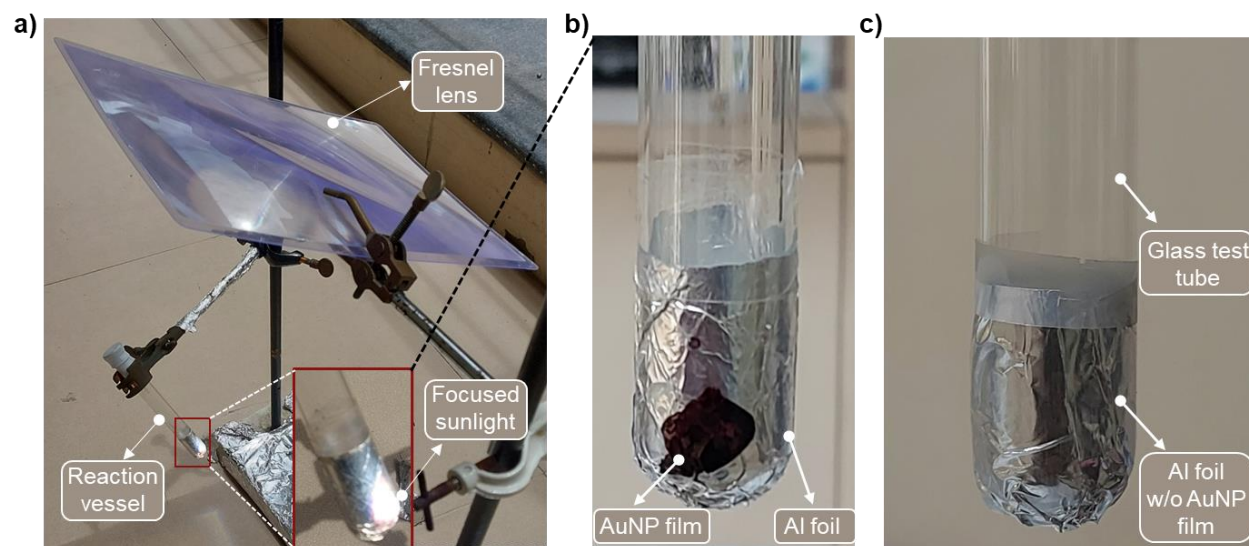

Figure 4.6. Reaction setup and the thermodynamically closed reactor. (a) and (b) Experimental setup for the plasmonic-heat driven Claisen rearrangement. A film of AuNPs was coated on the Al-foil wrapped test tube. The sunlight was focused on the AuNPs film using a Fresnel lens (28.5 cm × 19.5 cm). (c) The reactor setup for the control experiment where allyl phenyl ether reactant in an Al-foil wrapped test tube without AuNP film was irradiated with focused sunlight.

Claisen rearrangement was selected as the model reaction to study the potential of plasmonic heat in performing high-temperature organic synthesis. The intramolecular ortho rearrangement of the allylic group in allyl phenyl ether to form 2-allylphenol *via* [3,3] sigmatropic rearrangement is an

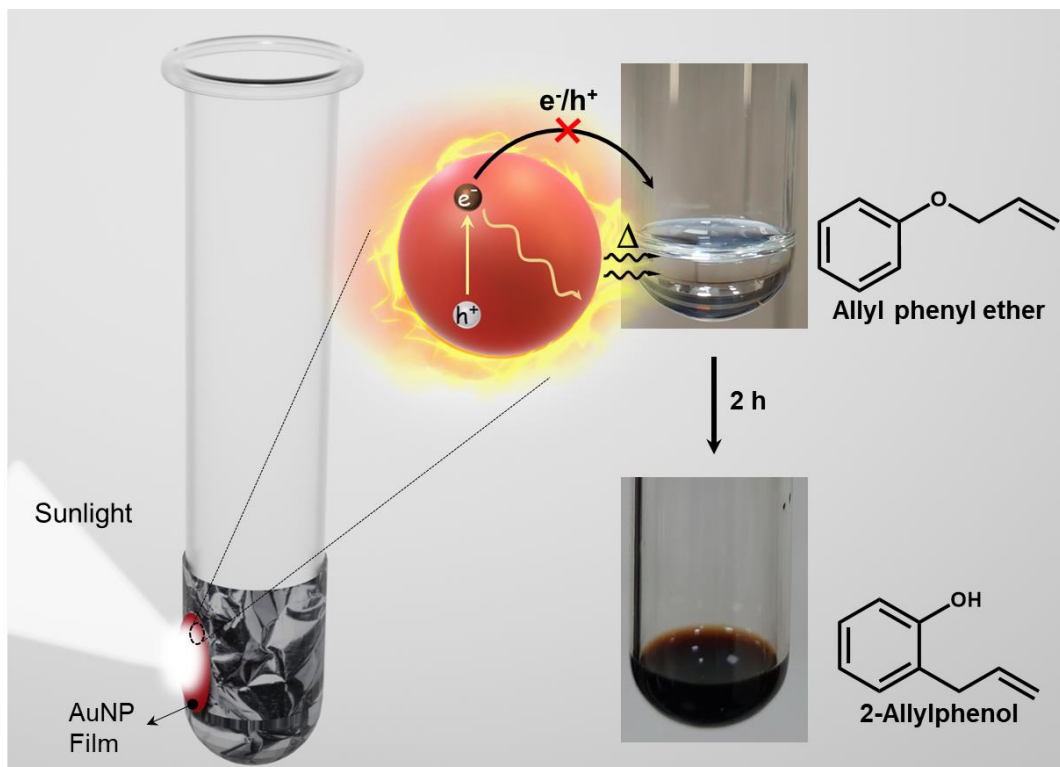energy intensive thermal transformation, which was conventionally performed at 250 °C (**Figure 4.7**).

Figure 4.7. Schematics of the thermodynamically closed reactor used for the plasmonic-heat driven Claisen rearrangement. The optical photographs of the reaction medium before and after 2 h of solar illumination are shown on the right side.

Our idea was to replace the traditional electrical-heat with plasmonic-heat generated from the solar irradiation of AuNPs (**Figure 4.8a**). In a typical photothermal experiment, the AuNP coated Al-foil wrapped test tube containing 1 mL of allyl phenyl ether was irradiated with focused sunlight (experimental details are provided in **Section 4.3.7**). The colourless reactant turned to reddish yellow within 2 h of solar irradiation (**Figure 4.7**), indicating the thermal conversion of allyl phenyl ether to 2-allylphenol. The reaction mixture was purified, and the product was characterized using ^{1}H-NMR and HRMS studies (**Figure 4.8** and **4.18** in the Appendix). The presence of all the characteristic peaks in proton NMR as well as molecular ion peak in HRMS spectrum confirms the formation of desired product. All the yields were calculated from the ^{1}H-NMR of the reaction

mixture using the internal standard method (1,1,2,2-tetrachloroethane was used as the internal standard) (see **Figure 4.3**, **4.10** and **Section 4.3.8** for details of yield calculation).
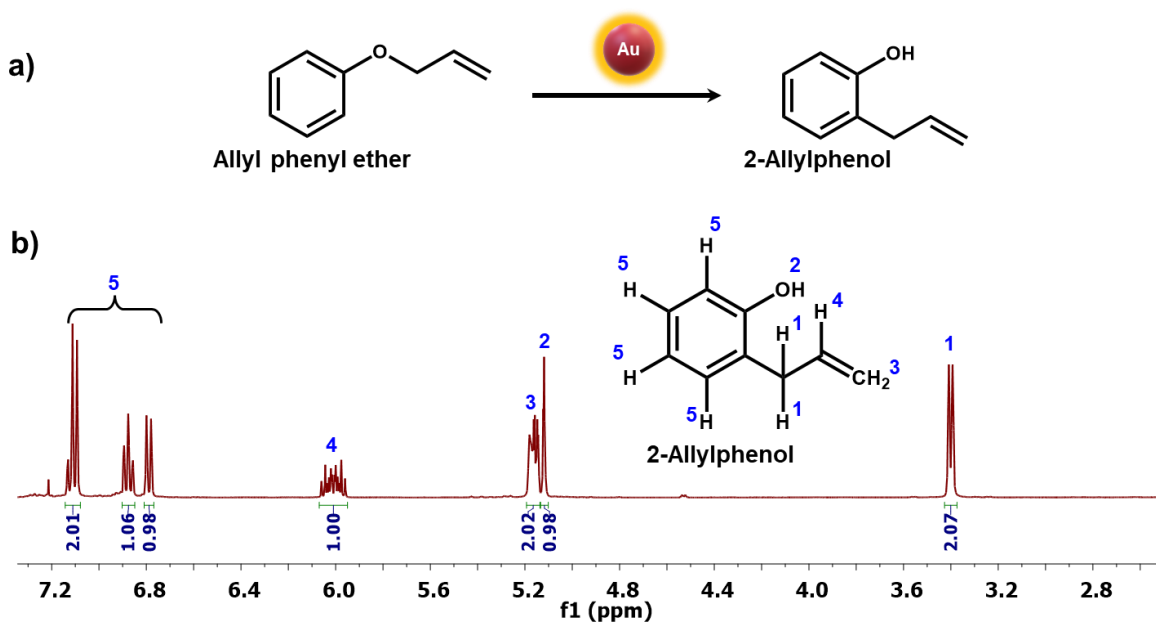

Figure 4.8. Product characterization. (a) Reaction scheme and (b) ^{1}H-NMR spectrum of the purified product obtained from the plasmonic-heat driven Claisen rearrangement. Presence of all the characteristic NMR peaks of the product, 2-allylphenol, confirms the successful chemical transformation using plasmonic-heat.
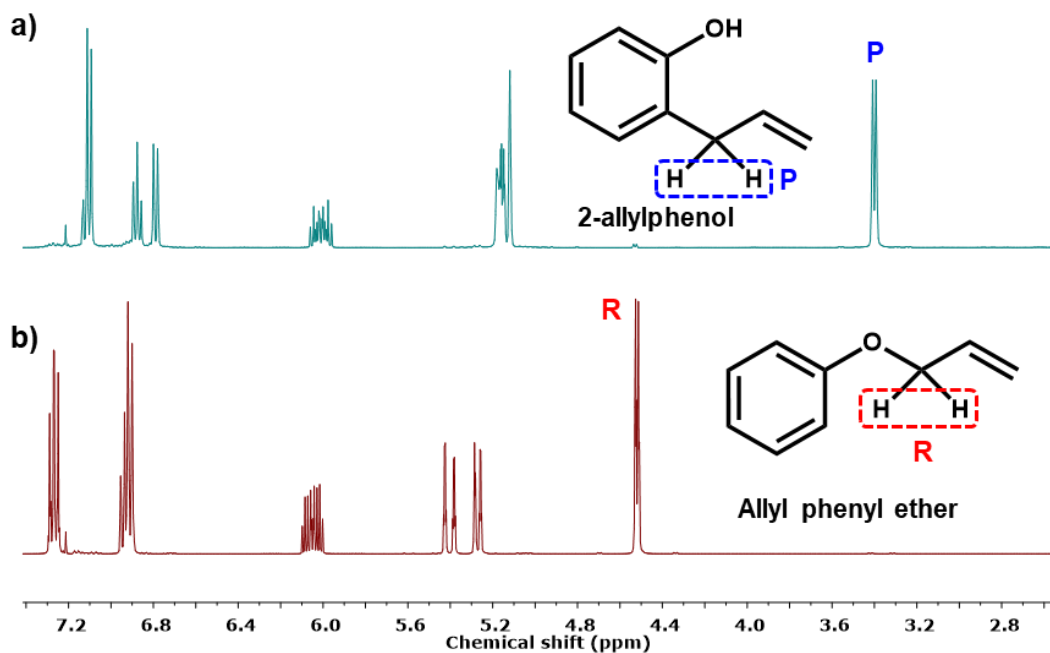
Figure 4.10. ¹H-NMR spectra of (a) product (2-allylphenol) and (b) reactant (allyl phenyl ether). The main characteristic peaks in product and reactant are marked as P and R, respectively.

The plasmonic-heat driven Claisen rearrangement resulted in a yield of ~80% after 2 h of solar irradiation (**Figure 4.11** and **4.12**), which was at least double the yield obtained from normal thermal reaction performed at 250 °C under similar experimental conditions (**Figure 4.12** and **4.19** in the Appendix).
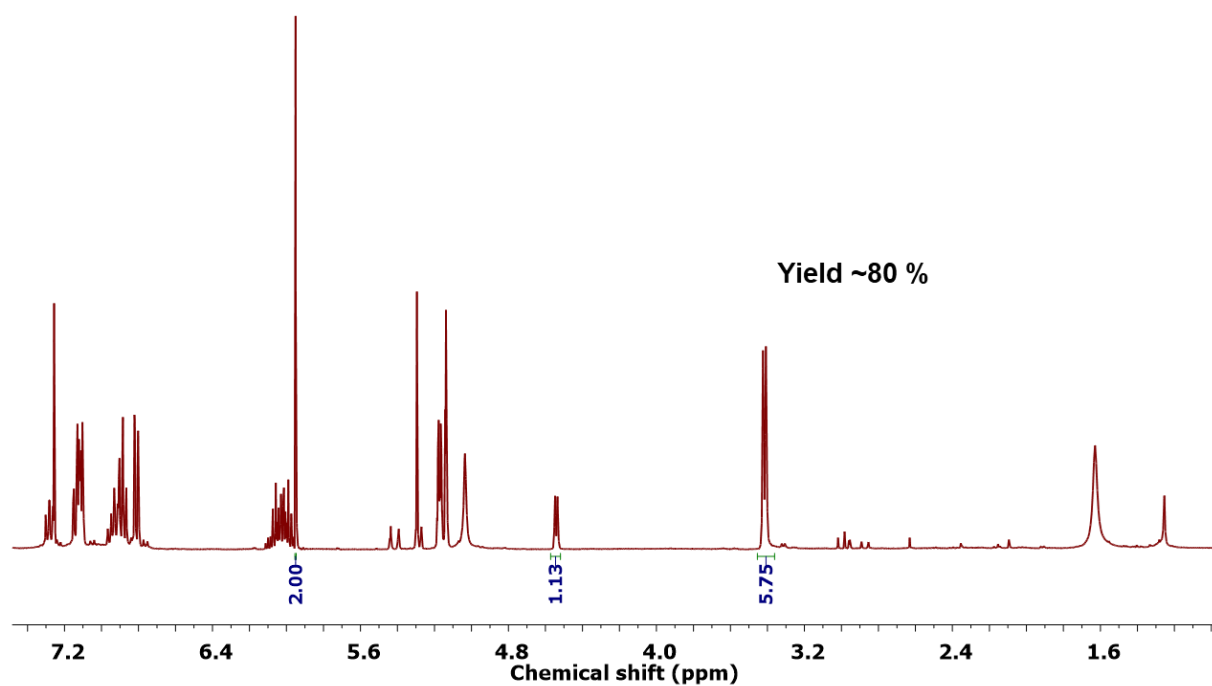
Figure 4.11 ^{1}H-NMR spectrum of the crude reaction mixture after 2 h sunlight irradiation of the reactant in a AuNP coated Al-foil wrapped test-tube (plasmonic-heat driven Claisen rearrangement).

The enhancement in the yield under solar irradiation can be explained as follows. The amount of energy absorbed by AuNPs upon solar irradiation is exceptionally high ($\sim 10^8$ M^{-1} cm^{-1}), because of the phenomenon of surface plasmon resonance.[1-3] The photoexcited AuNPs undergo a series of nonradiative relaxation processes (Landau damping, electron–electron, electron–phonon, and phonon–phonon interactions) to eventually dissipate the excess energy in the form of plasmonic-heat.[3] It has been shown that the plasmonic-heat can raise the surface temperature of AuNPs to 600 °C,[50] which will be finally dissipated to the surrounding medium. As a result, the temperature experienced by the surrounding medium close to the plasmonic AuNPs can be as high as $\sim$600 °C.[37,50] In the present study too, a higher steady-state temperature (>250 °C)[34] could have been experienced by the reactants because of the plasmonic-heat dissipated from the photoexcited AuNPs, leading to an improvement in the product yield under solar irradiation. Control experiments (i) in the dark at room temperature under similar experimental conditions with an AuNP film coated Al-foil wrapped test tube (**Figure 4.12** and **4.20** in the **Appendix**) and (ii) under

sunlight illumination of allyl phenyl ether reactant in an Al-foil wrapped test tube without the AuNP film produced negligible yields (**Figure 4.12** and **Figure 4.21** in the Appendix), confirming the necessity of plasmonic heat in performing the reaction. It is worth mentioning that the Al-foil completely blocks the focused sunlight from entering the test tube (**Figure 4.13**), which overrules the possibility of the thermal shielding effect arising from the confinement of light by Al-foil.
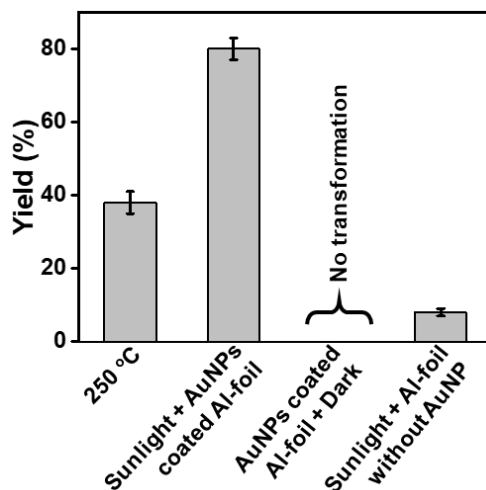

Figure 4.12. Bar diagram showing the yield obtained under different experimental conditions, which conclusively prove the sole role of plasmonic heat in driving the Claisen rearrangement.
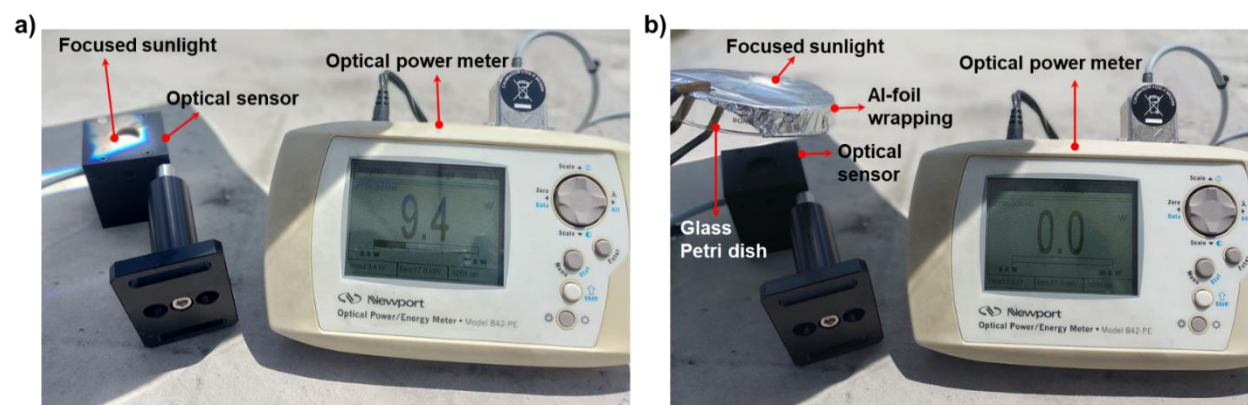

Figure 4.13. Focused solar power measured in the (a) absence and (b) presence of Al-foil wrapped glass Petri dish. The Al-foil completely blocks the focused sunlight.

Figure 4.17c (in the **Appendix**) clearly shows the vigorous boiling, along with a distinct color change to reddish yellow, when the AuNP coated test tube containing allyl phenyl ether reactant (b.p. = 191.7 °C) was irradiated with sunlight. In this particular experiment, the AuNP film was coated inside the glass test tube for the in-situ visualisation of the progress of the reaction (control

experiments in the absence of AuNPs fail to show any boiling as well as conversion of the reactant. Details are given in the **Section 4.3.9**). All these control experiments confirm the sole-involvement of plasmonic heat as the thermal energy source in the Claisen rearrangement of allyl phenyl ether to 2-allylphenol. The plasmonic heaters based on AuNPs also showed excellent reusability with negligible loss in the photothermal reaction yield for at least five cycles (**Figure 4.14**), which can be attributed to their high photostability under continuous solar irradiation (the time of the reaction was reduced to 90 min to complete multiple cycles under similar solar irradiation power).
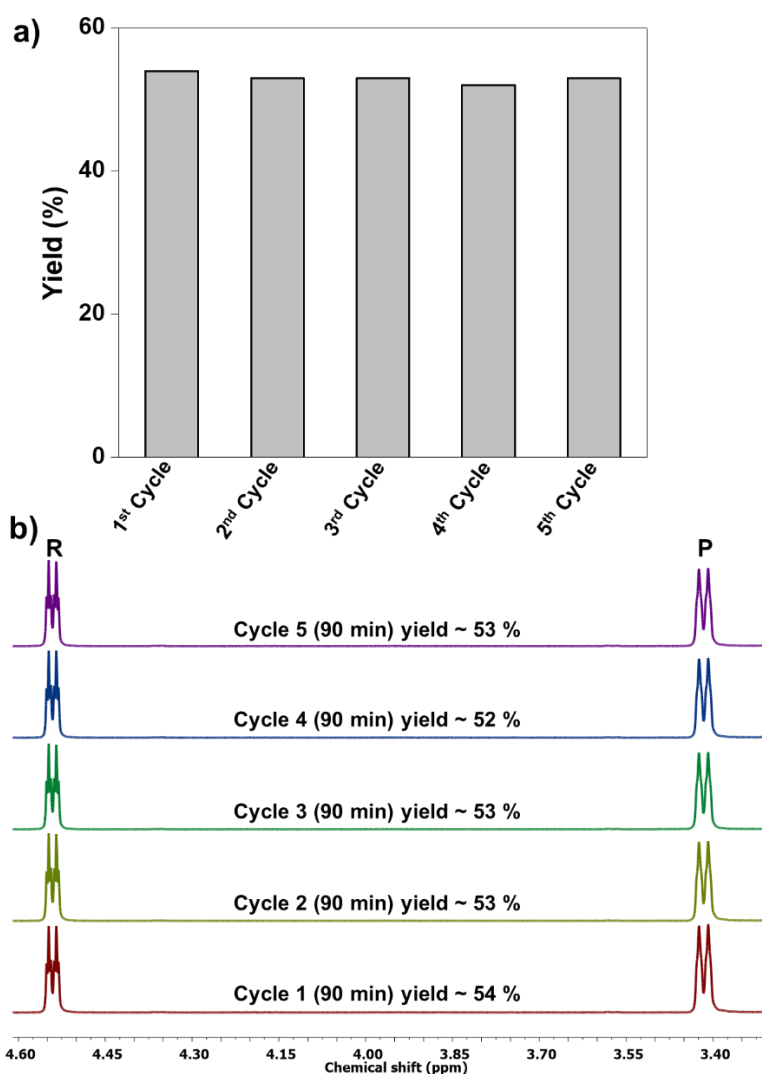

Figure 4.14. Reusability study of thermodynamically closed rector. (a) Bar diagram showing the retention of photothermal activity of plasmonic AuNPs for at least five cycles. (b) ^{1}H-NMR spectra of the reaction mixture obtained in each cycle during the reusability study are stacked together. R and P corresponds to the characteristic peaks of reactant and product, respectively.

Finally, the rate of the Claisen rearrangement under plasmonic- and electrical-heating was compared. The progress of the reaction was monitored by analysing the product yield in aliquots collected at different time intervals (see Section 4.3.11 for the experimental details). NMR studies revealed a gradual increase in the product yield with time (**Figure 4.15a** and **b**), for both plasmonic and electrical-heating driven Claisen rearrangement. The NMR signal at 3.5 ppm corresponding to the product increased with time of heating, accompanied by a decrease in the reactant signal at 4.55 ppm (**Figure 4.16**).
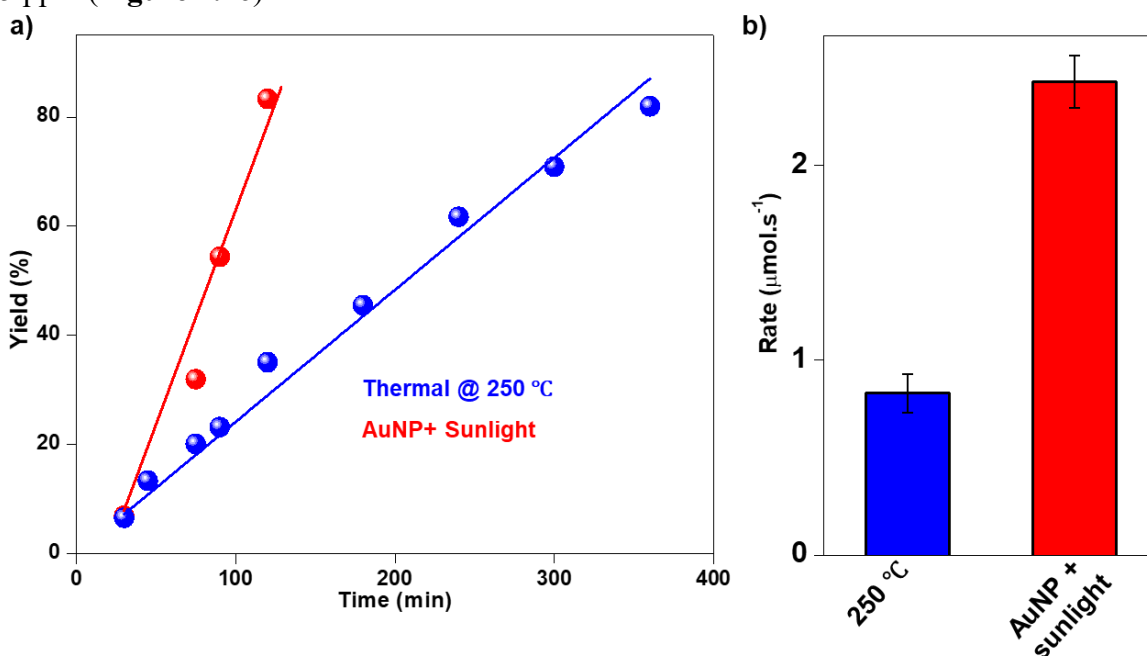

Figure 4.15. Kinetic study of Claisen rearrangement. (a) A plot showing the variation in the product yield with respect to time for plasmonic-heat (red) and electrical-heat (blue) driven Claisen rearrangement. (b) The bar diagram showing the corresponding reaction rates.

Approximately 80% product was formed under the plasmonic-heating condition after 2 h of solar irradiation. In contrast, the normal electrical-heating at 250 °C required ~6 h to yield ~80% product formation (**Figure 4.16b**). The rate of the reaction under plasmonic-heating conditions was at least two times higher than the one under electrical-heating, which confirms that the steady-state temperature achieved with plasmonic-heat is higher than 250 °C.
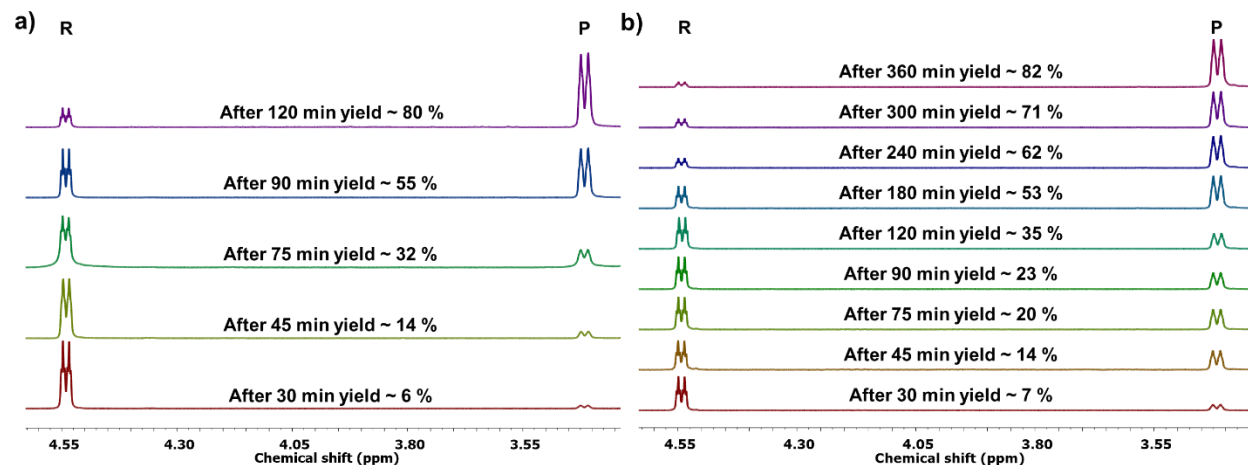
Figure 4.16. Time dependent ¹H NMR study. (a) A plot showing the variation in 1H-NMR signals with respect to time for plasmonic-heat driven Claisen rearrangement (only the region covering the distinguishable peaks of reactant and product is shown for clarity). (b) A plot showing the variation in ¹H-NMR signals with respect to time for thermal Claisen rearrangement performed at 250 °C with electrical heating. A gradual increase in the product peak intensity (marked P), along with a decrease in the reactant peak intensity (marked R), was observed with time.

4.5. Conclusion

In summary, the potential of the "heat" generated from the solar irradiation of plasmonic gold nanoparticles (AuNPs) in performing an energy intensive organic reaction, thereby showcasing a way to achieve sustainability in high-temperature chemical synthesis is studied. An energy-intensive high temperature Claisen rearrangement was performed with an excellent yield of ~80% using the plasmonic heat generated from the solar irradiation of AuNPs. Control experiments conclusively prove the sole role of plasmonic heat as the thermal energy source for driving the Claisen rearrangement. The high photostability of AuNPs ensured the constant supply of heat energy for performing the Claisen rearrangement, under continuous and repeated solar irradiations. More importantly, an appropriate design of a closed reactor enabled the physical separation of reactants from the source of the plasmonic-heat generator, which prevented the interference from the hot-charge carriers. The thermodynamically closed plasmonic reactor was found to be reusable till at least 5 cycles; an important feat that is scarcely discussed in the literature. In short, our study reveals the potential of plasmonic heating as an alternative to electrical-heating for high-

temperature organic reactions, thereby showcasing a way to achieve sustainability in high-temperature chemical synthesis. Moreover, the thermodynamically closed reactor that was designed in this work can be adapted in future to study the sole effects of photothermal effects in a plasmon-driven process. Thus, we strongly believe that the results summarized in this work will inspire the chemists to replace electrical heating with plasmonic-heating in high-temperature chemical reactions.

4.6. References

(1)   Link, S.; El-Sayed, M. A. Spectral Properties and Relaxation Dynamics of Surface Plasmon Electronic Oscillations in Gold and Silver Nanodots and Nanorods. *J. Phys. Chem. B* **1999**, *103*, 8410–8426.

(2)   Hodak, J. H.; Martini, I.; Hartland, G. V. Spectroscopy and Dynamics of Nanometer-Sized Noble Metal Particles. *J. Phys. Chem. B* **1998**, *102*, 6958–6967.

(3)   Bohren, C. F. How can a particle absorb more than the light incident on it? *Am. J. Phys*. **1983**, *51*, 323–327.

(4)   Sönnichsen, C.; Franzl, T.; Wilk, T.; von Plessen, G.; Feldmann, J.; Wilson, O.; Mulvaney, P. Drastic Reduction of Plasmon Damping in Gold Nanorods. *Phys. Rev. Lett*. **2002**, *88*, 077402.

(5)   Brown, A. M.; Sundararaman, R.; Narang, P.; Goddard, W. A. I.; Atwater, H. A. Nonradiative Plasmon Decay and Hot Carrier Dynamics: Effects of Phonons, Surfaces, and Geometry. *ACS Nano* **2016**, *10*, 957–966.

(6)   Inouye, H.; Tanaka, K.; Tanahashi, I.; Hirao, K. Ultrafast Dynamics of Nonequilibrium Electrons in A Gold Nanoparticle System. *Phys. Rev. B* **1998**, *57*, 11334–11340.

(7)   Link, S.; El-Sayed, M. A. Optical Properties and Ultrafast Dynamics of Metallic Nanocrystals. *Annu. Rev. Phys. Chem.* **2003**, *54*, 331–366.

(8)   Brongersma, M. L.; Halas, N. J.; Nordlander, P. Plasmon-Induced Hot Carrier Science and Technology. *Nat. Nanotechnol*. **2015**, *10*, 25–34.

(9)   Boerigter, C.; Aslam, U.; Linic, S. Mechanism of Charge Transfer from Plasmonic Nanostructures to Chemically Attached Materials. *ACS Nano* **2016**, *10*, 6108–6115.

(10) Jain, V.; Kashyap, R. K.; Pillai, P. P. Plasmonic Photocatalysis: Activating Chemical Bonds through Light and Plasmon. *Adv. Opt. Mater.* **2022**, *10*, 2200463.

(11) Linic, S.; Christopher, P.; Ingram, D. B. Plasmonic-Metal Nanostructures for Efficient Conversion of Solar to Chemical Energy. *Nat. Mater*. **2011**, *10*, 911–921.

(12) Mukherjee, S.; Libisch, F.; Large, N.; Neumann, O.; Brown, L. V.; Cheng, J.; Lassiter, J. B.; Carter, E. A.; Nordlander, P.; Halas, N. J. Hot Electrons Do the Impossible: Plasmon-Induced Dissociation of H_2 on Au. *Nano Lett*. **2013**, *13*, 240–247.

(13) Roy, S.; Roy, S.; Rao, A.; Devatha, G.; Pillai, P. P. Precise Nanoparticle–Reactant Interaction Outplays Ligand Poisoning in Visible-Light Photocatalysis. *Chem. Mater*. **2018**, *30*, 8415–8419.

(14) Roy, S.; Jain, V.; Kashyap, R. K.; Rao, A.; Pillai, P. P. Electrostatically Driven Multielectron Transfer for the Photocatalytic Regeneration of Nicotinamide Cofactor. *ACS Catal*. **2020**, *10*, 5522–5528.

(15) Jain, V.; Chakraborty, I. N.; Raj, R. B.; Pillai, P. P. Deciphering the Role of Light Excitation Attributes in Plasmonic Photocatalysis: The Case of Nicotinamide Cofactor Regeneration. *J. Phys. Chem. C* **2023**, *127*, 5153–5161.

(16) Dhankhar, A.; Jain, V.; Chakraborty, I. N.; Pillai, P. P. Enhancing the Photocatalytic Regeneration of Nicotinamide Cofactors with Surface Engineered Plasmonic Antenna-Reactor System. *J. Photochem. Photobiol. A* **2023**, *437*, 114472.

(17) Kuno, J.; Ledos, N.; Bouit, P.-A.; Kawai, T.; Hissler, M.; Nakashima, T. Chirality Induction at the Helically Twisted Surface of Nanoparticles Generating Circularly Polarized Luminescence. *Chem. Mater*. **2022**, *34*, 9111–9118.

(18) Verma, R.; Tyagi, R.; Voora, V. K.; Polshettiwar, V. Black Gold-Based "Antenna–Reactor" To Activate Non-Plasmonic Nickel: Photocatalytic Hydrodechlorination and Hydrogenation Reactions *ACS Catal.* **2023**, *13*, 7395–7406.

(19) Govorov, A. O.; Richardson, H. H. Generating Heat with Metal Nanoparticles. *Nano Today* **2007**, *2*, 30–38.

(20) Baffou, G.; Quidant, R. Thermo-Plasmonics: Using Metallic Nanostructures as Nano-Sources of Heat. *Laser Photonics Rev*. **2013**, *7*, 171–187.

(21) Jauffred, L.; Samadi, A.; Klingberg, H.; Bendix, P. M.; Oddershede, L. B. Plasmonic Heating of Nanostructures. *Chem. Rev*. **2019**, *119*, 8087–8130.

(22) Margeson, M. J.; Monfared, Y. E.; Dasog, M. Synthesis and Photothermal Properties of UV-Plasmonic Group IV Transition Metal Carbide Nanoparticles. *ACS Appl. Opt. Mater*. **2023**, *1*, 1004–1011.

(23) B.; Klemmed, L. V.; Besteiro, A.; Benad, Georgi, M.; Wang, Z.; Govorov, A. O.; Eychmüller, A. Hybrid Plasmonic–Aerogel Materials as Optical Superheaters with Engineered Resonances. *Angew. Chem. Int. Ed*. **2020**, *59*, 1696–1702.

(24) Dhiman, M.; Maity, A.; Das, A.; Belgamwar, R.; Chalke, B.; Lee, Y.; Sim, K.; Nam, J.-M.; Polshettiwar, V. Plasmonic Colloidosomes of Black Gold for Solar Energy Harvesting and Hotspots Directed Catalysis for CO_2 to Fuel Conversion. *Chem. Sci*. **2019**, *10*, 6594–6603.

(25) Mezzasalma, S. A.; Kruse, J.; Merkens, S.; Lopez, E.; Seifert, A.; Morandotti, R.; Grzelczak, M. Light-Driven Self-Oscillation of Thermoplasmonic Nanocolloids. *Adv. Mater*. **2023**, *35*, 2302987.

(26) Roy, S.; Kashyap, R. K.; Pillai, P. P. Thermoplasmonics Enable the Coupling of Light into the Solvent-Mediated Self-Assembly of Gold Nanoparticles. *J. Phys. Chem. C* **2023**, *127*, 10355–10365.

(27) Richardson, H. H.; Carlson, M. T.; Tandler, P. J.; Hernandez, P.; Govorov, A. O. Experimental and Theoretical Studies of Light-to-Heat Conversion and Collective Heating Effects in Metal Nanoparticle Solutions. *Nano Lett*. **2009**, *9*, 1139–1146.

(28) Breitenborn, H.; Dong, J.; Piccoli, R.; Bruhacs, A.; Besteiro, L. V.; Skripka, A.; Wang, Z. M.; Govorov, A. O.; Razzari, L.; Vetrone, F.; Naccache, R.; Morandotti, R. Quantifying the Photothermal Conversion Efficiency of Plasmonic Nanoparticles by Means of Terahertz Radiation. *APL Photonics* **2019**, *4*, 126106.

(29) Hirsch, L. R.; Stafford, R. J.; Bankson, J. A.; Sershen, S. R.; Rivera, B.; Price, R. E.; Hazle, J. D.; Halas, N. J.; West, J. L. Nanoshell-Mediated Near-Infrared Thermal Therapy of Tumors Under Magnetic Resonance Guidance. *Proc. Natl. Acad. Sci. U.S.A*. **2003**, *100*, 13549–13554.

(30) Huang, X.; El-Sayed, I. H.; Qian, W.; El-Sayed, M. A. Cancer Cell Imaging and Photothermal Therapy in the Near-Infrared Region by Using Gold Nanorods. *J. Am. Chem. Soc*. **2006**, *128*, 2115–2120.

(31) Sun, T.; Zhang, Y. S.; Pang, B.; Hyun, D. C.; Yang, M.; Xia, Y. Engineered Nanoparticles for Drug Delivery in Cancer Therapy. *Angew. Chem. Int. Ed*. **2014**, *53*, 12320–12364.

(32) Strozyk, M. S.; Carregal-Romero, S.; Henriksen-Lacey, M.; Brust, M.; Liz-Marzán, L. M. Biocompatible, Multiresponsive Nanogel Composites for Codelivery of Antiangiogenic and Chemotherapeutic Agents. *Chem. Mater*. **2017**, *29*, 2303–2313.

(33) Neumann, O.; Urban, A. S.; Day, J.; Lal, S.; Nordlander, P.; Halas, N. J. Solar Vapor Generation Enabled by Nanoparticles. *ACS Nano* **2013**, *7,* 42–49.

(34) Kashyap, R. K.; Dwivedi, I.; Roy, S.; Roy, S.; Rao, A.; Subramaniam, C.; Pillai, P. P. Insights into the Utilization and Quantification of Thermoplasmonic Properties in Gold Nanorod Arrays. *Chem. Mater*. **2022**, *34*, 7369–7378.

(35) Neumann, O.; Neumann, A. D.; Silva, E.; Ayala-Orozco, C.; Tian, S.; Nordlander, P.; Halas, N. J. Ultrafast Electron Dynamics in Single Aluminum Nanostructures. *Nano Lett*. **2015**, *15*, 7880–7885.

(36) Kamarudheen, R.; Kumari, G.; Baldi, A. Plasmon-Driven Synthesis of Individual Metal@Semiconductor Core@Shell Nanoparticles. *Nat. Commun*.**2020**, *11*, 3957.

(37) Fasciani, C.; Alejo, C. J. B.; Grenier, M.; Netto-Ferreira, J. C.; Scaiano, J. C. High-Temperature Organic Reactions at Room Temperature Using Plasmon Excitation: Decomposition of Dicumyl Peroxide. *Org. Lett*. **2011**, *13*, 204–207.

(38) Vázquez-Vázquez, C.; Vaz, B.; Giannini, V.; Pérez-Lorenzo, M.; Alvarez-Puebla, R. A.; Correa-Duarte, M. A. Nanoreactors for Simultaneous Remote Thermal Activation and Optical Monitoring of Chemical Reactions. *J. Am. Chem. Soc*. **2013**, *135*, 13616–13619.

(39) Qiu, J.; Wei, W. D. Surface Plasmon-Mediated Photothermal Chemistry. *J. Phys. Chem. C* **2014**, *118*, 20735–20749.

(40) Van Burns, E. N.; Lear, B. J. Controlled Rapid Formation of Polyurethane at 700 K: Thermodynamic and Kinetic Consequences of Extreme Photothermal Heating. *J. Phys. Chem. C* **2019**, *123*, 14774–14780.

(41) Zhou, L.; Swearer, D. F.; Zhang, C.; Robatjazi, H.; Zhao, H.; Henderson, L.; Dong, L.; Christopher, P.; Carter, E. A.; Nordlander, P.; Halas, N. J. *Science* **2018**, *362*, 69–72.

(42) Claisen, L. *Berichte der deutschen chemischen Gesellschaft*, **1912**, *45*, 3157–3166.

(43) Martín Castro, A. M. Claisen Rearrangement Over the Past Nine Decades. *Chem. Rev*. **2004**, *104*, 2939–3002;

(44) Han, X.; Armstrong, D. W. Using Geminal Dicationic Ionic Liquids as Solvents for High-Temperature Organic Reactions. *Org. Lett*. **2005**, *7*, 4205–4208.

(45) Hiersemann, M.; Nubbemeyer, U. *The Claisen Rearrangement*, Wiley-VCH, Weinheim, 2007.

(46) Jana, N. R.; Peng, X. Single-Phase and Gram-Scale Routes toward Nearly Monodisperse Au and Other Noble Metal Nanocrystals. *J. Am. Chem. Soc*. **2003**, *125*, 14280–14281.

(47) Rao, A.; Roy, S.; Unnikrishnan, M.; Bhosale, S. S.; Devatha, G.; Pillai, P. P. Regulation of Interparticle Forces Reveals Controlled Aggregation in Charged Nanoparticles. *Chem. Mater.* **2016**, *28*, 2348–2355.

(48) Kim, Y.; Smith, J. G.; Jain, P. K. Harvesting Multiple Electron–Hole Pairs Generated Through Plasmonic Excitation of Au Nanoparticles. *Nat. Chem.* **2018**, *10*, 763–769.

(49) Kashyap, R. K.; Parammal, M. J.; Pillai, P. P. Effect of Nanoparticle Size on Plasmonic Heat-Driven Organic Transformation. *ChemNanoMat* **2022**, *8*, e202200252.

(50) Wang, C.; Ranasingha, O.; Natesakhawat, S.; Ohodnicki, P. R.; Andio, M.; Lewis, J. P.; Matranga, C. Visible Light Plasmonic Heating of Au–ZnO for The Catalytic Reduction of CO_2. *Nanoscale* **2013**, *5*, 6968–6974.
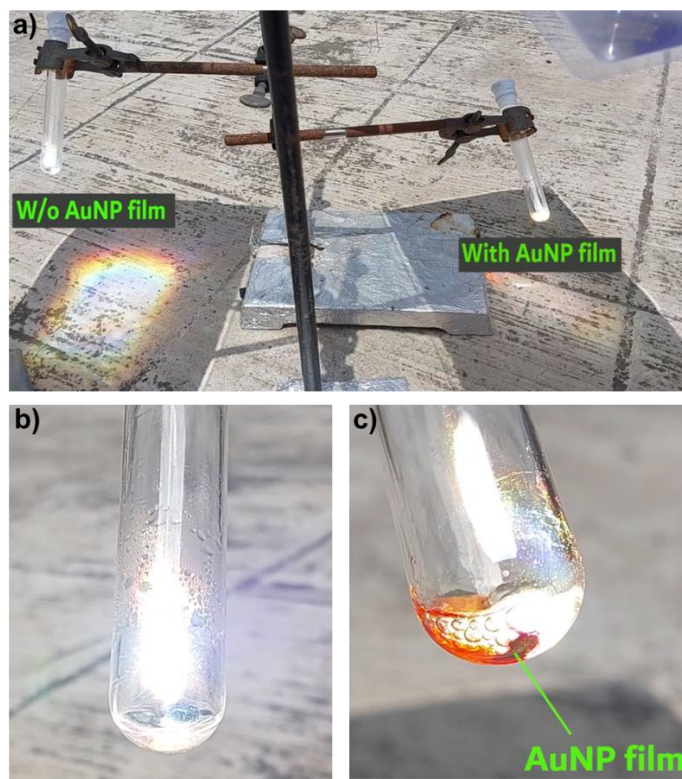
4.7. Appendix

Figure 4.17. In-situ visualization of photothermal Claisen rearrangement. (a) The reaction setup where both the test tube was irradiated with a focused sunlight using a Fresnel lens. (b) and (c) Test tubes containing reaction mixture under solar illumination with and without a AuNP film on the inner walls. A clear boiling as well as the color change from colorless to reddish yellow confirmed the role of plasmonic heat in driving the Claisen rearrangement. A negligible boiling as well as no observable color change was evident in the control experiment performed without AuNP film.
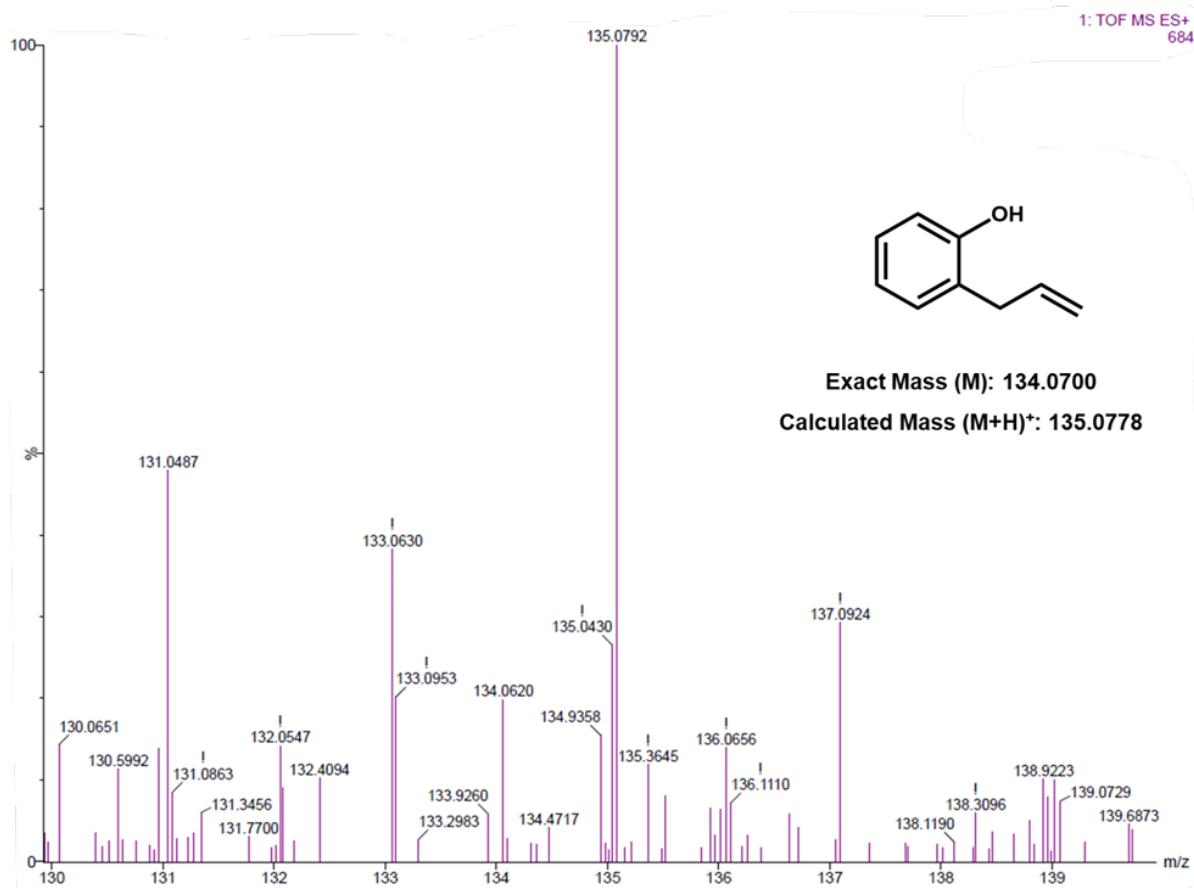
Figure 4.18. HRMS spectrum of the purified product, 2-allylphenol, obtained from plasmonic heat-driven Claisen rearrangement.
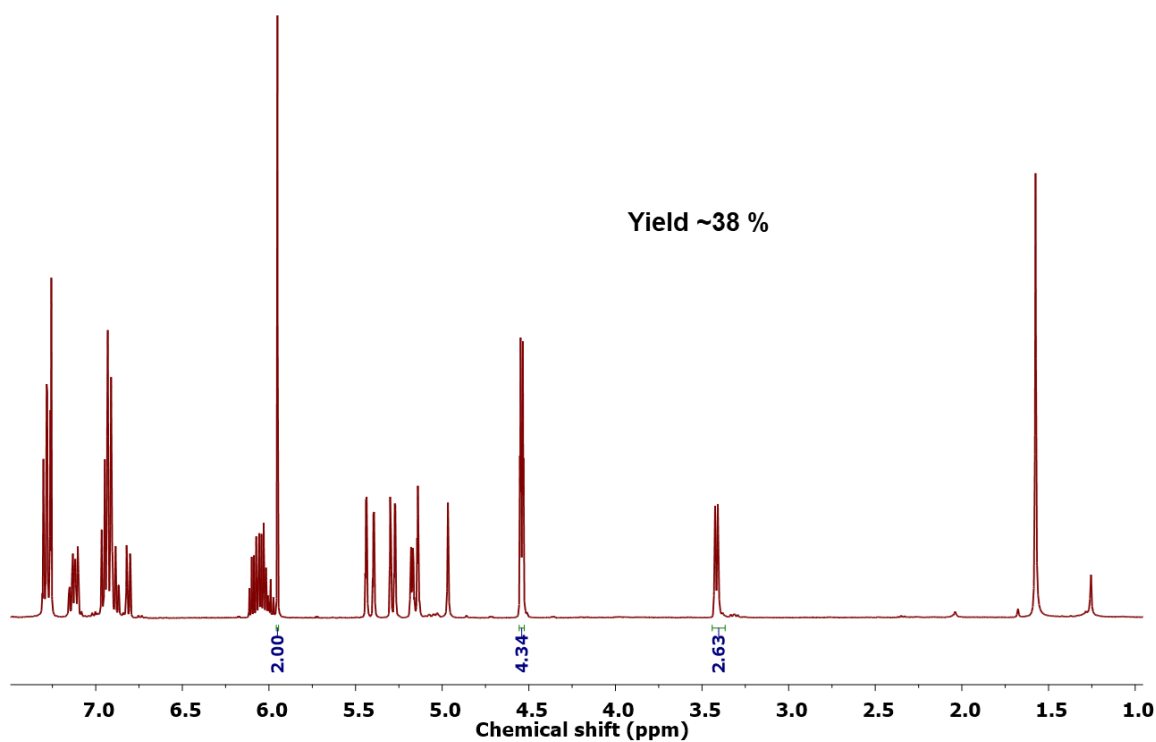
Figure 4.19. ¹H-NMR spectrum of the crude reaction mixture after 2 h under thermal condition at 250 °C with electrical heating.
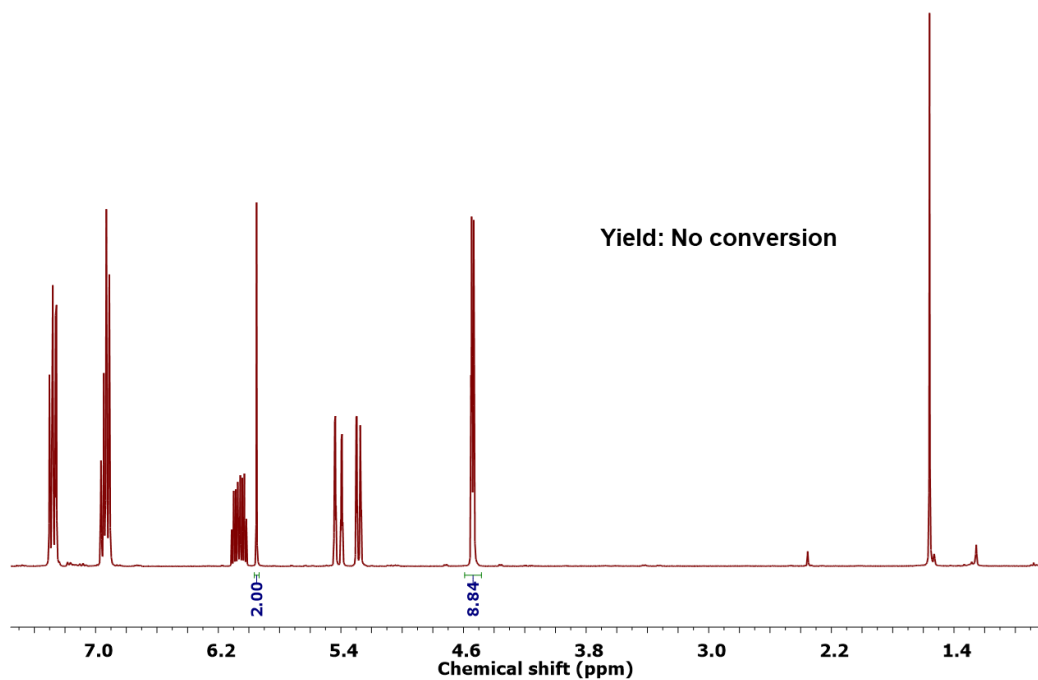

Figure 4.20. ¹H-NMR spectrum of the crude reaction mixture after 2 h in dark in a AuNP coated Al-foil wrapped test-tube.
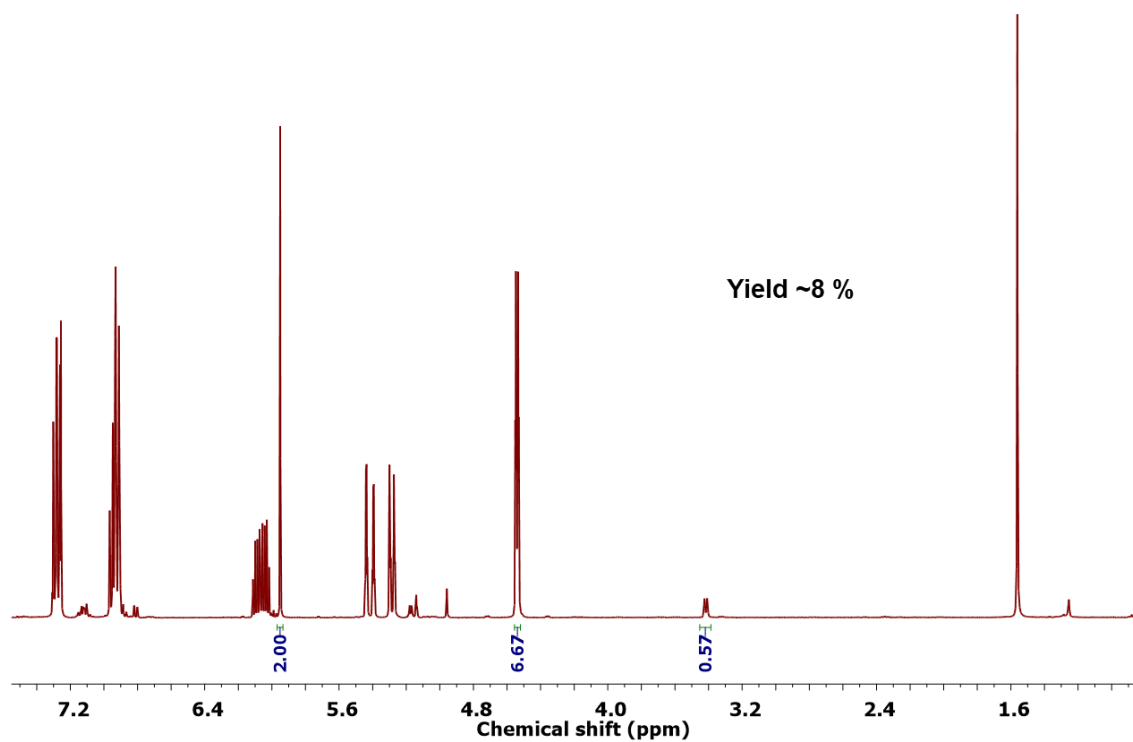
Figure 4.21. ^{1}H-NMR spectrum of the crude reaction mixture obtained after 2 h sunlight irradiation of the reactant in an Al-foil wrapped test-tube (**please note that the Al-foil doesn't contain any AuNP coating**).

Chapter – 5

Plasmonic Solar Absorbers Boost the Performance of Solar Thermoelectric Generators at Ambient Conditions
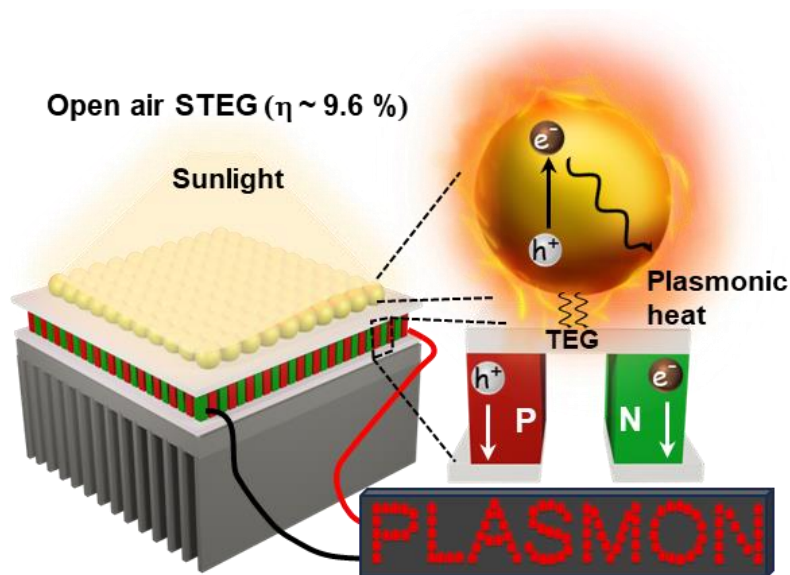
This chapter has been adapted from the following paper. Copyright 2024, American Chemical Society.

Kashyap, R. K.; Pillai, P. P. Plasmonic Nanoparticles Boost Solar-to-Electricity Generation at Ambient Conditions. *Nano Lett.* **2024**, *24*, 5585–559210.

5.1. Abstract

In order to expand the application horizon of plasmonic heating, it is important to investigate upon the possibility of conversion of plasmonic heat to a universal form of energy such as electricity. The current Chapter discusses this prospect where the high amount of heat generated from optically illuminated plasmonic nanomaterials may act as a greener and cost-effective alternative source of electricity. Our main goal is to convert solar-to-electrical energy using plasmonic nanomaterials in an efficient way: a desirable feat in the area of sustainable energy. IN this direction, sunlight-to-electricity conversion using solar thermoelectric generators (STEGs) is one of the proven technologies to meet the ever-growing energy demand. However, STEGs are often operated under vacuum with customized thermoelectric materials to achieve the high performance. In the present Chapter, the incorporation of plasmonic gold nanoparticle (AuNP) based solar absorbers enabled the efficient operation of STEGs at ambient conditions, and that too with commercially available thermoelectric devices. The incorporation of plasmonic AuNPs enhanced the performance of STEG by ~9 times, yielding an overall solar-to-electricity conversion efficiency of 9.6 % under 7.5 W.cm^{-2} solar irradiance at ambient conditions. To the best of our knowledge, this is the highest conversion efficiency reported so far among all the STEGs operated at ambient condition. The plasmonic heat dissipated by AuNPs upon solar irradiation was used as the thermal energy source for STEGs. Large light absorption cross section, high photothermal conversion efficiency (η_{PT} ~95 %), and high thermal conductivity of plasmonic AuNPs enabled the efficient generation and transfer of plasmonic heat to STEGs, with minimal radiative and convective heat losses. The power generated from plasmon-powered STEGs was used to run electrical devices, as well as produce green-hydrogen via the electrolysis of water. The results obtained here open up multiple avenues of possibility such as utilizing the electrical output obtained here for electro-driven chemical transformations. Additionally, the plasmon-powered STEG technology can be paired with already-in-use solar thermal water heating technology, improving the overall efficiency of solar energy utilization.

5.2. Introduction

Solar energy being the greener and renewable energy source has attracted much attention in recent past. The quest of harvesting solar energy has resulted two major technologies for its conversion to electricity: solar photovoltaic and solar thermal technologies (**Figure 5.1**). Solar photovoltaics works on the photovoltaic effect where material upon exposure to light generates charge carriers whose diffusion creates potential difference. On the other hand, solar thermal technology works on harvesting and storing the solar irradiance in the form of thermal energy using molten salt methodology. Later, the stored thermal energy is used to generate steam which rotates the turbine to ultimately give electricity. Both the technologies are well established; however, photovoltaics is limited with their efficiency and solar thermals require a lot of real estate and logistics to realize a high output.
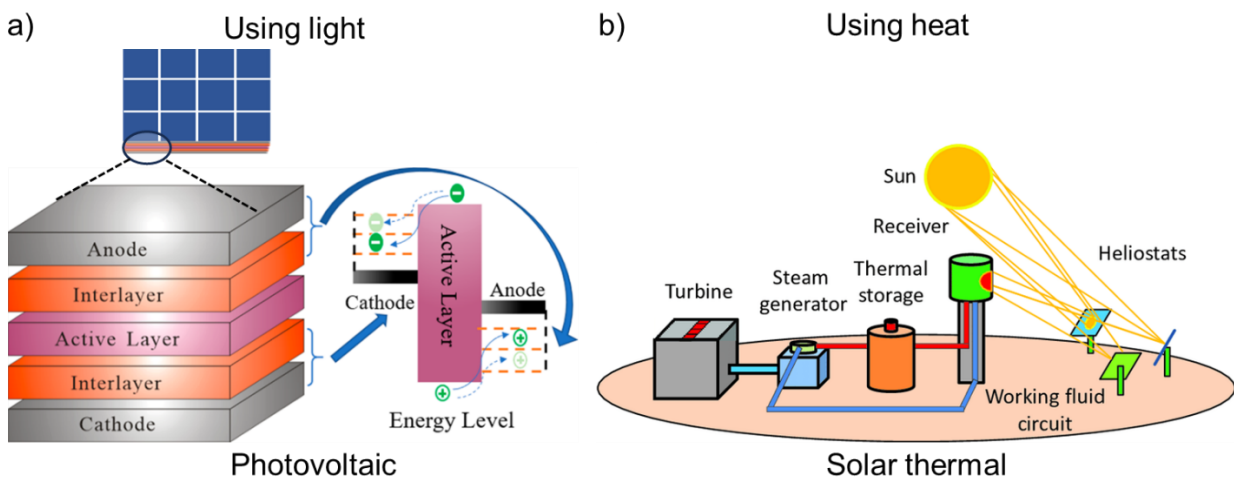

Figure 5.1. Solar-to-electricity conversion technologies. The schematic representation of **(a)** solar photovoltaic device architecture and its working principle. Solar photovoltaics utilizes optical energy of sun to excite the charge carriers which generates the potential difference. Reproduced with permission from ref. 14. Copyright: 2020, American Chemical Society. (b) Solar thermal plant working principle. All the core components are named. Reproduced with permission from ref. 15. Copyright: 2017 MDPI.

In recent years, solar thermoelectric generators (STEG) have emerged as an alternative and cost-effective alternative to photovoltaic devices to convert sunlight into electricity.[1] It can provide electrical supply to tropical regions where the entire day is mostly sunny. Along with the cost effectiveness, the STEGs can be easily integrated into existing light-harvesting technologies, including photovoltaics and solar water heating, to achieve a better solar energy utilisation. These

factors have made STEGs an attractive technology in modern solar energy research.[2,3] The core device architecture of a STEG (**Figure 5.2**) consists of a solar absorber in combination with a thermoelectric generator (TEG). In a typical STEG, the sunlight is converted into heat energy by solar absorbers, which is subsequently transferred to the thermoelectric materials for the generation of electricity.[1-4] Conversion of heat to electrical energy by thermoelectric generator (TEG) is based on the Seebeck effect,[5-12] wherein a large temperature difference across the two terminals of the TEG is the driving force. However, poor solar-to-electricity conversion efficiency is the major limitation of the technology, which is either because of poor solar absorber efficiency or possible heat and radiation losses.
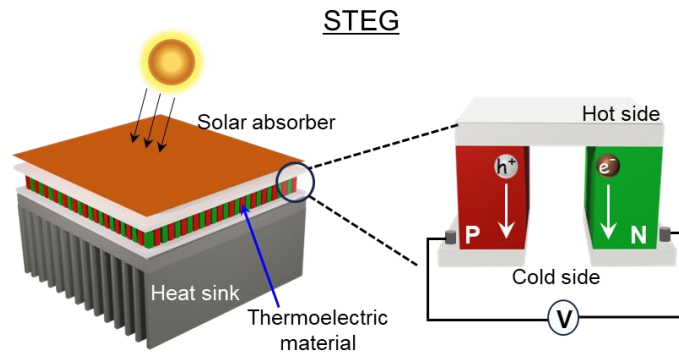

Figure 5.2. Schematic representation of a typical solar thermoelectric generator. The sunlight is absorbed by solar absorber followed by its conversion to heat. Finally, the heat is transferred to thermoelectric material where it gets converted to electricity.

Improving the efficiency of a STEG was of great attention, and experimental as well as modelling studies have shown that the overall solar-to-electricity conversion efficiency of STEGs can be improved by the appropriate choice of solar absorbers, thermoelectric materials, and operation conditions (such as optical concertation of sunlight, vacuum, cavity effect, etc.) (**Table 5.1**).[13,16] In terms of the device architecture, firstly, the major improvement was predicted to emerge with optical concentration using appropriate solar concentrator (**Figure 5.3a**).[17] The solar concentrator focuses the sunlight on solar absorber resulting in higher hot side temperature and in turn improving the overall efficiency. Next proposed modification was a vacuum encapsulation (**Figure 5.3b**) to minimize the convective heat losses for the improvement in the overall conversion efficiency.[18] Further, an optical cavity design was modeled (**Figure 5.3c**) which was proposed to mitigate the reflected optical as well as thermal losses from the solar absorber.[19] The working

principle for minimizing the loss here is based on total internal reflection of optical and thermal radiation towards the solar absorber by a perfectly designed reflector cavity. Finally, the vacuum encapsulation was suggested to minimize the nominal convective heat losses in the cavity designed architecture (**Figure 5.3d**).[20]
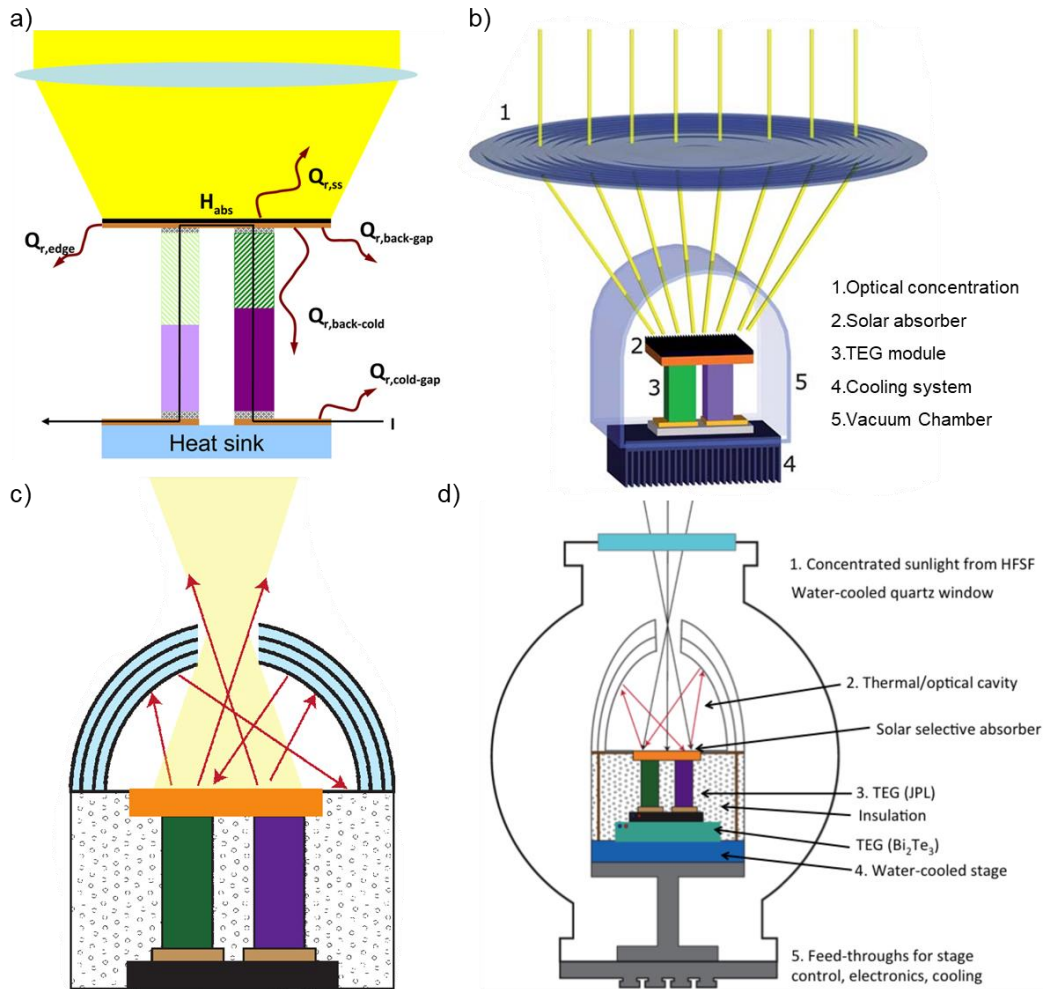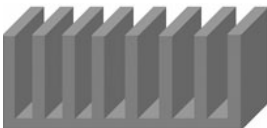

Figure 5.3. Modeling device architecture for efficiency improvement of STEG. (a) The optical concentration which can increase the hot side temperature effectively to enhance overall efficiency. Reproduced with permission from ref. 17. Copyright: 2011, American Institute of Physics Publishing. (b) Optical concentration in combination with vacuum encapsulation. The vacuum encapsulation was suggested for minimizing the convective heat losses. Reproduced with permission from ref. 18. Copyright: 2012, Royal Society of Chemistry. (c) Optical cavity design which could minimize the losses due to reflection as well as thermal emission from the solar absorber surface via internal reflection to the solar absorber. Reproduced with permission from ref. 19. Copyright: 2014, Springer Science. (d) Vacuum encapsulation of the STEG after cavity design which will further minimize the convective heat losses. Reproduced with permission from ref. 20. Copyright: 2014, Elsevier.

The highest solar-to-electricity conversion efficiency reported so far is 9.6 % with concentrated-STEG (211 sun, 21.1 $W.cm^{-2}$ solar irradiance) based on a customized TE device architecture operated under vacuum (10^{-3} – 10^{-2} Pa).[3] A spectrally selective solar absorber based on a double-cermet layer (W/Ni-filled Al_2O_3) was sputtered onto the stainless steel deposited on the customized TE material by a high-temperature vacuum brazing process. This path breaking study has accelerated and revived the research in the area of STEGs.[11,21,22] However, specialized device fabrication protocols were required to assemble the TE material, deposit the solar absorber, improve the spectral selectivity, and operate the STEG (under vacuum), in order to achieve the record solar-to-electricity conversion efficiency. Thus, there is a scope for simplifying the fabrication protocols and operating conditions in STEGs. In this context, the light absorptivity and thermal conductivity of solar absorbers play a crucial role in achieving a large temperature difference across the terminals of a TEG. Majority of the solar absorbers used so far exhibit low-to-moderate light absorptivity and/or thermal conductivity,[1-3, 21-26] which has forced the researchers to modify the design of the thermoelectric generator as well as to use harsh operating conditions, such as vacuum, to achieve a decent power output from STEGs.[2,3] Therefore, it is essential to identify and incorporate solar absorbers that can convert sunlight-to-heat efficiently, as well as transfer the heat to thermoelectric devices with minimal energy loss. This will ensure the operation of STEGs under ambient conditions and compatibility with commercially available thermoelectric devices, thereby enhancing the prospects of STEGs in solar energy technology.

Table 5.1. Summary of different methodologies and tools utilized to improve the efficiency of STEG. Reproduced with permission from ref. 16. Copyright: 2023, Wiley-VCH.

Optical concentrator	Fresnel lens Conical concentrators Parabolic concentrators Reflective mirrors Flat-plate panels
Thermal and selective absorbers	Metallic plates Solar collector plates MgF_2–Mo–CeO–Mo coating Mo–Al_2O_3 coating TiAlN/SiO_2 coating Multilayer SiO and Al thin film Ti/MgF_2 thin film Carbon black nanopowder polyvinylidene fluoride (CB/PVDF) Carbon nanotubes Other commercial selective absorbers
TE element	Zinc antimony (ZnSb) Lead telluride (PbTe) Bismuth telluride (BiTe) Lead antimony silver telluride (LAST) Silicone germanium (SiGe) Skutterudites ($CoSb_3$) ErAs:(InGaAs)$_{1−x}$(InAlAs)$_x$ (AgSbTe)$_x$(PbSnTe)$_{1−x}$ Half-HeuslersGapped metals (La_3Te_4/$Yb_{14}MnSb_{11}$) Commercial BiTe devices Multi/single-walled carbon nanotubes PEDOT:PSS
TE devices and architecture	Conventional TE leg (one TE material) Segments TE legs (two or more TE materials, direct contact) Cascaded TE legs (two or more TE materials, no direct contact) Asymmetric TE legs Planar (2D, thin or thick films) Circular
Heat sink	Natural air convection Controlled wind cooling Water convection (forced or natural) Water spray cooling Vapor cooling Metallic fin heat sink
Further methods	Sun tracking systems Heat storage units Vacuum enclosures Thermosyphons Organic light control methods

Inspired by the ability of plasmonic nanoparticles to efficiently convert sunlight into heat energy, we have incorporated gold nanoparticles (AuNPs) as solar absorbers into a STEG platform. Further, the thermal conductivity (κ) of AuNPs is significantly higher than the solar absorbers used in the best STEG reported so far (κ_{Au} = 310 wm^{-1}K^{-1} vs κ_W = 175 wm^{-1}K^{-1}, κ_{Ni} = 97.5 wm^{-1}K^{-1} and $\kappa_{alumina}$ = 12 wm^{-1}K^{-1}). Thus, the large light-absorptivity ($\sim10^8$-10^{10} M^{-1}cm^{-1}), high photothermal conversion efficiency (η_{PT} $\sim$95 %), and high thermal conductivity (κ_{Au} = 310 wm^{-1}K^{-1}) of plasmonic AuNPs will ensure the efficient generation and transfer of heat to STEGs, with minimal radiative and convective heat losses. In the present work, the plasmonic heat dissipated by $\sim$12 nm sized AuNP upon solar irradiation was used as the thermal energy source for the commercially available TEG (a typical example of TEG is Bi_2Te_3 based p-n diodes, TEC1-12706). The overall solar-to-electricity conversion efficiency significantly increased after the incorporation of plasmonic NPs as the solar absorbers in concentrated-STEGs. The plasmon-powered concentrated-STEG gave a peak efficiency of 9.6 % under 7.5 W cm^{-2} solar irradiance, at ambient conditions. To the best of our knowledge, this is the highest solar-to-electricity conversion efficiency reported so far among all the STEGs operated at ambient conditions. The use of a thin layer of plasmonic AuNPs ($\sim$2 μm) as the solar absorber resulted in a large temperature difference across the two sides of the STEG, which is the primary reason for the high performance of our plasmon-powered concentrated-STEG at ambient conditions (generally a vacuum system is necessary to use the greenhouse effect to achieve a larger temperature difference across the TEGs[3]). More importantly, the real-world application of plasmon-powered concentrated-STEGs in running low-to-medium power devices was demonstrated as well. The electricity generated from plasmon-powered STEGs was used to run 120 LEDs simultaneously (1.63 V each), a stopwatch (1.5 V), a calculator (1.5 V), and a 500 mW fan (5 V). Furthermore, plasmon-powered concentrated-STEGs were used for the production of green-hydrogen via the electrolysis of water. Thus, the excellent sunlight-to-heat generation and photostability of plasmonic AuNPs led the construction of efficient and durable (> one year) STEGs at ambient conditions from commercially available thermoelectric device.

5.3. Methods and Experimental Section

5.3.1. Materials and Reagents

Tetrachloroaurate trihydrate (HAuCl$_4$.3H$_2$O), tetramethylammonium hydroxide (TMAOH) 25% wt. in water, 11-mercaptoundecanoic acid (MUA), hydrazine monohydrate (N$_2$H$_4$.H$_2$O 50-60%), tetrabutylammonium borohydride (TBAB) and trisodium citrate dihydrate (SC) were purchased from Sigma-Aldrich. (Di-n-dodecyl) dimethylammonium bromide (DDAB) and dodecylamine (DDA) were purchased from Alfa Aesar. Tannic acid, and potassium carbonate (K$_2$CO$_3$) were purchased from Tokyo Chemical Industry (TCI). All the reagents were used as received without any further purification. All the stock solutions of metal ions were prepared in Milli-Q water. The TEG (Generic Thermoelectric Peltier Cooler, TEC1-12706, $40 \times 40 \times 4$ mm^3, proprietary TE legs) was purchased from Amazon.in and the relevant details provided by the manufacturer are given below:

Specification of Thermoelectric Module
TEC1-12706

Description

The 127 couples, 40 mm × 40 mm size single stage module is made of selected high performance ingot to achieve super ior cooling performance and greater delta T up to 70 °C, designed for superior cooling and heating up to 100 °C requirement. If higher operation or processing temperature is required, please specify, we can design and manufacture the custom made module according to your special requirements.

Features

● High effective cooling and efficiency.

● No moving parts, no noise, and solid-state

● Compact structure, small in size, light in weight

● Environmental friendly, RoHS compliant

● Precise temperature control

● Exceptionally reliable in quality, high performance

Application

● Food and beverage service refrigerator

● Portable cooler box for cars

● Liquid cooling

● Temperature stabilizer

● Photonic and medical systems

Peformance Specification Sheet

T_h(°C)	27	50	Hot side temperature at environment: dry air, N_2
DT_{max}(°C)	70	79	Temperature Difference between cold and hot side of the module when cooling capacity is zero at cold side
U_{max}(Voltage)	16.0	17.2	Voltage applied to the module at DT_{max}
I_{max}(amps)	6.1	6.1	DC current through the modules at DT_{max}
Q_{Cmax}(Watts)	61.4	66.7	Cooling capacity at cold side of the module under DT=0 °C
AC resistance(ohms)	2.0	2.2	The module resistance is tested under AC
Tolerance (%)	± 10		For thermal and electricity parameters
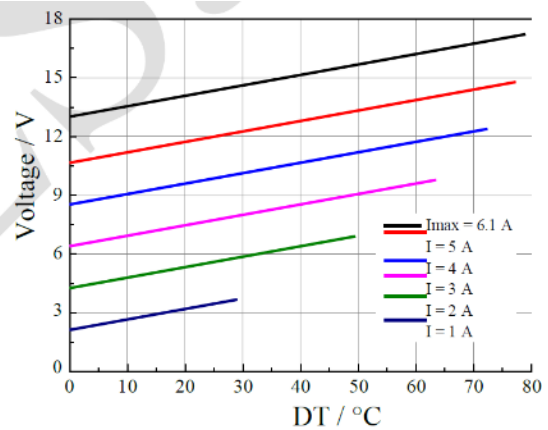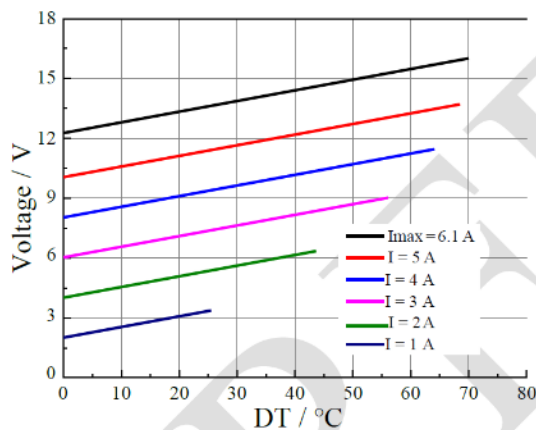
Standard Performance Graph V= f(ΔT)

5.3.2. UV-visible absorption spectroscopy

All UV-visible absorption spectra were recorded using SHIMADZU UV-3600 plus UV-vis-NIR spectrophotometer. The AuNPs for measurements were taken in a 3 mL quartz cuvette with a path length of 1 cm. The UV-visible spectrum of AuNPs film was collected under reflectance mode with external 2D detector and the collected diffused reflectance was transformed to get absorbance using Kubelka-Munk function.

5.3.3. Transmission electron microscopy (TEM) studies

The AuNPs were characterized using High resolution transmission electron microscopy (HR-TEM) studies on JEOL JEM2200FS (200 kV) HRTEM instrument. AuNPs were drop-casted on a 400- mesh carbon-coated copper grid (Tedpella Inc.) and dried overnight under vacuum to prepare the TEM sample.

5.3.4. Scanning electron microscopy (SEM) imaging

The AuNPs were immobilized on Si-wafer and dried under vacuum for imaging. The field emission scanning electron microscopic (FE-SEM) imaging was performed on ZEISS Ultra Plus FESEM instrument.

5.3.5. Electrical output measurement

Current and voltage were recorded using a Keithley 2450 source measurement unit (SMU) under a two-probe setup. All the measurements were done by connecting the output wires of STEG to SMU probes. For sunlight experiments, the current and voltage measurements were performed using a digital multimeter (Model 17B$^+$ ESP; Fluke, Everrit, Washington, USA).

5.3.6. Measurement of hot side temperature (T_h) of STEG

The temperature on the hot face of the thermoelectric generator (the one coated with AuNP) was measured using laser pointer digital infrared (IR) thermometer (EEE Instruments Inc., Kolkata), having measurement limit between -50°C to 550°C.

5.3.7. Synthesis of AuNPs

Spherical gold nanoparticles (AuNPs) were synthesized using a seed-mediated growth approach, following a modified literature procedure.[27,28]

5.3.7.1. Seed preparation: Hydrazine monohydrate ($N_2H_4.H_2O$) was used as the reducing agent. In a typical experiment, $HAuCl_4.3H_2O$ (12 mg), DDA (140 mg), and DDAB (140 mg) were mixed in toluene (4 mL) and sonicated for ~10 min for complete solubilization of Au (III) ions. This was followed by a rapid injection of another toluene solution containing 30 mg of TBAB and 46 mg of DDAB. The resulting solution was left stirring overnight to ensure the complete reduction of Au (III) ions.

5.3.7.2. Growth step -1: The seed particles (typically ~2-4 nm) were then grown to ~5.5 nm DDA-Au NPs. For this, a growth solution was prepared by adding 460 mg of DDAB, 1.4 g of DDA, 120 mg of $HAuCl_4.3H_2O$ and seed solution in 30 mL toluene. The growth solution was further reduced with a dropwise addition of another toluene solution containing 160 μL of $N_2H_4.H_2O$ and 560 mg of DDAB. The solution was stirred overnight for complete growth of the particles yielding monodisperse 5.5 ± 0.7 nm of DDA-Au NPs.

5.3.7.3. Growth step -2: The 5.5 ± 0.7 nm of DDA-Au NPs were further grown to ~12 nm DDA-AuNPs. A growth solution was prepared by adding 8 g of DDAB, 13.0 g of DDA, 1.1 g of $HAuCl_4.3H_2O$ and seed solution in 200 mL toluene. The growth solution was further reduced with a dropwise addition of another toluene solution containing 650 μL of $N_2H_4.H_2O$ and 4.4 g of DDAB. The solution was stirred overnight for complete growth of the particles yielding monodisperse 12.1 ± 0.5 nm of DDA-Au NPs, as confirmed through TEM analysis (**Figure 5.4c**).

5.3.8. Place exchange of AuNP with 11-mercaptoundecanoic acid (MUA) ligands

In a typical synthesis, 12.09 ± 0.48 nm DDA-Au NPs (15 mL) were first precipitated by adding 50 mL of methanol which yielded a black precipitate. The supernatant was carefully removed, and the precipitate was then re-dispersed in 20 mL toluene. MUA ligand (equal to the moles of Au (III) in solution) dissolved in 10 mL dichloromethane (DCM) was added. The solution was left overnight to ensure a complete ligand exchange. Next, the supernatant was decanted, and the precipitate was washed with DCM (3 × 50 mL) and acetone (50 mL), respectively. The precipitate was then dried and redispersed in Milli Q water by adding ~20 μL of TMAOH base (25 % wt. in water), to deprotonate the carboxylic acid group for further studies.

5.3.9. Calculation of NP concentration

The concentration of AuNPs in stock solution was calculated using Beer-Lambert's law according to the UV-vis absorption study in **Figure 5.18** in Appendix:[29]

$$A = \varepsilon \cdot c \cdot l$$

where,
A is the absorbance
ε is the molar extinction coefficient ($M^{-1}cm^{-1}$)
c is the concentration of the solution (M)
l is the optical path length (cm).

The molar extinction coefficient (*ε*) for AuNP was taken to be 2.7×10^8 M^{-1} cm^{-1} for ~12 nm diameter particles.[28]

The concentration of AuNP stock solution was estimated to be ~ 0.38 µM (in terms of AuNPs).

5.3.10. Preparation and performance measurement of plasmonic-powered STEG

On plasmon and light intensity dependent study

Under 532 nm CW laser light source

A commercially available thermoelectric generator based on Bi_2Te_3 based p-n diodes (TEC1-12706) was purchase from Amazon.in. One side of the TEG was attached to a metallic heat sink using a thermally conducting adhesive (HI-TECH heat sink compound, HI-TECH Chemical Corp., India). A circular thin film of AuNP was drop-cast on the other side of the TEG. In a typical experiment, 10 µL (~3.8 pmol) of AuNPs from ~0.38 µM stock solution were drop-cast on TEG. A circular plasmonic AuNP film of diameter ~1 cm was prepared by air drying the drop of aqueous AuNP colloid at room temperature. 1W 532 nm CW diode laser was used as the light source. The distance between the source and the AuNP film was kept constant at 15 cm. The power at the AuNP film was measured to be 1W with the help of thermopile optical power sensor (Model LM-10 HTD; Coherent, Santa Clara, CA 95054 USA). Current and voltage were recorded using a Keithley 2450 source measurement unit (SMU) under a two-probe setup. All the measurements were done by connecting the output wires of STEG to Keithley 2450 SMU probes. A peak voltage of ~95 mV and a current of ~18 mA was obtained, when AuNP-coated side of the TEG was irradiated with the 532 nm CW diode laser.

For intensity dependent studies, the AuNP coated and non-coated STEG were irradiated with a 532 nm CW diode laser at various intensities. First, the intensities were increased from 0 to 1000 mW (step size = 100 mW), and then reversed from 1000 to 0 mW. We waited for 3 min at each intensity, for the current and voltage to be stabilized before changing the optical intensity.

5.3.11. STEG performance studies under white light

In a typical experiment, 25 μL (~9.5 pmol) of AuNPs from ~0.38 μM stock solution were drop-cast on one side of the TEG following by air drying at room temperature (2.5 cm ✕ 2.5 cm). The other side was fixed on a metal heat sink using thermally conducting adhesive (HI-TECH heat sink compound, HI-TECH Chemical Corp., India). The AuNPs film was irradiated using a 20 W white LED and the electrical output was measured using Keithley's series 2450 source unit. The power at the AuNP film was measured to be 60 mW.cm^{-2} with the help of thermopile optical power sensor (Model LM-10 HTD; Coherent, Santa Clara, CA 95054 USA). The simultaneous temperature increase was measured using an IR thermometer (EEE Instruments Inc., Kolkata).

5.3.12. Synthesis of different sizes of AuNPs

In a typical synthesis, chloroauric acid (HAuCl$_4$) was reduced in the presence of trisodium citrate and tannic acid at 70 °C, followed by two rounds of growth at the same temperature with subsequent additions of HAuCl$_4$.[30] The average diameter of citrate stabilized AuNPs was estimated to be 5.0 ± 0.6 nm. A slightly different procedure was adopted for the preparation of higher sizes of AuNPs.[31] Trisodium citrate was used as the sole reducing-cum-capping agent, and the reduction was carried out at 100 °C to get AuNPs of ~12 nm diameter. Higher sizes of NPs were prepared by growing ~12 nm AuNPs at 90 °C by the subsequent additions of HAuCl$_4$, yielding ~25, ~45, ~55, ~68, and ~88 nm sized citrate capped AuNPs.

5.3.13. Size dependent and durability study

AuNPs of varying sizes ranging from ~5 nm to ~90 nm was synthesized as mentioned earlier. The effect of NP size on the plasmonic-heat generation and STEG performance was studied. In a typical experimental setup, a thin film of AuNP was drop-cast on one side of TEG as mentioned earlier. The other side was fixed on a metal heat sink using a thermally conducting adhesive. The AuNPs coated-TEG was irradiated using a 20 W white LED at a distance of ~2 cm and the electrical output was measured using Keithley's series 2450 source measure unit. The power at the AuNP film was

measured to be 60 mW.cm^{-2} with the help of thermopile optical power sensor (Model LM-10 HTD; Coherent, Santa Clara, CA 95054 USA). The simultaneous temperature increase was measured using an IR thermometer (EEE Instruments Inc., Kolkata). It is worth mentioning that the same TEG was used for all the sizes to have a fair comparison. The size effect was studied by normalizing the optical density at the surface plasmon band of each AuNP, which is a commonly used normalization strategy to study the size effect.[32,33]

The durability of the plasmon-powered STEG was tested for three different thermoelectric modules coated with a thin film of ~12 nm AuNPs. The AuNP-coated TEG film was irradiated using a 20 W white LED at a distance of ~2 cm and the electrical output was measured using Keithley's series 2450 source measure unit. The power at the AuNP film was measured to be 60 mW.cm^{-2} with the help of thermopile optical power sensor (Model LM-10 HTD; Coherent, Santa Clara, CA 95054 USA). The electrical outputs from all the three devices were monitored at regular intervals (The intervals were in terms of days, weeks and months **Table 5.4** in **Appendix**).

5.3.14. Measurement of AuNPs film thickness

The thickness of AuNP film on TEG was measured using an optical 3D surface profilometer (Bruker ContourX-200). In a typical experiment, a film of AuNPs was made and dried on the TEG as discussed previously (**Figure 5.5a**). The 3D optical surface profile measurement was performed across the boundary of the film (small red box in **Figure 5.5a**). The height profile (**Figure 5.5b**) and corresponding thickness plot along black-dotted line of the profile (**Figure 5.5c**) confirms the film thickness to be ~2 μm.

5.3.15. Photothermal conversion efficiency of AuNPs (under 532 nm illumination)

In a typical experiment, 1 mL water is taken in a quartz cuvette and 10 μL of AuNPs stock solution (~0.4 μM in terms of AuNPs) was added to it. The aqueous AuNP colloidal dispersion was irradiated using 532 nm CW diode laser with a power of 1W. The simultaneous temperature rise of the dispersion was monitored using a thermocouple dipped in the AuNP colloidal solution (thermocouple was attached to a digital multimeter Model 17B^{+} ESP; Fluke, Everrit, Washington, USA). A control experiment was performed with only water (without AuNP) keeping all the parameters constant (**Figure 5.7**).

Following a modified Roper's method,[35] the photothermal conversion efficiency (η_{PT}), was calculated using the equation:

$$\eta_{PT} = \frac{hS\,(T_{max} - T_{surr}) - Q_{dis}}{I(1 - 10^{-A_{532}})} \tag{1}$$

where,

η_{PT} = Photothermal conversion efficiency

h = Heat transfer coefficient

S = Surface area of the container

T_{max} = Maximum temperature achieved with AuNPs under irradiation (70.3 °C, see **Figure 5.7b**)

T_{surr} = Temperature before irradiation (20.8 °C, see **Figure 5.7b**)

Q_{dis} = Heat dissipated by light illumination without AuNPs

I = Light intensity (1 W)

A_{532} = Absorbance at 532 nm (0.5 OD, see **Figure 5.7a**)

hS can be expressed as

$$hS = \frac{m_s C_s}{\tau_s} \tag{2}$$

where,

m_s = mass of the system (here water, 1000 mg)

C_s = specific heat capacity of the system (4.2 J/g.°C)

τ_s = time constant of the test system (300 s)

Therefore,

$$hS = \frac{1000 \times 4.2}{300}\; mW/°C$$

$$= \mathbf{14\; mW/°C}$$

Q_{dis} can be calculated from the control experiment with only water in the absence of AuNPs

$$Q_{dis} = \frac{mC\Delta T}{t} \tag{3}$$

where,

m = mass of water (1000 mg)

C= specific heat capacity of water (4.2 J/g.°C)

ΔT = temperature increase in water (3 °C, see **Figure 5.7b**)

t = time of the irradiation (300 s)

Therefore,

$$Q_{dis} = \frac{1000 \times 4.2 \times 3}{300} \, mW$$

$$= 42 \, mW$$

By substituting all the values in equation (1), the photothermal conversion efficiency (η_{PT}) was calculated to be **95.2 %.**

5.3.16. Laboratory demonstration of running a fan using the electricity generated from plasmon-powered STEG

In a typical experiment, three plasmon-powered STEGs were connected in series. The AuNP film on the STEG was irradiated vertically with a warm simulated sunlight source (Rehbein GmbH & Co.). The distance between the lamp and the AuNP film was ~2 cm. The optical power of light falling on the AuNP film was measured to be ~500 mW/cm^2 using a thermopile optical power sensor (Model LM-10 HTD; Coherent, Santa Clara, CA 95054 USA). The voltage and current output were measured using a digital multimeter (Model 17B$^+$ ESP; Fluke, Everrit, Washington, USA). The overall light-electricity conversion efficiency was calculated using the equation explained later for the sunlight experiment. A control experiment was performed without AuNP-coated STEG, under similar conditions. A ~5-fold enhancement in power output as well as efficiency was observed, when AuNPs film was used as the solar absorber (**Figure 5.11**).

A $\geq$ 35 mW fan was connected at the output of the STEG devices, as shown in **Figure 5.11a**.

5.3.17. Sunlight experiments

A commercially available thermoelectric generator based on Bi$_2$Te$_3$ based p-n diodes (TEC1-12706) was purchase from Amazon.in. One side of the TEG was attached to a metallic heat sink using a thermally conducting adhesive (HI-TECH heat sink compound, HI-TECH Chemical Corp., India), which was dipped into ice water for the efficient thermal management. A thin film of AuNP was drop-cast on the other side of the TEG. In a typical experiment, 25 µL (~9.5 pmol) of ~12 nm

sized AuNPs from ~0.38 µM stock solution were drop-cast on TEG. A thin film of AuNP was made by air drying the drop of aqueous AuNP colloid at room temperature (2.5 × 2.5 cm). A Fresnel lens (19.5 × 28.5 cm^2) was used to focus the sunlight. The beam area and optical power after focusing was measured to be 1 cm^2 and 9.5 W.cm^{-2}, respectively. Current and voltage outputs were monitored using Keithley 2450 SMU or a digital multimeter (Model 17B$^+$ ESP; Fluke, Everrit, Washington, USA). Keithley 2450 SMU was used for measuring current and voltage for calculating power and overall solar-to-electricity conversion efficiency, shown in **Figures 5.12b** and **c**.

A digital multimeter (Model 17B$^+$ ESP; Fluke, Everrit, Washington, USA) was used to measure the current and voltage of plasmon-powered concentrated-STEGs while running various electrical devices and H$_2$ generation experiments.

5.3.18. Overall solar-to-electricity conversion efficiency calculation of STEGs

5.3.18.1. Power density (PD) calculation

As per **Figure 5.12b**, the measured peak voltage and current outputs are as follows for plasmon-powered STEG:

$$V_{out} = 1.71\ V$$

$$I_{out} = 0.478\ A$$

$$Area\ under\ irradiation\ (a) = 1\ cm^2$$

Thus, power density (PD)

$$PD = \frac{P_{out}}{a} = \frac{V_{out} \times I_{out}}{a}$$

$$= \frac{1.71\ V \times 0.478\ A}{1\ cm^2}$$

$$PD = \mathbf{0.817\ W.\,cm^{-2}}$$

5.3.18.2. Overall solar-to-electricity conversion efficiency (η)

The efficiency (η) can be calculated using the following equation,

$$\eta = \frac{PD}{P_{in}} \times 100$$

where,

$P_{in} = Input\ optical\ power\ (9.5\ W.cm^{-2})$

Thus,

$$\eta = \frac{0.817\ W.cm^{-2}}{9.5\ W.cm^{-2}} \times 100$$

$$= \mathbf{8.6}\ \%$$

Similarly, the η for STEG in the absence of plasmonic AuNPs was calculated and found to be 0.93 %.

5.3.19. Sunlight experiments (under vacuum)

In a typical experiment, a plasmon-powered STEG was kept in a glass vacuum desiccator under the similar experimental conditions explained above. The sunlight was focused onto the AuNP film made over the STEG using a Fresnel lens ($19.5 \times 28.5\ cm^2$). The electrical output was measured using a digital multimeter (Model 17B$^+$ ESP; Fluke, Everrit, Washington, USA). The control experiment without AuNP film was performed under similar experimental conditions. The optical power was measured using a thermopile optical power sensor (Model LM-10 HTD; Coherent, Santa Clara, CA 95054 USA).

5.3.20. Stability study of AuNPs based solar absorber under concentrated solar illumination

The stability of AuNPs after concentrated solar illumination was tested in solution as well as film states using microscopic and spectroscopic techniques (**Figure 5.16**).

5.3.20.1. In film state: In a typical experiment, 2 mL of AuNP solution (from ~0.38 µM stock solution) were drop-casted on a silicon wafer and dried under vacuum. This was followed by ~15 min of concentrated solar illumination. SEM images confirm that AuNPs retained their shape and size even after the concentrated solar illumination (**Figures 5.16a, b**). Likewise, negligible change was observed in the UV-vis-NIR absorption of AuNP film before and after concentrated solar illumination (**Figure 5.16c.** Absorption studies were performed on the AuNP film coated TEG, under the diffused reflectance mode).

5.3.20.2. In Colloidal state: In a typical experiment, a 3 mL solution of ~2 nM AuNP solution was illuminated under concentrated sunlight for ~15 min. It is worth mentioning that a clear boiling of the AuNP solution was observed, confirming the generation and dissipation of plasmonic-heat. A negligible change was observed in the UV-vis-NIR absorption of AuNP before and after concentrated solar illumination (**Figure 5.16c**).

All these experiments conclusively prove the stability of AuNPs under the concentrated solar illumination, both in solution and film states.

5.3.21. Storage of the electrical energy generated from plasmon-powered concentrated-STEG: H₂ production via water electrolysis

In a typical experiment, 1.5 L of 1 M KOH solution was prepared for the electrolysis experiment. Electrode chambers were made by inverting two 20 mL calibrated plastic syringes closed from the top. A platinum mesh electrode was inserted into each of the electrode chambers. The electrodes were connected to the electrical output of 3 plasmon-powered concentrated-STEGs arranged in series. The average solar concentration during the experiment was measured to be 80 sun (1 sun corresponds to 100 mW.cm^{-2}. Upon solar irradiation, instantaneous bubble formation was observed at each electrode which escaped and occupied the space in the respective electrode chambers. The continuous storage of gases in inverted electrode chambers was performed till 20 min. The total average voltage and current during the experiment was measured to be ~4 V and 300 mA, respectively. The average optical power falling on the AuNP during the experiment was measured to be ~8 W/cm^2 and the beam area ~1cm^2.

The hydrogen energy produced (E_{H_2}), can be calculated from the hydrogen combustion enthalpy.[34]

$$E_{H_2} = \frac{pv}{RT} \times \Delta H_{H_2}$$

Where, ΔH_{H_2} is the molar hydrogen combustion enthalpy (286 kJ/mol), p (Pa) and v (mL) are the pressure (the atmospheric pressure) and the volume of the H₂ produced, R is the gas constant (8.314 J mol^{-1}K^{-1}); T (K) is the temperature.

Under our experimental condition,

$v = 10\ mL = 10 \times 10^{-6} m^3$

$T = 307\ K$

Therefore,

$$E_{H_2} = \frac{101325\ Pa\ (kgm^{-1}s^{-2}) \times 10 \times 10^{-6}m^3}{8.314\ J\ mol^{-1}K^{-1}(J = kgm^2s^{-2}) \times 307\ K} \times 286\ kJ/mol$$

$$= 0.113536\ kJ$$

$$= \mathbf{113.536\ J}$$

Now, the efficiency of the electrical to hydrogen energy (η_{ETH}) can be calculated as

$$\eta_{ETH} = \frac{E_{H_2}}{IV \times t} \times 100$$

where,

$V = $ Total output voltages from 3 thermoelectric modules (V = 4 V)

$I = $ Current flowing through the circuit (300 mA)

$t = $ experimental time (1200 s)

Thus,

$$\eta_{ETH} = \frac{113.536\ J}{4\ V \times 0.3\ A \times 1200\ s} \times 100$$

$$= \mathbf{7.9\ \%}$$

The solar to hydrogen efficiency (η_{STH}) can be calculated as[33]

$$\eta_{ETH} = \frac{E_{H_2}}{Input\ solar\ energy} \times 100$$

$$Input\ solar\ energy = nq_iat$$

where,

n = number of devices

q_i = power of illuminated solar light (8 W.cm^{-2}),

a = spot area (1 cm^2)

t = time duration of illumination (1200 s)

$$\eta_{ETH} = \frac{113.536}{3 \times 1 \times 8 \times 1200} \times 100$$

$$\sim \mathbf{0.4\ \%}$$

5.4. Results and Discussion

5.4.1. Design of plasmon-powered STEG. The visible-light absorption ability of AuNPs is one of the best, as they can absorb light beyond their physical cross-section because of the unique phenomenon of localized surface plasmon resonance (LSPR).[36] As a result, the molar extinction coefficient of AuNPs is 10^8-10^{10} M^{-1}cm^{-1}, which is 10^3-10^5 times higher than the standard dye molecules.[36-39] A photoexcited plasmonic NP undergoes a series of non-radiative relaxation pathways (Landau damping, electron-electron, electron-phonon, and phonon-phonon interactions) to eventually dissipate its excess energy in the form of heat to the surroundings,[40-55] which is termed as plasmonic heat (**Figure 5.4a**).
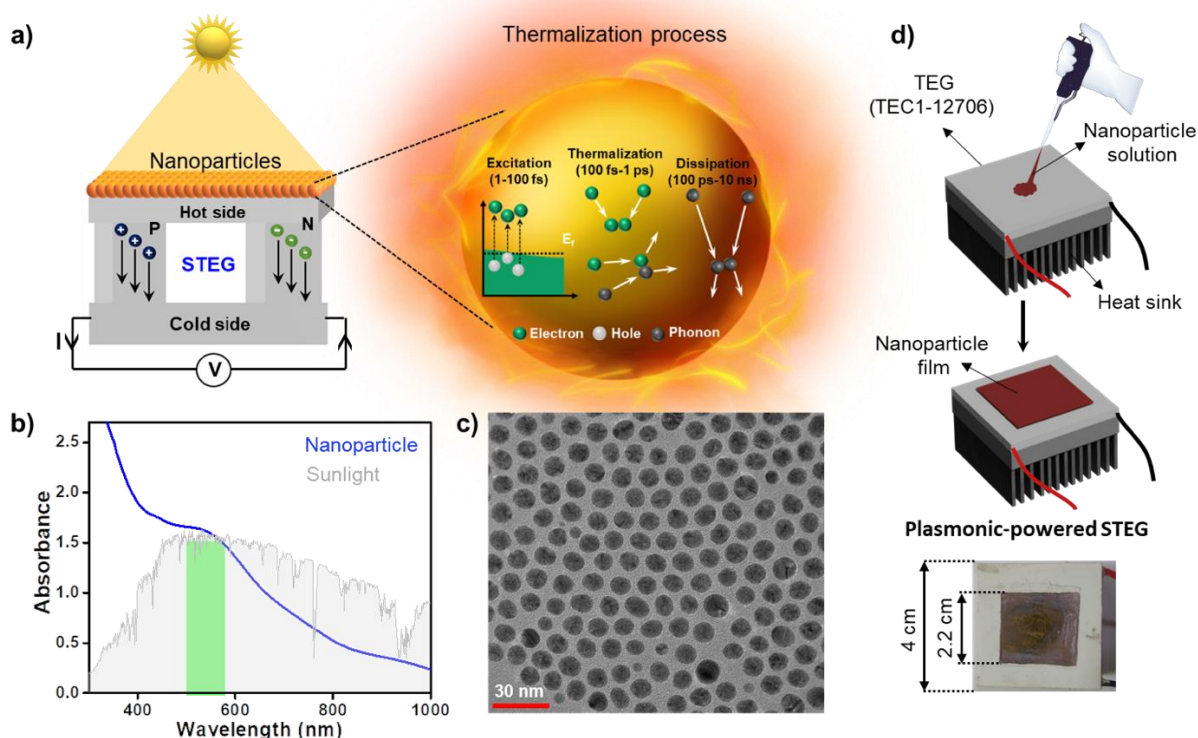

Figure 5.4. Construction of plasmon-powered STEG. (a) Schematics showing the working principle of plasmon-powered STEGs. The solar illumination of AuNPs leads to the plasmon excitation, followed by a series of non-radiative relaxation pathways (Landau damping, electron-electron, electron-phonon, and phonon-phonon interactions) to eventually dissipate the excess energy in the form of heat to the surroundings. This heat is termed as plasmon-heat, which was used as the thermal energy source for the STEG to generate electricity. (b) Absorption studies showing a strong overlap between the absorption of sunlight and plasmonic AuNP film. The AM1.5G reference solar spectrum was adapted from

DOE/NREL/ALLIANCE for the comparison. (c) A representative transmission electron microscope image of ~12 nm sized plasmonic AuNPs. (d) Schematics for the fabrication of a plasmon-powered STEG, along with the actual photograph of the device.

It is interesting to note that >90% of the light absorbed by a plasmonic NP is dissipated in the form of heat, especially in the size range of 5-25 nm.[33] As a result, the temperature experienced by the surroundings because to the dissipation of plasmon-heat can be as high as 600 °C.[56] Further, the strong overlap between the UV-visible absorption of AuNPs (absorption maximum ~520 nm) and the solar spectrum justifies the choice of plasmonic AuNPs (diameter ~12 nm, see **Figure 5.18** in the **Appendix**) as the solar absorber (**Figure 5.4b**). A simple drop and dry method were adopted to deposit a thin film (~2 μm, **Figure 5.5**) of plasmonic AuNPs on one side of a commercially available TEG (in a typical experiment, TEC1-12706 based on Bi_2Te_3 p-n diodes was used as the TEG) (**Figure 5.4c,d**). The other side of the STEG was attached to a metallic heat sink or ice water bath for the efficient thermal management.
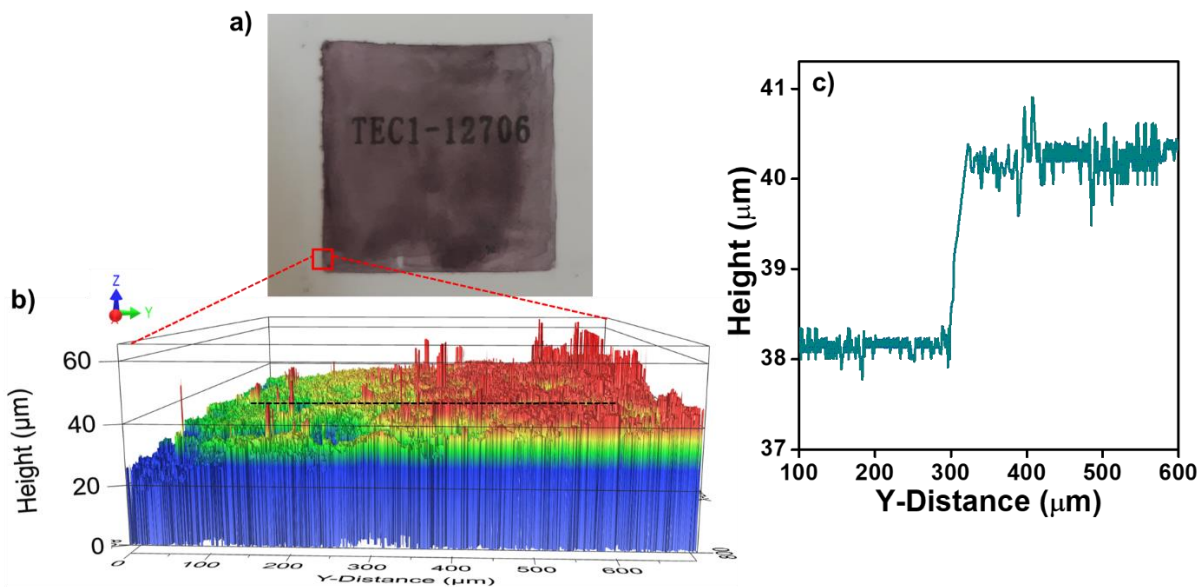

Figure 5.5. Measurement of the AuNP film thickness on the TEG surface using an optical 3D surface profilometer. (a) Optical photograph of AuNP deposited TEG, (b) height profile at the interface, and (c) thickness measured along the black dotted line in image (b). The data clearly shows that the film thickness is ~2 μm.

5.4.2. Laboratory optimization and durability studies. Optimization studies were performed inside the lab using monochromatic diode laser (spot diameter ~1 cm), white LED (irradiation area

4 cm ✕ 4 cm), and warm light sources (irradiation area 4 cm ✕ 4 cm) (experimental set-up is shown in **Figure 5.6, 5.7**).
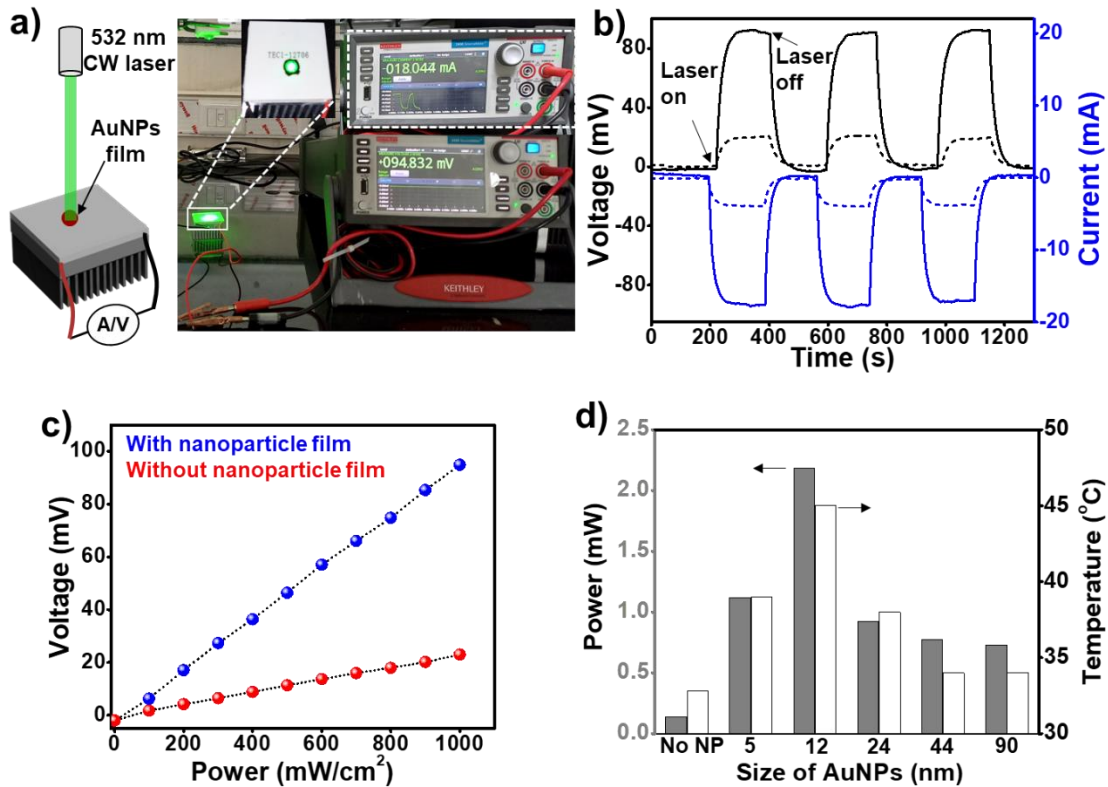

Figure 5.6. Laboratory optimization and durability studies. **(a)** Experimental setup for measuring output voltage and current using Keithley 2450 SMU, upon irradiation of plasmon-powered STEG with a 532 nm CW diode laser. **(b)** The light ON-OFF cycles of electrical output of plasmon-powered STEG. Dotted curves represent the data for STEG without the plasmonic AuNP coating. The light intensity on the AuNP film was measured to be 1 W.cm^{-2} for the data presented in **(a-c)**. **(c)** Light intensity variation in output voltage of STEG with and without plasmonic AuNP coating. **(d)** The AuNP size dependent study revealed that AuNP with d~12 nm gave the highest output electrical power, following the trend in temperature-rise caused by the irradiation of the NP film. A 20 W white LED was used as the light source, where the light intensity on the AuNP film was measured to be 60 mW.cm^{-2}. The same TEG was used in the size dependent study to have a fair comparison. All the studies were performed with the TEG module TEC1-12706.

To begin with, 1W continuous wave (CW) 532 nm diode laser was chosen as the light source, as it matches well with the λ_{LSPR} of AuNPs (~520 nm). A peak open-circuit voltage (V_{oc}) of ~95 mV and a short-circuit current (I_{sc}) of ~18 mA was obtained, when AuNP-coated side of the TEG was irradiated with the 532 nm CW diode laser (**Figures 5.6a,b**. The light intensity measured on the AuNP film was 1 Wcm^{-2}).
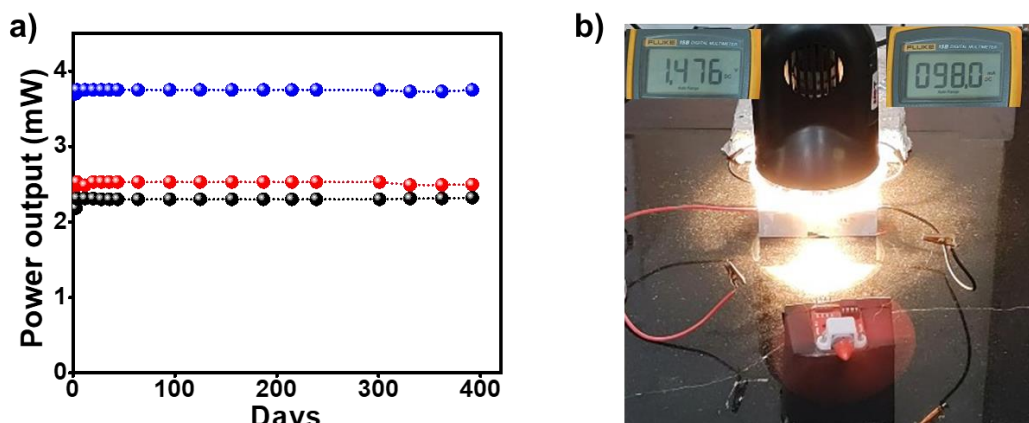
Figure 5.7. Device durability and laboratory demonstration. (a) Durability test of three different independent plasmon-powered STEGs, confirming the stability of the output power. A 20 W white LED was used as the light source, where the light intensity on the AuNP film was measured to be 60 mW.cm^{-2}. **(b)** Demonstration of an electrical fan ($P_{in} \geq 35$ mW) operated with the electricity generated from three plasmon-powered STEG connected in series. A warm-white light was used as the irradiation source (The light intensity measured on the AuNP film was 1 Wcm^{-2}). All the studies were performed with the TEG module TEC1-12706.

The use of plasmonic AuNPs helped in enhancing the power (I x V) output of the TEG by at least 20 times with 532 nm CW diode laser as the light source. The thermoelectric output enhancement in the presence of plasmonic light absorber can be corroborated to the excellent photothermal conversion efficiency of AuNPs (η_{PT} ~95 %, see **Figure 5.8** and **Section 5.3.15** for detailed calculation).
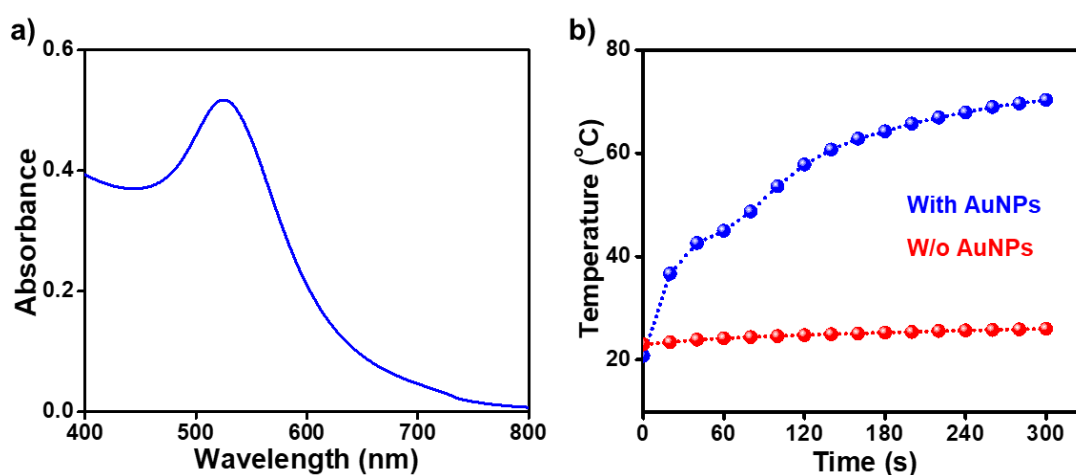

Figure 5.8. Photothermal conversion efficiency measurement. (a) UV-vis absorption spectrum of the AuNP dispersion in water. (b) Measurement of temperature rise in 1 mL aqueous solution with (blue) and without (red) AuNPs, under constant irradiation using 532 nm CW diode laser. The light intensity at the cuvette wall was measured to be 1 W.cm^{-2}.

A sharp change in the current and voltage profiles was observed in response to the laser ON-OFF cycles, which confirms the active involvement of light in the generation of electrical energy by plasmon-powered STEG (**Figure 5.6b**). The role of plasmonic-heat in enhancing the STEG performances was confirmed using light intensity experiment which showed a linear increase in the I-V profiles (**Figure 5.6c, 5.9** and **Table 5.2** in Appendix). This is in accordance with the equation (1), which predicts a linear increase in the temperature as a function of increase in the light intensity.[56]

$$T(I_{inc}) = T_{dark} + aI_{inc} \qquad\qquad (1)$$

where, T_{dark} and $T(I_{inc})$ are temperatures of plasmonic nanostructure in dark and under incident intensity of light (I_{inc}). Here 'a' is the photothermal conversion coefficient.
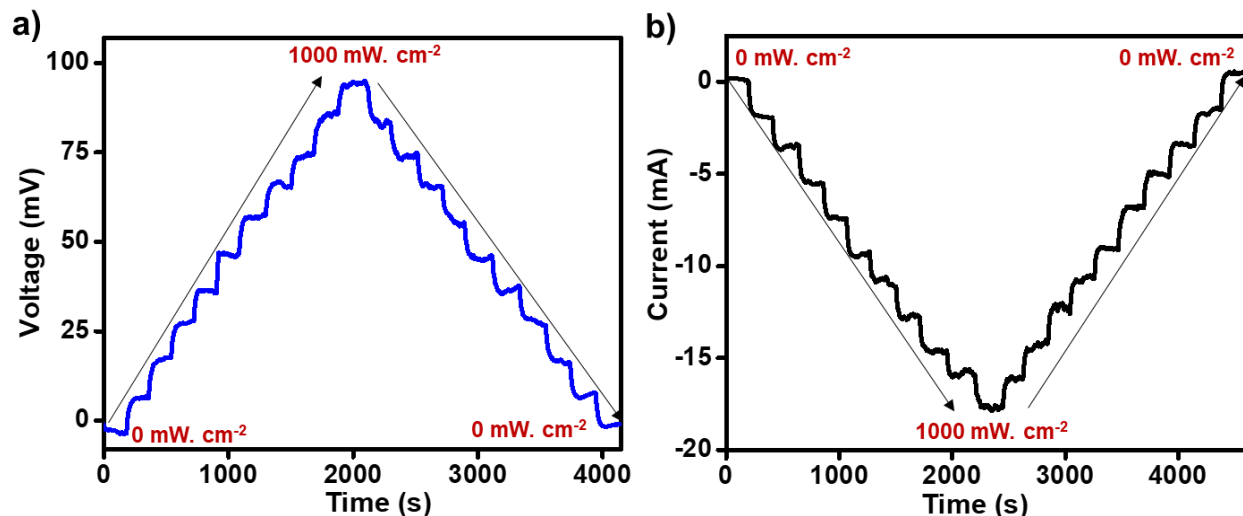

Figure 5.9. Light intensity dependent electrical output from plasmon-powered STEG. (a) A sharp increase, followed by saturation, in the output voltage was observed, as the light intensity was increased from 0 to 1000 mW (in 100 mW steps). Similarly, a sharp decrease, followed by saturation, in the output voltage was observed, as the light intensity was decreased from 1000 to 0 mW (in 100 mW steps). The corresponding changes in the current output is shown in **(b)**. A 1W 532 nm CW diode laser was used as the light source.

Next, the performance of plasmon-powered STEG was tested under white light LED before performing the sunlight experiments. The power output obtained upon illumination of the plasmon-powered STEG with a 20 W white LED was similar to that under green laser irradiation (the incident light intensity was measured to be ~60 mW.cm^{-2}). The effect of AuNP size was studied by using the AuNPs of different sizes ranging from ~5 nm to ~90 nm. Detailed microscopic

and spectroscopic characterization was performed for AuNPs of different sizes (**Figure 5.10** and **5.11**). The microscopic characterization reveals the shape and size homogeneity of synthesized AuNPs (**Figure 5.10**).
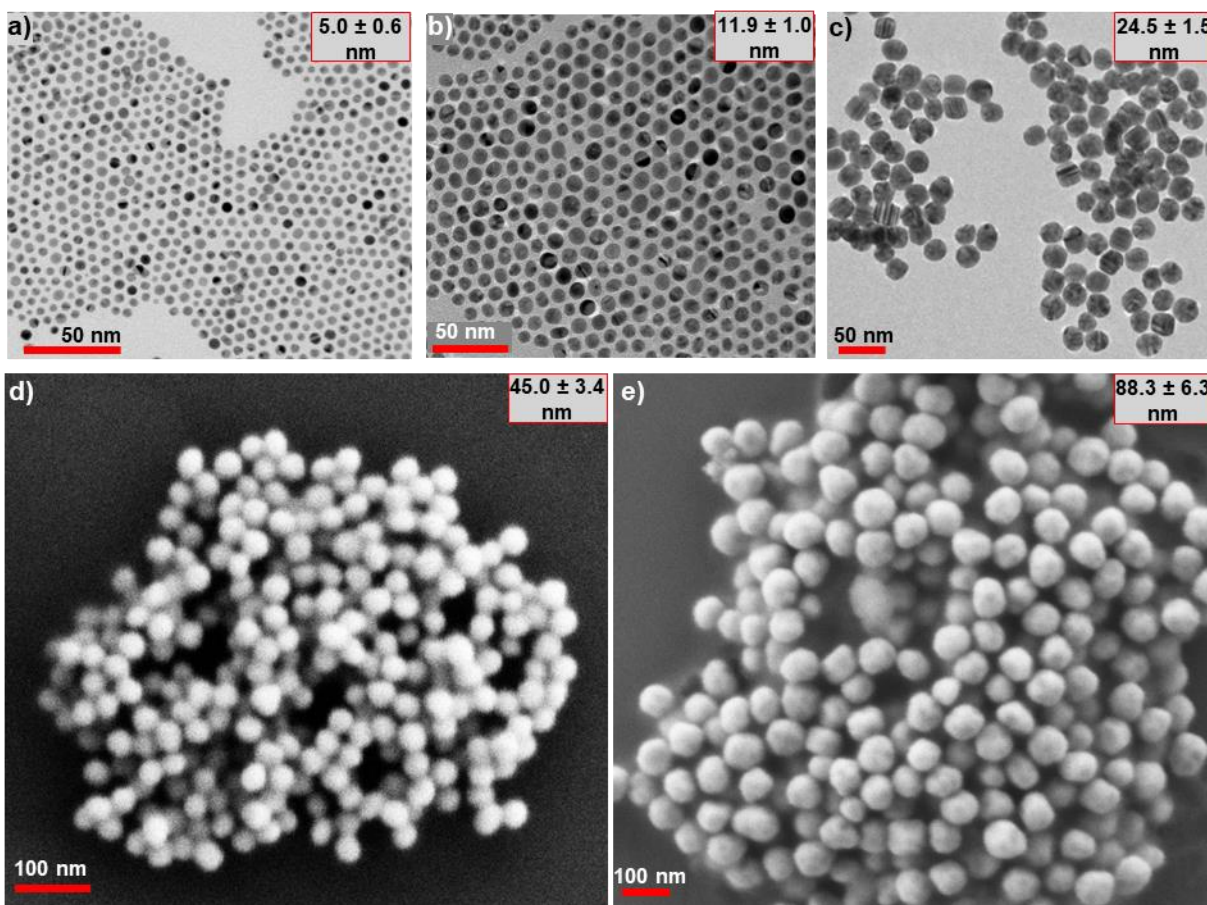

Figure 5.10. **Microscopic characterization of AuNPs of different sizes.** (a-c) TEM and (d,e) SEM images of AuNPs of different sizes.

A characteristic redshift in the UV-vis absorption was observed along with increase in the particle diameter (**Figure 5.11**). The maximum heat and electricity generation was obtained when 12 nm sized plasmonic AuNPs were used as the light absorber (**Figure 5.6d** and **Table 5.3** in Appendix) (working dimension was 2.5 cm x 2.5 cm). The trend in the electrical output power, as a function of the AuNP size, followed the temperature-rise caused by the irradiation of the NP film (**Figure 5.6d**). The plasmonic-heat generation within the NP lattice has a linear dependance on absorption cross-section of NPs.[46] Now, the scattering and absorption components of the extinction coefficient

scale as r^6 and r^3 (where r is the radius of the NP), respectively.[57] The outcome is that the absorption cross-section will plateau at a specific size regime, while the scattering cross-section will continue to increase as a function of NP size.[5] Therefore, the amount of heat generated first increase to a maxima followed by a decrease with further increase in the size. In our case, this maximum was observed for ~12 nm sized AuNPs. We would like to mention here that a similar trend in plasmonic heat dissipation was observed in our previous work as well.[33]
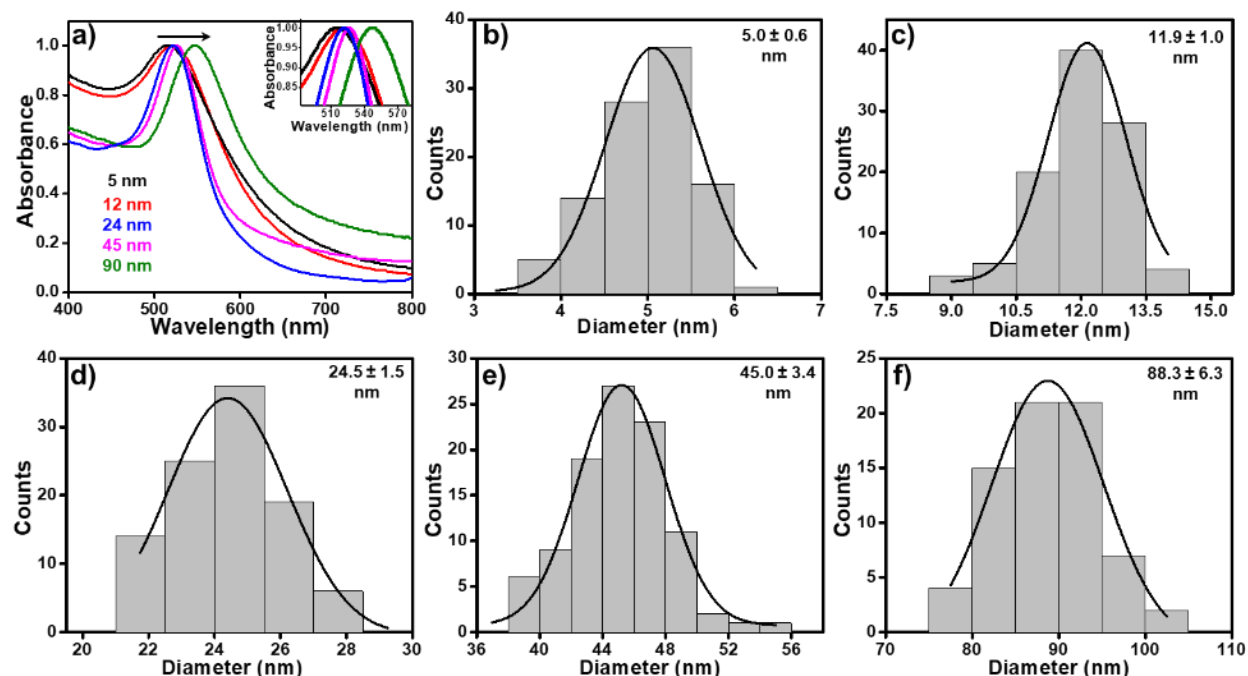

Figure 5.11. **Spectroscopic characterization and size distribution of AuNPs of different sizes.** (a) UV-vis absorption spectra and (b-f) size distribution charts of AuNPs of different sizes.

The durability studies confirmed that the power (I × V) output from the plasmon-powered STEG was stable for more than a year, which can be attributed to the excellent photostability of plasmonic AuNPs (**Figure 5.7a** and **Table 5.4** Durability was tested under intermittent illumination). A difference in the magnitude of power output was observed between the three plasmon-powered STEGs because of the variations in the internal resistance of TEG modules. At this moment, it is important to test whether the power generated from plasmon-powered STEGs under indoor illumination was sufficient to perform useful work. A power of 145 mW was obtained when three plasmon-powered STEGs were connected in series and illuminated with a warm-white light source, which was sufficient to run an electrical fan ($P_{in} \geq 35$ mW) (**Figure 5.7b,** The light intensity on the AuNP film was measured to be 0.5 W.cm^{-2}). Control experiments prove that the integration

of plasmonic AuNPs was essential to generate sufficient power from commercially available TEGs (**Figure 5.20** in the **Appendix**). Plasmonic AuNPs based light solar absorber helped in improving the power output by at least 5 times, under warm-white light illumination (**Figure 5.20** in the **Appendix**). All these optimization studies confirm that the plasmonic AuNP based light absorbers can be effectively integrated with a commercially available TEG for generating electricity from light, at ambient conditions. Moreover, the successful demonstration of plasmon-powered STEGs under white light irradiation proves their suitability for natural sunlight experiments as well.

5.4.3. Solar energy harvesting using plasmon-powered STEG. The performance of plasmon-powered STEG was tested under sunlight irradiation at ambient atmospheric conditions (1 atm pressure and 30-35 °C). Here too, a simple drop and dry method were adopted to integrate the plasmonic AuNP based solar absorber onto the TEG, which enhances its prospects of commercialization as no dedicated instrumentation was required (working dimension was 2.5 cm × 2.5 cm). The other side of the STEG was immersed in ice water bath to stabilize the electrical output for a longer time. Sunlight was focused on to the plasmonic AuNP film using a Fresnel lens (19.5 cm × 28.5 cm. Spot diameter ~1 cm). The average power output from a single plasmon-powered concentrated-STEG was estimated to be ~820 mW.cm^{-2} (corresponding to a voltage and current of 1.71 V and 0.478 A, respectively) at 95 sun irradiation (**Figure 5.12a-b** and see **Section 5.3.18** for detailed calculations). A ~9-fold increase in the concentrated-STEG power output
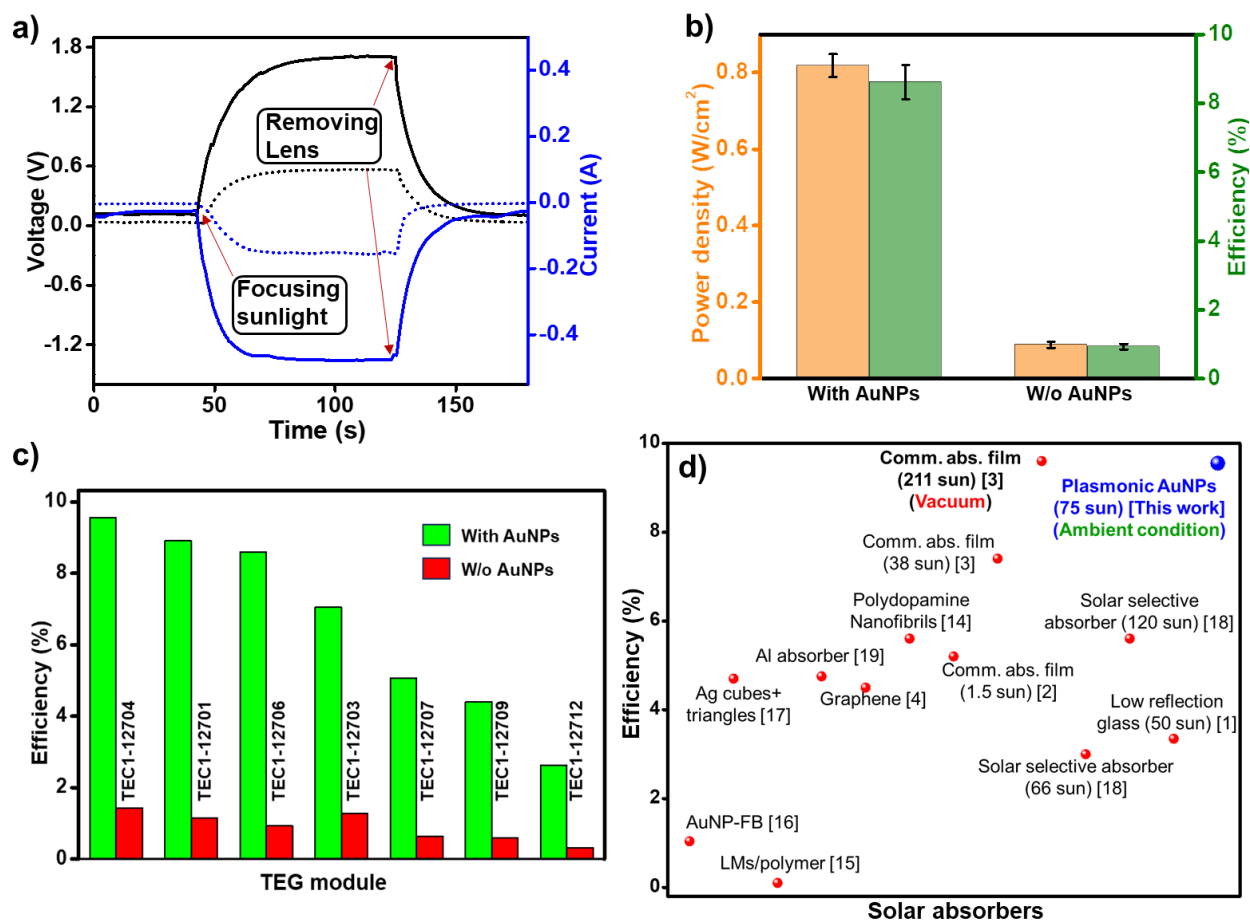
Figure 5.12. Solar energy harvesting using plasmon-powered concentrated-STEG. **(a)** Voltage and current generation upon irradiation of plasmon-powered concentrated-STEG with focused sunlight irradiation (95 sun). Dotted curves represent the data for concentrated-STEG without the plasmonic AuNP coating. **(b)** Comparison of output power density and solar-to-electricity conversion efficiency of concentrated-STEG with and without plasmonic AuNP coating. The data shown in **(a)** and **(b)** were collected with the TEG module TEC1-12706, under a solar illumination of 95 sun (1 sun corresponds to 100 mW.cm^{-2}). **(c)** Comparison of solar-to-electricity conversion efficiency of plasmon-powered STEGs prepared with different commercially available TEG modules. **(d)** Comparison of solar-to-electricity conversion efficiency of plasmon-powered STEG with various STEGs reported in the literature. The solar concentrations and reference numbers are mentioned in round and square brackets, respectively.

was obtained by using the plasmonic AuNPs as the solar absorber, which unambiguously confirms the active involvement of plasmonic-heat in enhancing the device performance. A peak solar-to-electricity conversion efficiency of 8.6 % (~9 times enhancement under 95 sun) was obtained for plasmon-powered concentrated-STEG with the TEG module TEC1-12706 (**Figure 5.12b,** see **Section 5.3.18** for detailed calculations). **Figure 5.12c** proves the suitability of plasmonic AuNPs in boosting the solar-to- electricity conversion efficiency of commercially available different TEG

modules (**Table 5.5**). The highest solar-to-electricity conversion efficiency of ~9.6 % was recorded for the plasmon-powered TEG module TEG-12704 under 75 sun, which is one of the highest reported for STEGs operable at ambient atmospheric conditions (**Figure 5.12d**, and **Table 5.6**). Under vacuum conditions, the efficiency of plasmon-powered STEG was measured to be 11.5 ± 1.5 % with TEG module TEC1-12706 under ~65 sun, which is the highest reported value so far for any STEGs (See **Figure 5.13**).

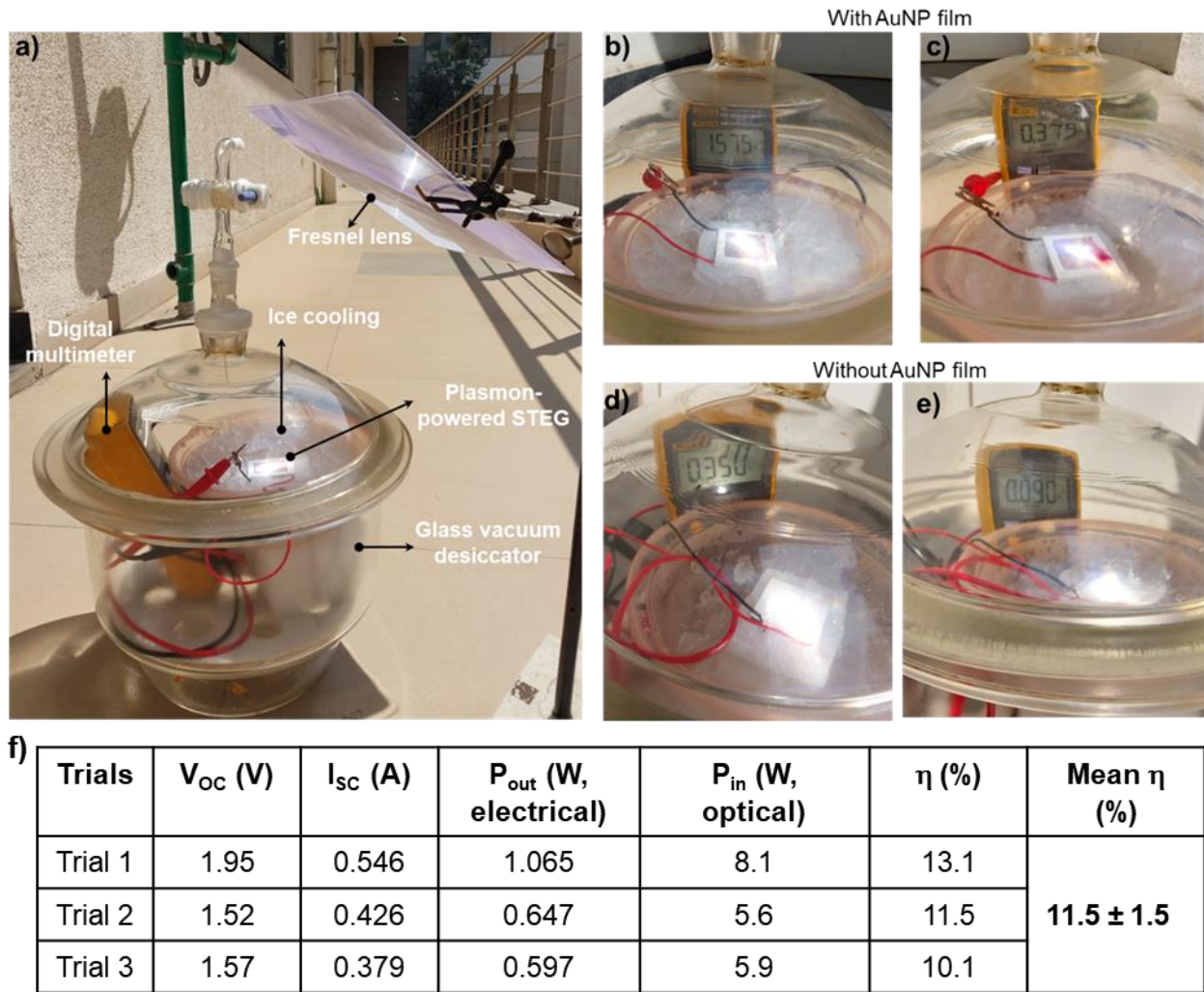| Trials	V_{OC} (V)	I_{SC} (A)	P_{out} (W, electrical)	P_{in} (W, optical)	η (%)	Mean η (%)
Trial 1	1.95	0.546	1.065	8.1	13.1	
Trial 2	1.52	0.426	0.647	5.6	11.5	**11.5 ± 1.5**
Trial 3	1.57	0.379	0.597	5.9	10.1	

Figure 5.13. Thermoelectric output measurement under vacuum. (a) The experimental setup (b) and (c) the output voltage and current measurement with plasmon-powered STEG respectively. (d) and (e) The output voltage and current measurement without AuNP film respectively. (f) The table of output voltage current and efficiency for plasmon-powered STEG under vacuum.

5.4.4. Working examples of electrical devices operated using plasmon-powered concentrated-STEG. According to the maximum power transport theorem (MPTT), the resistance of the external load should match with the internal resistance of an electrical power generator to extract the maximum power from the generator.[59] The internal resistance of the plasmon-powered STEG was determined to be 4.5 Ω from the I-V plot generated by varying the resistance of the load resistors (**Figure 5.14a,b** and **Table 5.7**).[60]
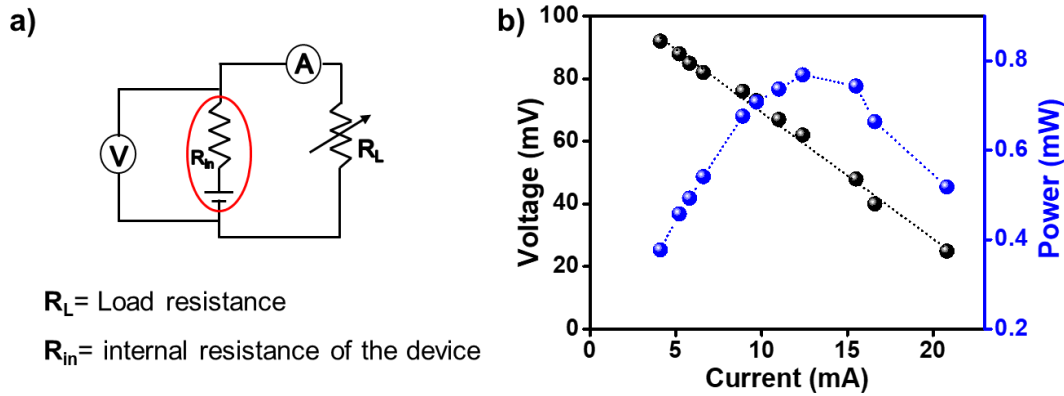

Figure 5.14. **(a)** A circuit diagram for the study of different resistors experiencing the output voltage and current from the plasmon-powered STEG. **(b)** A plot of voltage and power (I x V) output from a single plasmon-powered STEG obtained by varying the resistance of the load resistors. The maximum power output was observed when 4.5 Ω was connected to the circuit. A 20 W white LED was used as the light source, where the light intensity on the AuNP film was measured to be ~60 mW.cm^{-2}. A Keithley 2450 SMU was used to measure the I-V reported in **(a)** and **(b).** Details of different resistors used, and I-V output obtained are mentioned in **Table 5.7** of the Appendix.

Next, the real-world applications of plasmon-powered concentrated-STEG were demonstrated in running low-to-medium power electrical devices (The solar concentrations varied from 60-95 sun, as these experiments were performed on different days). Firstly, a low power ($P_{in} \geq 35$ mW) fan was operated using one plasmon-powered concentrated-STEG under focused solar irradiation (**Figure 5.15a**, and see **Figure 5.16** for circuit diagram). Secondly, a combination of calculator and timer, each requiring a minimum input voltage of 1.5 V, was operated using two plasmon-powered concentrated-STEGs connected in series (**Figure 5.15b**, and see **Figure 5.16** for circuit diagram).
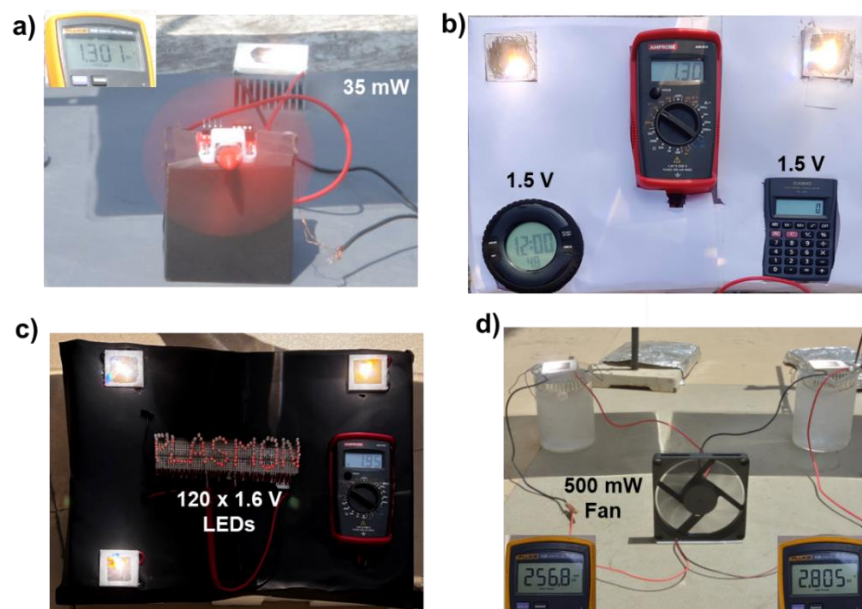
Figure 5.15. Real-world examples of electrical devices operated using plasmon-powered concentrated-STEG. **(a-d)** Photographs showing the working of electrical devices using the electricity generated from plasmon-powered concentrated-STEGs. The solar concentrations for the data shown in **(a-d)** were in the range of 60-95 sun, as these experiments were performed on different days (1 sun corresponds to 100 mW.cm^{-2}).

The maximum output voltage was measured to be 1.3 V, while the two electrical devices were working (electrical devices and multimeter were connected in parallel to the two plasmon-powered concentrated-STEGs. **Figure 5.15b**). Thirdly, a pattern of 'PLASMON' made of 120 red LEDs, each requiring a minimum input voltage of 1.63 V, was illuminated using the electrical output from three plasmon-powered concentrated-STEGs connected in series (**Figure 5.15c** and see **Figure 5.16** for circuit diagram).
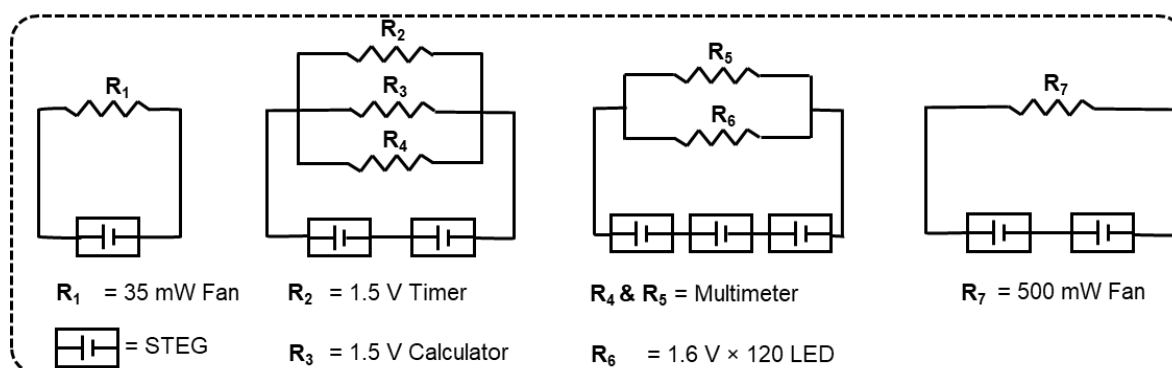

Figure 5.16. Circuit diagrams for powering to various electrical devices using the electricity generated from plasmon-powered concentrated-STEG. All the notations are elaborated at the bottom of the diagram.

The maximum output voltage of 1.95 V was measured, while the LED pattern was glowing. Finally, a cooling-fan requiring a minimum input power of 500 mW was operated using two plasmon-powered concentrated-STEGs connected in series (**Figure 5.15d,** and see **Figure 5.16** for circuit diagram). V_{oc} and I_{sc} during this experiment were measured to be 2.80 V and 257 mA, respectively. The excellent photostability of plasmonic AuNP based solar absorber (**Figure 5.17**) enabled us to run the electrical devices multiple times using the same plasmon-powered concentrated-STEGs for several months, without any drop in the output voltage. All these working examples prove that the electricity generated from the plasmon-powered concentrated-STEG can be used for running real-world electrical devices. In future, one can increase the working area or connect multiple plasmon-powered STEGs in series to run high-power electrical devices as well.
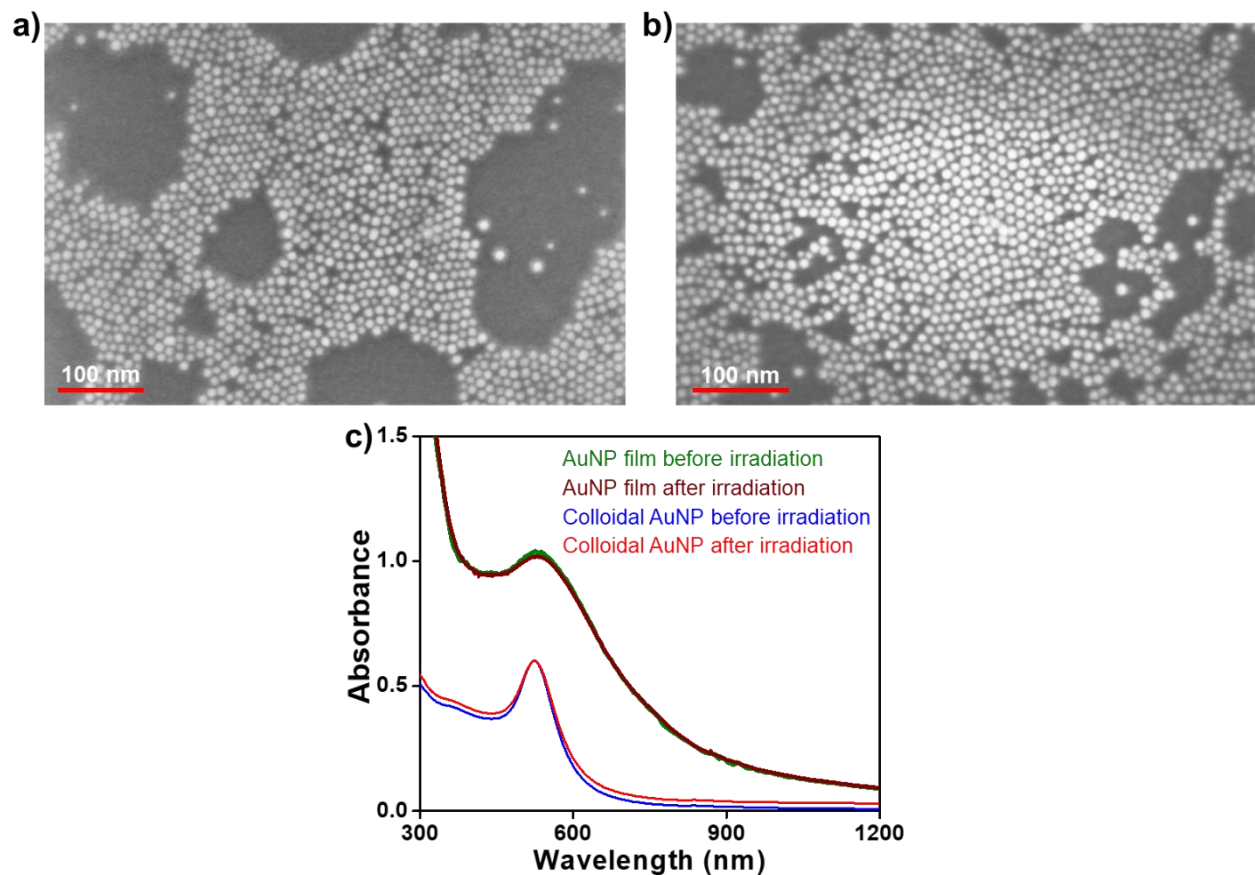

Figure 5.17: Photostability study of AuNP based solar absorber. FESEM images of AuNP film. (a) before and (b) after concentrated solar illumination. The morphology of AuNPs (size and shape) post illumination is retained, overruling any sintering effect under the concentrated solar illumination. (c) UV-vis-NIR spectra of AuNPs before and after illumination (both in colloidal and film states). A negligible change in absorption spectra proves the photostability of the AuNPs based solar absorber post illumination. UV-vis-NIR absorption of the AuNP film on TEG was measured under the diffused reflectance mode.

5.4.5. Storage of electrical energy generated from plasmon-powered concentrated-STEG. It is important to store the electrical energy generated from the plasmon-powered STEG in the form of chemical fuels, to use the energy in the dark as well. With this in mind, the electrical energy generated was stored in the form of hydrogen (H_2) gas via the electrolysis of water. Storing energy in the form of H_2 gas is a common practice in the energy sector, as H_2 has the highest energy density by weight (~140 MJ/kg).[61] As a result, the electrolysis of water is currently practiced in industry to produce H_2 fuel. However, most of the industrial plants use electricity produced from conventional non-renewable sources to perform the electrolysis of water. Our target was to replace this conventional electricity with the electricity generated from the plasmon-powered STEG. In this way, we can produce H_2 with net zero carbon emission, which will directly support our efforts to solve the challenges associated with energy crisis and climate change. In a typical experiment, three plasmon-powered concentrated-STEGs connected in series were used as the electrical energy input for the electrolysis of basic water (1M KOH. The average solar concentration during the experiment was measured to be 80 sun). Platinum mesh electrodes were used as cathode and anode. The H_2 and O_2 gases thus produced were collected in inverted columns at cathode and anode compartments, respectively (**Figure 5.18a,b**). The volume of H_2 gas collected at the cathode compartment steadily raised with increase in the solar irradiation time (**Figure 5.18c**). H_2 and O_2 gases were produced in a stoichiometric ratio of 2:1, which confirms the process of water splitting by the electrical energy produced from the plasmon-powered STEG (**Figure 5.18d**). Impressively, 10 mL of H_2 gas was produced upon ~20 min solar irradiation of plasmon-powered STEG, with an electrical-to-hydrogen energy efficiency (η_{ETH}) of ~8 % (see **Section 5.3.21** for detailed calculation).
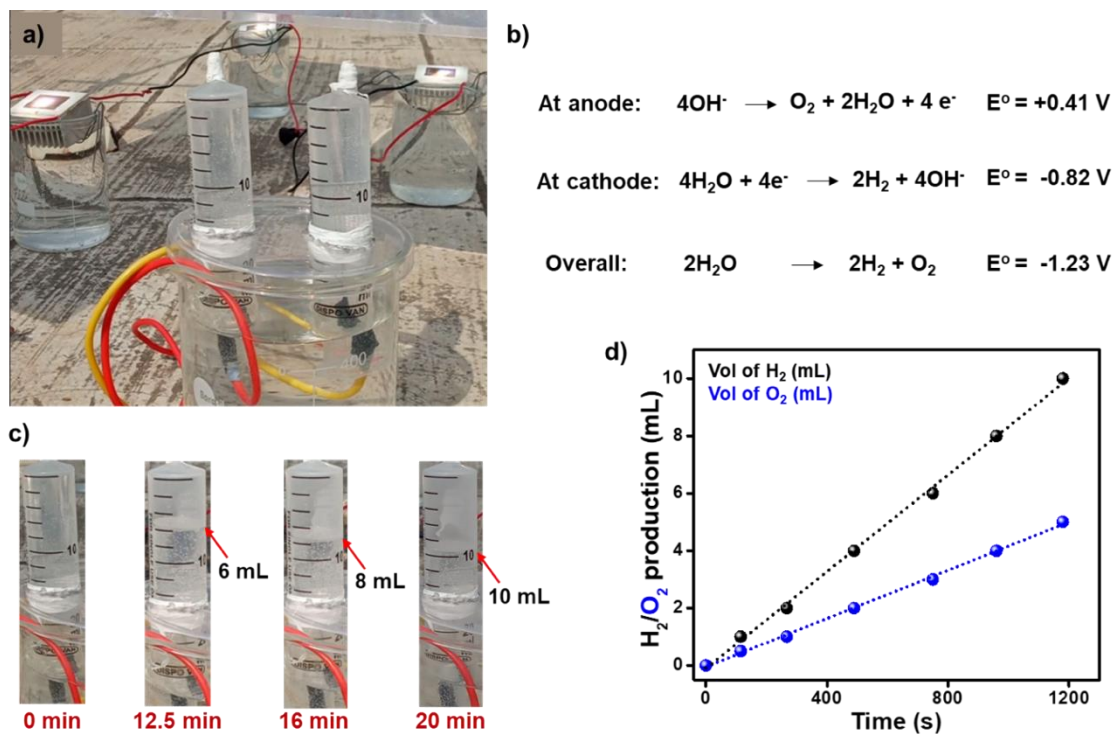
Figure 5.18. Production of green-H_2 using plasmon-powered concentrated-STEG. **(a)** The experimental setup for the splitting of water using plasmon-powered concentrated-STEG. **(b)** Half-cell and overall water-splitting reactions. **(c)** Photographs showing the storage of H_2 gas in inverted columns, as a function of solar irradiation time. **(d)** A plot showing the increase in the volume of H_2 and O_2 generated, as a function of solar irradiation time. H_2 and O_2 gases were collected in 2:1 volume ratio throughout the experiment, confirming the process of water splitting. The average solar concentration during the experiment was measured to be 80 sun (1 sun corresponds to 100 mW.cm^{-2}).

5.5. Conclusions

The excellent light-to-heat energy conversion property of plasmonic AuNPs was used for the construction of efficient and durable (> one year) STEGs at ambient conditions from commercially available thermoelectric devices. The incorporation of AuNPs as the solar absorber led to ~9 times enhancement in the overall solar-to-electricity conversion efficiency of concentrated-STEG (under 75 sun), with a peak efficiency of 9.6% at ambient conditions. An excellent efficiency of ~11.5% achieved with the plasmon-powered solar thermoelectric generator operated under vacuum is the highest value reported so far under any experimental condition to the best of our knowledge. Large light-absorptivity, high photothermal conversion efficiency, and high thermal conductivity of plasmonic AuNP ensured a large temperature difference across the two sides of the TEG, which was the primary reason for the high performance of our plasmon-powered STEG at ambient

conditions. The electricity generated from the plasmon-powered STEG process was used to run low-to-medium power electrical devices (35 mW to 500 mW), as well as for the green-H_2 production via the electrolysis of water. The design of our plasmon-powered STEGs is so simple that it could be easily integrated with other existing technologies, such as solar thermal technology to generate hot water. Such integrations of solar energy technologies are essential to achieve better solar energy utilization. In short, the use of plasmonic AuNPs as the solar absorber enabled us to construct efficient and durable (> one year) STEGs at ambient conditions from commercially available thermoelectric devices. The design of our plasmon-powered STEGs is so simple that it could be easily integrated to other clean energy harvesting technologies, including photovoltaics and solar water heaters. Thus, our work showcases how an appropriate choice of light-absorbing materials can significantly boost the solar energy conversion efficiency of thermoelectric materials for various applications, including powering of electric devices and green hydrogen production.

5.6. References

(1) Telkes, M. Solar Thermoelectric Generators. *J. Appl. Phys.* **1954**, *25*, 765–777.

(2) Kraemer, D.; Poudel, B.; Feng, H.-P.; Caylor, J. C.; Yu, B.; Yan, X.; Ma, Y.; Wang, X.; Wang, D.; Muto, A.; McEnaney, K.; Chiesa, M.; Ren, Z.; Chen, G. High-Performance Flat-Panel Solar Thermoelectric Generators with High Thermal Concentration. *Nat. Mater.* **2011**, *10*, 532–538.

(3) Kraemer, D.; Jie, Q.; McEnaney, K.; Cao, F.; Liu, W.; Weinstein, L. A.; Loomis, J.; Ren, Z.; Chen, G. Concentrating Solar Thermoelectric Generators with a Peak Efficiency of 7.4%. *Nat. Energy* **2016**, *1*, 16153.

(4) Girard, S. N.; He, J.; Li, C.; Moses, S.; Wang, G.; Uher, C.; Dravid, V. P.; Kanatzidis, M. G. *In Situ* Nanostructure Generation and Evolution within a Bulk Thermoelectric Material to Reduce Lattice Thermal Conductivity. *Nano Lett.* **2010**, *10*, 2825– 2831.

(5) Seebeck, T. J. *Magnetische Polarisation der Metalle und Erze durch Temperatur-Differenz* (Ed: A. J. V. Oettinger); W. Engelmann, 1895.

(6) Goldsmid, H. J. *Applications of Thermoelectricity*; Methuen: London 1960.

(7) Lee, J.-H.; Galli, G. A.; Grossman, J. C. Nanoporous Si as an Efficient Thermoelectric Material. *Nano Lett.* **2008**, *8*, 3750– 3754.

(8) Zhao, L. D.; Lo, S. H.; Zhang, Y. S.; Sun, H.; Tan, G. J.; Uher, C.; Wolverton, C.; Dravid, V. P.; Kanatzidis, M. G. Ultralow Thermal Conductivity and High Thermoelectric Figure of Merit in SnSe Crystals. *Nature* **2014**, *508*, 373–377.

(9) Roychowdhury, S.; Ghosh, T.; Arora, R.; Samanta, M.; Xie, L.; Singh, N. K.; Soni, A.; He, J.; Waghmare, U. V.; Biswas, K. Enhanced Atomic Ordering Leads to High Thermoelectric Performance in $AgSbTe_2$. *Science* **2021**, *371*, 722–727.

(10) Pornrungroj, C.; Andrei, V.; Reisner, E. Thermoelectric–Photoelectrochemical Water Splitting under Concentrated Solar Irradiation. *J. Am. Chem. Soc.* **2023**, *145*, 13709–13714.

(11) Wang, Q.; Pornrungroj, C.; Linley, S.; Reisner, E. Strategies to Improve Light Utilization in Solar Fuel Synthesis. *Nat. Energy* **2022**, *7*, 13–24.

(12) Buha, J.; Gaspari, R.; Del Rio Castillo, A. E.; Bonaccorso, F.; Manna, L. Thermal Stability and Anisotropic Sublimation of Two-Dimensional Colloidal Bi_2Te_3 and Bi_2Se_3 Nanocrystals. *Nano Lett.* **2016**, *16*, 4217– 4223.

(13) Toberer, E. Solar Thermoelectric Generators: Pushing the Efficiency Up. *Nat. Energy* **2016**, *1*, 16172.

(14) Li, T.; Chen, Z.; Wang, Y.; Tu, J.; Deng, X.; Li, Q.; Li, Z. Materials for Interfaces in Organic Solar Cells and Photodetectors. *ACS Appl. Mater. Interfaces* **2020**, *12*, 3301– 3326.

(15) Cruz, N.C.; Alvarez, J.D.; Redondo, J.L.; Fernandez-Reche, J.; Berenguel, M.; Monterreal, R.; Ortigosa, P.M. A New Methodology for Building-up a Robust Model for Heliostat Field Flux Characterization. *Energies* **2017**, *10*, 730.

(16) Ayachi, S.; He, X.; Yoon, H. J. Solar Thermoelectricity for Power Generation. *Adv. Energy Mater.* **2023**, *13* (28), 2300937.

(17) McEnaney, K.; Kraemer, D.; Ren, Z.; Chen, G. Modeling of Concentrating Solar Thermoelectric Generators. *J. Appl. Phys.* **2011**, *110*, 074502.

(18) Baranowski, L. L.; Snyder, G. J.; Toberer, E. S. Concentrated Solar Thermoelectric Generators. *Energy Environ. Sci.* **2012**, *5*, 9055– 9067.

(19) Baranowski, L.; Warren, E.; Toberer, E. High-Temperature High-Efficiency Solar Thermoelectric Generators. *J. Electron. Mater.* **2014**, *43*, 2348– 2355.

(20) Olsen, M. L.; Warren, E. L.; Parilla, P. A.; Toberer, E. S.; Kennedy, C. E.; Snyder, G. J.; Firdosy, S. A.; Nesmith, B.; Zakutayev, A.; Goodrich, A.; Turchi, C. S.; Netter, J.; Gray, M. H.; Ndione, P. F.; Tirawat,R.; Baranowski, L. L.; Gray, A.; Ginley, D. S. A High-Temperature, High-Efficiency Solar Thermoelectric Generator Prototype. *Energy Procedia* **2014**, 49, 1460-1469.

(21) Zong, L.; Li, M.; Li, C. Intensifying Solar-Thermal Harvest of Low-Dimension Biologic Nanostructures for Electric Power and Solar Desalination. *Nano Energy* **2018**, *50*, 308–315.

(22) Huang, X.; Liu, J.; Zhou, P.; Su, G.; Zhou, T.; Zhang, X.; Zhang, C. Ultrarobust Photothermal Materials via Dynamic Crosslinking for Solar Harvesting. *Small* **2022**, *18*, 2104048.

(23) Kosuga, A.; Yamamoto, Y.; Miyai, M.; Matsuzawa, M.; Nishimura, Y.; Hidaka, S.; Yamamoto, K.; Tanaka, S.; Yamamoto, Y.; Tokonami, S.; Iida, T. High Performance Photothermal Film with Spherical Shell-type Metallic Nanocomposites for Solar Thermoelectric Conversion. *Nanoscale* **2015**, *7*, 7580–7584.

(24) Xiong, Y.; Long, R.; Liu, D.; Zhong, X.; Wang, C.; Li, Z.-Y.; Xie, Y. Solar Energy Conversion with Tunable Plasmonic Nanostructures for Thermoelectric Devices. *Nanoscale* **2012**, *4*, 4416– 4420.

(25) Amatya, R.; Ram, R. J. Solar Thermoelectric Generator for Micropower Applications. *J. Electron. Mater.* **2010**, *39*, 1735 –1740.

(26) Wang, N.; Han, L.; He, H.; Park, N.-H.; Koumoto, K. A Novel High-Performance Photovoltaic-Thermoelectric Hybrid Device. *Energy Environ. Sci.* **2011**, *4*, 3676– 3679.

(27) Jana, N. R.; Peng, X. Single-Phase and Gram-Scale Routes toward Nearly Monodisperse Au and Other Noble Metal Nanocrystals. *J. Am. Chem. Soc.* **2003**, *125*, 14280–14281.

(28) Rao, A.; Roy, S.; Unnikrishnan, M.; Bhosale, S. S.; Devatha, G.; Pillai, P. P. Regulation of Interparticle Forces Reveals Controlled Aggregation in Charged Nanoparticles *Chem. Mater.* **2016**, *28*, 2348-2355.

(29) Kim, Y.; Smith, J. G.; Jain, P. K. Harvesting Multiple Electron–Hole Pairs Generated through Plasmonic Excitation of Au Nanoparticles. *Nat. Chem.* **2018**, *10*, 763–769.

(30) Piella, J.; Bastús, N. G.; Puntes, V. Size-Controlled Synthesis of Sub-10-nanometer Citrate-Stabilized Gold Nanoparticles and Related Optical Properties. *Chem. Mater.* **2016**, *28*, 1066–1075.

(31) Bastús, N. G.; Comenge, J.; Puntes, V. Kinetically Controlled Seeded Growth Synthesis of Citrate-Stabilized Gold Nanoparticles of up to 200 nm: Size Focusing versus Ostwald Ripening. *Langmuir* **2011**, *27*, 11098–11105.

(32) Kim, S.; Lee, S.; Yoon, S. Effect of Nanoparticle Size on Plasmon-Driven Reaction Efficiency. *ACS Appl. Mater. Interfaces* **2022**, *14*, 4163–4169.

(33) Kashyap, R. K.; Parammal, M. J.; Pillai, P. P. Effect of Nanoparticle Size on Plasmonic Heat-Driven Organic Transformation. *ChemNanoMat* **2022**, *8*, e202200252.

(34) Roper, D. K.; Ahn, W.; Hoepfner, M. Microscale Heat Transfer Transduced by Surface Plasmon Resonant Gold Nanoparticles. *J. Phys. Chem. C* **2007**, *111*, 3636–3641.

(35) Chen, X.; Jiang, C.; Shehzad, M. A.; Wang, Y.; Feng, H.; Yang, Z.; Xu, T. Water-Dissociation-Assisted Electrolysis for Hydrogen Production in a Salinity Power Cell. *ACS Sustainable Chem. Eng.* **2019**, *7*, 13023– 13030.

(36) Bohren, C. F. How Can a Particle Absorb More Than the Light Incident on It? *Am. J. Phys.* **1983**, *51*, 323–327.

(37) Hodak, J. H.; Martini, I.; Hartland, G. V. Spectroscopy and Dynamics of Nanometer-Sized Noble Metal Nanoparticles. *J. Phys. Chem. B* **1998**, *102*, 6958–6967.

(38) Link, S.; El-Sayed, M. A. Spectral Properties and Relaxation Dynamics of Surface Plasmon Electronic Oscillations in Gold and Silver Nanodots and Nanorods. *J. Phys. Chem. B* **1999**, *103*, 8410–8426.

(39) Jain, V. Kashyap, R. K. Pillai, P. P. Plasmonic Photocatalysis: Activating Chemical Bonds through Light and Plasmon. *Adv. Opt. Mater.* **2022**, *10*, 2200463.

(40) Link, S.; El-Sayed, M. A. Optical Properties and Ultrafast Dynamics of Metallic Nanocrystals. *Annu. Rev. Phys. Chem.* **2003**, *54*, 331-366.

(41) Hartland, G. V. Optical Studies of Dynamics in Noble Metal Nanostructures. *Chem. Rev.* **2011**, *111*, 3858– 3887.

(42) Brongersma, M. L.; Halas, N. J.; Nordlander, P. Plasmon-Induced Hot Carrier Science and Technology. *Nat. Nanotechnol.* **2015**, *10*, 25–34.

(43) Boyer, D.; Tamarat, P.; Maali, A.; Lounis, B.; Orrit, M. Photothermal Imaging of Nanometer-Sized Metal Particles among Scatterers. *Science* **2002**, *297*, 1160– 1163.

(44) Govorov, A. O.; Richardson, H. H. Generating Heat with Metal Nanoparticles. *Nano Today* **2007**, *2*, 30−38.

(45) Baffou, G. *Thermoplasmonics: Heating Metal Nanoparticles Using Light*; Cambridge University Press, 2017.

(46) Jauffred, L.; Samadi, A.; Klingberg, H.; Bendix, P. M.; Oddershede, L. B. Plasmonic Heating of Nanostructures. *Chem. Rev.* **2019**, *119*, 8087−8130.

(47) Baffou, G.; Cichos, F.; Quidant, R. Applications and Challenges of Thermoplasmonics. *Nat. Mater.* **2020**, *19*, 946−958.

(48) Dhiman, M.; Maity, A.; Das, A.; Belgamwar, R.; Chalke, B.; Lee, Y.; Sim, K.; Nam, J. M.; Polshettiwar, V. Plasmonic Colloidosomes of Black Gold for Solar Energy Harvesting and Hotspots Directed Catalysis for CO_2 to Fuel Conversion. *Chem. Sci.* **2019**, *10*, 6594–6603.

(49) Klemmed, B.; Besteiro, L.; Benad, A.; Georgi, M.; Wang, Z.; Govorov, A.; Eychmüller, A. Hybrid Plasmonic−Aerogel Materials as Optical Superheaters with Engineered Resonances. *Angew. Chem., Int. Ed.* **2020**, *59*, 1696−1702.

(50) Qiu, J.; Wu, Y.-C.; Wang, Y.-C.; Engelhard, M. H.; McElwee-White, L.; Wei, W. D. Surface Plasmon Mediated Chemical Solution Deposition of Gold Nanoparticles on a Nanostructured Silver Surface at Room Temperature. *J. Am. Chem. Soc.* **2013**, *135*, 38– 41.

(51) Reinhardt, P. A.; Crawford, A. P.; West, C. A.; DeLong, G.; Link, S.; Masiello, D. J.; Willets, K. A. Toward Quantitative Nanothermometry Using Single-Molecule Counting. *J. Phys. Chem. B* **2021**, *125*, 12197– 12205.

(52) Kashyap, R. K.; Dwivedi, I.; Roy, S.; Roy, S.; Rao, A.; Subramaniam, C.; Pillai, P. P. Insights into the Utilization and Quantification of Thermoplasmonic Properties in Gold Nanorod Arrays. *Chem Mater.* **2022**, *34*, 7369–7378.

(53) Dasog, M. Transition Metal Nitrides Are Heating Up the Field of Plasmonics. *Chem. Mater.* **2022**, *34*, 4249– 4258.

(54) Coppens, Z. J.; Li, W.; Walker, D. G.; Valentine, J. G. Probing and Controlling Photothermal Heat Generation in Plasmonic Nanostructures. *Nano Lett.* **2013**, *13*, 1023– 1028.

(55) de la Encarnación, C.; Jungwirth, F.; Vila-Liarte, D.; Renero-Lecuna, C.; Kavak, S.; Orue, I.; Wilhelm, C.; Bals, S.; Henriksen-Lacey, M.; Jimenez de Aberasturi, D.; Liz-Marzán, L. M. Hybrid Core-Shell Nanoparticles for Cell-Specific Magnetic Separation and Photothermal Heating. *J. Mater. Chem. B* **2023**, *11*, 5574– 5585.

(56) Wang, C. J.; Ranasingha, O.; Natesakhawat, S.; Ohodnicki Jr., P. R.; Andio, M.; Lewis, J. P.; Matranga, C. Visible Light Plasmonic Heating of Au–ZnO for the Catalytic Reduction of CO_2. *Nanoscale* **2013**, *5*, 6968 – 6974.

(57) Dubi, Y.; Un, I. W.; Sivan, Y. Thermal Effects – an Alternative Mechanism for Plasmon-Assisted Photocatalysis. *Chem. Sci.* **2020**, *11*, 5017–5027.

(58) Jain, P. K.; Lee, K. S.; El-Sayed, I. H.; El-Sayed, M. A. Calculated Absorption and Scattering Properties of Gold Nanoparticles of Different Size, Shape, and Composition: Applications in Biological Imaging and Biomedicine. *J. Phys. Chem. B* **2006**, *110*, 7238– 7248.

(59) Montecucco, A.; Siviter, J.; Knox, A. R. The Effect of Temperature Mismatch on Thermoelectric Generators Electrically Connected in Series and Parallel. *Appl. Energy* **2014**, *123*, 47– 54.

(60) Min, G.; Singh, T.; Garcia-Canadas, J.; Ellor, R. Evaluation of Thermoelectric Generators by I–V Curves. *J. Electron. Mater.* **2016**, *45*, 1700- 1704.

(61) Chu, S.; Majumdar, A. Opportunities and Challenges for a Sustainable Energy Future. *Nature* **2012**, *488*, 294−303.
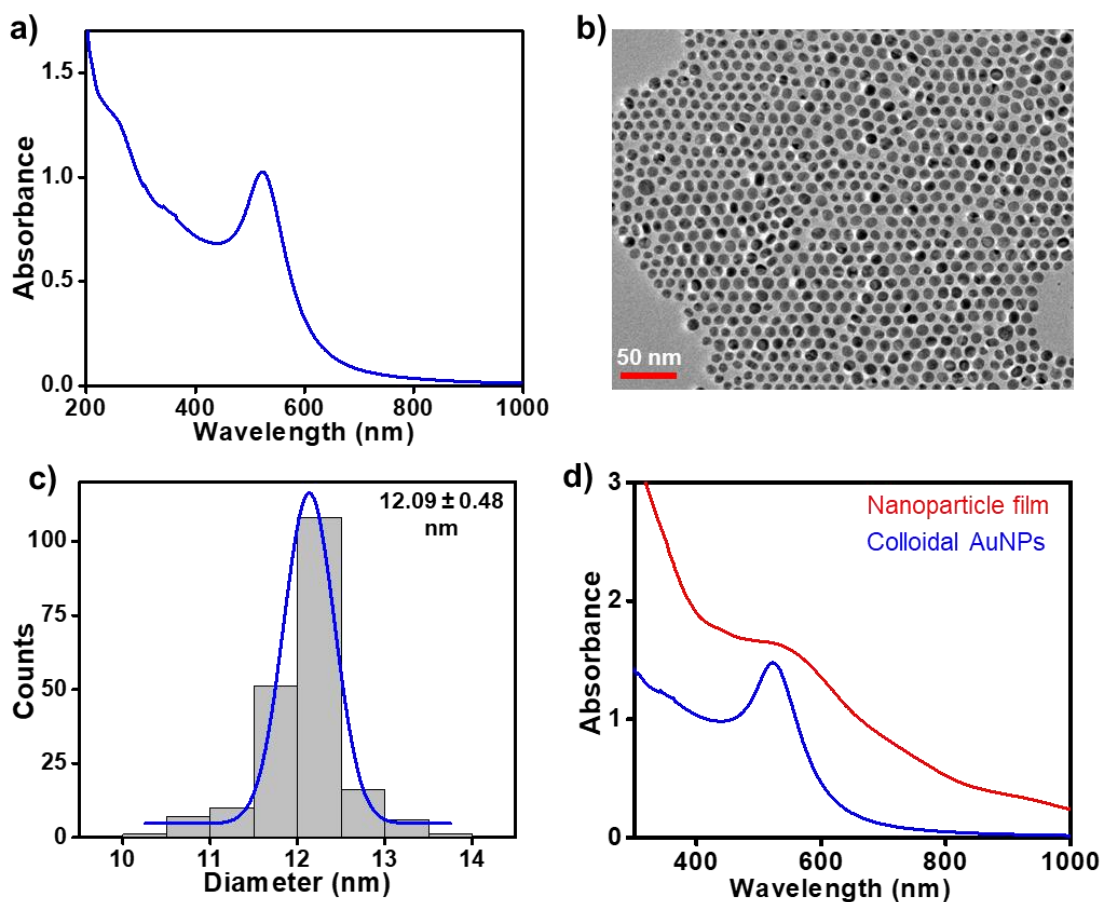
5.7. Appendix

Figure 5.19. Spectroscopic and microscopic characterization of AuNPs. (a) UV-vis absorption spectrum of ~12 nm sized AuNP, showing the surface plasmon band at 522 nm, (b) A representative TEM image and (c) the size distribution of ~12 nm AuNPs, proving the homogeneity with respect to shape and size. (d) Comparison between the UV-vis absorption spectra of ~12 nm sized AuNP in colloidal solution (blue trace) and film (red trace) states. The spectral broadness of the AuNP film on TEG is attributed to the NP coupling.

Table 5.2. Light intensity dependent voltage and current output from plasmon-powered STEG corresponding to **Figure 5.8**.

Light Intensity (mW)	V_{OC} (mV)	I_{SC} (mA)
0	-2.94 ± 0.53	0.16 ± 0.04
100	6.33 ± 0.15	-1.88 ± 0.01
200	17.63 ± 0.11	-3.52 ± 0.09
300	27.23 ± 0.06	-5.48 ± 0.07
400	36.24 ± 0.25	-7.40 ± 0.05

500	46.43 ± 0.31	-9.40 ± 0.08
600	56.98 ± 0.36	-10.98 ± 0.10
700	66.02 ± 0.56	-12.84 ± 0.05
800	74.11 ± 0.46	-14.63 ± 0.06
900	85.68 ± 0.44	-15.86 ± 0.12
1000	94.43 ± 0.27	-17.70 ± 0.07

Table 5.3. AuNPs size dependent electrical output from plasmon-powered STEG. A 20 W white LED was used as the light source. The light intensity at the AuNP film was measured to be 60 mW.cm^{-2} in all the cases.

AuNP diameter	V_{OC} (mV)	I_{SC} (mA)	P_{out} (mW)	T_h (°C)[a]
No AuNPs	28	5	0.14	32.8
5 nm	80	14	1.12	39
12 nm	91	24	2.184	45
24 nm	71	13	0.923	38
44 nm	64	12.1	0.7744	34
90 nm	65	11.2	0.728	34

[a]The simultaneous temperature increase was measured using an IR thermometer (EEE Instruments Inc., Kolkata).

Table 5.4. Table summarizing the time-dependent electrical output from plasmon-powered STEG. A 20 W white LED was used as the light source.

| Day	STEG-1			STEG-2			STEG-3		
	V_{OC} (mV)	I_{SC} (mA)	P_{out} (mW)	V_{OC} (mV)	I_{SC} (mA)	P_{out} (mW)	V_{OC} (mV)	I_{SC} (mA)	P_{out} (mW)
1	148	25	3.7	110	22.6	2.486	104	21	2.184
2	148	25	3.7	110	22.6	2.486	104	21	2.184
3	148	25	3.7	110	22.5	2.475	104	21	2.184
4	150	25	3.75	110	23	2.53	106	21.8	2.3108
12	150	25	3.75	110	22.6	2.486	106	21.7	2.3002
20	150	25	3.75	110	22.6	2.486	106	21.7	2.3002
28	150	25	3.75	110	22.63	2.4893	106	21.8	2.3108
36	150	24.9	3.73	110	22.7	2.497	106	21.7	2.3002
42	150	25	3.75	110	22.7	2.497	106	21.7	2.3002
44	150	25	3.75	110	22.6	2.486	106	21.8	2.3108
64	150	25	3.75	110	22.7	2.497	106	21.9	2.3214
95	150	25	3.75	110	22.6	2.486	106	21.9	2.3214
125	149.9	25	3.74	110	22.7	2.497	106	21.8	2.3108
156	150	25	3.75	110	22.62	2.4882	106	21.9	2.3214
187	150	24.9	3.73	110	22.61	2.4871	106	21.8	2.3108
215	150	24.9	3.73	110	22.7	2.497	106	21.7	2.3002
239	150	25	3.75	110	22.6	2.486	106	21.8	2.3108
301	150	25	3.75	110	22.63	2.4893	106	21.7	2.3002
331	150	24.9	3.73	110	22.65	2.4915	106	21.8	2.3108
362	150	24.9	3.73	110	22.64	2.4904	106	21.8	2.3108
392	150	25	3.75	110	22.7	2.497	106	21.9	2.3214
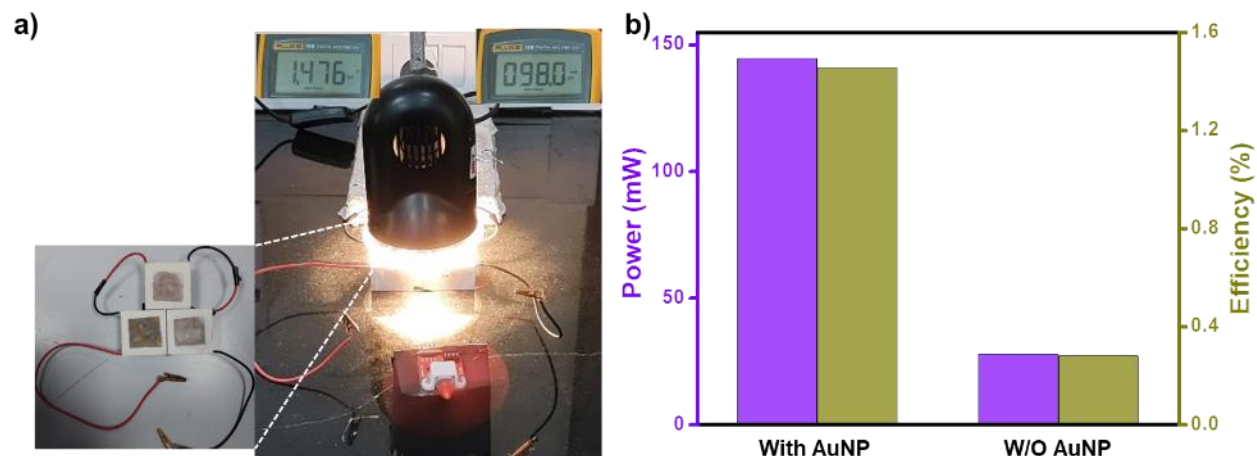
Figure 5.20. **Laboratory demonstration plasmon-powered STEG**. (a) The experimental setup for running a ≥35 mW fan with the electricity produced from three plasmon-powered STEGs. The current and voltage output is shown in the inset. (b) the power output (violet) and light-electricity conversion efficiency (dark yellow) of STEGs operated with and without AuNP film.

Table 5.5. Comparison of solar-to-electricity conversion efficiency (η) of different TEG modules.

TEG module	V_{OC} (V)		I_{SC} (mA)		P_{out} (W) (electrical power)		P_{in} (W.cm^{-2}) (optical power)	Efficiency (%)	
	With AuNP	W/o AuNP	With AuNP	W/o AuNP	With AuNP	W/o AuNP		With AuNP	W/o AuNP
TEC1-12701	3.06	1	230	90	0.7038	0.0900	7.9	8.91	1.14
TEC1-12703	1.55	0.65	350	150	0.5425	0.0975	7.7	7.04	1.26
TEC1-12704	1.76	0.67	407	160	0.7163	0.1072	7.5	**9.55**	1.43
TEC1-12705	1.05	0.44	320	125	0.3360	0.0550	7	4.80	0.78
TEC1-12706	1.71	0.565	478	156	0.8173	0.0881	9.5	8.60	0.93
TEC1-12707	0.85	0.3	375	135	0.3187	0.0405	6.3	5.06	0.64
TEC1-12709	0.78	0.292	350	126	0.2730	0.0368	6.2	4.40	0.59
TEC1-12710	0.68	0.237	340	130	0.2312	0.0308	6.1	3.79	0.50
TEC1-12712	0.45	0.16	350	120	0.1575	0.0192	6	2.62	0.32
TEC1-12715	0.38	0.15	347	120	0.1318	0.0180	5.9	2.23	0.30

Table 5.6. Comparison of solar-to-electricity conversion efficiency (η) of STEGs and concentrated-STEGs.

Solar absorber	Solar concentration	Efficiency (η) (%)	Reference
AuNP-FB/AgNP-FB	1 Sun	1.04	*Nanoscale* **2015**, *7*, 7580
Ag cubed + triangles	1 Sun	4.7	*Nanoscale* **2012**, *4*, 4416
LMs/polymer	1 Sun	0.1	*Small* **2022**, *18*, 2104048
Al-Absorber	1 Sun	4.75	*Energy Environ. Sci.* **2011**, *4*, 3676
Graphene	1 Sun	4.5	*Nano Energy* **2018**, *50*, 308
Polydopamine nanofibrils	1 Sun	5.6	*Nano Energy* **2018**, *50*, 308
Commercial absorber film	1.5 sun	5.2	*Nat. Mater.* **2011**, *10*, 532
Commercial absorber film	38 Sun	7.4	*Nat. Energy* **2016**, *1*, 16153
Commercial absorber film	211 Sun	9.6	*Nat. Energy* **2016**, *1*, 16153
Solar selective absorber	66 Sun	3	*J. Electron. Mater.* **2010**, *39*, 1735
Solar selective absorber	120 Sun	5.6	*J. Electron. Mater.* **2010**, *39*, 1735
Low reflection glass plate	50 Sun	3.35	*J. Appl. Phys.* **1954**, *25*, 765
AuNP film + TEC1-12706	95 Sun	8.6	This work
AuNP film + TEC1-12704	75 Sun	9.6	This work

Table 5.7. I-V characteristics of plasmon-powered STEG with different load resistances.

Load resistance (Ω)	V (mV)	I (mA)	P (mW)
1	24.9	20.8	0.51792
2	40	16.6	0.664
3	48	15.5	0.744
4	62	12.4	0.7688
5	67	11	0.737
7	73	9.7	0.7081
8	76	8.9	0.6764
12	82	6.6	0.5412
14	85	5.8	0.493
16	88	5.2	0.4576
22	92	4.1	0.3772

Chapter – 6

Thesis Summary and Future Directions

6.1. Thesis summary

The thesis revolves around the phenomenon of plasmonic heat which is the heat dissipated in a plasmonic nanomaterial due to its interaction with light, as a result of a series of nonradiative relaxation pathways such as electron-electron, electron-phonon, and phonon-phonon interactions. To begin with, the factors affecting thermalization and dissipation have been experimentally investigated, with a focus on the effect of shape and configuration. A thermally-driven synthetic organic reaction, namely the Diels-Alder reaction between trans-β-nitrostyrene and 2,3-dimethyl-1,3-butadiene, was performed and the yield of the reaction was used as a marker for the amount of heat generated and dissipated from plasmonic nanostructures. For the shape effect, the plasmonic heat generation in spherical Au nanoparticles was compared with the Au nanorod geometry; whereas the assembling effect was studied using a bundled geometry of AuNR array. The result suggested that nanorods were better thermoplasmonic substrates, and the assembly had an added advantage for plasmonic heat generation and/or dissipation. Throughout the thesis, the plasmonic heat was utilized for a broad range of applications such as thermal PDMS polymerization, solar-vapor generation, crystal-to-crystal phase transformation, and high-temperature reactions in synthetic organic chemistry (Diels-Alder reaction and Claisen rearrangement). One of the desired feats achieved in this direction was the deconvolution of thermal and hot carrier contribution in plasmon-driven chemistry. A thermodynamically closed reactor setup was proposed for extricating the role of hot carriers and achieving a sole plasmonic heat-driven chemistry. Further, the thermodynamically closed plasmonic reactor was advantageous with respect to the recyclability aspect as well. Next, a simple, yet effective, strategy based on thermochromism was developed to quantify the temperature rise caused by the plasmonic heat generated. The result suggested the attainment of ~250 °C within 15 min of irradiation from a 532 nm CW diode laser. The proposed quantification technique based on thermochromism was verified with three independent techniques, such as melting point, Raman spectroscopy, and infrared-based thermometric imaging studies. Finally, the prospect of conversion of plasmonic heat to electricity was discussed, which is a crucial step towards establishment of the plasmonic heat as a universal energy source. For this, the plasmonic AuNPs were integrated into a solar thermoelectric generator (STEG), which boosted the solar-to-electricity conversion efficiency by ~9 times (overall efficiency ~9.6% under ambient conditions). The electrical output from the plasmon-powered solar thermoelectric generators was used to run low-to-medium power electrical devices. Finally, the electrical energy generated from

plasmon-powered solar thermoelectric generators was stored in the form of chemical energy in the form of green hydrogen via the electrolysis of water.
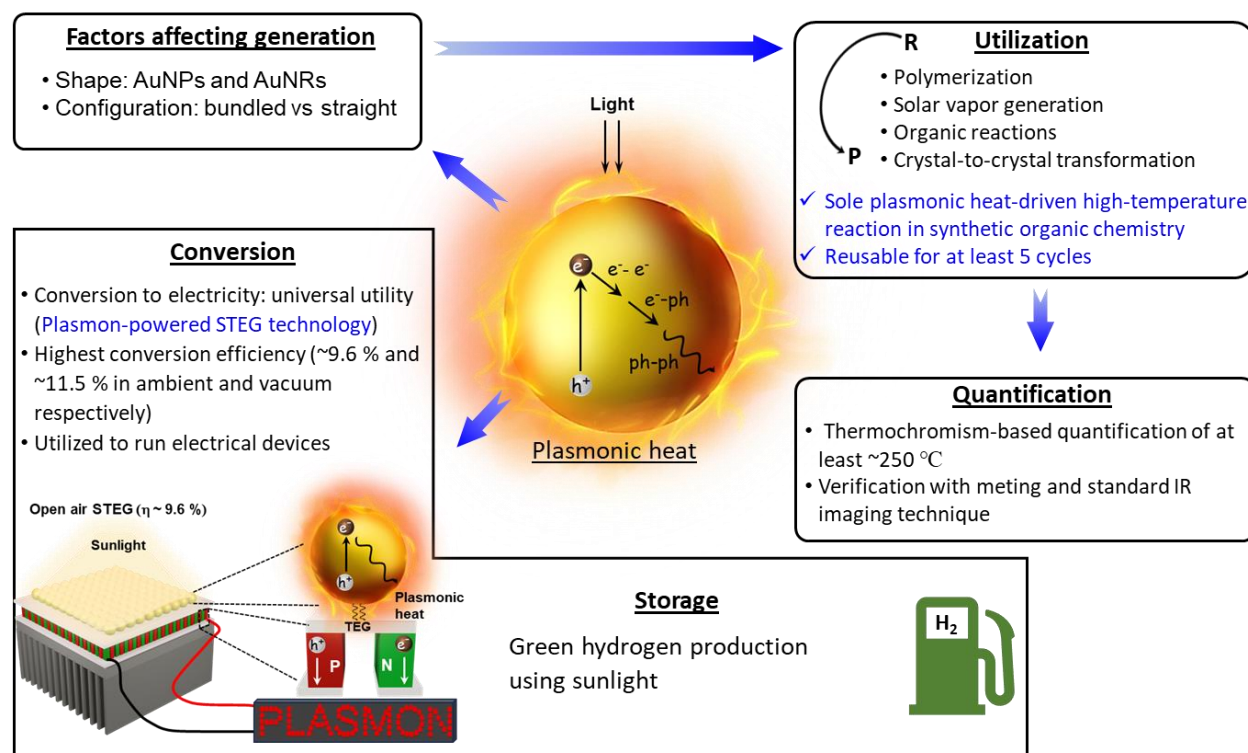

Figure 6.1. Summary of the thesis. Thesis covers various aspects of thermoplasmonics including factors influencing the generation and dissipation of plasmonic heat, quantification technique, alternate source of thermal energy for doing high-temperature chemical reactions, solar vapor generation, and electricity generation and storage.

In summary, the current thesis is an attempt to fill some of the gaps in the field of thermoplasmonics with respect to fundamental as well as applied perspectives. Our attempt is expected to help in installing sustainability in chemical synthesis, which can have direct impact in solving some of the challenges associated with energy crisis and climate change.

6.2. Future directions

The work summarized in this thesis unambiguously prove the versatility in the use of plasmonic heat in doing high-temperature chemical and physical transformations with sunlight. In future, several aspects related to thermoplasmonics can be focused to popularize the use of plasmonic

heat. From a fundamental perspective, there is an urgent need for developing plasmonic materials based on affordable and readily available precursors, which can be used as an alternative to conventional Au and Ag NPs. A few options include Cu-based NPs (Cu, CuO, CuS, etc.), Al NPs, metal carbides, metal nitrides, etc.[1-4] (marked 1 in **Figure 6.2**). The second direction could be expanding the scope of plasmonic heat in various energy-intensive important chemical transformations (CO_2 reduction, nitrogen fixation, water splitting, etc.), towards achieving the goal of sustainability in chemical synthesis (marked 2 in **Figure 6.2**).
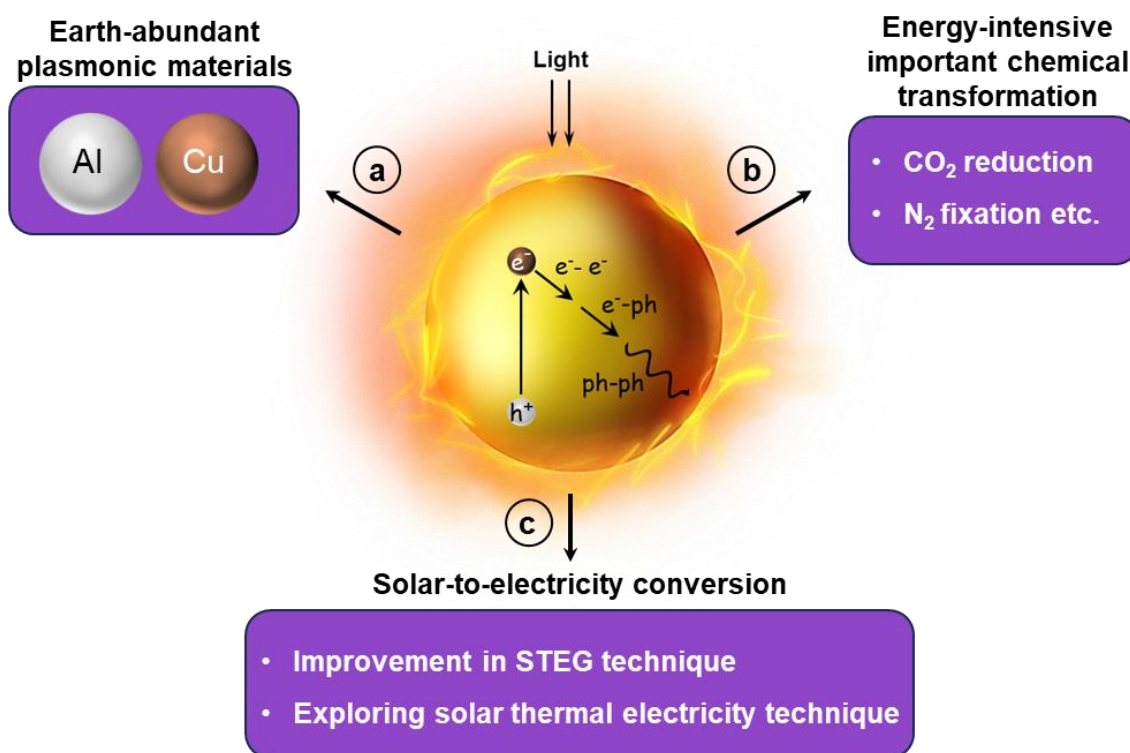
Figure 6.2. Future directions. (a) Exploring plasmonic materials from earth-abundant as a cost-effective alternative to noble metal-based material, for the lab-to-industry upscaling of thermoplasmonic-based technologies. (b) The second direction can be the utilization of plasmonic heating to carry out important energy-intensive chemical transformations such as CO_2 reduction and N_2 fixation, by integrating plasmonic materials with thermocatalysts. (c) The solar-to-electricity conversion studies could be expanded either by using plasmonic board-band solar absorbers or by integrating plasmonic materials with solar heaters.

As shown in Chapter 4 of the thesis, plasmonic heat can be used to carry out high-temperature transformation using sunlight as the sole energy source. This idea could be extended towards thermocatalytic reactions[5] where the visible-light active plasmonic materials can be used as a thermal energy source in combination with standard thermocatalysts to drive the reactions. For

this, the integration of material (thermocatalysts + plasmonic materials) as well as the reactor design will be crucial.

The final work of the thesis is an important advancement in producing electricity from sunlight. In the future, the efficiency of plasmon-powered solar thermoelectric generators can be improved by using plasmon-based materials capable of absorbing a broad solar spectrum (marked 3 in **Figure 6.2**). The other direction can be the integration of plasmonic materials with other technologies such as solar water heaters[6], which could be further extended to melt salts for generating electricity through steam turbines.

6.3. References

(51) Lalisse, A.; Tessier, G.; Plain, J.; Baffou, G. Quantifying the Efficiency of Plasmonic Materials for Near-Field Enhancement and Photothermal Conversion. *J. Phys. Chem. C* **2015**, *119*, 25518– 25528.

(52) Knight, M. W.; King, N. S.; Liu, L. F.; Everitt, H. O.; Nordlander, P.; Halas, N. J. Aluminum for plasmonics. *ACS Nano* **2014**, *8*, 834– 840.

(53) Lyu, Z.; Shang, Y.; Xia, Y. Shape-Controlled Synthesis of Copper Nanocrystals for Plasmonic, Biomedical, and Electrocatalytic Applications. *Acc. Mater. Res.* **2022***, 3,* 1137-1148.

(54) Dasog, M. Transition Metal Nitrides are Heating Up the Field of Plasmonics. *Chem. Mater.* **2022**, *34*, 4249– 4258.

(55) Tackett, B. M.; Gomez, E.; Chen, J. G. Net Reduction of CO2 via Its Thermocatalytic and Electrocatalytic Transformation Reactions in Standard and Hybrid Processes. *Nat. Catal.* **2019**, *2*, 381– 386.

(56) Mills, D. Advances in Solar Thermal Electricity Technology. *Solar Energy* **2004**, *76*, 19.

List of publication

Included in thesis

1. **Radha Krishna Kashyap**, Itisha Dwivedi, Soumendu Roy, Sumit Roy, Anish Rao, Chandramouli Subramaniam, Pramod P. Pillai* Insights into the Utilization and Quantification of Thermoplasmonic Properties in Gold Nanorod Arrays. *Chem. Mater.* **2022**, *34*, 7369– 7378.

2. **Radha Krishna Kashyap**, Shreya Tyagi, Pramod P. Pillai* Plasmon Enabled Claisen Rearrangement with Sunlight. *Chem. Commun.* **2023**, *59*, 13293-13296.

3. Vanshika Jain, **Radha Krishna Kashyap**, Pramod P. Pillai* Plasmonic Photocatalysis: Activating Chemical Bonds Through Light and Plasmon. *Adv. Opt. Mater.* **2022**, *10*, 2200463.

4. **Radha Krishna Kashyap**, Pramod P. Pillai* Plasmonic Nanoparticles Boost Solar-to-Electricity Generation at Ambient Conditions. *Nano Lett.* **2024**, *24*, 5585–5592.

Other

5. Shreya Tyagi, **Radha Krishna Kashyap**, Ankit Dhankhar, Pramod P Pillai* Plasmon-Powered Chemistry with Visible-Light Active Copper Nanoparticles. *Chem. Sci.* **2024**, DOI: 10.1039/D4SC04806G.

6. **Radha Krishna Kashyap**, Muhammed Jibin Parammal, Pramod P. Pillai* Effect of Nanoparticle Size on Plasmonic Heat-Driven Organic Transformation. *ChemNanoMat* **2022**, *8*, e202200252.

7. Sumit Roy, **Radha Krishna Kashyap**, Pramod P. Pillai* Thermoplasmonics Enable the Coupling of Light into the Solvent-Mediated Self-Assembly of Gold Nanoparticles. *J. Phys. Chem. C* **2023**, *127*, 10355– 10365

8. Soumendu Roy, Vanshika Jain, **Radha Krishna Kashyap**, Anish Rao, Pramod P. Pillai* Electrostatically Driven Multielectron Transfer for the Photocatalytic Regeneration of Nicotinamide Cofactor. *ACS Catal.* **2020**, *10*, 5522– 5528**.**

Chapter 1

JOHN WILEY AND SONS LICENSE
TERMS AND CONDITIONS

Jul 23, 2024

This Agreement between Radha Krishna Kashyap ("You") and John Wiley and Sons ("John Wiley and Sons") consists of your license details and the terms and conditions provided by John Wiley and Sons and Copyright Clearance Center.

License Number	5834810119478
License date	Jul 23, 2024
Licensed Content Publisher	John Wiley and Sons
Licensed Content Publication	Advanced Optical Materials
Licensed Content Title	Plasmonic Photocatalysis: Activating Chemical Bonds through Light and Plasmon
Licensed Content Author	Pramod P. Pillai, Radha Krishna Kashyap, Vanshika Jain
Licensed Content Date	Jun 12, 2022
Licensed Content Volume	10
Licensed Content Issue	15
Licensed Content Pages	33
Type of use	Dissertation/Thesis
Requestor type	Author of this Wiley article
Format	Print and electronic

Portion	Full article
Will you be translating?	No
Title of new work	Light-Powered Plasmonic Heaters: Extracting the Heat Out of Plasmons for Photothermal Applications
Institution name	Indian Institute of Science Education and Research (IISER), Pune
Expected presentation date	Sep 2024
The Requesting Person / Organization to Appear on the License	Radha Krishna Kashyap
Requestor Location	Mr. Radha Krishna Kashyap Chemistry Department, IISER Pune Dr. Homi Bhabha Road, Pashan Pune, 411008 India Attn: Mr. Radha Krishna Kashyap
Publisher Tax ID	EU826007151
Total	0.00 USD

Terms and Conditions

TERMS AND CONDITIONS

- You are hereby granted a personal, non-exclusive, non-sub licensable (on a stand-alone basis), non-transferable, worldwide, limited license <u>to reproduce the Wiley Materials for the purpose specified in the licensing process.</u> This license, **and any CONTENT (PDF or image file) purchased as part of your order,** is for a one-time use only and limited to any maximum distribution number specified in the license. The first instance of republication or reuse granted by this license must be completed within two years of the date of the grant of this license (although copies prepared before the end date may be distributed thereafter). The Wiley Materials shall not be used in any other manner or for any other purpose, beyond what is granted in the license. Permission is granted subject to an appropriate acknowledgement given to the author, title of the material/book/journal and the publisher. You shall also duplicate the copyright notice that appears in the Wiley publication in your use of the Wiley Material. Permission is also granted on the understanding that nowhere in the text is a previously published source acknowledged for all or part of this Wiley Material. Any third party content is expressly excluded from this permission.

- With respect to the Wiley Materials, all rights are reserved. Except as expressly granted by the terms of the license, no part of the Wiley Materials may be copied, modified, adapted (except for minor reformatting required by the new Publication), translated, reproduced, transferred or distributed, in any form or by any means, and no derivative works may be made based on the Wiley Materials without the prior permission of the respective copyright owner.**For STM Signatory Publishers clearing permission under the terms of the [STM Permissions Guidelines](#) only, the terms of the license are extended to include subsequent editions and for editions in other languages, provided such editions are for the work as a whole in situ and does not involve the separate exploitation of the permitted figures or extracts,** You may not alter, remove or suppress in any manner any copyright, trademark or other notices displayed by the Wiley Materials. You may not license, rent, sell, loan, lease, pledge, offer as security, transfer or assign the Wiley Materials on a stand-alone basis, or any of the rights granted to you hereunder to any other person.

- The Wiley Materials and all of the intellectual property rights therein shall at all times remain the exclusive property of John Wiley & Sons Inc, the Wiley Companies, or their respective licensors, and your interest therein is only that of having possession of and the right to reproduce the Wiley Materials pursuant to Section 2 herein during the continuance of this Agreement. You agree that you own no right, title or interest in or to the Wiley Materials or any of the intellectual property rights therein. You shall have no rights hereunder other than the license as provided for above in Section 2. No right, license or interest to any trademark, trade name, service mark or other branding ("Marks") of WILEY or its licensors is granted hereunder, and you agree that you shall not assert any such right, license or interest with respect thereto

- NEITHER WILEY NOR ITS LICENSORS MAKES ANY WARRANTY OR REPRESENTATION OF ANY KIND TO YOU OR ANY THIRD PARTY, EXPRESS, IMPLIED OR STATUTORY, WITH RESPECT TO THE MATERIALS OR THE ACCURACY OF ANY INFORMATION CONTAINED IN THE MATERIALS, INCLUDING, WITHOUT LIMITATION, ANY IMPLIED WARRANTY OF MERCHANTABILITY, ACCURACY, SATISFACTORY QUALITY, FITNESS FOR A PARTICULAR PURPOSE, USABILITY, INTEGRATION OR NON-INFRINGEMENT AND ALL SUCH WARRANTIES ARE HEREBY EXCLUDED BY WILEY AND ITS LICENSORS AND WAIVED BY YOU.

- WILEY shall have the right to terminate this Agreement immediately upon breach of this Agreement by you.

- You shall indemnify, defend and hold harmless WILEY, its Licensors and their respective directors, officers, agents and employees, from and against any actual or threatened claims, demands, causes of action or proceedings arising from any breach of this Agreement by you.

- IN NO EVENT SHALL WILEY OR ITS LICENSORS BE LIABLE TO YOU OR ANY OTHER PARTY OR ANY OTHER PERSON OR ENTITY FOR ANY SPECIAL, CONSEQUENTIAL, INCIDENTAL, INDIRECT, EXEMPLARY OR PUNITIVE DAMAGES, HOWEVER CAUSED, ARISING OUT OF OR IN CONNECTION WITH THE DOWNLOADING, PROVISIONING, VIEWING OR USE OF THE MATERIALS REGARDLESS OF THE FORM OF ACTION, WHETHER FOR BREACH OF CONTRACT, BREACH OF WARRANTY, TORT, NEGLIGENCE, INFRINGEMENT OR OTHERWISE (INCLUDING, WITHOUT LIMITATION, DAMAGES BASED ON LOSS OF PROFITS, DATA, FILES, USE, BUSINESS OPPORTUNITY OR CLAIMS OF THIRD PARTIES), AND WHETHER OR NOT THE PARTY HAS BEEN ADVISED OF THE POSSIBILITY OF SUCH DAMAGES. THIS LIMITATION SHALL APPLY NOTWITHSTANDING ANY FAILURE OF ESSENTIAL PURPOSE OF ANY LIMITED REMEDY PROVIDED HEREIN.

- Should any provision of this Agreement be held by a court of competent jurisdiction to be illegal, invalid, or unenforceable, that provision shall be deemed amended to achieve as nearly as possible the same economic effect as the original provision, and the legality, validity and enforceability of the remaining provisions of this Agreement shall not be affected or impaired thereby.

- The failure of either party to enforce any term or condition of this Agreement shall not constitute a waiver of either party's right to enforce each and every term and condition of this Agreement. No breach under this agreement shall be deemed waived or excused by either party unless such waiver or consent is in writing signed by the party granting such waiver or consent. The waiver by or consent of a party to a breach of any provision of this Agreement shall not operate or be construed as a waiver of or consent to any other or subsequent breach by such other party.

- This Agreement may not be assigned (including by operation of law or otherwise) by you without WILEY's prior written consent.

- Any fee required for this permission shall be non-refundable after thirty (30) days from receipt by the CCC.

- These terms and conditions together with CCC's Billing and Payment terms and conditions (which are incorporated herein) form the entire agreement between you and WILEY concerning this licensing transaction and (in the absence of fraud) supersedes all prior agreements and representations of the parties, oral or written. This Agreement may not be amended except in writing signed by both parties. This Agreement shall be binding upon and inure to the benefit of the parties' successors, legal representatives, and authorized assigns.

- In the event of any conflict between your obligations established by these terms and conditions and those established by CCC's Billing and Payment terms and conditions, these terms and conditions shall prevail.

- WILEY expressly reserves all rights not specifically granted in the combination of (i) the license details provided by you and accepted in the course of this licensing transaction, (ii) these terms and conditions and (iii) CCC's Billing and Payment

terms and conditions.

- This Agreement will be void if the Type of Use, Format, Circulation, or Requestor Type was misrepresented during the licensing process.

- This Agreement shall be governed by and construed in accordance with the laws of the State of New York, USA, without regards to such state's conflict of law rules. Any legal action, suit or proceeding arising out of or relating to these Terms and Conditions or the breach thereof shall be instituted in a court of competent jurisdiction in New York County in the State of New York in the United States of America and each party hereby consents and submits to the personal jurisdiction of such court, waives any objection to venue in such court and consents to service of process by registered or certified mail, return receipt requested, at the last known address of such party.

WILEY OPEN ACCESS TERMS AND CONDITIONS

Wiley Publishes Open Access Articles in fully Open Access Journals and in Subscription journals offering Online Open. Although most of the fully Open Access journals publish open access articles under the terms of the Creative Commons Attribution (CC BY) License only, the subscription journals and a few of the Open Access Journals offer a choice of Creative Commons Licenses. The license type is clearly identified on the article.

The Creative Commons Attribution License

The Creative Commons Attribution License (CC-BY) allows users to copy, distribute and transmit an article, adapt the article and make commercial use of the article. The CC-BY license permits commercial and non-

Creative Commons Attribution Non-Commercial License

The Creative Commons Attribution Non-Commercial (CC-BY-NC)License permits use, distribution and reproduction in any medium, provided the original work is properly cited and is not used for commercial purposes.(see below)

Creative Commons Attribution-Non-Commercial-NoDerivs License

The Creative Commons Attribution Non-Commercial-NoDerivs License (CC-BY-NC-ND) permits use, distribution and reproduction in any medium, provided the original work is properly cited, is not used for commercial purposes and no modifications or adaptations are made. (see below)

Use by commercial "for-profit" organizations

Use of Wiley Open Access articles for commercial, promotional, or marketing purposes requires further explicit permission from Wiley and will be subject to a fee.

Further details can be found on Wiley Online Library
http://olabout.wiley.com/WileyCDA/Section/id-410895.html

Other Terms and Conditions:

v1.10 Last updated September 2015

Questions? customercare@copyright.com.

CCC

RightsLink

RK

Insights into the Utilization and Quantification of Thermoplasmonic Properties in Gold Nanorod Arrays

Author: Radha Krishna Kashyap, Itisha Dwivedi, Soumendu Roy, et al

Publication: Chemistry of Materials

Publisher: American Chemical Society

Date: Aug 1, 2022

Copyright © 2022, American Chemical Society

Chapter 2,3

RK

Plasmonic Nanoparticles Boost Solar-to-Electricity Generation at Ambient Conditions

Author: Radha Krishna Kashyap, Pramod P. Pillai

Publication: Nano Letters

Publisher: American Chemical Society

Date: May 1, 2024

Copyright © 2024, American Chemical Society

PERMISSION/LICENSE IS GRANTED FOR YOUR ORDER AT NO CHARGE

BACK　　　　　　　　　　　　　　　　　CLOSE WINDOW

Privacy - Terms

Figures adapted from open access papers –

1. Figure 1.5b, c, d
2. Figure 5b

SPRINGER NATURE LICENSE
TERMS AND CONDITIONS

Figure 1.1

Jul 18, 2024

This Agreement between Radha Krishna Kashyap ("You") and Springer Nature ("Springer Nature") consists of your license details and the terms and conditions provided by Springer Nature and Copyright Clearance Center.

License Number	5831710797833
License date	Jul 18, 2024
Licensed Content Publisher	Springer Nature
Licensed Content Publication	Nature Nanotechnology
Licensed Content Title	Plasmon-induced hot carrier science and technology
Licensed Content Author	Mark L. Brongersma et al
Licensed Content Date	Jan 6, 2015
Type of Use	Thesis/Dissertation
Requestor type	academic/university or research institute
Format	print and electronic
Portion	figures/tables/illustrations
Number of figures/tables/illustrations	1
Would you like a high resolution image with your order?	no

Will you be translating?	no
Circulation/distribution	1 - 29
Author of this Springer Nature content	no
Title of new work	Light-Powered Plasmonic Heaters: Extracting the Heat Out of Plasmons for Photothermal Applications
Institution name	Indian Institute of Science Education and Research (IISER), Pune
Expected presentation date	Sep 2024
Portions	Figure 2
The Requesting Person / Organization to Appear on the License	Radha Krishna Kashyap
Requestor Location	Mr. Radha Krishna Kashyap Chemistry Department, IISER Pune Dr. Homi Bhabha Road, Pashan Pune, 411008 India Attn: Mr. Radha Krishna Kashyap
Billing Type	Invoice
Billing Address	Mr. Radha Krishna Kashyap Chemistry Department, IISER Pune Dr. Homi Bhabha Road, Pashan Pune, India 411008 Attn: Mr. Radha Krishna Kashyap
Total	0.00 USD

Terms and Conditions

Springer Nature Customer Service Centre GmbH Terms and Conditions

The following terms and conditions ("Terms and Conditions") together with the terms specified in your [RightsLink] constitute the License ("License") between you as Licensee and Springer Nature Customer Service Centre GmbH as Licensor. By clicking 'accept' and completing the transaction for your use of the material ("Licensed Material"), you confirm your acceptance of and obligation to be bound by these Terms and Conditions.

1. Grant and Scope of License

1. 1. The Licensor grants you a personal, non-exclusive, non-transferable, non-sublicensable, revocable, world-wide License to reproduce, distribute, communicate to the public, make available, broadcast, electronically transmit or create derivative works using the Licensed Material for the purpose(s) specified in your RightsLink Licence Details only. Licenses are granted for the specific use requested in the order and for no other use, subject to these Terms and Conditions. You acknowledge and agree that the rights granted to you under this License do not include the right to modify, edit, translate, include in collective works, or create derivative works of the Licensed Material in whole or in part unless expressly stated in your RightsLink Licence Details. You may use the Licensed Material only as permitted under this Agreement and will not reproduce, distribute, display, perform, or otherwise use or exploit any Licensed Material in any way, in whole or in part, except as expressly permitted by this License.

1. 2. You may only use the Licensed Content in the manner and to the extent permitted by these Terms and Conditions, by your RightsLink Licence Details and by any applicable laws.

1. 3. A separate license may be required for any additional use of the Licensed Material, e.g. where a license has been purchased for print use only, separate permission must be obtained for electronic re-use. Similarly, a License is only valid in the language selected and does not apply for editions in other languages unless additional translation rights have been granted separately in the License.

1. 4. Any content within the Licensed Material that is owned by third parties is expressly excluded from the License.

1. 5. Rights for additional reuses such as custom editions, computer/mobile applications, film or TV reuses and/or any other derivative rights requests require additional permission and may be subject to an additional fee. Please apply to journalpermissions@springernature.com or bookpermissions@springernature.com for these rights.

2. Reservation of Rights

Licensor reserves all rights not expressly granted to you under this License. You acknowledge and agree that nothing in this License limits or restricts Licensor's rights in or use of the Licensed Material in any way. Neither this License, nor any act, omission, or statement by Licensor or you, conveys any ownership right to you in any Licensed Material, or to any element or portion thereof. As between Licensor and you, Licensor owns and retains all right, title, and interest in and to the Licensed Material subject to the license granted in Section 1.1. Your permission to use the Licensed Material is expressly conditioned on you not impairing Licensor's or the applicable copyright owner's rights in the Licensed Material in any way.

3. Restrictions on use

3. 1. Minor editing privileges are allowed for adaptations for stylistic purposes or formatting purposes provided such alterations do not alter the original meaning or

intention of the Licensed Material and the new figure(s) are still accurate and representative of the Licensed Material. Any other changes including but not limited to, cropping, adapting, and/or omitting material that affect the meaning, intention or moral rights of the author(s) are strictly prohibited.

3. 2. You must not use any Licensed Material as part of any design or trademark.

3. 3. Licensed Material may be used in Open Access Publications (OAP), but any such reuse must include a clear acknowledgment of this permission visible at the same time as the figures/tables/illustration or abstract and which must indicate that the Licensed Material is not part of the governing OA license but has been reproduced with permission. This may be indicated according to any standard referencing system but must include at a minimum 'Book/Journal title, Author, Journal Name (if applicable), Volume (if applicable), Publisher, Year, reproduced with permission from SNCSC'.

4. STM Permission Guidelines

4. 1. An alternative scope of license may apply to signatories of the STM Permissions Guidelines ("STM PG") as amended from time to time and made available at https://www.stm-assoc.org/intellectual-property/permissions/permissions-guidelines/.

4. 2. For content reuse requests that qualify for permission under the STM PG, and which may be updated from time to time, the STM PG supersede the terms and conditions contained in this License.

4. 3. If a License has been granted under the STM PG, but the STM PG no longer apply at the time of publication, further permission must be sought from the Rightsholder. Contact journalpermissions@springernature.com or bookpermissions@springernature.com for these rights.

5. Duration of License

5. 1. Unless otherwise indicated on your License, a License is valid from the date of purchase ("License Date") until the end of the relevant period in the below table:

Reuse in a medical communications project	Reuse up to distribution or time period indicated in License
Reuse in a dissertation/thesis	Lifetime of thesis
Reuse in a journal/magazine	Lifetime of journal/magazine
Reuse in a book/textbook	Lifetime of edition
Reuse on a website	1 year unless otherwise specified in the License
Reuse in a presentation/slide kit/poster	Lifetime of presentation/slide kit/poster. Note: publication whether electronic or in print of presentation/slide kit/poster may require further permission.
Reuse in conference proceedings	Lifetime of conference proceedings
Reuse in an annual report	Lifetime of annual report
Reuse in training/CME materials	Reuse up to distribution or time period indicated in License
Reuse in newsmedia	Lifetime of newsmedia

Reuse in coursepack/classroom materials	Reuse up to distribution and/or time period indicated in license

6. Acknowledgement

6. 1. The Licensor's permission must be acknowledged next to the Licensed Material in print. In electronic form, this acknowledgement must be visible at the same time as the figures/tables/illustrations or abstract and must be hyperlinked to the journal/book's homepage.

6. 2. Acknowledgement may be provided according to any standard referencing system and at a minimum should include "Author, Article/Book Title, Journal name/Book imprint, volume, page number, year, Springer Nature".

7. Reuse in a dissertation or thesis

7. 1. Where 'reuse in a dissertation/thesis' has been selected, the following terms apply: Print rights of the Version of Record are provided for; electronic rights for use only on institutional repository as defined by the Sherpa guideline (www.sherpa.ac.uk/romeo/) and only up to what is required by the awarding institution.

7. 2. For theses published under an ISBN or ISSN, separate permission is required. Please contact journalpermissions@springernature.com or bookpermissions@springernature.com for these rights.

7. 3. Authors must properly cite the published manuscript in their thesis according to current citation standards and include the following acknowledgement: '*Reproduced with permission from Springer Nature*'.

8. License Fee

You must pay the fee set forth in the License Agreement (the "License Fees"). All amounts payable by you under this License are exclusive of any sales, use, withholding, value added or similar taxes, government fees or levies or other assessments. Collection and/or remittance of such taxes to the relevant tax authority shall be the responsibility of the party who has the legal obligation to do so.

9. Warranty

9. 1. The Licensor warrants that it has, to the best of its knowledge, the rights to license reuse of the Licensed Material. **You are solely responsible for ensuring that the material you wish to license is original to the Licensor and does not carry the copyright of another entity or third party (as credited in the published version).** If the credit line on any part of the Licensed Material indicates that it was reprinted or adapted with permission from another source, then you should seek additional permission from that source to reuse the material.

9. 2. EXCEPT FOR THE EXPRESS WARRANTY STATED HEREIN AND TO THE EXTENT PERMITTED BY APPLICABLE LAW, LICENSOR PROVIDES THE LICENSED MATERIAL "AS IS" AND MAKES NO OTHER REPRESENTATION OR WARRANTY. LICENSOR EXPRESSLY DISCLAIMS ANY LIABILITY FOR ANY CLAIM ARISING FROM OR OUT OF THE CONTENT, INCLUDING BUT NOT LIMITED TO ANY ERRORS, INACCURACIES, OMISSIONS, OR DEFECTS CONTAINED THEREIN, AND ANY IMPLIED OR EXPRESS WARRANTY AS TO MERCHANTABILITY OR FITNESS FOR A PARTICULAR PURPOSE. IN NO EVENT SHALL LICENSOR

BE LIABLE TO YOU OR ANY OTHER PARTY OR ANY OTHER PERSON OR
FOR ANY SPECIAL, CONSEQUENTIAL, INCIDENTAL, INDIRECT,
PUNITIVE, OR EXEMPLARY DAMAGES, HOWEVER CAUSED, ARISING
OUT OF OR IN CONNECTION WITH THE DOWNLOADING, VIEWING OR
USE OF THE LICENSED MATERIAL REGARDLESS OF THE FORM OF
ACTION, WHETHER FOR BREACH OF CONTRACT, BREACH OF
WARRANTY, TORT, NEGLIGENCE, INFRINGEMENT OR OTHERWISE
(INCLUDING, WITHOUT LIMITATION, DAMAGES BASED ON LOSS OF
PROFITS, DATA, FILES, USE, BUSINESS OPPORTUNITY OR CLAIMS OF
THIRD PARTIES), AND WHETHER OR NOT THE PARTY HAS BEEN
ADVISED OF THE POSSIBILITY OF SUCH DAMAGES. THIS LIMITATION
APPLIES NOTWITHSTANDING ANY FAILURE OF ESSENTIAL PURPOSE
OF ANY LIMITED REMEDY PROVIDED HEREIN.

10. Termination and Cancellation

10. 1. The License and all rights granted hereunder will continue until the end of the
applicable period shown in Clause 5.1 above. Thereafter, this license will be
terminated and all rights granted hereunder will cease.

10. 2. Licensor reserves the right to terminate the License in the event that payment
is not received in full or if you breach the terms of this License.

11. General

11. 1. The License and the rights and obligations of the parties hereto shall be
construed, interpreted and determined in accordance with the laws of the Federal
Republic of Germany without reference to the stipulations of the CISG (United
Nations Convention on Contracts for the International Sale of Goods) or to
Germany´s choice-of-law principle.

11. 2. The parties acknowledge and agree that any controversies and disputes
arising out of this License shall be decided exclusively by the courts of or having
jurisdiction for Heidelberg, Germany, as far as legally permissible.

11. 3. This License is solely for Licensor's and Licensee's benefit. It is not for the
benefit of any other person or entity.

Questions? For questions on Copyright Clearance Center accounts or website issues
please contact springernaturesupport@copyright.com or +1-855-239-3415 (toll free in
the US) or +1-978-646-2777. For questions on Springer Nature licensing please visit
https://www.springernature.com/gp/partners/rights-permissions-third-party-distribution

Other Conditions:

Version 1.4 - Dec 2022

Questions? customercare@copyright.com.

ELSEVIER LICENSE
TERMS AND CONDITIONS

Figure 1.3,2.1a

Jul 23, 2024

This Agreement between Radha Krishna Kashyap ("You") and Elsevier ("Elsevier") consists of your license details and the terms and conditions provided by Elsevier and Copyright Clearance Center.

License Number	5834820950662
License date	Jul 23, 2024
Licensed Content Publisher	Elsevier
Licensed Content Publication	Nano Today
Licensed Content Title	Generating heat with metal nanoparticles
Licensed Content Author	Alexander O. Govorov,Hugh H. Richardson
Licensed Content Date	Feb 1, 2007
Licensed Content Volume	2
Licensed Content Issue	1
Licensed Content Pages	9
Start Page	30
End Page	38
Type of Use	reuse in a thesis/dissertation
Portion	figures/tables/illustrations

Number of figures/tables/illustrations	1
Format	both print and electronic
Are you the author of this Elsevier article?	No
Will you be translating?	No
Title of new work	Light-Powered Plasmonic Heaters: Extracting the Heat Out of Plasmons for Photothermal Applications
Institution name	Indian Institute of Science Education and Research (IISER), Pune
Expected presentation date	Sep 2024
Portions	Figure 1b
The Requesting Person / Organization to Appear on the License	Radha Krishna Kashyap
Requestor Location	Mr. Radha Krishna Kashyap Chemistry Department, IISER Pune Dr. Homi Bhabha Road, Pashan Pune, 411008 India Attn: Mr. Radha Krishna Kashyap
Publisher Tax ID	GB 494 6272 12
Total	0.00 USD

Terms and Conditions

INTRODUCTION

1. The publisher for this copyrighted material is Elsevier. By clicking "accept" in connection with completing this licensing transaction, you agree that the following terms and conditions apply to this transaction (along with the Billing and Payment terms and conditions established by Copyright Clearance Center, Inc. ("CCC"), at the time that you opened your RightsLink account and that are available at any time at https://myaccount.copyright.com).

GENERAL TERMS

2. Elsevier hereby grants you permission to reproduce the aforementioned material subject to the terms and conditions indicated.

3. Acknowledgement: If any part of the material to be used (for example, figures) has appeared in our publication with credit or acknowledgement to another source, permission must also be sought from that source. If such permission is not obtained then that material may not be included in your publication/copies. Suitable acknowledgement to the source must be made, either as a footnote or in a reference list at the end of your publication, as follows:

"Reprinted from Publication title, Vol /edition number, Author(s), Title of article / title of chapter, Pages No., Copyright (Year), with permission from Elsevier [OR APPLICABLE SOCIETY COPYRIGHT OWNER]." Also Lancet special credit - "Reprinted from The Lancet, Vol. number, Author(s), Title of article, Pages No., Copyright (Year), with permission from Elsevier."

4. Reproduction of this material is confined to the purpose and/or media for which permission is hereby given. The material may not be reproduced or used in any other way, including use in combination with an artificial intelligence tool (including to train an algorithm, test, process, analyse, generate output and/or develop any form of artificial intelligence tool), or to create any derivative work and/or service (including resulting from the use of artificial intelligence tools).

5. Altering/Modifying Material: Not Permitted. However figures and illustrations may be altered/adapted minimally to serve your work. Any other abbreviations, additions, deletions and/or any other alterations shall be made only with prior written authorization of Elsevier Ltd. (Please contact Elsevier's permissions helpdesk here). No modifications can be made to any Lancet figures/tables and they must be reproduced in full.

6. If the permission fee for the requested use of our material is waived in this instance, please be advised that your future requests for Elsevier materials may attract a fee.

7. Reservation of Rights: Publisher reserves all rights not specifically granted in the combination of (i) the license details provided by you and accepted in the course of this licensing transaction, (ii) these terms and conditions and (iii) CCC's Billing and Payment terms and conditions.

8. License Contingent Upon Payment: While you may exercise the rights licensed immediately upon issuance of the license at the end of the licensing process for the transaction, provided that you have disclosed complete and accurate details of your proposed use, no license is finally effective unless and until full payment is received from you (either by publisher or by CCC) as provided in CCC's Billing and Payment terms and conditions. If full payment is not received on a timely basis, then any license preliminarily granted shall be deemed automatically revoked and shall be void as if never granted. Further, in the event that you breach any of these terms and conditions or any of CCC's Billing and Payment terms and conditions, the license is automatically revoked and shall be void as if never granted. Use of materials as described in a revoked license, as well as any use of the materials beyond the scope of an unrevoked license, may constitute copyright infringement and publisher reserves the right to take any and all action to protect its copyright in the materials.

9. Warranties: Publisher makes no representations or warranties with respect to the licensed material.

10. Indemnity: You hereby indemnify and agree to hold harmless publisher and CCC, and their respective officers, directors, employees and agents, from and against any and all

claims arising out of your use of the licensed material other than as specifically authorized pursuant to this license.

11. No Transfer of License: This license is personal to you and may not be sublicensed, assigned, or transferred by you to any other person without publisher's written permission.

12. No Amendment Except in Writing: This license may not be amended except in a writing signed by both parties (or, in the case of publisher, by CCC on publisher's behalf).

13. Objection to Contrary Terms: Publisher hereby objects to any terms contained in any purchase order, acknowledgment, check endorsement or other writing prepared by you, which terms are inconsistent with these terms and conditions or CCC's Billing and Payment terms and conditions. These terms and conditions, together with CCC's Billing and Payment terms and conditions (which are incorporated herein), comprise the entire agreement between you and publisher (and CCC) concerning this licensing transaction. In the event of any conflict between your obligations established by these terms and conditions and those established by CCC's Billing and Payment terms and conditions, these terms and conditions shall control.

14. Revocation: Elsevier or Copyright Clearance Center may deny the permissions described in this License at their sole discretion, for any reason or no reason, with a full refund payable to you. Notice of such denial will be made using the contact information provided by you. Failure to receive such notice will not alter or invalidate the denial. In no event will Elsevier or Copyright Clearance Center be responsible or liable for any costs, expenses or damage incurred by you as a result of a denial of your permission request, other than a refund of the amount(s) paid by you to Elsevier and/or Copyright Clearance Center for denied permissions.

LIMITED LICENSE

The following terms and conditions apply only to specific license types:

15. **Translation**: This permission is granted for non-exclusive world **English** rights only unless your license was granted for translation rights. If you licensed translation rights you may only translate this content into the languages you requested. A professional translator must perform all translations and reproduce the content word for word preserving the integrity of the article.

16. **Posting licensed content on any Website**: The following terms and conditions apply as follows: Licensing material from an Elsevier journal: All content posted to the web site must maintain the copyright information line on the bottom of each image; A hyper-text must be included to the Homepage of the journal from which you are licensing at http://www.sciencedirect.com/science/journal/xxxxx or the Elsevier homepage for books at http://www.elsevier.com; Central Storage: This license does not include permission for a scanned version of the material to be stored in a central repository such as that provided by Heron/XanEdu.

Licensing material from an Elsevier book: A hyper-text link must be included to the Elsevier homepage at http://www.elsevier.com . All content posted to the web site must maintain the copyright information line on the bottom of each image.

Posting licensed content on Electronic reserve: In addition to the above the following clauses are applicable: The web site must be password-protected and made available only to bona fide students registered on a relevant course. This permission is granted for 1 year only. You may obtain a new license for future website posting.

17. **For journal authors:** the following clauses are applicable in addition to the above:

Preprints:

A preprint is an author's own write-up of research results and analysis, it has not been peer-reviewed, nor has it had any other value added to it by a publisher (such as formatting, copyright, technical enhancement etc.).

Authors can share their preprints anywhere at any time. Preprints should not be added to or enhanced in any way in order to appear more like, or to substitute for, the final versions of articles however authors can update their preprints on arXiv or RePEc with their Accepted Author Manuscript (see below).

If accepted for publication, we encourage authors to link from the preprint to their formal publication via its DOI. Millions of researchers have access to the formal publications on ScienceDirect, and so links will help users to find, access, cite and use the best available version. Please note that Cell Press, The Lancet and some society-owned have different preprint policies. Information on these policies is available on the journal homepage.

Accepted Author Manuscripts: An accepted author manuscript is the manuscript of an article that has been accepted for publication and which typically includes author-incorporated changes suggested during submission, peer review and editor-author communications.

Authors can share their accepted author manuscript:

- immediately
    - via their non-commercial person homepage or blog
    - by updating a preprint in arXiv or RePEc with the accepted manuscript
    - via their research institute or institutional repository for internal institutional uses or as part of an invitation-only research collaboration work-group
    - directly by providing copies to their students or to research collaborators for their personal use
    - for private scholarly sharing as part of an invitation-only work group on commercial sites with which Elsevier has an agreement
- After the embargo period
    - via non-commercial hosting platforms such as their institutional repository
    - via commercial sites with which Elsevier has an agreement

In all cases accepted manuscripts should:

- link to the formal publication via its DOI
- bear a CC-BY-NC-ND license - this is easy to do
- if aggregated with other manuscripts, for example in a repository or other site, be shared in alignment with our hosting policy not be added to or enhanced in any way to appear more like, or to substitute for, the published journal article.

Published journal article (JPA): A published journal article (PJA) is the definitive final record of published research that appears or will appear in the journal and embodies all value-adding publishing activities including peer review co-ordination, copy-editing, formatting, (if relevant) pagination and online enrichment.

Policies for sharing publishing journal articles differ for subscription and gold open access articles:

Subscription Articles: If you are an author, please share a link to your article rather than the full-text. Millions of researchers have access to the formal publications on ScienceDirect, and so links will help your users to find, access, cite, and use the best available version.

Theses and dissertations which contain embedded PJAs as part of the formal submission can be posted publicly by the awarding institution with DOI links back to the formal publications on ScienceDirect.

If you are affiliated with a library that subscribes to ScienceDirect you have additional private sharing rights for others' research accessed under that agreement. This includes use for classroom teaching and internal training at the institution (including use in course packs and courseware programs), and inclusion of the article for grant funding purposes.

Gold Open Access Articles: May be shared according to the author-selected end-user license and should contain a CrossMark logo, the end user license, and a DOI link to the formal publication on ScienceDirect.

Please refer to Elsevier's posting policy for further information.

18. **For book authors** the following clauses are applicable in addition to the above: Authors are permitted to place a brief summary of their work online only. You are not allowed to download and post the published electronic version of your chapter, nor may you scan the printed edition to create an electronic version. **Posting to a repository:** Authors are permitted to post a summary of their chapter only in their institution's repository.

19. **Thesis/Dissertation**: If your license is for use in a thesis/dissertation your thesis may be submitted to your institution in either print or electronic form. Should your thesis be published commercially, please reapply for permission. These requirements include permission for the Library and Archives of Canada to supply single copies, on demand, of the complete thesis and include permission for Proquest/UMI to supply single copies, on demand, of the complete thesis. Should your thesis be published commercially, please reapply for permission. Theses and dissertations which contain embedded PJAs as part of the formal submission can be posted publicly by the awarding institution with DOI links back to the formal publications on ScienceDirect.

Elsevier Open Access Terms and Conditions

You can publish open access with Elsevier in hundreds of open access journals or in nearly 2000 established subscription journals that support open access publishing. Permitted third party re-use of these open access articles is defined by the author's choice of Creative Commons user license. See our open access license policy for more information.

Terms & Conditions applicable to all Open Access articles published with Elsevier:

Any reuse of the article must not represent the author as endorsing the adaptation of the article nor should the article be modified in such a way as to damage the author's honour or reputation. If any changes have been made, such changes must be clearly indicated.

The author(s) must be appropriately credited and we ask that you include the end user license and a DOI link to the formal publication on ScienceDirect.

If any part of the material to be used (for example, figures) has appeared in our publication with credit or acknowledgement to another source it is the responsibility of the user to ensure their reuse complies with the terms and conditions determined by the rights holder.

Additional Terms & Conditions applicable to each Creative Commons user license:

CC BY: The CC-BY license allows users to copy, to create extracts, abstracts and new works from the Article, to alter and revise the Article and to make commercial use of the Article (including reuse and/or resale of the Article by commercial entities), provided the user gives appropriate credit (with a link to the formal publication through the relevant DOI), provides a link to the license, indicates if changes were made and the licensor is not represented as endorsing the use made of the work. The full details of the license are available at http://creativecommons.org/licenses/by/4.0.

CC BY NC SA: The CC BY-NC-SA license allows users to copy, to create extracts, abstracts and new works from the Article, to alter and revise the Article, provided this is not done for commercial purposes, and that the user gives appropriate credit (with a link to the formal publication through the relevant DOI), provides a link to the license, indicates if changes were made and the licensor is not represented as endorsing the use made of the work. Further, any new works must be made available on the same conditions. The full details of the license are available at http://creativecommons.org/licenses/by-nc-sa/4.0.

CC BY NC ND: The CC BY-NC-ND license allows users to copy and distribute the Article, provided this is not done for commercial purposes and further does not permit distribution of the Article if it is changed or edited in any way, and provided the user gives appropriate credit (with a link to the formal publication through the relevant DOI), provides a link to the license, and that the licensor is not represented as endorsing the use made of the work. The full details of the license are available at http://creativecommons.org/licenses/by-nc-nd/4.0. Any commercial reuse of Open Access articles published with a CC BY NC SA or CC BY NC ND license requires permission from Elsevier and will be subject to a fee.

Commercial reuse includes:

- Associating advertising with the full text of the Article
- Charging fees for document delivery or access
- Article aggregation
- Systematic distribution via e-mail lists or share buttons

Posting or linking by commercial companies for use by customers of those companies.

20. **Other Conditions**:

v1.10

Questions? customercare@copyright.com.

CCC
RightsLink

RK

Plasmon-Assisted Local Temperature Control to Pattern Individual Semiconductor Nanowires and Carbon Nanotubes

ACS Publications
Most Trusted. Most Cited. Most Read.

Author: Linyou Cao, David N. Barsic, Alex R. Guichard, et al

Publication: Nano Letters

Publisher: American Chemical Society

Date: Nov 1, 2007

Copyright © 2007, American Chemical Society

PERMISSION/LICENSE IS GRANTED FOR YOUR ORDER AT NO CHARGE

BACK CLOSE WINDOW

Figure 1.4

CCC
RightsLink

RK

Plasmon Resonant Enhancement of Carbon Monoxide Catalysis

ACS Publications
Most Trusted. Most Cited. Most Read.

Author: Wei Hsuan Hung, Mehmet Aykol, David Valley, et al

Publication: Nano Letters

Publisher: American Chemical Society

Date: Apr 1, 2010

Copyright © 2010, American Chemical Society

PERMISSION/LICENSE IS GRANTED FOR YOUR ORDER AT NO CHARGE

This type of permission/license, instead of the standard Terms and Conditions, is sent to you because no fee is being charged for your order. Please note the following:

- Permission is granted for your request in both print and electronic formats, and translations.
- If figures and/or tables were requested, they may be adapted or used in part.
- Please print this page for your records and send a copy of it to your publisher/graduate school.
- Appropriate credit for the requested material should be given as follows: "Reprinted (adapted) with permission from {COMPLETE REFERENCE CITATION}. Copyright {YEAR} American Chemical Society." Insert appropriate information in place of the capitalized words.
- One-time permission is granted only for the use specified in your RightsLink request. No additional uses are granted (such as derivative works or other editions). For any uses, please submit a new request.

If credit is given to another source for the material you requested from RightsLink, permission must be obtained from that source.

BACK   CLOSE WINDOW

Figure 1.6

Radha Krishna Kashyap <krishna.kashyap@students.iiserpune.ac.in>

Case #02103878 - Request of copyright permission
1 message

customercare@copyright.com <customercare@copyright.com>   Tue, Jul 23, 2024 at 10:36 PM
To: "krishna.kashyap@students.iiserpune.ac.in" <krishna.kashyap@students.iiserpune.ac.in>

Figure 1.7,1.8, 2.1b,c

Dear Radha Krishna Kashyap,

My name is Zach with CCC's customer service team. As you may know, we partner with copyright owners to assist with processing permissions requests through our online platforms RightsLink and Marketplace.

That is a great question. On the articles website for "Gold nanoparticle ensembles as heaters and actuators: melting and collective plasmon resonances" within the Rights and Permissions section Springer Nature has provided the following about reuse of the material:

> **Open Access** *This article is distributed under the terms of the Creative Commons Attribution 2.0 International License (https://creativecommons.org/licenses/by/2.0), which permits unrestricted use, distribution, and reproduction in any medium, provided the original work is properly cited.*

I hope this has been helpful. If you need further assistance please let me know.

Kind regards,

Zachary

Zachary Hall
Customer Account Specialist
Copyright Clearance Center
222 Rosewood Drive
Danvers, MA 01923
www.copyright.com
Toll Free US +1.855.239.3415
International +1.978-646-2600

Facebook - Twitter - LinkedIn

--------------- Original Message ---------------
From: Radha Krishna Kashyap [krishna.kashyap@students.iiserpune.ac.in]
Sent: 7/23/2024 11:04 AM
To: springernaturesupport@copyright.com
Subject: Request of copyright permission

Dear Springer Nature Copyright Team,
I am Radha Krishna Kashyap a PhD student at Indian Institute of Science Education and Research (IISER), Pune.
IISER Pune is a non-profit academic institute. I would like to take permission to reuse figures (Fig.1, Fig. 5, and Fig. 6)
from the article (doi: 10.1007/s11671-006-9015-7) for my PhD thesis.
The details are as follows for your ready reference:
Title of the article: Gold nanoparticle ensembles as heaters and actuators: melting and collective plasmon
resonances
Doi: 10.1007/s11671-006-9015-7
Detail of the figures taken: Fig.1, Fig. 5 and Fig. 6

Thanks and regards
Kashyap

Radha Krishna Kashyap
Senior Research Fellow
Dr. Pramod P. Pillai's Group
IISER Pune- 411008

CCC
RightsLink

RK

Quantifying the Efficiency of Plasmonic Materials for Near-Field Enhancement and Photothermal Conversion

ACS Publications
Most Trusted. Most Cited. Most Read.

Author: Adrien Lalisse, Gilles Tessier, Jérome Plain, et al

Publication: The Journal of Physical Chemistry C

Publisher: American Chemical Society

Date: Nov 1, 2015

Copyright © 2015, American Chemical Society

PERMISSION/LICENSE IS GRANTED FOR YOUR ORDER AT NO CHARGE

This type of permission/license, instead of the standard Terms and Conditions, is sent to you because no fee is being charged for your order. Please note the following:

- Permission is granted for your request in both print and electronic formats, and translations.
- If figures and/or tables were requested, they may be adapted or used in part.
- Please print this page for your records and send a copy of it to your publisher/graduate school.
- Appropriate credit for the requested material should be given as follows: "Reprinted (adapted) with permission from {COMPLETE REFERENCE CITATION}. Copyright {YEAR} American Chemical Society." Insert appropriate information in place of the capitalized words.
- One-time permission is granted only for the use specified in your RightsLink request. No additional uses are granted (such as derivative works or other editions). For any uses, please submit a new request.

If credit is given to another source for the material you requested from RightsLink, permission must be obtained from that source.

BACK   CLOSE WINDOW

Figure 1.9,2.2

CCC

RightsLink

RK

Cancer Photothermal Therapy with ICG-Conjugated Gold Nanoclusters

ACS Publications
Most Trusted. Most Cited. Most Read.

Author: Xingya Jiang, Bujie Du, Yingyu Huang, et al

Publication: Bioconjugate Chemistry

Publisher: American Chemical Society

Date: May 1, 2020

Copyright © 2020, American Chemical Society

BACK   CLOSE WINDOW

Figure 1.10a

CCC
RightsLink

Plasmonic Photothermal Nanoparticles for Biomedical Applications

WILEY

Author: Jwa-Min Nam, Jung-Hoon Lee, Minho Kim

Publication: Advanced Science

Publisher: John Wiley and Sons

Date: Jul 22, 2019

© 2019 The Authors. Published by WILEY-VCH Verlag GmbH & Co. KGaA, Weinheim

Figure 1.10b

SPRINGER NATURE LICENSE
TERMS AND CONDITIONS

Figure 1.11

Jul 23, 2024

This Agreement between Radha Krishna Kashyap ("You") and Springer Nature ("Springer Nature") consists of your license details and the terms and conditions provided by Springer Nature and Copyright Clearance Center.

License Number	5835061174614
License date	Jul 23, 2024
Licensed Content Publisher	Springer Nature
Licensed Content Publication	Nature Photonics
Licensed Content Title	3D self-assembly of aluminium nanoparticles for plasmon-enhanced solar desalination
Licensed Content Author	Lin Zhou et al
Licensed Content Date	Apr 25, 2016
Type of Use	Thesis/Dissertation
Requestor type	academic/university or research institute
Format	print and electronic
Portion	figures/tables/illustrations
Number of figures/tables/illustrations	1
Would you like a high resolution image with your order?	no

Print This Page

JOHN WILEY AND SONS LICENSE
TERMS AND CONDITIONS

Jul 23, 2024   # Figure 1.12a

This Agreement between Radha Krishna Kashyap ("You") and John Wiley and Sons
("John Wiley and Sons") consists of your license details and the terms and conditions
provided by John Wiley and Sons and Copyright Clearance Center.

License Number	5835060447039
License date	Jul 23, 2024
Licensed Content Publisher	John Wiley and Sons
Licensed Content Publication	Angewandte Chemie International Edition
Licensed Content Title	An Efficient Method Based on the Photothermal Effect for the Release of Molecules from Metal Nanoparticle Surfaces
Licensed Content Author	Neil R. Branda, Byron D. Gates, Guoxia Jin, et al
Licensed Content Date	May 19, 2009
Licensed Content Volume	48
Licensed Content Issue	23
Licensed Content Pages	4
Type of use	Dissertation/Thesis
Requestor type	University/Academic
Format	Print and electronic

Portion	Figure/table

Number of figures/tables	1

Will you be translating?	No

Title of new work	Light-Powered Plasmonic Heaters: Extracting the Heat Out of Plasmons for Photothermal Applications

Institution name	Indian Institute of Science Education and Research (IISER), Pune

Expected presentation date	Sep 2024

Portions	Figure 1

The Requesting Person / Organization to Appear on the License	Radha Krishna Kashyap

Requestor Location	Mr. Radha Krishna Kashyap Chemistry Department, IISER Pune Dr. Homi Bhabha Road, Pashan Pune, 411008 India Attn: Mr. Radha Krishna Kashyap

Publisher Tax ID	EU826007151

Total	0.00 USD

Terms and Conditions

TERMS AND CONDITIONS

This copyrighted material is owned by or exclusively licensed to John Wiley & Sons, Inc. or one of its group companies (each a"Wiley Company") or handled on behalf of a society with which a Wiley Company has exclusive publishing rights in relation to a particular work (collectively "WILEY"). By clicking "accept" in connection with completing this licensing transaction, you agree that the following terms and conditions apply to this transaction (along with the billing and payment terms and conditions established by the Copyright Clearance Center Inc., ("CCC's Billing and Payment terms and conditions"), at the time that you opened your RightsLink account (these are available at any time at http://myaccount.copyright.com).

Terms and Conditions

- The materials you have requested permission to reproduce or reuse (the "Wiley Materials") are protected by copyright.

- You are hereby granted a personal, non-exclusive, non-sub licensable (on a stand-alone basis), non-transferable, worldwide, limited license <u>to reproduce the Wiley Materials for the purpose specified in the licensing process.</u> This license, **and any CONTENT (PDF or image file) purchased as part of your order,** is for a one-time use only and limited to any maximum distribution number specified in the license. The first instance of republication or reuse granted by this license must be completed within two years of the date of the grant of this license (although copies prepared before the end date may be distributed thereafter). The Wiley Materials shall not be used in any other manner or for any other purpose, beyond what is granted in the license. Permission is granted subject to an appropriate acknowledgement given to the author, title of the material/book/journal and the publisher. You shall also duplicate the copyright notice that appears in the Wiley publication in your use of the Wiley Material. Permission is also granted on the understanding that nowhere in the text is a previously published source acknowledged for all or part of this Wiley Material. Any third party content is expressly excluded from this permission.

- With respect to the Wiley Materials, all rights are reserved. Except as expressly granted by the terms of the license, no part of the Wiley Materials may be copied, modified, adapted (except for minor reformatting required by the new Publication), translated, reproduced, transferred or distributed, in any form or by any means, and no derivative works may be made based on the Wiley Materials without the prior permission of the respective copyright owner.**For STM Signatory Publishers clearing permission under the terms of the STM Permissions Guidelines only, the terms of the license are extended to include subsequent editions and for editions in other languages, provided such editions are for the work as a whole in situ and does not involve the separate exploitation of the permitted figures or extracts,** You may not alter, remove or suppress in any manner any copyright, trademark or other notices displayed by the Wiley Materials. You may not license, rent, sell, loan, lease, pledge, offer as security, transfer or assign the Wiley Materials on a stand-alone basis, or any of the rights granted to you hereunder to any other person.

- The Wiley Materials and all of the intellectual property rights therein shall at all times remain the exclusive property of John Wiley & Sons Inc, the Wiley Companies, or their respective licensors, and your interest therein is only that of having possession of and the right to reproduce the Wiley Materials pursuant to Section 2 herein during the continuance of this Agreement. You agree that you own no right, title or interest in or to the Wiley Materials or any of the intellectual property rights therein. You shall have no rights hereunder other than the license as provided for above in Section 2. No right, license or interest to any trademark, trade name, service mark or other branding ("Marks") of WILEY or its licensors is granted hereunder, and you agree that you shall not assert any such right, license or interest with respect thereto

- NEITHER WILEY NOR ITS LICENSORS MAKES ANY WARRANTY OR REPRESENTATION OF ANY KIND TO YOU OR ANY THIRD PARTY, EXPRESS, IMPLIED OR STATUTORY, WITH RESPECT TO THE MATERIALS OR THE ACCURACY OF ANY INFORMATION CONTAINED IN THE MATERIALS, INCLUDING, WITHOUT LIMITATION, ANY IMPLIED WARRANTY OF MERCHANTABILITY, ACCURACY, SATISFACTORY QUALITY, FITNESS FOR A PARTICULAR PURPOSE, USABILITY,

INTEGRATION OR NON-INFRINGEMENT AND ALL SUCH WARRANTIES ARE HEREBY EXCLUDED BY WILEY AND ITS LICENSORS AND WAIVED BY YOU.

- WILEY shall have the right to terminate this Agreement immediately upon breach of this Agreement by you.

- You shall indemnify, defend and hold harmless WILEY, its Licensors and their respective directors, officers, agents and employees, from and against any actual or threatened claims, demands, causes of action or proceedings arising from any breach of this Agreement by you.

- IN NO EVENT SHALL WILEY OR ITS LICENSORS BE LIABLE TO YOU OR ANY OTHER PARTY OR ANY OTHER PERSON OR ENTITY FOR ANY SPECIAL, CONSEQUENTIAL, INCIDENTAL, INDIRECT, EXEMPLARY OR PUNITIVE DAMAGES, HOWEVER CAUSED, ARISING OUT OF OR IN CONNECTION WITH THE DOWNLOADING, PROVISIONING, VIEWING OR USE OF THE MATERIALS REGARDLESS OF THE FORM OF ACTION, WHETHER FOR BREACH OF CONTRACT, BREACH OF WARRANTY, TORT, NEGLIGENCE, INFRINGEMENT OR OTHERWISE (INCLUDING, WITHOUT LIMITATION, DAMAGES BASED ON LOSS OF PROFITS, DATA, FILES, USE, BUSINESS OPPORTUNITY OR CLAIMS OF THIRD PARTIES), AND WHETHER OR NOT THE PARTY HAS BEEN ADVISED OF THE POSSIBILITY OF SUCH DAMAGES. THIS LIMITATION SHALL APPLY NOTWITHSTANDING ANY FAILURE OF ESSENTIAL PURPOSE OF ANY LIMITED REMEDY PROVIDED HEREIN.

- Should any provision of this Agreement be held by a court of competent jurisdiction to be illegal, invalid, or unenforceable, that provision shall be deemed amended to achieve as nearly as possible the same economic effect as the original provision, and the legality, validity and enforceability of the remaining provisions of this Agreement shall not be affected or impaired thereby.

- The failure of either party to enforce any term or condition of this Agreement shall not constitute a waiver of either party's right to enforce each and every term and condition of this Agreement. No breach under this agreement shall be deemed waived or excused by either party unless such waiver or consent is in writing signed by the party granting such waiver or consent. The waiver by or consent of a party to a breach of any provision of this Agreement shall not operate or be construed as a waiver of or consent to any other or subsequent breach by such other party.

- This Agreement may not be assigned (including by operation of law or otherwise) by you without WILEY's prior written consent.

- Any fee required for this permission shall be non-refundable after thirty (30) days from receipt by the CCC.

- These terms and conditions together with CCC's Billing and Payment terms and conditions (which are incorporated herein) form the entire agreement between you and WILEY concerning this licensing transaction and (in the absence of fraud) supersedes all prior agreements and representations of the parties, oral or written. This Agreement may not be amended except in writing signed by both parties. This Agreement shall be binding upon and inure to the benefit of the parties' successors, legal representatives, and authorized assigns.

- In the event of any conflict between your obligations established by these terms and conditions and those established by CCC's Billing and Payment terms and

conditions, these terms and conditions shall prevail.

- WILEY expressly reserves all rights not specifically granted in the combination of (i) the license details provided by you and accepted in the course of this licensing transaction, (ii) these terms and conditions and (iii) CCC's Billing and Payment terms and conditions.

- This Agreement will be void if the Type of Use, Format, Circulation, or Requestor Type was misrepresented during the licensing process.

- This Agreement shall be governed by and construed in accordance with the laws of the State of New York, USA, without regards to such state's conflict of law rules. Any legal action, suit or proceeding arising out of or relating to these Terms and Conditions or the breach thereof shall be instituted in a court of competent jurisdiction in New York County in the State of New York in the United States of America and each party hereby consents and submits to the personal jurisdiction of such court, waives any objection to venue in such court and consents to service of process by registered or certified mail, return receipt requested, at the last known address of such party.

WILEY OPEN ACCESS TERMS AND CONDITIONS

Wiley Publishes Open Access Articles in fully Open Access Journals and in Subscription journals offering Online Open. Although most of the fully Open Access journals publish open access articles under the terms of the Creative Commons Attribution (CC BY) License only, the subscription journals and a few of the Open Access Journals offer a choice of Creative Commons Licenses. The license type is clearly identified on the article.

The Creative Commons Attribution License

The Creative Commons Attribution License (CC-BY) allows users to copy, distribute and transmit an article, adapt the article and make commercial use of the article. The CC-BY license permits commercial and non-

Creative Commons Attribution Non-Commercial License

The Creative Commons Attribution Non-Commercial (CC-BY-NC)License permits use, distribution and reproduction in any medium, provided the original work is properly cited and is not used for commercial purposes.(see below)

Creative Commons Attribution-Non-Commercial-NoDerivs License

The Creative Commons Attribution Non-Commercial-NoDerivs License (CC-BY-NC-ND) permits use, distribution and reproduction in any medium, provided the original work is properly cited, is not used for commercial purposes and no modifications or adaptations are made. (see below)

Use by commercial "for-profit" organizations

Use of Wiley Open Access articles for commercial, promotional, or marketing purposes requires further explicit permission from Wiley and will be subject to a fee.

Further details can be found on Wiley Online Library
http://olabout.wiley.com/WileyCDA/Section/id-410895.html

Other Terms and Conditions:

v1.10 Last updated September 2015

Questions? customercare@copyright.com.

CCC
RightsLink

RK

High-Temperature Organic Reactions at Room Temperature Using Plasmon Excitation: Decomposition of Dicumyl Peroxide

ACS Publications
Most Trusted. Most Cited. Most Read.

Author: Chiara Fasciani, Carlos J. Bueno Alejo, Michel Grenier, et al

Publication: Organic Letters

Publisher: American Chemical Society

Date: Jan 1, 2011

Copyright © 2011, American Chemical Society

PERMISSION/LICENSE IS GRANTED FOR YOUR ORDER AT NO CHARGE

This type of permission/license, instead of the standard Terms and Conditions, is sent to you because no fee is being charged for your order. Please note the following:

- Permission is granted for your request in both print and electronic formats, and translations.
- If figures and/or tables were requested, they may be adapted or used in part.
- Please print this page for your records and send a copy of it to your publisher/graduate school.
- Appropriate credit for the requested material should be given as follows: "Reprinted (adapted) with permission from {COMPLETE REFERENCE CITATION}. Copyright {YEAR} American Chemical Society." Insert appropriate information in place of the capitalized words.
- One-time permission is granted only for the use specified in your RightsLink request. No additional uses are granted (such as derivative works or other editions). For any uses, please submit a new request.

If credit is given to another source for the material you requested from RightsLink, permission must be obtained from that source.

BACK　　　　　　　　　　　　　　　　　　　CLOSE WINDOW

Figure 1.12b, 4.1, 1.5a

Privacy - Terms

CCC
RightsLink

RK

Nanoreactors for Simultaneous Remote Thermal Activation and Optical Monitoring of Chemical Reactions

ACS Publications
Most Trusted. Most Cited. Most Read.

Author: Carmen Vázquez-Vázquez, Belén Vaz, Vincenzo Giannini, et al

Publication: Journal of the American Chemical Society

Publisher: American Chemical Society

Date: Sep 1, 2013

Copyright © 2013, American Chemical Society

BACK   CLOSE WINDOW

Figure 1.12c,4.2

CCC

RightsLink

Quantifying Photothermal and Hot Charge Carrier Effects in Plasmon-Driven Nanoparticle Syntheses

ACS Publications
Most Trusted. Most Cited. Most Read.

Author: Rifat Kamarudheen, Gabriel W. Castellanos, Leon P. J. Kamp, et al

Publication: ACS Nano

Publisher: American Chemical Society

Date: Aug 1, 2018

Copyright © 2018, American Chemical Society

BACK   CLOSE WINDOW

Figure 1.13

Privacy - Terms

CCC

RightsLink

Quantifying Surface Temperature of Thermoplasmonic Nanostructures

Author: Shu Hu, Bi-Ju Liu, Jia-Min Feng, et al

Publication: Journal of the American Chemical Society

Publisher: American Chemical Society

Date: Oct 1, 2018

Copyright © 2018, American Chemical Society

PERMISSION/LICENSE IS GRANTED FOR YOUR ORDER AT NO CHARGE

This type of permission/license, instead of the standard Terms and Conditions, is sent to you because no fee is being charged for your order. Please note the following:

- Permission is granted for your request in both print and electronic formats, and translations.
- If figures and/or tables were requested, they may be adapted or used in part.
- Please print this page for your records and send a copy of it to your publisher/graduate school.
- Appropriate credit for the requested material should be given as follows: "Reprinted (adapted) with permission from {COMPLETE REFERENCE CITATION}. Copyright {YEAR} American Chemical Society." Insert appropriate information in place of the capitalized words.
- One-time permission is granted only for the use specified in your RightsLink request. No additional uses are granted (such as derivative works or other editions). For any uses, please submit a new request.

If credit is given to another source for the material you requested from RightsLink, permission must be obtained from that source.

BACK　　　　　　　　　　　　　　　　　　　CLOSE WINDOW

Figure 1.15b

CCC
RightsLink

RK

Quantifying Surface Temperature of Thermoplasmonic Nanostructures

ACS Publications
Most Trusted. Most Cited. Most Read.

Author: Shu Hu, Bi-Ju Liu, Jia-Min Feng, et al

Publication: Journal of the American Chemical Society

Publisher: American Chemical Society

Date: Oct 1, 2018

Copyright © 2018, American Chemical Society

PERMISSION/LICENSE IS GRANTED FOR YOUR ORDER AT NO CHARGE

This type of permission/license, instead of the standard Terms and Conditions, is sent to you because no fee is being charged for your order. Please note the following:

- Permission is granted for your request in both print and electronic formats, and translations.
- If figures and/or tables were requested, they may be adapted or used in part.
- Please print this page for your records and send a copy of it to your publisher/graduate school.
- Appropriate credit for the requested material should be given as follows: "Reprinted (adapted) with permission from {COMPLETE REFERENCE CITATION}. Copyright {YEAR} American Chemical Society." Insert appropriate information in place of the capitalized words.
- One-time permission is granted only for the use specified in your RightsLink request. No additional uses are granted (such as derivative works or other editions). For any uses, please submit a new request.

If credit is given to another source for the material you requested from RightsLink, permission must be obtained from that source.

BACK   CLOSE WINDOW

Privacy - Terms

SPRINGER NATURE LICENSE
TERMS AND CONDITIONS

Jul 23, 2024

Figure 3.1, 3.2, 3.3

This Agreement between Radha Krishna Kashyap ("You") and Springer Nature ("Springer Nature") consists of your license details and the terms and conditions provided by Springer Nature and Copyright Clearance Center.

License Number	5835090446492
License date	Jul 23, 2024
Licensed Content Publisher	Springer Nature
Licensed Content Publication	Nature Reviews Chemistry
Licensed Content Title	Experimental characterization techniques for plasmon-assisted chemistry
Licensed Content Author	Emiliano Cortés et al
Licensed Content Date	Mar 28, 2022
Type of Use	Thesis/Dissertation
Requestor type	academic/university or research institute
Format	print and electronic
Portion	figures/tables/illustrations
Number of figures/tables/illustrations	1
Would you like a high resolution image with your order?	no

Will you be translating?	no
Circulation/distribution	200 - 499
Author of this Springer Nature content	no
Title of new work	Light-Powered Plasmonic Heaters: Extracting the Heat Out of Plasmons for Photothermal Applications
Institution name	Indian Institute of Science Education and Research (IISER), Pune
Expected presentation date	Sep 2024
Portions	Figure 6
The Requesting Person / Organization to Appear on the License	Radha Krishna Kashyap
Requestor Location	Mr. Radha Krishna Kashyap Chemistry Department, IISER Pune Dr. Homi Bhabha Road, Pashan Pune, 411008 India Attn: Mr. Radha Krishna Kashyap
Billing Type	Invoice
Billing Address	Mr. Radha Krishna Kashyap Chemistry Department, IISER Pune Dr. Homi Bhabha Road, Pashan Pune, India 411008 Attn: Mr. Radha Krishna Kashyap
Total	0.00 USD

Terms and Conditions

Springer Nature Customer Service Centre GmbH Terms and Conditions

The following terms and conditions ("Terms and Conditions") together with the terms specified in your [RightsLink] constitute the License ("License") between you as Licensee and Springer Nature Customer Service Centre GmbH as Licensor. By clicking 'accept' and completing the transaction for your use of the material ("Licensed Material"), you confirm your acceptance of and obligation to be bound by these Terms and Conditions.

1. Grant and Scope of License

1. 1. The Licensor grants you a personal, non-exclusive, non-transferable, non-sublicensable, revocable, world-wide License to reproduce, distribute, communicate to the public, make available, broadcast, electronically transmit or create derivative works using the Licensed Material for the purpose(s) specified in your RightsLink Licence Details only. Licenses are granted for the specific use requested in the order and for no other use, subject to these Terms and Conditions. You acknowledge and agree that the rights granted to you under this License do not include the right to modify, edit, translate, include in collective works, or create derivative works of the Licensed Material in whole or in part unless expressly stated in your RightsLink Licence Details. You may use the Licensed Material only as permitted under this Agreement and will not reproduce, distribute, display, perform, or otherwise use or exploit any Licensed Material in any way, in whole or in part, except as expressly permitted by this License.

1. 2. You may only use the Licensed Content in the manner and to the extent permitted by these Terms and Conditions, by your RightsLink Licence Details and by any applicable laws.

1. 3. A separate license may be required for any additional use of the Licensed Material, e.g. where a license has been purchased for print use only, separate permission must be obtained for electronic re-use. Similarly, a License is only valid in the language selected and does not apply for editions in other languages unless additional translation rights have been granted separately in the License.

1. 4. Any content within the Licensed Material that is owned by third parties is expressly excluded from the License.

1. 5. Rights for additional reuses such as custom editions, computer/mobile applications, film or TV reuses and/or any other derivative rights requests require additional permission and may be subject to an additional fee. Please apply to journalpermissions@springernature.com or bookpermissions@springernature.com for these rights.

2. Reservation of Rights

Licensor reserves all rights not expressly granted to you under this License. You acknowledge and agree that nothing in this License limits or restricts Licensor's rights in or use of the Licensed Material in any way. Neither this License, nor any act, omission, or statement by Licensor or you, conveys any ownership right to you in any Licensed Material, or to any element or portion thereof. As between Licensor and you, Licensor owns and retains all right, title, and interest in and to the Licensed Material subject to the license granted in Section 1.1. Your permission to use the Licensed Material is expressly conditioned on you not impairing Licensor's or the applicable copyright owner's rights in the Licensed Material in any way.

3. Restrictions on use

3. 1. Minor editing privileges are allowed for adaptations for stylistic purposes or formatting purposes provided such alterations do not alter the original meaning or

intention of the Licensed Material and the new figure(s) are still accurate and representative of the Licensed Material. Any other changes including but not limited to, cropping, adapting, and/or omitting material that affect the meaning, intention or moral rights of the author(s) are strictly prohibited.

3. 2. You must not use any Licensed Material as part of any design or trademark.

3. 3. Licensed Material may be used in Open Access Publications (OAP), but any such reuse must include a clear acknowledgment of this permission visible at the same time as the figures/tables/illustration or abstract and which must indicate that the Licensed Material is not part of the governing OA license but has been reproduced with permission. This may be indicated according to any standard referencing system but must include at a minimum 'Book/Journal title, Author, Journal Name (if applicable), Volume (if applicable), Publisher, Year, reproduced with permission from SNCSC'.

4. STM Permission Guidelines

4. 1. An alternative scope of license may apply to signatories of the STM Permissions Guidelines ("STM PG") as amended from time to time and made available at https://www.stm-assoc.org/intellectual-property/permissions/permissions-guidelines/.

4. 2. For content reuse requests that qualify for permission under the STM PG, and which may be updated from time to time, the STM PG supersede the terms and conditions contained in this License.

4. 3. If a License has been granted under the STM PG, but the STM PG no longer apply at the time of publication, further permission must be sought from the Rightsholder. Contact journalpermissions@springernature.com or bookpermissions@springernature.com for these rights.

5. Duration of License

5. 1. Unless otherwise indicated on your License, a License is valid from the date of purchase ("License Date") until the end of the relevant period in the below table:

Reuse in a medical communications project	Reuse up to distribution or time period indicated in License
Reuse in a dissertation/thesis	Lifetime of thesis
Reuse in a journal/magazine	Lifetime of journal/magazine
Reuse in a book/textbook	Lifetime of edition
Reuse on a website	1 year unless otherwise specified in the License
Reuse in a presentation/slide kit/poster	Lifetime of presentation/slide kit/poster. Note: publication whether electronic or in print of presentation/slide kit/poster may require further permission.
Reuse in conference proceedings	Lifetime of conference proceedings
Reuse in an annual report	Lifetime of annual report
Reuse in training/CME materials	Reuse up to distribution or time period indicated in License
Reuse in newsmedia	Lifetime of newsmedia

Reuse in coursepack/classroom materials	Reuse up to distribution and/or time period indicated in license

6. Acknowledgement

6. 1. The Licensor's permission must be acknowledged next to the Licensed Material in print. In electronic form, this acknowledgement must be visible at the same time as the figures/tables/illustrations or abstract and must be hyperlinked to the journal/book's homepage.

6. 2. Acknowledgement may be provided according to any standard referencing system and at a minimum should include "Author, Article/Book Title, Journal name/Book imprint, volume, page number, year, Springer Nature".

7. Reuse in a dissertation or thesis

7. 1. Where 'reuse in a dissertation/thesis' has been selected, the following terms apply: Print rights of the Version of Record are provided for; electronic rights for use only on institutional repository as defined by the Sherpa guideline (www.sherpa.ac.uk/romeo/) and only up to what is required by the awarding institution.

7. 2. For theses published under an ISBN or ISSN, separate permission is required. Please contact journalpermissions@springernature.com or bookpermissions@springernature.com for these rights.

7. 3. Authors must properly cite the published manuscript in their thesis according to current citation standards and include the following acknowledgement: '*Reproduced with permission from Springer Nature*'.

8. License Fee

You must pay the fee set forth in the License Agreement (the "License Fees"). All amounts payable by you under this License are exclusive of any sales, use, withholding, value added or similar taxes, government fees or levies or other assessments. Collection and/or remittance of such taxes to the relevant tax authority shall be the responsibility of the party who has the legal obligation to do so.

9. Warranty

9. 1. The Licensor warrants that it has, to the best of its knowledge, the rights to license reuse of the Licensed Material. **You are solely responsible for ensuring that the material you wish to license is original to the Licensor and does not carry the copyright of another entity or third party (as credited in the published version).** If the credit line on any part of the Licensed Material indicates that it was reprinted or adapted with permission from another source, then you should seek additional permission from that source to reuse the material.

9. 2. EXCEPT FOR THE EXPRESS WARRANTY STATED HEREIN AND TO THE EXTENT PERMITTED BY APPLICABLE LAW, LICENSOR PROVIDES THE LICENSED MATERIAL "AS IS" AND MAKES NO OTHER REPRESENTATION OR WARRANTY. LICENSOR EXPRESSLY DISCLAIMS ANY LIABILITY FOR ANY CLAIM ARISING FROM OR OUT OF THE CONTENT, INCLUDING BUT NOT LIMITED TO ANY ERRORS, INACCURACIES, OMISSIONS, OR DEFECTS CONTAINED THEREIN, AND ANY IMPLIED OR EXPRESS WARRANTY AS TO MERCHANTABILITY OR FITNESS FOR A PARTICULAR PURPOSE. IN NO EVENT SHALL LICENSOR

BE LIABLE TO YOU OR ANY OTHER PARTY OR ANY OTHER PERSON OR
FOR ANY SPECIAL, CONSEQUENTIAL, INCIDENTAL, INDIRECT,
PUNITIVE, OR EXEMPLARY DAMAGES, HOWEVER CAUSED, ARISING
OUT OF OR IN CONNECTION WITH THE DOWNLOADING, VIEWING OR
USE OF THE LICENSED MATERIAL REGARDLESS OF THE FORM OF
ACTION, WHETHER FOR BREACH OF CONTRACT, BREACH OF
WARRANTY, TORT, NEGLIGENCE, INFRINGEMENT OR OTHERWISE
(INCLUDING, WITHOUT LIMITATION, DAMAGES BASED ON LOSS OF
PROFITS, DATA, FILES, USE, BUSINESS OPPORTUNITY OR CLAIMS OF
THIRD PARTIES), AND WHETHER OR NOT THE PARTY HAS BEEN
ADVISED OF THE POSSIBILITY OF SUCH DAMAGES. THIS LIMITATION
APPLIES NOTWITHSTANDING ANY FAILURE OF ESSENTIAL PURPOSE
OF ANY LIMITED REMEDY PROVIDED HEREIN.

10. Termination and Cancellation

10. 1. The License and all rights granted hereunder will continue until the end of the
applicable period shown in Clause 5.1 above. Thereafter, this license will be
terminated and all rights granted hereunder will cease.

10. 2. Licensor reserves the right to terminate the License in the event that payment
is not received in full or if you breach the terms of this License.

11. General

11. 1. The License and the rights and obligations of the parties hereto shall be
construed, interpreted and determined in accordance with the laws of the Federal
Republic of Germany without reference to the stipulations of the CISG (United
Nations Convention on Contracts for the International Sale of Goods) or to
Germany´s choice-of-law principle.

11. 2. The parties acknowledge and agree that any controversies and disputes
arising out of this License shall be decided exclusively by the courts of or having
jurisdiction for Heidelberg, Germany, as far as legally permissible.

11. 3. This License is solely for Licensor's and Licensee's benefit. It is not for the
benefit of any other person or entity.

Questions? For questions on Copyright Clearance Center accounts or website issues
please contact springernaturesupport@copyright.com or +1-855-239-3415 (toll free in
the US) or +1-978-646-2777. For questions on Springer Nature licensing please visit
https://www.springernature.com/gp/partners/rights-permissions-third-party-distribution

Other Conditions:

Version 1.4 - Dec 2022

Questions? customercare@copyright.com.

CCC
RightsLink

RK ? 💬

Materials for Interfaces in Organic Solar Cells and Photodetectors

ACS Publications
Most Trusted. Most Cited. Most Read.

Author: Tianhao Li, Zixuan Chen, Yangyang Wang, et al

Publication: Applied Materials

Publisher: American Chemical Society

Date: Jan 1, 2020

Copyright © 2020, American Chemical Society

PERMISSION/LICENSE IS GRANTED FOR YOUR ORDER AT NO CHARGE

This type of permission/license, instead of the standard Terms and Conditions, is sent to you because no fee is being charged for your order. Please note the following:

- Permission is granted for your request in both print and electronic formats, and translations.
- If figures and/or tables were requested, they may be adapted or used in part.
- Please print this page for your records and send a copy of it to your publisher/graduate school.
- Appropriate credit for the requested material should be given as follows: "Reprinted (adapted) with permission from {COMPLETE REFERENCE CITATION}. Copyright {YEAR} American Chemical Society." Insert appropriate information in place of the capitalized words.
- One-time permission is granted only for the use specified in your RightsLink request. No additional uses are granted (such as derivative works or other editions). For any uses, please submit a new request.

If credit is given to another source for the material you requested from RightsLink, permission must be obtained from that source.

BACK   CLOSE WINDOW

Figure 5.1a

JOHN WILEY AND SONS LICENSE
TERMS AND CONDITIONS

Jul 24, 2024   # Table 5.1

This Agreement between Radha Krishna Kashyap ("You") and John Wiley and Sons
("John Wiley and Sons") consists of your license details and the terms and conditions
provided by John Wiley and Sons and Copyright Clearance Center.

License Number	5835381476567
License date	Jul 24, 2024
Licensed Content Publisher	John Wiley and Sons
Licensed Content Publication	Advanced Energy Materials
Licensed Content Title	Solar Thermoelectricity for Power Generation
Licensed Content Author	Hyo Jae Yoon, Xin He, Sahar Ayachi
Licensed Content Date	Jun 13, 2023
Licensed Content Volume	13
Licensed Content Issue	28
Licensed Content Pages	20
Type of use	Dissertation/Thesis
Requestor type	University/Academic
Format	Print and electronic
Portion	Figure/table

Number of figures/tables	1
Will you be translating?	No
Title of new work	Light-Powered Plasmonic Heaters: Extracting the Heat Out of Plasmons for Photothermal Applications
Institution name	Indian Institute of Science Education and Research (IISER), Pune
Expected presentation date	Sep 2024
Portions	Table 6
The Requesting Person / Organization to Appear on the License	Radha Krishna Kashyap
Requestor Location	Mr. Radha Krishna Kashyap Chemistry Department, IISER Pune Dr. Homi Bhabha Road, Pashan Pune, 411008 India Attn: Mr. Radha Krishna Kashyap
Publisher Tax ID	EU826007151
Total	0.00 USD

Terms and Conditions

TERMS AND CONDITIONS

Terms and Conditions

- The materials you have requested permission to reproduce or reuse (the "Wiley Materials") are protected by copyright.

- You are hereby granted a personal, non-exclusive, non-sub licensable (on a stand-alone basis), non-transferable, worldwide, limited license <u>to reproduce the Wiley Materials for the purpose specified in the licensing process.</u> This license, **and any CONTENT (PDF or image file) purchased as part of your order,** is for a one-time use only and limited to any maximum distribution number specified in the license. The first instance of republication or reuse granted by this license must be completed within two years of the date of the grant of this license (although copies prepared before the end date may be distributed thereafter). The Wiley Materials shall not be used in any other manner or for any other purpose, beyond what is granted in the license. Permission is granted subject to an appropriate acknowledgement given to the author, title of the material/book/journal and the publisher. You shall also duplicate the copyright notice that appears in the Wiley publication in your use of the Wiley Material. Permission is also granted on the understanding that nowhere in the text is a previously published source acknowledged for all or part of this Wiley Material. Any third party content is expressly excluded from this permission.

- With respect to the Wiley Materials, all rights are reserved. Except as expressly granted by the terms of the license, no part of the Wiley Materials may be copied, modified, adapted (except for minor reformatting required by the new Publication), translated, reproduced, transferred or distributed, in any form or by any means, and no derivative works may be made based on the Wiley Materials without the prior permission of the respective copyright owner.**For STM Signatory Publishers clearing permission under the terms of the [STM Permissions Guidelines](#) only, the terms of the license are extended to include subsequent editions and for editions in other languages, provided such editions are for the work as a whole in situ and does not involve the separate exploitation of the permitted figures or extracts,** You may not alter, remove or suppress in any manner any copyright, trademark or other notices displayed by the Wiley Materials. You may not license, rent, sell, loan, lease, pledge, offer as security, transfer or assign the Wiley Materials on a stand-alone basis, or any of the rights granted to you hereunder to any other person.

- The Wiley Materials and all of the intellectual property rights therein shall at all times remain the exclusive property of John Wiley & Sons Inc, the Wiley Companies, or their respective licensors, and your interest therein is only that of having possession of and the right to reproduce the Wiley Materials pursuant to Section 2 herein during the continuance of this Agreement. You agree that you own no right, title or interest in or to the Wiley Materials or any of the intellectual property rights therein. You shall have no rights hereunder other than the license as provided for above in Section 2. No right, license or interest to any trademark, trade name, service mark or other branding ("Marks") of WILEY or its licensors is granted hereunder, and you agree that you shall not assert any such right, license or interest with respect thereto

- NEITHER WILEY NOR ITS LICENSORS MAKES ANY WARRANTY OR REPRESENTATION OF ANY KIND TO YOU OR ANY THIRD PARTY, EXPRESS, IMPLIED OR STATUTORY, WITH RESPECT TO THE MATERIALS OR THE ACCURACY OF ANY INFORMATION CONTAINED IN THE MATERIALS, INCLUDING, WITHOUT LIMITATION, ANY IMPLIED WARRANTY OF MERCHANTABILITY, ACCURACY, SATISFACTORY QUALITY, FITNESS FOR A PARTICULAR PURPOSE, USABILITY, INTEGRATION OR NON-INFRINGEMENT AND ALL SUCH WARRANTIES ARE HEREBY EXCLUDED BY WILEY AND ITS LICENSORS AND WAIVED

BY YOU.

- WILEY shall have the right to terminate this Agreement immediately upon breach of this Agreement by you.

- You shall indemnify, defend and hold harmless WILEY, its Licensors and their respective directors, officers, agents and employees, from and against any actual or threatened claims, demands, causes of action or proceedings arising from any breach of this Agreement by you.

- IN NO EVENT SHALL WILEY OR ITS LICENSORS BE LIABLE TO YOU OR ANY OTHER PARTY OR ANY OTHER PERSON OR ENTITY FOR ANY SPECIAL, CONSEQUENTIAL, INCIDENTAL, INDIRECT, EXEMPLARY OR PUNITIVE DAMAGES, HOWEVER CAUSED, ARISING OUT OF OR IN CONNECTION WITH THE DOWNLOADING, PROVISIONING, VIEWING OR USE OF THE MATERIALS REGARDLESS OF THE FORM OF ACTION, WHETHER FOR BREACH OF CONTRACT, BREACH OF WARRANTY, TORT, NEGLIGENCE, INFRINGEMENT OR OTHERWISE (INCLUDING, WITHOUT LIMITATION, DAMAGES BASED ON LOSS OF PROFITS, DATA, FILES, USE, BUSINESS OPPORTUNITY OR CLAIMS OF THIRD PARTIES), AND WHETHER OR NOT THE PARTY HAS BEEN ADVISED OF THE POSSIBILITY OF SUCH DAMAGES. THIS LIMITATION SHALL APPLY NOTWITHSTANDING ANY FAILURE OF ESSENTIAL PURPOSE OF ANY LIMITED REMEDY PROVIDED HEREIN.

- Should any provision of this Agreement be held by a court of competent jurisdiction to be illegal, invalid, or unenforceable, that provision shall be deemed amended to achieve as nearly as possible the same economic effect as the original provision, and the legality, validity and enforceability of the remaining provisions of this Agreement shall not be affected or impaired thereby.

- The failure of either party to enforce any term or condition of this Agreement shall not constitute a waiver of either party's right to enforce each and every term and condition of this Agreement. No breach under this agreement shall be deemed waived or excused by either party unless such waiver or consent is in writing signed by the party granting such waiver or consent. The waiver by or consent of a party to a breach of any provision of this Agreement shall not operate or be construed as a waiver of or consent to any other or subsequent breach by such other party.

- This Agreement may not be assigned (including by operation of law or otherwise) by you without WILEY's prior written consent.

- Any fee required for this permission shall be non-refundable after thirty (30) days from receipt by the CCC.

- These terms and conditions together with CCC's Billing and Payment terms and conditions (which are incorporated herein) form the entire agreement between you and WILEY concerning this licensing transaction and (in the absence of fraud) supersedes all prior agreements and representations of the parties, oral or written. This Agreement may not be amended except in writing signed by both parties. This Agreement shall be binding upon and inure to the benefit of the parties' successors, legal representatives, and authorized assigns.

- In the event of any conflict between your obligations established by these terms and conditions and those established by CCC's Billing and Payment terms and conditions, these terms and conditions shall prevail.

- WILEY expressly reserves all rights not specifically granted in the combination of (i) the license details provided by you and accepted in the course of this licensing transaction, (ii) these terms and conditions and (iii) CCC's Billing and Payment terms and conditions.

- This Agreement will be void if the Type of Use, Format, Circulation, or Requestor Type was misrepresented during the licensing process.

- This Agreement shall be governed by and construed in accordance with the laws of the State of New York, USA, without regards to such state's conflict of law rules. Any legal action, suit or proceeding arising out of or relating to these Terms and Conditions or the breach thereof shall be instituted in a court of competent jurisdiction in New York County in the State of New York in the United States of America and each party hereby consents and submits to the personal jurisdiction of such court, waives any objection to venue in such court and consents to service of process by registered or certified mail, return receipt requested, at the last known address of such party.

WILEY OPEN ACCESS TERMS AND CONDITIONS

Wiley Publishes Open Access Articles in fully Open Access Journals and in Subscription journals offering Online Open. Although most of the fully Open Access journals publish open access articles under the terms of the Creative Commons Attribution (CC BY) License only, the subscription journals and a few of the Open Access Journals offer a choice of Creative Commons Licenses. The license type is clearly identified on the article.

The Creative Commons Attribution License

The Creative Commons Attribution License (CC-BY) allows users to copy, distribute and transmit an article, adapt the article and make commercial use of the article. The CC-BY license permits commercial and non-

Creative Commons Attribution Non-Commercial License

The Creative Commons Attribution Non-Commercial (CC-BY-NC)License permits use, distribution and reproduction in any medium, provided the original work is properly cited and is not used for commercial purposes.(see below)

Creative Commons Attribution-Non-Commercial-NoDerivs License

The Creative Commons Attribution Non-Commercial-NoDerivs License (CC-BY-NC-ND) permits use, distribution and reproduction in any medium, provided the original work is properly cited, is not used for commercial purposes and no modifications or adaptations are made. (see below)

Use by commercial "for-profit" organizations

Use of Wiley Open Access articles for commercial, promotional, or marketing purposes requires further explicit permission from Wiley and will be subject to a fee.

Further details can be found on Wiley Online Library
http://olabout.wiley.com/WileyCDA/Section/id-410895.html

Other Terms and Conditions:

v1.10 Last updated September 2015

Questions? customercare@copyright.com.

AIP PUBLISHING LICENSE
TERMS AND CONDITIONS

Jul 23, 2024

Figure 5.3a

This Agreement between Radha Krishna Kashyap ("You") and AIP Publishing ("AIP Publishing") consists of your license details and the terms and conditions provided by AIP Publishing and Copyright Clearance Center.

License Number	5835071391214
License date	Jul 23, 2024
Licensed Content Publisher	AIP Publishing
Licensed Content Publication	Journal of Applied Physics
Licensed Content Title	Modeling of concentrating solar thermoelectric generators
Licensed Content Author	McEnaney, Kenneth; Kraemer, Daniel
Licensed Content Date	Oct 3, 2011
Licensed Content Volume	110
Licensed Content Issue	7
Type of Use	Thesis/Dissertation
Requestor type	Student
Format	Print and electronic
Portion	Figure/Table
Number of figures/tables	1

Will you be translating?	No
Title of new work	Light-Powered Plasmonic Heaters: Extracting the Heat Out of Plasmons for Photothermal Applications
Institution name	Indian Institute of Science Education and Research (IISER), Pune
Expected presentation date	Sep 2024
Portions	Figure 1
The Requesting Person / Organization to Appear on the License	Radha Krishna Kashyap
Requestor Location	Mr. Radha Krishna Kashyap Chemistry Department, IISER Pune Dr. Homi Bhabha Road, Pashan Pune, 411008 India Attn: Mr. Radha Krishna Kashyap
Billing Type	Invoice
Billing Address	Mr. Radha Krishna Kashyap Chemistry Department, IISER Pune Dr. Homi Bhabha Road, Pashan Pune, India 411008 Attn: Mr. Radha Krishna Kashyap
Total	0.00 USD

Terms and Conditions

AIP Publishing -- Terms and Conditions: Permissions Uses

AIP Publishing hereby grants to you the non-exclusive right and license to use and/or distribute the Material according to the use specified in your order, on a one-time basis, for the specified term, with a maximum distribution equal to the number that you have ordered. Any links or other content accompanying the Material are not the subject of this license.

1. You agree to include the following copyright and permission notice with the reproduction of the Material:"Reprinted from [FULL CITATION], with the permission of AIP Publishing." For an article, the credit line and permission notice must be printed on the first page of the article or book chapter. For photographs, covers, or tables, the notice may appear with the Material, in a footnote, or in the reference list.

2. If you have licensed reuse of a figure, photograph, cover, or table, it is your responsibility to ensure that the material is original to AIP Publishing and does not contain the copyright of another entity, and that the copyright notice of the figure, photograph, cover, or table does not indicate that it was reprinted by AIP Publishing, with permission, from another source. Under no circumstances does AIP Publishing purport or intend to grant permission to reuse material to which it does not hold appropriate rights.

   You may not alter or modify the Material in any manner. You may translate the Material into another language only if you have licensed translation rights. You may not use the Material for promotional purposes.

3. The foregoing license shall not take effect unless and until AIP Publishing or its agent, Copyright Clearance Center, receives the Payment in accordance with Copyright Clearance Center Billing and Payment Terms and Conditions, which are incorporated herein by reference.

4. AIP Publishing or Copyright Clearance Center may, within two business days of granting this license, revoke the license for any reason whatsoever, with a full refund payable to you. Should you violate the terms of this license at any time, AIP Publishing, or Copyright Clearance Center may revoke the license with no refund to you. Notice of such revocation will be made using the contact information provided by you. Failure to receive such notice will not nullify the revocation.

5. AIP Publishing makes no representations or warranties with respect to the Material. You agree to indemnify and hold harmless AIP Publishing, and their officers, directors, employees or agents from and against any and all claims arising out of your use of the Material other than as specifically authorized herein.

6. The permission granted herein is personal to you and is not transferable or assignable without the prior written permission of AIP Publishing. This license may not be amended except in a writing signed by the party to be charged.

7. If purchase orders, acknowledgments or check endorsements are issued on any forms containing terms and conditions which are inconsistent with these provisions, such inconsistent terms and conditions shall be of no force and effect. This document, including the CCC Billing and Payment Terms and Conditions, shall be the entire agreement between the parties relating to the subject matter hereof.

This Agreement shall be governed by and construed in accordance with the laws of the State of New York. Both parties hereby submit to the jurisdiction of the courts of New York County for purposes of resolving any disputes that may arise hereunder.

V1.2

Questions? customercare@copyright.com.

CCC Marketplace

Order Confirmation   Figure 5.3b

Thank you, your order has been placed. An email confirmation has been sent to you. Your order license details and printable licenses will be available within 24 hours. Please access Manage Account for final order details.

This is not an invoice. Please go to manage account to access your order history and invoices.

CUSTOMER INFORMATION

Payment by invoice: You can cancel your order until the invoice is generated by contacting customer service.

📖 Billing Address

Mr. Radha Krishna Kashyap
Chemistry Department, IISER Pune
Dr. Homi Bhabha Road, Pashan
Pune, 411008
India

+91 9717078301
krishna.kashyap@students.iiserpune.ac.in

📍 Customer Location

Mr. Radha Krishna Kashyap
Chemistry Department, IISER Pune
Dr. Homi Bhabha Road, Pashan
Pune, 411008
India

📄 PO Number (optional)

N/A

💳 Payment options

Invoice

PENDING ORDER CONFIRMATION

Confirmation Number: Permission granted

Order Date: 24-Jul-2024

1. Energy & environmental science   0.00 USD

Article: Concentrated solar thermoelectric generators

Order License ID ISSN Type of Use	Permission granted 1754-5706 Republish in a thesis/dissertation	Publisher Portion	RSC Publishing Chart/graph/table/figure

LICENSED CONTENT

Publication Title	Energy & environmental science	**Rightsholder**	Royal Society of Chemistry
Article Title	Concentrated solar thermoelectric generators	**Publication Type**	e-Journal
		Start Page	9055
Author / Editor	Royal Society of Chemistry (Great Britain)	**Issue**	10
		Volume	5
Date	01/01/2008	**URL**	http://www.rsc.org/Publishing/Journals/EE/Index.asp
Language	English		
Country	United Kingdom of Great Britain and Northern Ireland		

REQUEST DETAILS

Portion Type	Chart/graph/table/figure	**Distribution**	Worldwide
Number of Charts / Graphs / Tables / Figures Requested	1	**Translation**	Original language of publication

Format (select all that apply)	Print, Electronic	Copies for the Disabled?	No
Who Will Republish the Content?	Not-for-profit entity	Minor Editing Privileges?	No
		Incidental Promotional Use?	No
Duration of Use	Life of current edition	Currency	USD
Lifetime Unit Quantity	Up to 499		
Rights Requested	Main product		

NEW WORK DETAILS

Title	Light-Powered Plasmonic Heaters: Extracting the Heat Out of Plasmons for Photothermal Applications	Institution Name	Indian Institute of Science Education and Research, Pune
		Expected Presentation Date	2024-09-02
Instructor Name	Radha Krishna Kashyap		

ADDITIONAL DETAILS

Order Reference Number	N/A	The Requesting Person / Organization to Appear on the License	Radha Krishna Kashyap

REQUESTED CONTENT DETAILS

Title, Description or Numeric Reference of the Portion(s)	Figure 2a	Title of the Article / Chapter the Portion Is From	Concentrated solar thermoelectric generators
Editor of Portion(s)	Baranowski, Lauryn L.; Snyder, G. Jeffrey; Toberer, Eric S.	Author of Portion(s)	Baranowski, Lauryn L.; Snyder, G. Jeffrey; Toberer, Eric S.
Volume / Edition	5	Issue, if Republishing an Article From a Serial	10
Page or Page Range of Portion	9055	Publication Date of Portion	2012-09-20

Total Items: 1

Total Due: 0.00 USD

SPRINGER NATURE LICENSE
TERMS AND CONDITIONS

Jul 23, 2024

Figure 5.3c

This Agreement between Radha Krishna Kashyap ("You") and Springer Nature ("Springer Nature") consists of your license details and the terms and conditions provided by Springer Nature and Copyright Clearance Center.

License Number	5835081437339
License date	Jul 23, 2024
Licensed Content Publisher	Springer Nature
Licensed Content Publication	Journal of Electronic Materials
Licensed Content Title	High-Temperature High-Efficiency Solar Thermoelectric Generators
Licensed Content Author	Lauryn L. Baranowski et al
Licensed Content Date	Mar 1, 2014
Type of Use	Thesis/Dissertation
Requestor type	academic/university or research institute
Format	print and electronic
Portion	figures/tables/illustrations
Number of figures/tables/illustrations	1
Will you be translating?	no
Circulation/distribution	200 - 499

Author of this Springer Nature content	no
Title of new work	Light-Powered Plasmonic Heaters: Extracting the Heat Out of Plasmons for Photothermal Applications
Institution name	Indian Institute of Science Education and Research (IISER), Pune
Expected presentation date	Sep 2024
Portions	Figure 2
The Requesting Person / Organization to Appear on the License	Radha Krishna Kashyap
Requestor Location	Mr. Radha Krishna Kashyap Chemistry Department, IISER Pune Dr. Homi Bhabha Road, Pashan Pune, 411008 India Attn: Mr. Radha Krishna Kashyap
Billing Type	Invoice
Billing Address	Mr. Radha Krishna Kashyap Chemistry Department, IISER Pune Dr. Homi Bhabha Road, Pashan Pune, India 411008 Attn: Mr. Radha Krishna Kashyap
Total	0.00 USD

Terms and Conditions

Springer Nature Customer Service Centre GmbH Terms and Conditions

The following terms and conditions ("Terms and Conditions") together with the terms specified in your [RightsLink] constitute the License ("License") between you as Licensee and Springer Nature Customer Service Centre GmbH as Licensor. By clicking 'accept' and completing the transaction for your use of the material ("Licensed Material"), you confirm your acceptance of and obligation to be bound by these Terms and Conditions.

1. Grant and Scope of License

1. 1. The Licensor grants you a personal, non-exclusive, non-transferable, non-sublicensable, revocable, world-wide License to reproduce, distribute, communicate to the public, make available, broadcast, electronically transmit or create derivative works using the Licensed Material for the purpose(s) specified in your RightsLink Licence Details only. Licenses are granted for the specific use requested in the order and for no other use, subject to these Terms and Conditions. You acknowledge and agree that the rights granted to you under this License do not include the right to modify, edit, translate, include in collective works, or create derivative works of the Licensed Material in whole or in part unless expressly stated in your RightsLink Licence Details. You may use the Licensed Material only as permitted under this Agreement and will not reproduce, distribute, display, perform, or otherwise use or exploit any Licensed Material in any way, in whole or in part, except as expressly permitted by this License.

1. 2. You may only use the Licensed Content in the manner and to the extent permitted by these Terms and Conditions, by your RightsLink Licence Details and by any applicable laws.

1. 3. A separate license may be required for any additional use of the Licensed Material, e.g. where a license has been purchased for print use only, separate permission must be obtained for electronic re-use. Similarly, a License is only valid in the language selected and does not apply for editions in other languages unless additional translation rights have been granted separately in the License.

1. 4. Any content within the Licensed Material that is owned by third parties is expressly excluded from the License.

1. 5. Rights for additional reuses such as custom editions, computer/mobile applications, film or TV reuses and/or any other derivative rights requests require additional permission and may be subject to an additional fee. Please apply to journalpermissions@springernature.com or bookpermissions@springernature.com for these rights.

2. Reservation of Rights

Licensor reserves all rights not expressly granted to you under this License. You acknowledge and agree that nothing in this License limits or restricts Licensor's rights in or use of the Licensed Material in any way. Neither this License, nor any act, omission, or statement by Licensor or you, conveys any ownership right to you in any Licensed Material, or to any element or portion thereof. As between Licensor and you, Licensor owns and retains all right, title, and interest in and to the Licensed Material subject to the license granted in Section 1.1. Your permission to use the Licensed Material is expressly conditioned on you not impairing Licensor's or the applicable copyright owner's rights in the Licensed Material in any way.

3. Restrictions on use

3. 1. Minor editing privileges are allowed for adaptations for stylistic purposes or formatting purposes provided such alterations do not alter the original meaning or intention of the Licensed Material and the new figure(s) are still accurate and representative of the Licensed Material. Any other changes including but not limited to, cropping, adapting, and/or omitting material that affect the meaning, intention or moral rights of the author(s) are strictly prohibited.

3. 2. You must not use any Licensed Material as part of any design or trademark.

3. 3. Licensed Material may be used in Open Access Publications (OAP), but any such reuse must include a clear acknowledgment of this permission visible at the same time as the figures/tables/illustration or abstract and which must indicate that the Licensed Material is not part of the governing OA license but has been reproduced with permission. This may be indicated according to any standard referencing system but must include at a minimum 'Book/Journal title, Author, Journal Name (if applicable), Volume (if applicable), Publisher, Year, reproduced with permission from SNCSC'.

4. STM Permission Guidelines

4. 1. An alternative scope of license may apply to signatories of the STM Permissions Guidelines ("STM PG") as amended from time to time and made available at https://www.stm-assoc.org/intellectual-property/permissions/permissions-guidelines/.

4. 2. For content reuse requests that qualify for permission under the STM PG, and which may be updated from time to time, the STM PG supersede the terms and conditions contained in this License.

4. 3. If a License has been granted under the STM PG, but the STM PG no longer apply at the time of publication, further permission must be sought from the Rightsholder. Contact journalpermissions@springernature.com or bookpermissions@springernature.com for these rights.

5. Duration of License

5. 1. Unless otherwise indicated on your License, a License is valid from the date of purchase ("License Date") until the end of the relevant period in the below table:

Reuse in a medical communications project	Reuse up to distribution or time period indicated in License
Reuse in a dissertation/thesis	Lifetime of thesis
Reuse in a journal/magazine	Lifetime of journal/magazine
Reuse in a book/textbook	Lifetime of edition
Reuse on a website	1 year unless otherwise specified in the License
Reuse in a presentation/slide kit/poster	Lifetime of presentation/slide kit/poster. Note: publication whether electronic or in print of presentation/slide kit/poster may require further permission.
Reuse in conference proceedings	Lifetime of conference proceedings
Reuse in an annual report	Lifetime of annual report
Reuse in training/CME materials	Reuse up to distribution or time period indicated in License
Reuse in newsmedia	Lifetime of newsmedia
Reuse in coursepack/classroom materials	Reuse up to distribution and/or time period indicated in license

6. Acknowledgement

6. 1. The Licensor's permission must be acknowledged next to the Licensed Material in print. In electronic form, this acknowledgement must be visible at the

same time as the figures/tables/illustrations or abstract and must be hyperlinked to the journal/book's homepage.

6. 2. Acknowledgement may be provided according to any standard referencing system and at a minimum should include "Author, Article/Book Title, Journal name/Book imprint, volume, page number, year, Springer Nature".

7. Reuse in a dissertation or thesis

7. 1. Where 'reuse in a dissertation/thesis' has been selected, the following terms apply: Print rights of the Version of Record are provided for; electronic rights for use only on institutional repository as defined by the Sherpa guideline (www.sherpa.ac.uk/romeo/) and only up to what is required by the awarding institution.

7. 2. For theses published under an ISBN or ISSN, separate permission is required. Please contact journalpermissions@springernature.com or bookpermissions@springernature.com for these rights.

7. 3. Authors must properly cite the published manuscript in their thesis according to current citation standards and include the following acknowledgement: '*Reproduced with permission from Springer Nature*'.

8. License Fee

You must pay the fee set forth in the License Agreement (the "License Fees"). All amounts payable by you under this License are exclusive of any sales, use, withholding, value added or similar taxes, government fees or levies or other assessments. Collection and/or remittance of such taxes to the relevant tax authority shall be the responsibility of the party who has the legal obligation to do so.

9. Warranty

9. 1. The Licensor warrants that it has, to the best of its knowledge, the rights to license reuse of the Licensed Material. **You are solely responsible for ensuring that the material you wish to license is original to the Licensor and does not carry the copyright of another entity or third party (as credited in the published version).** If the credit line on any part of the Licensed Material indicates that it was reprinted or adapted with permission from another source, then you should seek additional permission from that source to reuse the material.

9. 2. EXCEPT FOR THE EXPRESS WARRANTY STATED HEREIN AND TO THE EXTENT PERMITTED BY APPLICABLE LAW, LICENSOR PROVIDES THE LICENSED MATERIAL "AS IS" AND MAKES NO OTHER REPRESENTATION OR WARRANTY. LICENSOR EXPRESSLY DISCLAIMS ANY LIABILITY FOR ANY CLAIM ARISING FROM OR OUT OF THE CONTENT, INCLUDING BUT NOT LIMITED TO ANY ERRORS, INACCURACIES, OMISSIONS, OR DEFECTS CONTAINED THEREIN, AND ANY IMPLIED OR EXPRESS WARRANTY AS TO MERCHANTABILITY OR FITNESS FOR A PARTICULAR PURPOSE. IN NO EVENT SHALL LICENSOR BE LIABLE TO YOU OR ANY OTHER PARTY OR ANY OTHER PERSON OR FOR ANY SPECIAL, CONSEQUENTIAL, INCIDENTAL, INDIRECT, PUNITIVE, OR EXEMPLARY DAMAGES, HOWEVER CAUSED, ARISING OUT OF OR IN CONNECTION WITH THE DOWNLOADING, VIEWING OR USE OF THE LICENSED MATERIAL REGARDLESS OF THE FORM OF ACTION, WHETHER FOR BREACH OF CONTRACT, BREACH OF WARRANTY, TORT, NEGLIGENCE, INFRINGEMENT OR OTHERWISE (INCLUDING, WITHOUT LIMITATION, DAMAGES BASED ON LOSS OF

PROFITS, DATA, FILES, USE, BUSINESS OPPORTUNITY OR CLAIMS OF THIRD PARTIES), AND WHETHER OR NOT THE PARTY HAS BEEN ADVISED OF THE POSSIBILITY OF SUCH DAMAGES. THIS LIMITATION APPLIES NOTWITHSTANDING ANY FAILURE OF ESSENTIAL PURPOSE OF ANY LIMITED REMEDY PROVIDED HEREIN.

10. Termination and Cancellation

10. 1. The License and all rights granted hereunder will continue until the end of the applicable period shown in Clause 5.1 above. Thereafter, this license will be terminated and all rights granted hereunder will cease.

10. 2. Licensor reserves the right to terminate the License in the event that payment is not received in full or if you breach the terms of this License.

11. General

11. 1. The License and the rights and obligations of the parties hereto shall be construed, interpreted and determined in accordance with the laws of the Federal Republic of Germany without reference to the stipulations of the CISG (United Nations Convention on Contracts for the International Sale of Goods) or to Germany´s choice-of-law principle.

11. 2. The parties acknowledge and agree that any controversies and disputes arising out of this License shall be decided exclusively by the courts of or having jurisdiction for Heidelberg, Germany, as far as legally permissible.

11. 3. This License is solely for Licensor's and Licensee's benefit. It is not for the benefit of any other person or entity.

Questions? For questions on Copyright Clearance Center accounts or website issues please contact springernaturesupport@copyright.com or +1-855-239-3415 (toll free in the US) or +1-978-646-2777. For questions on Springer Nature licensing please visit https://www.springernature.com/gp/partners/rights-permissions-third-party-distribution

Other Conditions:

Version 1.4 - Dec 2022

Questions? customercare@copyright.com.

ELSEVIER LICENSE
TERMS AND CONDITIONS

Jul 23, 2024

Figure 5.3d

This Agreement between Radha Krishna Kashyap ("You") and Elsevier ("Elsevier") consists of your license details and the terms and conditions provided by Elsevier and Copyright Clearance Center.

License Number	5835080957777
License date	Jul 23, 2024
Licensed Content Publisher	Elsevier
Licensed Content Publication	Energy Procedia
Licensed Content Title	A High-temperature, High-efficiency Solar Thermoelectric Generator Prototype
Licensed Content Author	M.L. Olsen,E.L. Warren,P.A. Parilla,E.S. Toberer,C.E. Kennedy,G.J. Snyder,S.A. Firdosy,B. Nesmith,A. Zakutayev,A. Goodrich,C.S. Turchi,J. Netter,M.H. Gray,P.F. Ndione,R. Tirawat,L.L. Baranowski,A. Gray,D.S. Ginley
Licensed Content Date	Jan 1, 2014
Licensed Content Volume	49
Licensed Content Issue	n/a
Licensed Content Pages	10
Start Page	1460
End Page	1469

Type of Use	reuse in a thesis/dissertation
Portion	figures/tables/illustrations
Number of figures/tables/illustrations	1
Format	both print and electronic
Are you the author of this Elsevier article?	No
Will you be translating?	No
Title of new work	Light-Powered Plasmonic Heaters: Extracting the Heat Out of Plasmons for Photothermal Applications
Institution name	Indian Institute of Science Education and Research (IISER), Pune
Expected presentation date	Sep 2024
Portions	Figure 1
The Requesting Person / Organization to Appear on the License	Radha Krishna Kashyap
Requestor Location	Mr. Radha Krishna Kashyap Chemistry Department, IISER Pune Dr. Homi Bhabha Road, Pashan Pune, 411008 India Attn: Mr. Radha Krishna Kashyap
Publisher Tax ID	GB 494 6272 12
Total	0.00 USD

Terms and Conditions

INTRODUCTION

1. The publisher for this copyrighted material is Elsevier. By clicking "accept" in connection with completing this licensing transaction, you agree that the following terms and conditions apply to this transaction (along with the Billing and Payment terms and conditions established by Copyright Clearance Center, Inc. ("CCC"), at the time that you opened your RightsLink account and that are available at any time at https://myaccount.copyright.com).

GENERAL TERMS

2. Elsevier hereby grants you permission to reproduce the aforementioned material subject to the terms and conditions indicated.

3. Acknowledgement: If any part of the material to be used (for example, figures) has appeared in our publication with credit or acknowledgement to another source, permission must also be sought from that source. If such permission is not obtained then that material may not be included in your publication/copies. Suitable acknowledgement to the source must be made, either as a footnote or in a reference list at the end of your publication, as follows:

"Reprinted from Publication title, Vol /edition number, Author(s), Title of article / title of chapter, Pages No., Copyright (Year), with permission from Elsevier [OR APPLICABLE SOCIETY COPYRIGHT OWNER]." Also Lancet special credit - "Reprinted from The Lancet, Vol. number, Author(s), Title of article, Pages No., Copyright (Year), with permission from Elsevier."

4. Reproduction of this material is confined to the purpose and/or media for which permission is hereby given. The material may not be reproduced or used in any other way, including use in combination with an artificial intelligence tool (including to train an algorithm, test, process, analyse, generate output and/or develop any form of artificial intelligence tool), or to create any derivative work and/or service (including resulting from the use of artificial intelligence tools).

5. Altering/Modifying Material: Not Permitted. However figures and illustrations may be altered/adapted minimally to serve your work. Any other abbreviations, additions, deletions and/or any other alterations shall be made only with prior written authorization of Elsevier Ltd. (Please contact Elsevier's permissions helpdesk here). No modifications can be made to any Lancet figures/tables and they must be reproduced in full.

6. If the permission fee for the requested use of our material is waived in this instance, please be advised that your future requests for Elsevier materials may attract a fee.

7. Reservation of Rights: Publisher reserves all rights not specifically granted in the combination of (i) the license details provided by you and accepted in the course of this licensing transaction, (ii) these terms and conditions and (iii) CCC's Billing and Payment terms and conditions.

8. License Contingent Upon Payment: While you may exercise the rights licensed immediately upon issuance of the license at the end of the licensing process for the transaction, provided that you have disclosed complete and accurate details of your proposed use, no license is finally effective unless and until full payment is received from you (either by publisher or by CCC) as provided in CCC's Billing and Payment terms and conditions. If full payment is not received on a timely basis, then any license preliminarily granted shall be deemed automatically revoked and shall be void as if never granted. Further, in the event that you breach any of these terms and conditions or any of CCC's Billing and Payment terms and conditions, the license is automatically revoked and shall be void as if never granted. Use of materials as described in a revoked license, as well as any use of the materials beyond the scope of an unrevoked license, may constitute

copyright infringement and publisher reserves the right to take any and all action to protect its copyright in the materials.

9. Warranties: Publisher makes no representations or warranties with respect to the licensed material.

10. Indemnity: You hereby indemnify and agree to hold harmless publisher and CCC, and their respective officers, directors, employees and agents, from and against any and all claims arising out of your use of the licensed material other than as specifically authorized pursuant to this license.

11. No Transfer of License: This license is personal to you and may not be sublicensed, assigned, or transferred by you to any other person without publisher's written permission.

12. No Amendment Except in Writing: This license may not be amended except in a writing signed by both parties (or, in the case of publisher, by CCC on publisher's behalf).

13. Objection to Contrary Terms: Publisher hereby objects to any terms contained in any purchase order, acknowledgment, check endorsement or other writing prepared by you, which terms are inconsistent with these terms and conditions or CCC's Billing and Payment terms and conditions. These terms and conditions, together with CCC's Billing and Payment terms and conditions (which are incorporated herein), comprise the entire agreement between you and publisher (and CCC) concerning this licensing transaction. In the event of any conflict between your obligations established by these terms and conditions and those established by CCC's Billing and Payment terms and conditions, these terms and conditions shall control.

14. Revocation: Elsevier or Copyright Clearance Center may deny the permissions described in this License at their sole discretion, for any reason or no reason, with a full refund payable to you. Notice of such denial will be made using the contact information provided by you. Failure to receive such notice will not alter or invalidate the denial. In no event will Elsevier or Copyright Clearance Center be responsible or liable for any costs, expenses or damage incurred by you as a result of a denial of your permission request, other than a refund of the amount(s) paid by you to Elsevier and/or Copyright Clearance Center for denied permissions.

LIMITED LICENSE

The following terms and conditions apply only to specific license types:

15. **Translation**: This permission is granted for non-exclusive world **English** rights only unless your license was granted for translation rights. If you licensed translation rights you may only translate this content into the languages you requested. A professional translator must perform all translations and reproduce the content word for word preserving the integrity of the article.

16. **Posting licensed content on any Website**: The following terms and conditions apply as follows: Licensing material from an Elsevier journal: All content posted to the web site must maintain the copyright information line on the bottom of each image; A hyper-text must be included to the Homepage of the journal from which you are licensing at http://www.sciencedirect.com/science/journal/xxxxx or the Elsevier homepage for books at http://www.elsevier.com; Central Storage: This license does not include permission for a scanned version of the material to be stored in a central repository such as that provided by Heron/XanEdu.

Licensing material from an Elsevier book: A hyper-text link must be included to the Elsevier homepage at http://www.elsevier.com . All content posted to the web site must maintain the copyright information line on the bottom of each image.

Posting licensed content on Electronic reserve: In addition to the above the following clauses are applicable: The web site must be password-protected and made available only to bona fide students registered on a relevant course. This permission is granted for 1 year only. You may obtain a new license for future website posting.

17. **For journal authors:** the following clauses are applicable in addition to the above:

Preprints:

A preprint is an author's own write-up of research results and analysis, it has not been peer-reviewed, nor has it had any other value added to it by a publisher (such as formatting, copyright, technical enhancement etc.).

Authors can share their preprints anywhere at any time. Preprints should not be added to or enhanced in any way in order to appear more like, or to substitute for, the final versions of articles however authors can update their preprints on arXiv or RePEc with their Accepted Author Manuscript (see below).

If accepted for publication, we encourage authors to link from the preprint to their formal publication via its DOI. Millions of researchers have access to the formal publications on ScienceDirect, and so links will help users to find, access, cite and use the best available version. Please note that Cell Press, The Lancet and some society-owned have different preprint policies. Information on these policies is available on the journal homepage.

Accepted Author Manuscripts: An accepted author manuscript is the manuscript of an article that has been accepted for publication and which typically includes author-incorporated changes suggested during submission, peer review and editor-author communications.

Authors can share their accepted author manuscript:

- immediately
    - via their non-commercial person homepage or blog
    - by updating a preprint in arXiv or RePEc with the accepted manuscript
    - via their research institute or institutional repository for internal institutional uses or as part of an invitation-only research collaboration work-group
    - directly by providing copies to their students or to research collaborators for their personal use
    - for private scholarly sharing as part of an invitation-only work group on commercial sites with which Elsevier has an agreement
- After the embargo period
    - via non-commercial hosting platforms such as their institutional repository
    - via commercial sites with which Elsevier has an agreement

In all cases accepted manuscripts should:

- link to the formal publication via its DOI
- bear a CC-BY-NC-ND license - this is easy to do
- if aggregated with other manuscripts, for example in a repository or other site, be shared in alignment with our hosting policy not be added to or enhanced in any way to appear more like, or to substitute for, the published journal article.

Published journal article (JPA): A published journal article (PJA) is the definitive final record of published research that appears or will appear in the journal and embodies all value-adding publishing activities including peer review co-ordination, copy-editing, formatting, (if relevant) pagination and online enrichment.

Policies for sharing publishing journal articles differ for subscription and gold open access articles:

Subscription Articles: If you are an author, please share a link to your article rather than the full-text. Millions of researchers have access to the formal publications on ScienceDirect, and so links will help your users to find, access, cite, and use the best available version.

Theses and dissertations which contain embedded PJAs as part of the formal submission can be posted publicly by the awarding institution with DOI links back to the formal publications on ScienceDirect.

If you are affiliated with a library that subscribes to ScienceDirect you have additional private sharing rights for others' research accessed under that agreement. This includes use for classroom teaching and internal training at the institution (including use in course packs and courseware programs), and inclusion of the article for grant funding purposes.

Gold Open Access Articles: May be shared according to the author-selected end-user license and should contain a CrossMark logo, the end user license, and a DOI link to the formal publication on ScienceDirect.

Please refer to Elsevier's posting policy for further information.

18. **For book authors** the following clauses are applicable in addition to the above: Authors are permitted to place a brief summary of their work online only. You are not allowed to download and post the published electronic version of your chapter, nor may you scan the printed edition to create an electronic version. **Posting to a repository:** Authors are permitted to post a summary of their chapter only in their institution's repository.

19. **Thesis/Dissertation**: If your license is for use in a thesis/dissertation your thesis may be submitted to your institution in either print or electronic form. Should your thesis be published commercially, please reapply for permission. These requirements include permission for the Library and Archives of Canada to supply single copies, on demand, of the complete thesis and include permission for Proquest/UMI to supply single copies, on demand, of the complete thesis. Should your thesis be published commercially, please reapply for permission. Theses and dissertations which contain embedded PJAs as part of the formal submission can be posted publicly by the awarding institution with DOI links back to the formal publications on ScienceDirect.

Elsevier Open Access Terms and Conditions

You can publish open access with Elsevier in hundreds of open access journals or in nearly 2000 established subscription journals that support open access publishing. Permitted third party re-use of these open access articles is defined by the author's choice of Creative Commons user license. See our open access license policy for more information.

Terms & Conditions applicable to all Open Access articles published with Elsevier:

Any reuse of the article must not represent the author as endorsing the adaptation of the article nor should the article be modified in such a way as to damage the author's honour or reputation. If any changes have been made, such changes must be clearly indicated.

The author(s) must be appropriately credited and we ask that you include the end user license and a DOI link to the formal publication on ScienceDirect.

If any part of the material to be used (for example, figures) has appeared in our publication with credit or acknowledgement to another source it is the responsibility of the user to ensure their reuse complies with the terms and conditions determined by the rights holder.

Additional Terms & Conditions applicable to each Creative Commons user license:

CC BY: The CC-BY license allows users to copy, to create extracts, abstracts and new works from the Article, to alter and revise the Article and to make commercial use of the Article (including reuse and/or resale of the Article by commercial entities), provided the user gives appropriate credit (with a link to the formal publication through the relevant DOI), provides a link to the license, indicates if changes were made and the licensor is not represented as endorsing the use made of the work. The full details of the license are available at http://creativecommons.org/licenses/by/4.0.

CC BY NC SA: The CC BY-NC-SA license allows users to copy, to create extracts, abstracts and new works from the Article, to alter and revise the Article, provided this is not done for commercial purposes, and that the user gives appropriate credit (with a link to the formal publication through the relevant DOI), provides a link to the license, indicates if changes were made and the licensor is not represented as endorsing the use made of the work. Further, any new works must be made available on the same conditions. The full details of the license are available at http://creativecommons.org/licenses/by-nc-sa/4.0.

CC BY NC ND: The CC BY-NC-ND license allows users to copy and distribute the Article, provided this is not done for commercial purposes and further does not permit distribution of the Article if it is changed or edited in any way, and provided the user gives appropriate credit (with a link to the formal publication through the relevant DOI), provides a link to the license, and that the licensor is not represented as endorsing the use made of the work. The full details of the license are available at http://creativecommons.org/licenses/by-nc-nd/4.0. Any commercial reuse of Open Access articles published with a CC BY NC SA or CC BY NC ND license requires permission from Elsevier and will be subject to a fee.

Commercial reuse includes:

- Associating advertising with the full text of the Article
- Charging fees for document delivery or access
- Article aggregation
- Systematic distribution via e-mail lists or share buttons

Posting or linking by commercial companies for use by customers of those companies.

20. **Other Conditions**:

v1.10

Questions? customercare@copyright.com.

Radha Krishna Kashyap <krishna.kashyap@students.iiserpune.ac.in>

RE: Copyright permission required
1 message

CONTRACTS-COPYRIGHT (shared) <Contracts-Copyright@rsc.org>   Wed, Jul 24, 2024 at 8:39 PM
To: "krishna.kashyap@students.iiserpune.ac.in" <krishna.kashyap@students.iiserpune.ac.in>

Dear Radha Krishna Kashyap   # Chapter 4

The Royal Society of Chemistry (RSC) hereby grants permission for the use of your paper(s) specified below in the printed and microfilm version of your thesis. You may also make available the PDF version of your paper(s) that the RSC sent to the corresponding author(s) of your paper(s) upon publication of the paper(s) in the following ways: in your thesis via any website that your university may have for the deposition of theses, via your university's Intranet or via your own personal website. We are however unable to grant you permission to include the PDF version of the paper(s) on its own in your institutional repository. The Royal Society of Chemistry is a signatory to the STM Guidelines on Permissions (available on request).

Please note that if the material specified below or any part of it appears with credit or acknowledgement to a third party then you must also secure permission from that third party before reproducing that material.

Please ensure that the thesis includes the correct acknowledgement (see http://rsc.li/permissions for details) and a link is included to the paper on the Royal Society of Chemistry's website.

Please also ensure that your co-authors are aware that you are including the paper in your thesis.

Best wishes

Becky

Becky Roberts
Contracts & Copyright Executive, Sales Operations

Royal Society of Chemistry

www.rsc.org

From: do-not-reply@rsc.org <do-not-reply@rsc.org>
Sent: Wednesday, July 24, 2024 4:05 PM
To: CONTRACTS-COPYRIGHT (shared) <Contracts-Copyright@rsc.org>
Subject: Copyright permission required

PLEASE DO NOT REPLY DIRECTLY TO THIS EMAIL AS THE INBOX IS NOT MONITORED.
The email address below can be used to reply to the person who submitted this form.

Name: Radha Krishna Kashyap
Email address (please reply to this address): krishna.kashyap@students.iiserpune.ac.in
Message: I am Radha Krishna Kashyap a PhD student at Indian Institute of Science Education and Research (IISER), Pune. IISER Pune is a non-profit academic institute. I would like to take permission to reuse content of (doi: 10.1039/D3CC04278B) for my PhD thesis. I am the leading author of it.
details of the article:
Title: Plasmon enabled Claisen rearrangement with sunlight
Doi: 10.1039/D3CC04278B
Detail part to be used: Full article

More information on The Royal Society of Chemistry can be found on our website: www.rsc.org

PLS Clear

Figure 1.14

PARTIES:

1. **Cambridge University Press** (Licensor); and
2. **Radha Krishna Kashyap** (Licensee).

Thank you for your recent permission request. Some permission requests for use of material published by the Licensor, such as this one, are now being facilitated by PLSclear.

Set out in this licence cover sheet (the **Licence Cover Sheet**) are the principal terms under which Licensor has agreed to license certain Licensed Material (as defined below) to Licensee. The terms in this Licence Cover Sheet are subject to the attached General Terms and Conditions, which together with this Licence Cover Sheet constitute the licence agreement (the **Licence**) between Licensor and Licensee as regards the Licensed Material. The terms set out in this Licence Cover Sheet take precedence over any conflicting provision in the General Terms and Conditions.

Free Of Charge Licence Terms

Licence Date:	24/07/2024
PLSclear Ref No:	96195

The Licensor

Company name:	Cambridge University Press
Address:	University Printing House
	Shaftesbury Road
	Cambridge
	CB2 8BS
	GB

The Licensee

Licensee Contact Name:	Radha Krishna Kashyap
Licensee Address:	Indian Institute of Science Education and Research,
	Pune, India
	411008
	India

Licensed Material

title:	Thermoplasmonics Heating Metal Nanoparticles Using Light
ISBN:	9781108418324
publisher:	Cambridge University Press

Are you requesting permission to reuse the cover of the publication?	No
Figure number & title	Fig. 4.2 Chronology of the articles reporting on temperature mapping for investigation in plasmonics
Page numbers	104
Name of illustrator	Radha Krishna Kashyap
Are you the author of the content that you are requesting to reuse?	No
Additional Information	I am Radha Krishna Kashyap a PhD student at Indian Institute of Science Education and Research (IISER), Pune. IISER Pune is a non-profit academic institute. I would like to take permission to reuse Fig. 4.2 for my PhD thesis.
Will you be changing or editing the image?	Yes
Will it be cropped?	No

For Use In Licensee's Publication(s)

usage type	Book, Journal, Magazine or Academic Paper-Thesis or Dissertation
Will your dissertation be placed in an online repository?	Yes
Author	Radha Krishna Kashyap
Estimated publication date	02/09/2024
Language	English
Title of dissertation/thesis	Light-Powered Plasmonic Heaters: Extracting the Heat Out of Plasmons for Photothermal Applications
University or institution	Indian Institute of Science Education and Research, Pune
Unlimited circulation?	No

Rights Granted

Exclusivity:	Non-Exclusive
Format:	Thesis or Dissertation
Language:	English
Territory:	UK & Commonwealth
Duration:	Lifetime of Licensee's Edition
Maximum Circulation:	100

GENERAL TERMS AND CONDITIONS

1. Definitions and Interpretation

1.1 Capitalised words and expressions in these General Terms and Conditions have the meanings given to them in the Licence Cover Sheet.

1.2 In this Licence any references (express or implied) to statutes or provisions are references to those statutes or provisions as amended or re-enacted from time to time. The term including will be construed as illustrative, without limiting the sense or scope of the words preceding it. A reference to in writing or written includes faxes and email. The singular includes the plural and vice versa.

2. Grant of Rights

2.1 The Licensor grants to Licensee the non-exclusive right to use the Licensed Material as specified in the Licence Cover Sheet.

2.2 The rights licensed to Licensee under this Licence do not include the right to use any third party copyright material incorporated in the Licensed Material. Licensee should check the Licensed Material carefully and seek permission for the use of any such third party copyright material from the relevant copyright owner(s).

2.3 Unless otherwise stated in the Licence Cover Sheet, the Licensed Material may be:

2.3.1 subjected to minor editing, including for the purposes of creating alternative formats to provide access for a beneficiary person (provided that any such editing does not amount to derogatory treatment); and/or

2.3.2 used for incidental promotional use (such as online retail providers' search facilities).

2.4 Save as expressly permitted in this Licence or as otherwise permitted by law, no use or modification of the Licensed Material may be made by Licensee without Licensor's prior written permission.

3. Copyright Notice and Acknowledgement

3.1 Licensee must ensure that the following notices and acknowledgements are reproduced prominently alongside each reproduction by Licensee of the Licensed Material:

3.1.1 the title and author of the Licensed Material;

3.1.2 the copyright notice included in the Licensed Material; and

3.1.3 the statement "Reproduced with permission of The Licensor through PLSclear."

4. Reversion of Rights

4.1 The rights licensed to Licensee under this Licence will terminate immediately and automatically upon the earliest of the following events to occur:

4.1.1 the Licensed Material not being used by Licensee within 18 months of the Licence Date;

4.1.2 expiry of the Licence Duration; or

4.1.3 the Maximum Circulation being reached.

5. <u>Miscellaneous</u>

5.1 By using the Licensed Material, Licensee will be deemed to have accepted all the terms and conditions contained in this Licence.

5.2 This Licence contains the entire understanding and agreement of the parties relating to its subject matter and supersedes in all respects any previous or other existing arrangements, agreements or understandings between the parties whether oral or written in relation to its subject matter.

5.3 Licensee may not assign this Licence or any of its rights or obligations hereunder to any third party without Licensor's prior written consent.

5.4 This Licence is governed by and shall be construed in accordance with the laws of England and Wales and the parties hereby irrevocably submit to the non-exclusive jurisdiction of the Courts of England and Wales as regards any claim, dispute or matter arising under or in relation to this Licence.

Radha Krishna Kashyap <krishna.kashyap@students.iiserpune.ac.in>

RE: Copyright permission required

1 message

CONTRACTS-COPYRIGHT (shared) <Contracts-Copyright@rsc.org>   Wed, Jul 24, 2024 at 10:58 PM
To: "krishna.kashyap@students.iiserpune.ac.in" <krishna.kashyap@students.iiserpune.ac.in>

Dear Radha Krishna Kashyap

Figure 5.3b

Thank you for your enquiry.

The Royal Society of Chemistry (RSC) hereby grants permission for the use of the material specified below in the printed and microfilm version of your thesis, and as part of your thesis in your university's digital repository. Permission is granted as long as the articles are fully acknowledged and a link is given back to the articles on our Platform. Please go to rsc.li/permissions for details.   Please note that if the material specified above or any part of it appears with credit or acknowledgement to a third party then you must also secure permission from that third party before reproducing that material.

Best wishes

Becky

Becky Roberts
Contracts & Copyright Executive, Sales Operations

Royal Society of Chemistry

www.rsc.org

ROYAL SOCIETY OF CHEMISTRY

From: do-not-reply@rsc.org <do-not-reply@rsc.org>
Sent: Wednesday, July 24, 2024 5:30 PM
To: CONTRACTS-COPYRIGHT (shared) <Contracts-Copyright@rsc.org>
Subject: Copyright permission required

PLEASE DO NOT REPLY DIRECTLY TO THIS EMAIL AS THE INBOX IS NOT MONITORED.
The email address below can be used to reply to the person who submitted this form.

Name: Copyright permission required
Email address (please reply to this address): krishna.kashyap@students.iiserpune.ac.in
Message: Dear RSC Team,
I am Radha Krishna Kashyap a PhD student at Indian Institute of Science Education and Research (IISER), Pune.
IISER Pune is a non-profit academic institute. I would like to take permission to reuse a figure (Fig.2a) from the article
(doi: 10.1039/C2EE22248E) for my PhD thesis.
The details are as follows:
Title of the article: Concentrated solar thermoelectric generators
Doi: 10.1039/C2EE22248E
Detail of the figures taken: Fig.2a

Thanks and regards
Kashyap